Microphase Separation Studies in Styrene-Diene Block Copolymer-based Hot-Melt Pressure-Sensitive Adhesives

Ninad Dixit

Dissertation submitted to the faculty of Virginia Polytechnic Institute and State University in partial fulfillment of the requirements for the degree of

DOCTOR OF PHILOSOPHY

in

Chemistry

Stephen M. Martin

Robert B. Moore

Eugene Joseph

Sam R. Turner

December 12, 2014

Blacksburg, VA

Keywords: block copolymer, tackifier, SAXS, rheology, microphase separation

Microphase Separation Studies in Styrene-Diene Block Copolymer-based Hot-Melt Pressure-Sensitive Adhesives

Ninad Dixit

Abstract

This dissertation is aimed at understanding the microstructure evolution in styrene – diene block copolymer – based pressure-sensitive adhesive compositions in melt. The work also focuses on determining the microphase separation mechanism in adhesive melts containing various amounts of low molecular weight resin (tackifiers) blended with styrene – diene block copolymers. To understand the correlation between adhesive morphology and their dynamic mechanical behavior, small angle X-ray scattering (SAXS) and rheological analysis were performed on blends with different compositions.

A modified Percus – Yevick model combined with Gaussian functions was used fit the liquid like disordered and bcc – ordered peaks of the SAXS intensity profiles. The morphological parameters derived from SAXS analysis corresponded to features such as the size and extent of ordering of the microphase separated polystyrene domains. The variation in these parameters with respect to temperature and adhesive composition correlated reasonably well with the trends observed in the shear modulus measured using rheological analysis. It was found that the ordering of polystyrene domains was influenced by the tackifier content in the adhesive blends. Polymer chain mobility was determined to be the dominant factor governing ordering kinetics, which depended on both the quench temperature and tackifier content in the blends. The addition of increasing amounts of tackifier eventually leads to a shift from a nucleation and growth type mechanism to a spinodal decomposition mechanism for phase separation and ordering. The compatibility of the tackifier

with the polystyrene chains had a significant impact on the morphological transitions and microphase separation in adhesive blends. The blends containing a styrene – incompatible tackifier showed ordering over a broader range of temperatures compared to the blends containing a polystyrene – compatible tackifier.

Acknowledgements

I would like to thank Dr. Stephen M. Martin for his support and guidance throughout the duration of this project. I would also like to thank Dr. Robert B. Moore for his valuable advice during my days at Virginia Tech. I would like to extend gratitude to Dr. Eugene Joseph, who took the initiative during the early stages of this project and has been a constant source of encouragement since then. I am grateful to Dr. S. Richard Turner, whose support was critical for successful completion of my graduate studies.

I also recognize valuable contribution of the following people in the achievement of my goals:

- My parents, who inspired me to become a scientist
- My extended family, who provided financial support during my stay in the United States
- Past and present members of the Martin research group – Alicia, Feras, Du Hyun, and Martha
- Undergraduate students who worked on this project – Conor, Brent, Teja, and Sahel
- Past and present members of the Moore research group – Gilles, Park, Sonya, Scott, Ming, Orkun, Elise, Amanda, and Jeremy
- Dr. Paul Deck and Dr. John Morris
- Chemistry and Chemical Engineering department staff
- Fellow teaching assistants and instructors

Format of Dissertation

The chapters 3, 4, and 5 of this dissertation will be submitted for journal publication. These chapters follow the formatting guidelines of a scientific journal (Macromolecules).

Table of Contents

List of Figures

Chapter 2

Chapter 3

Chapter 5

List of Tables

Chapter 1

Introduction

1.1 Research Background and Objectives

Pressure – sensitive adhesives (PSAs) are a class of adhesives that stick to a substrate without a chemical reaction when applied under light pressure.[1] In order to function as an adhesive, these materials must establish contact with the substrate at the molecular level. In other classes of adhesives, such as epoxies, intimate contact is achieved in the liquid state and is followed by a chemical reaction (heat or radiation curing) that imparts mechanical strength to the adhesive. In PSAs, good contact and adhesive strength are obtained through the viscoelastic properties of soft materials. The work of adhesion corresponds to the difference in the energy of substrate – adhesive interactions and the energy required to peel the adhesive layer. In the case of PSAs, van der Waal's forces are predominantly responsible for these adhesive interactions.[2,3]

PSAs are primarily based on three classes of polymers – natural rubber, acrylic and styrene-based block copolymers. Other polymers such as silicones are also used in specific PSA formulations. The styrene-based block copolymers are usually employed as a blend of triblock and diblock copolymers to obtain the desired viscoelastic behavior. High molecular weight styrene – diene based triblock copolymers undergo microphase separation at certain temperatures.[4] The microphase separated polystyrene domains dispersed in the diene-rich matrix provide physical crosslinks, which lead to excellent creep resistance, peel strength and good tack at service temperatures. Polydiene chains that bridge the two polystyrene domains significantly affect the tensile strength of an adhesive at large strains.[5] Hence, it is necessary to study the microphase separation process that controls the adhesive behavior of block copolymer – based adhesive compositions.

Fine-tuning of adhesive properties can be a critical issue for certain applications such as packaging tapes and labels, where long-term performance is required. In the case of block

copolymer – based adhesives, the desired properties can be achieved by carefully controlling the microphase separation process in the melt or in solution. However, a comprehensive study focusing on the microphase separation kinetics and resulting morphology is not available in the literature. The precise chemical structure of many adhesive components is not publicly available due to intellectual property protection rights. However, the variety in the chemistry of block copolymers involved in PSAs suggests that pressure – sensitive adhesion is a polymer physics problem. In this study we sought to understand the relationship between the morphology of the adhesive blends and their rheological behavior even though the precise chemistry of the materials was not available.

The key objectives of this study were as follows:

a. To analyze the microphase separation kinetics in block copolymers employed in pressure – sensitive adhesive formulations by small angle X-ray scattering and oscillatory rheological analysis; and to identify how processing temperature affects the behavior of morphological parameters obtained by correlating scattering and rheological analysis.
b. To extend the morphological model developed for block copolymers to their blends with tackifiers; to study the effect of tackifier on the microphase separation mechanism and kinetics; and to identify the trends in shear moduli of the adhesive melts as the tackifier content increases.
c. To evaluate the effect of tackifier compatibility with the hard and soft segments of the block copolymer on microphase separation in adhesive compositions by analyzing the rheological behavior of adhesive melts.

The dissertation is organized into chapters, several of which correspond to journal articles that have been submitted for publication, or will be shortly. The second chapter of this dissertation is

a brief literature review of microphase separation in block copolymers as well as the relationship between rheological behavior and the performance properties of the adhesives. The third chapter is focused on the establishment of morphological parameters for a commercially available block copolymer that is used in PSA formulations, and on the kinetics of microphase separation and ordering in the pure block copolymer. In the fourth chapter, the effect of tackifier on the microphase separation mechanism and kinetics in PSA compositions is discussed. The fifth chapter describes the effect of tackifier – block copolymer compatibility on the microphase separation kinetics in various PSA compositions. The sixth chapter contains a brief summary of the work, including the key contributions, and a discussion of areas for future research.

1.2 References

(1) Satas, D. *Handbook of pressure sensitive adhesive technology*; Satas & Associates: Warwick, RI, 1999.

(2) Creton, C.; Leibler, L. *Journal of Polymer Science Part B: Polymer Physics* **1996**, *34*, 545.

(3) Zosel, A. *Journal of Adhesion Science and Technology* **1997**, *11*, 1447.

(4) Bates, F. S.; Fredrickson, G. H. *Annu. Rev. Phys. Chem.* **1990**, *41*, 525.

(5) Roos, A.; Creton, C. *Macromolecules* **2005**, *38*, 7807.

Chapter 2

Literature review

2.1. Theory of microphase separation in block copolymers

Block copolymers undergo microphase separation due to repulsion between different blocks. However, complete separation of blocks is not achieved due to chemical bonds between them. Under various conditions, the microphase separated domains may form a periodic structure.[1,2] The most commonly observed structures include cubic arrangement of spheres, two-dimensional hexagonal cylinders, and one-dimensional lamellae. The existence of disordered phase in low molecular weight block copolymer melts has also been confirmed.[3,4] Significant efforts were made to develop a theory for block copolymer melts,[5-9] which attempted to calculate and minimize the free energy of a mesophase with its characteristic dimensions. A linear diblock copolymer consisting of two types of monomer units (A and B) was considered for theoretical purposes. Helfand[7] proposed a theory based on molecular parameters of the block copolymer, but it requires a complicated numerical analysis to understand the simplest possible phase (lamellae). The assumption of narrow interfacial thickness compared to the domain size greatly simplified the analysis of the lamellar and cubic phases.[8-10] However, when microphase separation takes place from homogeneous melt, a broad interface must be taken into account. Thus, this theory appeared to be inadequate to study the microphase separation in block copolymers. The 'random phase approximation' was proposed by de Gennes[11] to study the density correlation function of monomer A in A-B diblock copolymer. Leibler[2] used this approach and observed the appearance of a wave vector with an unstable mode under critical conditions. The introduction of instability was assigned to the microphase separation transition (also called 'order-disorder transition'). Leibler determined the correlation functions, and then used statistical physics to calculate the free energy of the system as a function of order parameter. The analysis showed that only two components,

system composition (f), and χN (product of Flory's interaction parameter and degree of polymerization respectively) were necessary to analyze the microphase separation transition.

For a compositionally symmetric copolymer (f = 0.5), the transition between ordered and disordered (order-disorder transition or ODT) phase occurs when $\chi N \sim 10$. For low values of χN (<<1), the system behaves as a disordered melt. However, block junctions and melt incompressibility leads to correlation hole.[11] As a result, a peak is observed in scattering (X-ray or neutron) analysis corresponding to length scale $D \sim R_g \sim aN^{1/2}$, where 'R_g' is radius of gyration, and 'a' is characteristic segment length. As χN nears 10, the balance between entropic and enthalpic factors leads to the order-disorder transition. Near the ODT, A-B interactions are considered weak enough so that the copolymer chains remain unperturbed. This regime is called 'weak segregation limit' (WSL), which simplifies the calculations. When $\chi N >> 10$, nearly pure domains of A and B are postulated, with a narrow interface. Minimization of A-B contacts comes at the expense of entropy, hence chains now exhibit perturbed dimensions. The domain spacing now scales as $D \sim aN^{2/3}\chi^{1/6}$. This regime is called 'strong segregation limit' (SSL). Most theories proposed to describe the phase behavior of block copolymer fall into either WSL or SSL. Treating the region near ODT as WSL has been more convenient for calculation purposes. Block copolymer compositions results in much limited range of χN values, thus a solvent neutral with respect to A and B is added to the block copolymer, which reduces the number of A-B contacts and lowers the interaction parameter (χ). Addition of a neutral solvent can lead to a wide range of χN values, and thus experimental verification of the theories becomes feasible. These concentrated solutions behave similar to undiluted block copolymers except that the interaction parameter is proportional to copolymer concentration.

According to the predictions by Helfand,[8,9,12] five ordered structures are observed in the SSL regime (two spherical, two cylindrical, and lamellar morphology). Hashimoto and coworkers[13-16] extensively studied the phase behavior of model styrene – isoprene diblock copolymers. The authors determined the interfacial thickness to be 20 ± 5 Å irrespective of the molecular weight and microstructure. Bates and coworkers[17] also observed similar results in a small angle neutron scattering (SANS) study. The authors[18] also verified a body centered cubic packing of polystyrene spheres predicted by Leibler. However, Richards and Thomason[19] proposed a face centered cubic packing of polystyrene spheres based on SANS studies. Roe et al determined the interfacial thickness (t) for styrene – isoprene diblock and triblock copolymers to be $10 \leq t \leq 17$ Å in WSL regime. These results were consistent with the predictions of Helfand and Wasserman[8] that

$$t \approx \sqrt{\frac{2}{3}} a\chi^{-1/2} \cong 23 \text{ Å} \quad \text{..... (1)}$$

Where, 'a' is statistical segment length of the copolymer.

Spontak et al[20] performed transmission electron microscopy (TEM) analysis, and determined an interfacial thickness of ~ 26 Å, slightly larger than found in previous studies. One of the significant discoveries was that of the ordered 'bicontinuous double diamond' morphology (OBDD) of polystyrene[21-24] in star copolymers, deduced from the correlation of SAXS and TEM analysis (Figures 1 and 2). Hasegawa et al[25] on the other hand, discovered the presence of the "tetrapod network structure" in linear styrene – isoprene diblock copolymers containing 62 – 66 volume % polystyrene. The tetrapod network structure was essentially a polyisoprene equivalent of OBDD structure observed in star copolymers. These morphologies appeared to be stable over a narrow range of polystyrene volume fractions (28 – 34 volume % for polystyrene OBDD, and 62

– 66 volume % for polyisoprene OBDD). Thomas and coworkers reported that the OBDD structures could be classified as "constant mean curvature" (CMC) surfaces.[26]

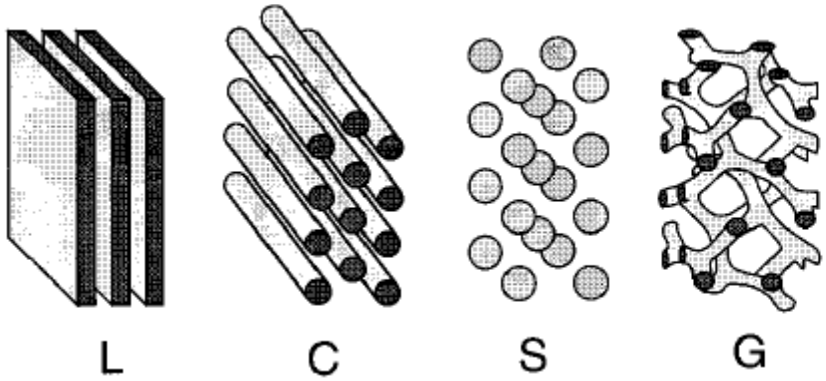

Figure 1: Microstructures in phase separated block copolymers: Lamellae (L), Cylinders (C), Spheres (S), and Gyroid (G) or 'ordered bicontinuous double diamond'. Reprinted with permission from Matsen, M. W.; Bates, F. S. *The Journal of Chemical Physics* **1997**, *106*, 2436. Copyright 1997, AIP Publishing LLC.

The concept of extended chain conformation is central to the theory of strong segregation. The relationship between periodic spacing and copolymer molecular weight is given as $D \sim N^{\delta}$, where $\delta = 2/3$ in SSL, and 1/2 in WSL which assumes unperturbed chain conformations. Initial work by Leary and Williams[27], and Helfand and Wasserman[8,28] established the principles governing the size and shape of microphase separated domains. Helfand and Wasserman in particular identified factors contributing to free energy in the strong segregation regime – (1) enthalpy of contact between nearly pure A and B domains at the interface, (2) entropy loss due to extended chain configuration, and (3) entropic contribution of A – B joints at the interface. These authors showed that the interfacial thickness $t \sim a\chi^{-1/2}$. They also used self-consistent mean field theory to propose the domain spacing $D \sim aN^{\delta}\chi^{\mu}$, where $\delta \approx 9/14$ and $\mu \approx 1/7$. Numerical techniques developed by these authors enabled construction of phase diagram in strong segregation regime, and stability limits of different ordered phases excluding the OBDD structure. However, the

application of Helfand-Wasserman theory has been limited due to necessity of complex calculations. The focus has rather been to determine the free energy when $\chi N \rightarrow \infty$.

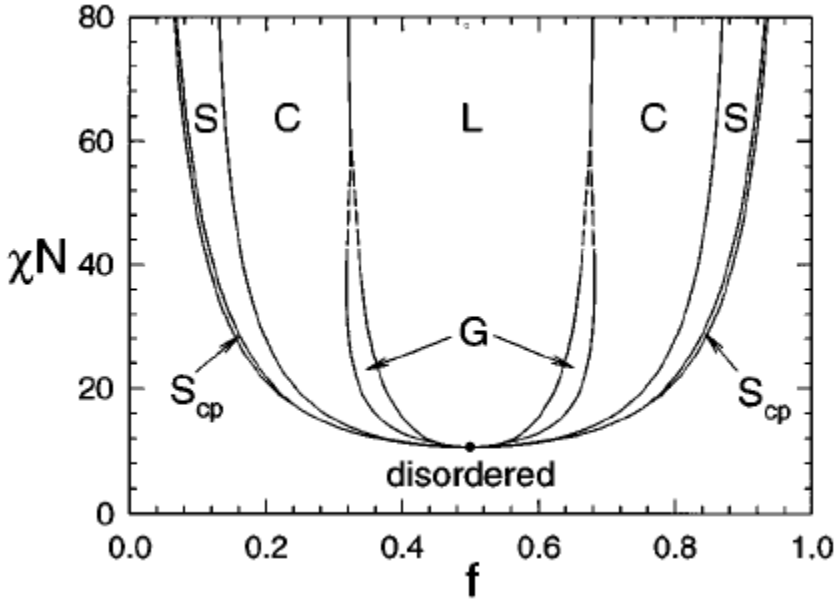

Figure 2: Phase diagram of a block copolymer based on mean-field theory. Reproduced from Matsen and Bates, 1997. Reprinted with permission from Matsen, M. W.; Bates, F. S. *The Journal of Chemical Physics* **1997**, *106*, 2436. Copyright 1997, AIP Publishing LLC.

Semenov[29] suggested that the asymmetric copolymer systems can be significantly more complicated compared to weak segregation theory predictions. Semenov used strong segregation theories to conclude that the formation of micelles is energetically favorable at a certain incompatibility $(\chi N)_M$, which is lower than $(\chi N)_{ODT}$. The weak segregation regime cannot access the long, large amplitude composition fluctuations i.e. micelles. Semenov not only predicted the existence of a micellar phase, he also postulated disordered micelles forming face-centered cubic (fcc) structure as χN increased. These micelles have been observed in triblock copolymers[30] as well as in concentrated and semi-dilute solutions of block copolymers in a neutral solvent.[31,32] In case of solutions, assuming that the solvent is uniformly distributed within microphases, one can obtain a phase diagram using $\phi\chi$ instead of χ, ϕ being copolymer volume fraction in the solution. However, Frederickson and Leibler[31] showed that such approach does not consider several aspects

of solutions, accumulation of solvent molecules at the A-B interface in particular. Such partition reduces the number of A-B contacts, but results in loss of translational entropy. In addition, in block copolymer solutions, an ODT exists between a solvent rich disordered phase and solvent poor ordered phase. Good solvents show such transition over a narrow range, but poorer solvents show broader range of $\phi\chi$.

2.2. Analysis of microphase separation

2.2.1. SAXS and microphase separation

Small angle X-ray scattering (SAXS) is one of the commonly used techniques to characterize the order-disorder transition (ODT) and phase structure. Numerous studies employing SAXS and/or SANS (small angle neutron scattering) to understand the block copolymer phase behavior are available in the literature.[15,33-38] The observable length (L) in scattering analysis is $\lambda/2sin\theta$. In case of SAXS, λ is approximately 0.15 nm, and $2\theta \sim 0.17 – 2.7^{o}$. Thus, domains within the size range 5 – 50 nm can be detected by SAXS analysis. Microphase separated domains in block copolymers can be observed using TEM as well, but a SAXS set up enables measurements over a wide temperature range, and does not require staining of samples. The efficiency of TEM analysis may depend on how well the samples are stained to achieve the contrast. In SAXS analysis, the electron density difference between different blocks provides the contrast. By analyzing the relative positions of scattering peaks, specific phase structures can be determined. Also, the interfacial thickness between two phases can be calculated by observing the scattering intensity.

Table 1: Relative scattering peak positions for classic microstructures[39]

Microdomain Structure	Relative scattering peak positions
Lamellae	1, 2, 3, 4, 5
Hexagonally packed cylinders	1, √3, √4, √7, √9
Simple cubic	1, √2, √3, √4, √5
Body-centered cubic	1, √2, √3, √4, √5
Face-centered cubic	√3,√4, √8, √11, √12

The intensity of scattered radiation *I(q)* can be given by the following equation

$$I(q) \sim (\rho_A - \rho_B) S(q) \quad \text{..... (2)}$$

where, $(\rho_A - \rho_B)$ is the electron density difference between A and B blocks, and *S(q)* is the structure factor that represents the interaction between microphase separated domains. Using Leibler's mean field theory, the intensity of the scattering maximum can be described as

$$I(q^*)^{-1} \sim \frac{F(x^*)}{N} - 2(a + \frac{b}{T}) \quad \text{..... (3)}$$

where $x = q^{*2}R_g^2$, R_g is the radius of gyration, and *F(x,f)* is a function related to Debye correlation functions of Gaussian chains a block copolymer. The values of constants *a* and *b* depend on the block copolymer chemistry. According to equation (3), the inverse of the scattering peak intensity should be proportional to inverse of the temperature. Many studies have determined this relationship between $1/I(q^*)$ and $1/T$ to calculate χ.[40-45] The linearity of $1/I(q^*)$ vs $1/T$ plots has also been used to determine the order-disorder transition temperature (T_{ODT}) in microphase separated systems. As the system transitions from ordered to disordered state (or vice versa), manifestation of (or departure from) the mean-field behavior should be reflected in $1/I(q^*)$ vs $1/T$ plots.[41,43,46,47]

The square of half width at half maximum (σ_q^2)of the primary scattering peak intensity was first used by Stuhn[48] to determine the ODT. Hashimoto and coworkers[41,43,46,47] used discontinuity in σ_q^2 vs *1/T* plots to determine the ODT in block copolymers. A theoretical basis of σ_q^2 was also established using the mean-field theory.[41]

2.2.2. Rheological analysis and phase separation

Time-temperature superposition (TTS) has been commonly used to study the linear viscoelastic behavior of homopolymers over a wide range of timescales. In TTS analysis, various plots of log(*G'*) or log(*G"*) vs angular frequency of oscillation (ω) are shifted along the ω-axis to generate a master curve. Application of TTS would fail in a microphase-separated systems due to presence of incompatible blocks with multiple relaxation times. However, numerous studies[49-65] have erroneously used TTS analysis to study the block copolymer systems. Alternatively, Han et al[66,67] proposed analysis of *G'* vs *G"* plots to determine ODT. The authors concluded that the G' vs G" plots should be linear, and overlap in the disordered state, and deviation from such behavior constitutes ODT. The ODT in block copolymers is also determined by isochronal temperature sweep analysis. Gouinlock and Porter[55] proposed that *G'* begins to drop drastically at T_{ODT}. However, the transition may not necessarily appear clearly in the *G'* vs *T* plots.[68]

2.2.3. Other methods

The anisotropic ordered structure in microphase separated block copolymer systems should exhibit birefringence. At ODT, the birefringence should disappear due to disappearance of ordered structures. Hence, by observing the intensity of scattered depolarized light, phase behavior of block copolymers with cylindrical or lamellar domains can be characterized. Spherical and gyroid structure are symmetrical, hence they do not demonstrate birefringence. Results of birefringence

measurements and isochronal temperature sweep experiments were found to be consistent.[69] However, these methods do not determine whether the ODT is a first or second order transition in terms of changes in thermodynamic parameters. Differential scanning calorimetry measures the change in enthalpy, and dilatometry tracks the volume change. Hence, these methods have also been used to characterize ODT. The DSC analysis of several block copolymers showed a small endothermic peak in the vicinity of ODT.[70-73] Ryu et al[70] also observed a small peak corresponding to the transition from hexagonal-close-packed structure to body-centered-cubic structure in asymmetric styrene-*b*-isoprene-*b*-styrene (SIS) block copolymers. Dilatometry analysis by Kasten and Stuhn[71], and Ryu et al[74] showed discontinuity in volume changes near ODT of styrene-based diblock copolymers.

2.3 Phase transitions in highly asymmetric block copolymers

An asymmetric block copolymer contains one of the monomers in significant excess compared to the other. E.g. a block copolymer containing 70 mol % isoprene is an asymmetric block copolymer. The symmetric copolymers contain 50 mol % of each of the monomers. The compositional asymmetry of a block copolymer has a pronounced effect on its phase behavior. E.g. log *G'* vs log *G''* plots of compositionally symmetric and highly asymmetric styrene-isoprene (SI) block copolymers show very different temperature dependence, as seen in Figure 3. In the case of nearly symmetric block copolymer (Figure 3A), the slope changes between 100 °C and 125 °C. For the asymmetric copolymer (Figure 3B), the plots run parallel between temperatures 140 °C and 180 °C. This difference puts forth two questions – do highly asymmetric copolymers undergo the same phase transitions as symmetric (or nearly symmetric) copolymers? And do highly asymmetric copolymers follow a different phase transition mechanism than that for phase transitions in symmetric copolymers?

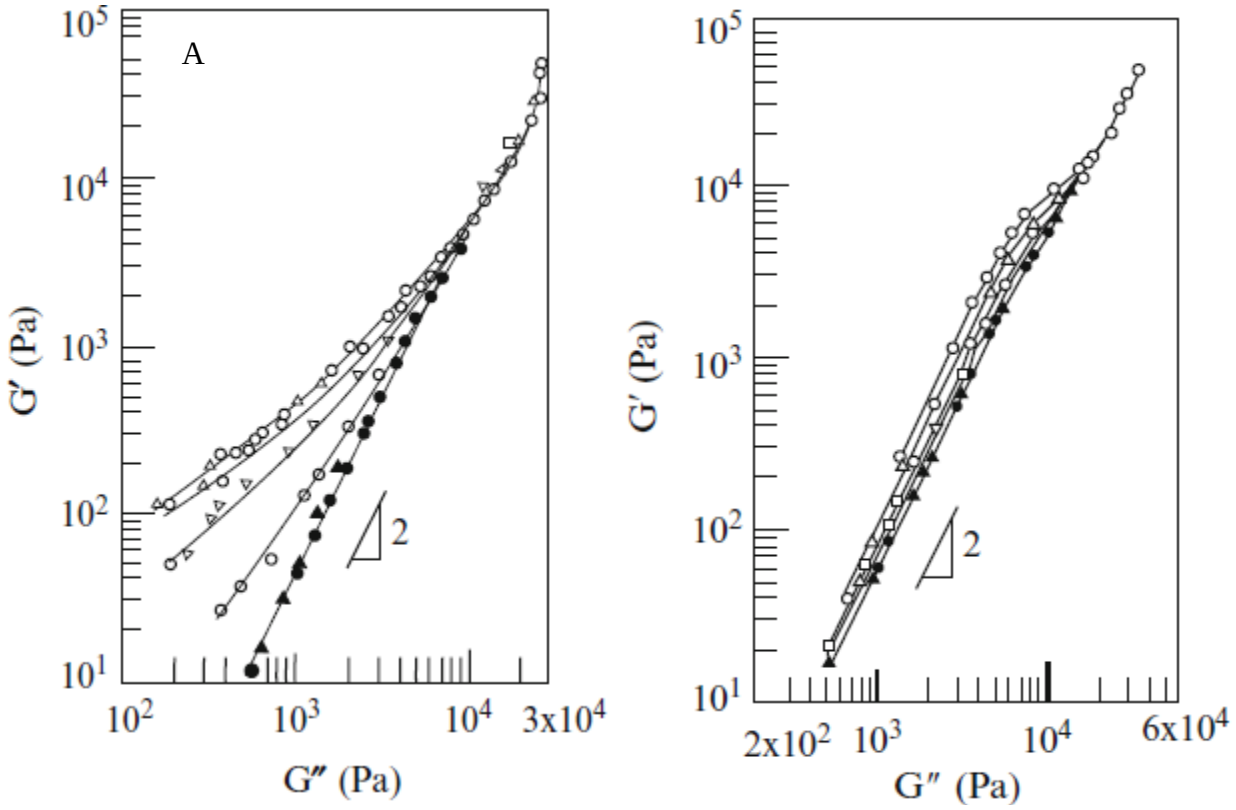

Figure 3: log *G'* vs log *G"* plots for SI block copolymers with (A) nearly symmetric composition (f_{PS} = 0.464) and (B) symmetric composition (f_{PS} = 0.81). Reprinted with permission from Han, C. D.; Baek, D. M.; Kim, J. K.; Ogawa, T.; Sakamoto, N.; Hashimoto, T. *Macromolecules* **1995**, *28*, 5043. Copyright 1995, American Chemical Society.

Figure 4 shows log *G'* vs log *G"* plots of an SIS block copolymer (w_{PS} = 0.16, M_n = 1.06 x 10^5) recorded at various temperatures, when the sample was heated from 140 ºC to 214 ºC.[75] The plots recorded at temperatures between 164 ºC and 200 ºC show a parallel shift. Such shift is also observed in other highly asymmetric systems, which is assigned to the presence of disordered micelles (or spherical domains).[76-78] Inset of Figure 4 shows temperature sweep analysis for the same block copolymer sample. The temperature sweep analysis shows loss of long-range order beginning at 166 ºC, resulting in sharp decrease in *G'*. This transition is called the lattice disorder-order transition (LDOT), which leads to formation of disordered micelles that show liquid-like behavior. At higher temperatures, the log *G'* vs log *G"* plots become temperature independent. Such behavior is assigned to formation of a disordered state with only composition fluctuations

present in the system. This transition indicates the disappearance of micelles and is called demicellization-micellization transition (DMT).

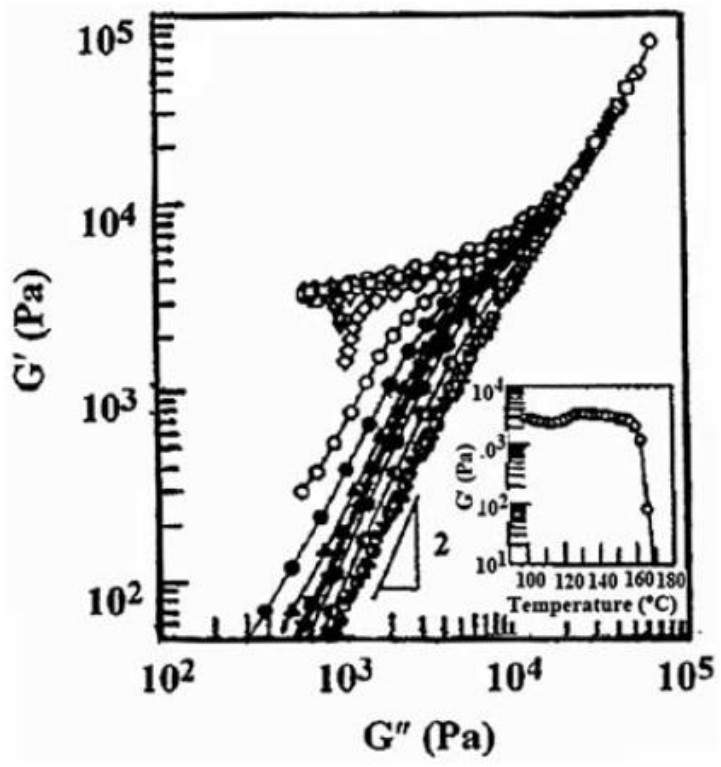

Figure 4: Frequency and temperature sweep (inset) analysis for an asymmetric SIS block copolymer during heating at different temperatures (ºC): (○)140, (△)151, (□)155, (▽)160, (◇)162, (⎔)164, (●)166, (▲)168, (■)170, (▼)172, (♦)174, (⬢)180, (◐)190, (◭)200, (◧)202, (▼)204, (◓)206, (◑)208, (◭)210, (◨)212, (⧩)214. Samples were annealed at 110 ºC for 3 days before performing rheological measurements. Temperature sweep experiment performed at ω = 0.01 rad/s. Reprinted with permission from Choi, S.; Vaidya, N. Y.; Han, C. D.; Sota, N.; Hashimoto, T. *Macromolecules* **2003**, *36*, 7707. Copyright 2003 American Chemical Society.

According to Sakamoto et al[76] and Han et al[77], LDOT is a first order transition similar to the ODT in symmetric block copolymers. However, it is important to understand that DMT, which is also a phase transition, takes place above LDOT. The inset in Figure 4 shows that the *G'* reaches a minimum around 120 ºC, which corresponds to the transition between hexagonal-close-packed (hcp) and body-centered-cubic (bcc) structure. The parallel shift in log *G'* vs log *G''* plots was also observed in nearly symmetric block copolymers by Rosedale and Bates.[61] The authors assigned

the shift to composition fluctuations near ODT. However, the analysis of symmetric SI diblock[68,75] and SIS triblock[75] copolymers has not shown such shift, thus casting doubt on whether the PEP-*b*-PEE copolymers analyzed by Rosedale and Bates were indeed symmetric in composition or not.

SAXS[47,75] and TEM[75] analysis have confirmed the presence of disordered micelles at temperatures above T_{LDOT}. The temperature range for an order-order transitions or OOT (between hcp and bcc structures), LDOT and DMT as determined by SAXS experiments matches reasonably well with the rheological analysis. The TEM analysis of samples quenched from a temperature between T_{LDOT} and T_{DMT} show a sharp interface, which is not due to trapped composition fluctuations.[79] Hence, LDOT should be considered a distinct transition rather than just an ODT for asymmetric block copolymers. Abuzania et al[80] showed that the hcp domains in an asymmetric SI copolymer (f_{PS} = 0.18) went through LDOT and formed micelles, whereas SI copolymer with f_{PS} = 0.23 did not form micelles following the disordering of hexagonal domains. Hence, the parallel shift observed in log *G'* vs log *G"* plots is likely due to formation of disordered micelles with a sharp interface. In case of a single phase system, log *G'* vs log *G"* plots overlap, and such behavior was concluded by the theory as well.[81,82]

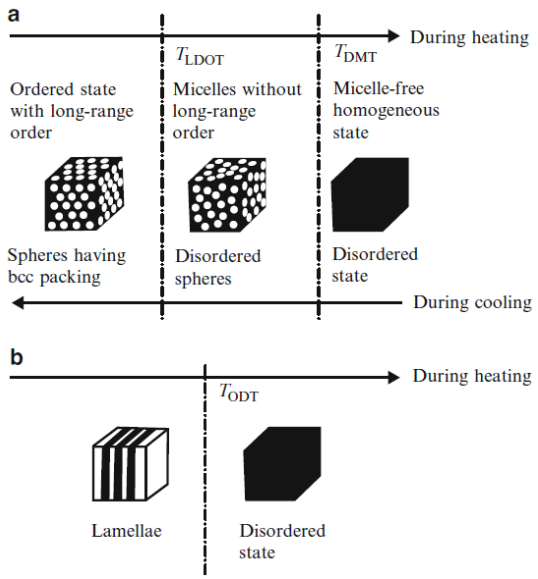

Figure 5: Trends in phase transition of (a) highly asymmetric and (b) symmetric / nearly symmetric block copolymers as the copolymer is heated up or cooled down. Highly asymmetric block copolymer shows 'bcc → disordered micelles → disordered phase' transitions upon heating. Symmetric / nearly symmetric copolymer shows 'lamellae → disordered phase' transition upon heating. All transitions are thermally reversible. Reprinted with permission from Han, C. D.; Vaidya, N. Y.; Kim, D.; Shin, G.; Yamaguchi, D.; Hashimoto, T. *Macromolecules* **2000**, *33*, 3767. Copyright 2000 American Chemical Society.

Figure 5 shows the phase transitions in symmetric and asymmetric block copolymers.[47,77] The DMT takes place approximately 40 ºC above LDOT. Theoretically, one would not expect to observe any other transition above the disordering transition (which is a first order transition). However, this condition is not followed in the analysis of asymmetric block copolymers, hence whether or not LDOT is a first order transition remains an unsolved issue. Dormidontova and Lodge[83] postulated the presence of micelles in the disordered phase, but essentially only used a classical terminology (T_{ODT} instead of T_{LDOT}). They also identified T_{CMT} (critical micelle temperature), which is similar to T_{DMT} described before. The predicted T_{CMT} was found to be in a reasonable agreement with experimentally observed T_{DMT}. However, the authors considered the micelles to be a part of the disordered phase. Matsen[84] and Wang et al[85] have followed similar approach.

2.4. Ordering Kinetics

Microphase separation can occur via two possible mechanisms – spinodal decomposition, and nucleation and growth. Depending on the magnitude of the driving force under given conditions, one of the two mechanisms is preferred. Using the theories described previously, one can determine disordered, metastable and spinodal (unstable) regions in the theoretical phase diagram for a given copolymer. The nucleation and growth mechanism is preferred when the system is in the metastable region, and spinodal decomposition is the dominant mechanism in the unstable region.[86]

2.4.1. Nucleation and Growth

There are two steps of development of an ordered phase in the metastable region. In the 'nucleation' step, nuclei of the ordered phase are formed in the disordered phase. In order to overcome the energy barrier, concentration fluctuations of large magnitude are necessary for nucleation to occur. The nuclei can be formed homogeneously - throughout the bulk of disordered phase, or heterogeneously – on impurities or on existing ordered structures.[87] Formation of nuclei is a result of the competition between interfacial energy and free energy of nucleus formation. Nuclei are formed only when their radius is above a critical value (r^*), above which the decrease in free energy of the system overcomes the interfacial energy. In the case of heterogeneous nucleation, the interfacial energy between a nucleus and substrate must also be considered (i.e. surface tension).[87]

Polymers usually undergo heterogeneous nucleation, cylindrical being the most common type of nucleus shape. Fredrickson and Binder[88] estimated the free energy required for nucleation in block copolymer melts by the following equation.

$$\Delta F^* \approx \frac{k_B T}{N^{1/3}\delta^2} \quad \text{..... (4)}$$

The time scale of growth was proposed using equation (4) as

$$\theta_c \sim N^{1/12}\delta^{-3/4}\tau_d e^{\Delta F^*/4k_B T} \quad \text{..... (5)}$$

where N is the degree of polymerization, δ is the difference between temperature of the system and ODT temperature, and τ_d is the chain relaxation time under given conditions. However, it is important to note that experimental data does not necessarily match with all theoretical predictions.[53,61]

Avrami Equation:

The Avrami model[89-91] was initially developed to describe the kinetics of phase change, and can be extended to microphase separation process in block copolymer melts. The model is derived from a previous free growth model which assumes non-interfering nuclei.[87] The model also assumes that the nucleation process is instantaneous. Since this model does not take into account nucleus impingement, there is no prediction of process termination as well. Avrami[89-91] proposed consideration of phantom nuclei that account for nuclei growing on existing ordered structures. Assuming constant nucleation and growth rates, the Avrami equation was proposed as follows.

$$1 - \lambda(t) = 1 - e^{-kt^n} \quad \text{..... (6)}$$

where $\lambda(t)$ is the fraction of material in the disordered state, k is the rate constant, and n is Avrami exponent for the given system under given conditions. The equation predicts sigmoidal behavior of ordering process, while 'k' and 'n' determine the precise shape of the curve. The effect of Avrami exponent and rate constant on the ordering process can be understood by determining the

time scale of ordering or half time of ordering. The values for Avrami exponent can vary between 1 and 6, and can be correlated to the type of growth process and the structure of the ordered phase. Following table shows possible growth types for various Avrami exponents.

Table 2: Relationship between Avrami exponent and type of growth. Reproduced from Mandelkern, 2002.[87]

Growth type	Homogeneous nucleation				Heterogeneous nucleation
	Linear growth		Diffusion controlled		
	growth	Steady state	$t = 0^a$	Steady state	Linear growth
			t = 0		
Sheaf-like	6	5	7/2	5/2	$5 \leq n \leq 6$
Three dimensional	4	3	5/2	3/2	$3 \leq n \leq 4$
Two-dimensional	3	2	2	1	$2 \leq n \leq 3$
One-dimensional	2	1	3/2	1/2	$1 \leq n \leq 2$

[a]All nuclei activated at t = 0

In the case of homogeneous nucleation, the linear and diffusion controlled growth processes can be distinguished based on the value of the Avrami coefficient. The '*n*' values are integers for the former type, and fractions for the latter. One-dimensional growth corresponds to formation of lamellae, two-dimensional growth corresponds to cylindrical geometry, and three-dimensional growth indicates spherulitic growth. However, it is clear from the table that different growth types can yield the same Avrami exponent. In the case of heterogeneous nucleation, the Avrami exponent may lie anywhere between the boundary values. It is also important to note that the growth rate may change with time during the crystallization process.[92] However, it seems

reasonable to neglect this assumption during the initial stages of ordering. Complete transformation of disordered phase into crystals is usually not observed in polymers.[87] Hence, the maximum possible fraction of ordered phase needs to be considered for the analysis. However, such modification does not necessarily change the interpretation of the Avrami exponent.

Floudas et al.[53,93] proposed that the volume fraction of the ordered phase $\phi(t)$ instead of $\lambda(t)$, be tracked to study ordering kinetics. Small angle X-ray scattering (SAXS) and rheology can be used to determine $\phi(t)$ to calculate the Avrami parameters. Considering the maximum possible volume of ordered phase V_∞, the modified Avrami equation is described as follows.[87,92]

$$ln\left[\frac{V_\infty - V_t}{V_t - V_0}\right] = \frac{1}{1-\lambda(\infty)} kt^n \quad \text{..... (7)}$$

where V_0 is the volume fraction of disordered phase. It is thus proposed that the ordering process in block copolymers is similar to that during polymer crystallization. However, physical meaning of the Avrami parameters is yet to be understood fully. It is still not clear whether the Avrami exponent corresponds to the shape of each domain (sphere/cylinder) or the resulting ordered structure (bcc, hcp etc.).

2.4.2. Spinodal decomposition

Microphase separation in the unstable (spinodal) region occurs due to composition fluctuations. Unlike nucleation, which occurs at a limited number of sites, composition fluctuations with sinusoidal profile are manifested throughout the sample.[94] Fluctuations of shorter wavelengths are energetically unfavorable, while fluctuations with large wavelengths would require polymer chains to diffuse through large distances. Hence, the fluctuations formed on the intermediate scale are usually responsible for microphase separation. During the initial times, the

fluctuations are relatively small in wavelength, but they grow in time as time progresses. The growth rate of amplitude of a fluctuation *R(q)* is given as follows.

$$R(q) = -D_{eff}q^2\left(1 + \frac{2\kappa q^2}{f_0^{"}}\right) \quad \text{..... (8)}$$

where, D_{eff} is the effective diffusion coefficient of a polymer chain through the given medium, κ is coefficient of gradient energy, q is wave vector, and $f_0^{"}$ is the second derivative of the free energy. Although the mechanisms of onset of phase separation may be different in metastable and spinodal regions, the growth processes at longer times appear to be similar. At longer times, the growth is predominantly driven by interfacial tension. The interfaces of phase separated domains become narrow to reduce the interfacial tension, and the growth rate is proportional to $t^{1/3}$.[94]

2.4.3. Order-disorder kinetics:

Hashimoto et al[95] reported one of the earliest studies of ordering kinetics in block copolymer, which have been followed by many researchers.[33,35,43,47,50,53,61,64,76,93,96-116] These studies involve quenching of block copolymer samples from a disordered state to a metastable state. The ordering of domains was observed using various techniques including SAXS, rheology, dynamic light scattering (DLS), polarized optical microscopy (POM), static birefringence, and transmission electron microscopy (TEM). However, POM and TEM analysis can result in large discrepancies when large grains of microphase separated domains overlap.[111,115] Static birefringence also fails to account for the growth of cubic and bicontinuous domains as they are structurally symmetrical and do not exhibit birefringence.[80,111,117]

Rheology and SAXS are the most commonly used techniques to track ordering when used in combination. The changes in intensity of the primary scattering maximum are used to determine the volume fraction of the ordered phase in SAXS analysis. Rheological measurements performed under oscillatory shear are used to determine the shear modulus of a sample, which then leads to calculation of the ordered phase volume fraction. These measurements are performed within the linear viscoelasticity limit of the sample to obtain the shear modulus independent of applied strain. It also negates development of an ordered structure (or orientation) due to applied shear.[103,118] Oscillatory shear is preferred in kinetics studies due to possible ordering of microphase separated domains under steady shear.[98] Similar to the crystallization process, the ordering in block copolymers follows sigmoidal behavior. Hence, application of the Avrami model to these systems is feasible.[53,93,96,109,116,119]

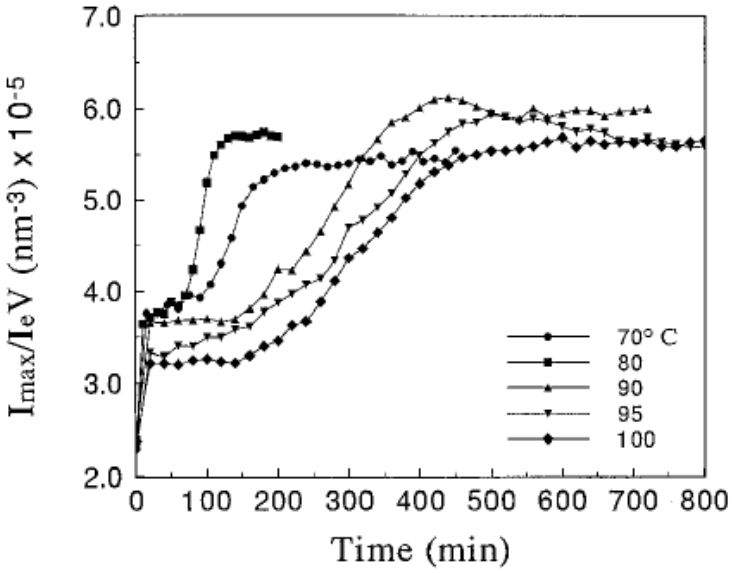

Figure 6: Absolute peak intensity of quenched SI diblock copolymer samples recorded as a function of time. Reprinted with permission from Adams, J. L.; Quiram, D. J.; Graessley, W. W.; Register, R. A.; Marchand, G. R. *Macromolecules* **1996**, *29*, 2929. Copyright 1996 American Chemical Society.

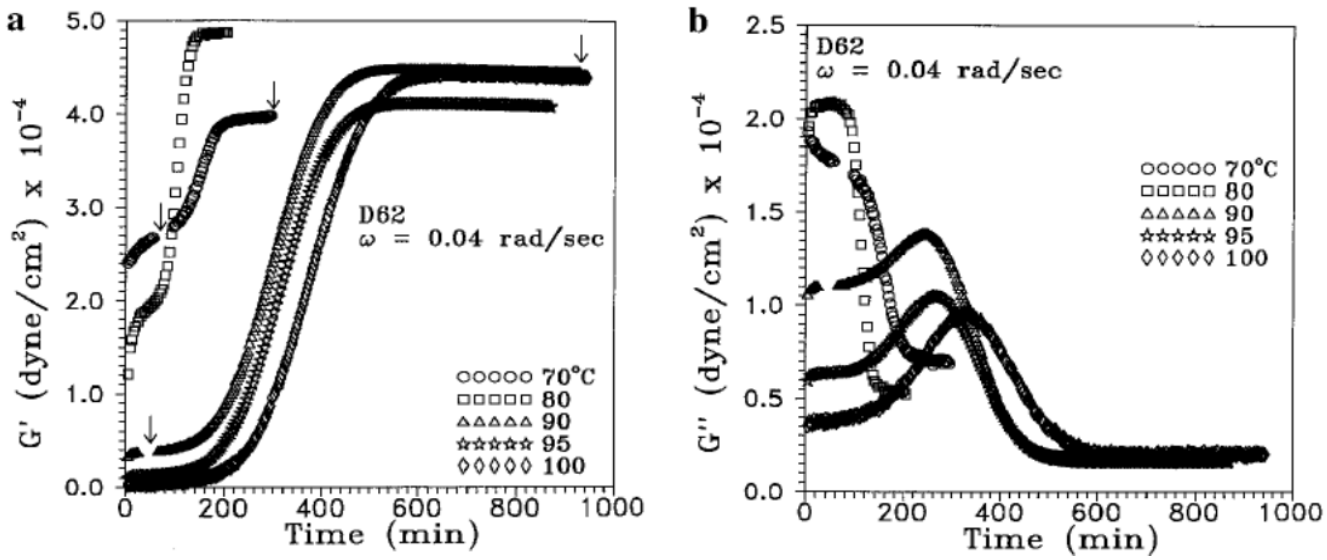

Figure 7: Storage (*G'*) and loss (*G''*) modulus of quenched SI diblock copolymer samples recorded as a function of time. Reprinted with permission from Adams, J. L.; Quiram, D. J.; Graessley, W. W.; Register, R. A.; Marchand, G. R. *Macromolecules* **1996**, *29*, 2929. Copyright 1996 American Chemical Society.

The ordering process in block copolymers occurs over several hours. The initial rise in modulus and scattering intensity is thought to be due to the incubation period, which accounts for the time taken for evolution of composition fluctuations from an undercooled disordered phase. The first step of the ordering process is microphase separation of blocks, which occurs over several minutes. The second step is the evolution of the macrolattice at longer times, which may take place over several hours, and accounts for the increase in shear modulus and scattering intensity.[64,101] The first step of local separation may not necessarily be detected by rheological analysis at certain quench depths relative to T_{ODT}.[112]

Avrami analysis of various block copolymer systems has led to observation of the Avrami exponent as being between 3 and 4.[53,109] However, Rosedale and Bates[61] have reported Avrami exponent values between 2 and 4 for different quench temperatures. Floudas et al[93] proposed that linear plots of ordering half times ($t_{1/2}$) vs inverse of quench depths (δ^{-1}) relative to T_{ODT} indicate that heterogeneous nucleation is the likely mechanism. Linear plots of $t_{1/2}$ *vs* δ^{-2} were indicative of

homogeneous nucleation. The authors concluded that for $n = 3$, heterogeneous nucleation occurs during the ordering process. It was also suggested that for $n = 4$, spinodal decomposition leads to microphase separation, however without offering a proof. Sakamoto and Hashimoto[47] on the other hand, suggested that homogeneous nucleation leads to microphase separation for Avrami exponent values between 3 and 4.

Ordering time usually decreases with increasing quench depth, since greater temperature difference leads to greater thermodynamic driving force. However, at a certain critical point, kinetic effects become predominant, and chain mobility is primarily responsible for the ordering rate. Thus, the relationship between ordering rate and quench temperature is usually parabolic in nature.[112,116] Floudas et al[120] also observed a parabolic relationship between Avrami exponents and quench temperature in SI diblock copolymers. The increase in Avrami exponent at lower temperature was assigned to shift from 'nucleation and growth' to 'spinodal decomposition' mechanism. Chastek and Lodge[115] also confirmed heterogeneous nucleation via POM analysis for cylinder forming SI solutions that showed Avrami exponents between 2.6 and 2.8.

2.4.4 Order-order kinetics

Kinetics of transformation from one type of microstructure to other has been studied extensively.[117,121-125] The time scale of these transitions varies between several seconds and few hours. These transitions result in changes in modulus and scattering peak intensity as observed in disorder-order kinetics. The Avrami exponents for cylinder-to-lamellae and cylinder-to-gyroid transition were found to be between 2 and 3, with heterogeneous nucleation being proposed as the likely mechanism.

2.4.5 Ordering in Selective Solvents

Solubilization of a block in a copolymer by the selective solvent leads to formation of micelles. Depending on the polymer concentration, the micelles can be in a disordered or ordered state as observed in several studies.[96,126,127] In disordered state, the micelles exhibit similar behavior that of a disordered liquid (no spatial order). In a symmetric ABA triblock copolymer solution, micelle formation largely depends on whether the solvent in soluble in midblock (B) or end blocks (A).[128] The end block selective solvents usually lead to formation of looped micelles, where midblock selective solvents lead to a mixture of looped and bridged micelles. Raspaud et al[129,130] performed small-angle neutron scattering studies on SIS triblock copolymer micelles formed in a midblock selective solvent, and observed cubic morphology at high polymer concentrations. Kleppinger et al[126] also observed cubic morphology for micelles of polystyrene-poly(ethylene-co-butylene)-polystyrene (SEBS) copolymer solutions in a midblock selective solvent. However, majority of the studies evaluated only the equilibrium structures, and very few studies describe the ordering kinetics in diblock[96,103,106,131,132] and triblock copolymers.

2.4.6. Modeling small angle scattering data for disordered polymer micelles

Several early studies[16,17,133,134] of block copolymers and their blends suggested the existence of disordered spheres in the bulk. Kinning and Thomas[135] successfully used the Percus – Yevick hard sphere model[136] to characterize the scattering behavior of highly asymmetric block copolymer blends. One of the key modifications of the hard sphere model came from Fournet's assumption of an impenetrable layer of other molecules surrounding the hard spheres. The fits obtained using the 'core and corona' approach provided a much better fit at lower angles for the block copolymer samples. According to this modified hard sphere model, the scattering from a

monodisperse particles can be expressed as a product of form factor *P(q)*, and structure factor *S(q)* as follows,

$$I_s = KNP(q)S(q) \quad \text{.....(9)}$$

Where, *K* is the contrast factor, and *N* is the number density of scattering entities. The form factor for a hard sphere is expressed by following equation,

$$P(q) = v_c^2 f^2(qR_c) \quad \text{.....(10)}$$

Where, $v_c = \frac{4}{3}\pi R_c^3$, hard sphere volume, and

$$f(x) = \frac{3}{x^3}(sinx - xcosx) \quad \text{.....(11)}$$

Following the Percus – Yevick model, the structure factor for hard spheres is described by the following equation,

$$S(q) = \frac{1}{1+24\varphi G(2qR_{hs})/(2qR_{hs})} \quad \text{.....(12)}$$

Where, R_{hs} is the radius of hard sphere, φ is the volume fraction of hard spheres, and

$$G(x) = \frac{\alpha}{x^2}(sinx - xcosx) + \frac{\beta}{x^3}[2xsinx + (2 - x^2)cosx - 2] + \frac{\gamma}{x^5}\{-x^4cosx + 4[(3x^2 - 6)cosx + (x^3 - 6x)sinx + 6]\} \quad \text{.....(13)}$$

The experimental data used by Kinning and Thomas[137] showed deviation from the model fit at higher scattering angles, possibly due to a diffused interface, which was not considered in the calculations. The primary scattering maximum was assigned to the formation of a microphase separated morphology. Another shoulder was observed at higher scattering angles, which was consistent with the Percus – Yevick model.[135,136] Several studies have successfully applied the

modified hard sphere model to study the scattering behavior of block copolymer micelles in solution.[62,65,127,135,138]

SAXS measurements of SEBS solutions in mineral oil have shown formation of a cubic morphology at temperatures below ODT during temperature ramp experiments.[126,139,140] However, these measurements are significantly affected by ramp rate, and cooling ramp experiments are susceptible to hysteresis and heat transfer issues in the sample cell. Hence, a better option to study the kinetics is isothermal experiments so that the ordering via nucleation and growth mechanism is possible.[88,141] The model developed by Avrami[89-91] is frequently used to study the nucleation and growth kinetics. Several studies report the ordering kinetics in diblock copolymer solutions.[96,131,142] However, the evolution of parameters such as hard sphere and core radius, has not been studied in detail. Ordering kinetics of bcc structure in SIS triblock[103] and cylindrical structure[64] have been reported, but the evolution of structural parameters has not been reported. Several potential colloidal systems have been reviewed by Pedersen[143] in order to model the structure of block copolymer micelles. Bansil et al[110,144] have modeled the scattering from bcc-ordered spheres as a sum of Gaussian functions.

$$I_b = \sum_{i=1}^{n} A_i(t)\exp[-\frac{1}{2}\left(\frac{q-q_i}{\sigma_i}\right)^2] \quad \text{..... (14)}$$

Hence, using equations (9) and (14), the total scattering intensity could be represented as the sum of scattering from micelles in liquid-like order and bcc-ordered structures.

$$I_{tot} = I_s + I_b \quad \text{..... (15)}$$

A two-step ordering process has been observed in diblock copolymer solutions, when quenched below ODT.[96,110,144] The first step represents supercooling of the liquid, and second step represents ordering of the micelles. The first step involves temperature equilibration and saturation

of concentration fluctuations, which should exhibit exponential relaxation behavior.[145] Hence, the scattering intensity during the first step can be characterized using an exponential function. The second step can be characterized by the Avrami theory.

2.5. Pressure-Sensitive Adhesives

Pressure-sensitive adhesives (PSAs) provide adhesion to the substrate when applied at low external pressure and over a short time (1-5 s). Several mechanisms including adsorption, electrostatic interaction, and diffusion have been proposed to be responsible for adhesion.[146] The phenomenon of adhesion was initially described empirically. However, several rheological studies provided a relationship between the viscoelastic properties and adhesion strength of adhesives.[147-154] To describe the adhesion, de Gennes[155] proposed a qualitative "trumpet" model (Figure 8). According to the "trumpet" model, the crack developed during the peeling experiments depends primarily on two factors – the storage modulus ratio of hard and soft components (obtained at very high and very low frequency respectively), and the relaxation time of polymer chains. The stresses developed during peeling relax along the crack. The model also demonstrated that when stresses are relaxed completely, the crack length might be on the same length scale as the adhesive thickness. The shape of the crack in weakly crosslinked polymers appeared trumpet-like.

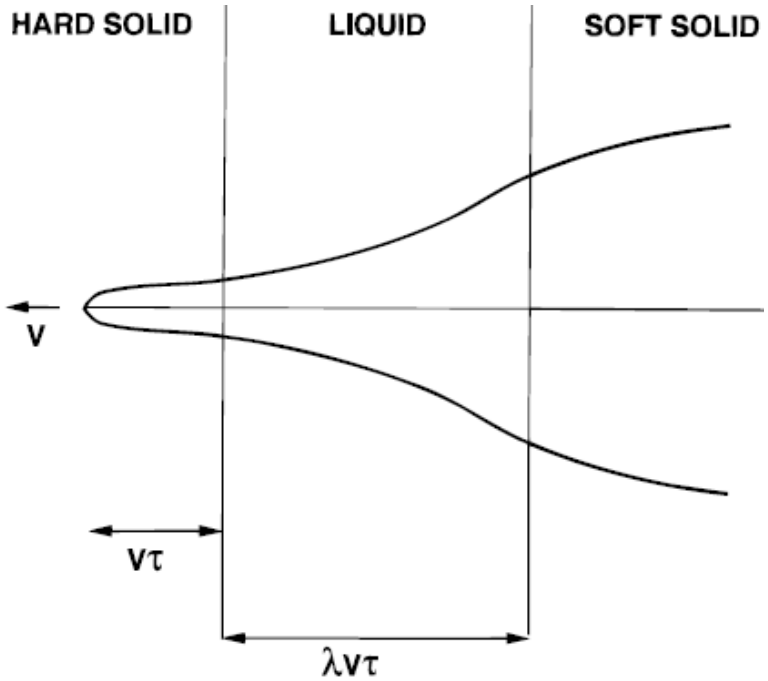

Figure 8: "Trumpet"-like fracture profile in a soft adhesive, where *V* is the fracture propagation rate, τ is the material relaxation time, and λ is the ratio of material modulus at very high frequency (μ_∞) and very low frequency (μ_0). Reprinted with permission from de Gennes, P. G. *Langmuir* **1996**, *12*, 4497. Copyright 1996 American Chemical Society.

Various techniques that characterize adhesives measure the mechanical energy necessary for adhesive failure. During these tests, PSAs undergo tensile deformation and fibril formation, and the energy contribution from deformation and fibrillation constitutes a major part of the mechanical energy necessary for adhesive failure.[156] The adhesion energy calculated by only taking into account the surface energies of adhesive and substrate thus fails to corroborate with results of tack and peel tests.[149] High tack is essential for pressure-sensitive adhesion[156], however it is not the only necessary material characteristic required in adhesives.[157,158] A good adhesive requires cohesion strength as well as flow properties to establish a good contact with the substrate. To achieve a good contact with the substrate at short times and under light pressure (1-10 Pa), the adhesive must behave as a liquid. In order to achieve good cohesive strength, the adhesive should behave as an elastic solid. Due to such requirements, PSAs contain rubber-like polymers for which the viscoelastic behavior can be carefully controlled.

Some commonly used polymers in adhesives are natural rubber, styrene-diene-styrene copolymers (SIS / SBS), silicone, ethyl-vinyl acetate copolymers, and acrylic block copolymers.[158] The wide variety in chemical structures in these polymers indicates that the adhesive behavior of a system does not necessarily come from its chemistry, but perhaps from physics. One should understand the molecular architecture of polymers and its effect on the adhesive properties, which will allow for selection of the best possible materials for a given adhesive application. This section reviews several approaches that correlated the macroscopic adhesive properties and micro- and nano-scale molecular architectures in polymers.

2.5.1. PSA debonding mechanism

The probe tack test is commonly used to characterize the adhesive performance, which imitates touching the adhesive surface with a finger and determining the force required for detachment from the substrate. Typical adhesives show four stages during the test, which are listed below.

1. Homogeneous deformation of adhesive film below the maximum in the stress-strain curve (σ_{max}).
2. Cavity formation in adhesive film around σ_{max}.
3. Sharp decrease in nominal stress accompanied by lateral growth of cavities.
4. Extension of cavities in vertical direction (fibrillation)

The fibrils can break cohesively or undergo adhesive failure by detachment from the substrate. The most important parameter obtained from this test is work of separation per unit area (W_a) i.e. the total area under the stress-strain curve multiplied by the initial thickness of the adhesive layer.

A good PSA should show a large W_a required for debonding, and it involves a significant contribution from elastic deformation and structural change in the adhesive.

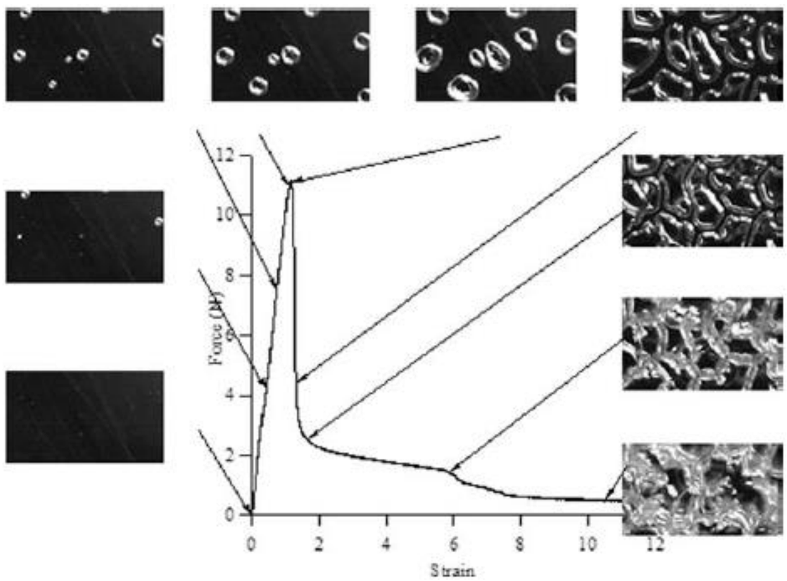

Figure 9: Force vs strain curve in a probe tack test of a poly(vinyl pyrrole) – poly(ethylene glycol) blend containing 36 wt. % PEG. Each micrograph corresponds to designated point on the force-strain curve. Reprinted with permission from Roos, A.; Creton, C.; Novikov, M. B.; Feldstein, M. M. *Journal of Polymer Science Part B: Polymer Physics* **2002**, *40*, 2395. Copyright 2002 Wiley Periodicals, Inc.

The cavitation begins in the vicinity of σ_{max}. Usually the peak stress is related to the mechanical modulus (E) of the material. The peak stress is achieved when the polymer chains begin orient themselves in the direction of applied force. Cavitation and coalescence in the adhesive lead to a sharp decrease in stress required for extension of polymer chains. The oriented polymer chains then lead to a plateau in the stress-strain plot. The final stage corresponds to fibrillation after which the adhesive fails.

The relationship between the peel force (P), and stress-strain curve is given by the following equation

$$P = kbl \int_0^{\varepsilon_b} \sigma . d\varepsilon \quad (17)$$

where b is the width and l is the thickness of adhesive layer, σ is tensile stress and ε is relative strain, ε_b is the strain at the break, and k is a dimensionless constant accounting for substrate deformation and adhesive-substrate interaction. Assuming $k = 1$ and linear viscoelasticity i.e. $\sigma = E\varepsilon$, equation (17) can be written in a form similar to Kaeble equation.[160]

$$P = \frac{bl\sigma_b^2}{4E} \quad \text{(18)}$$

Using the Maxwell model, $E = 3\eta/\tau$ the above equation can be re-written as

$$P = \frac{bl\tau\sigma_b^2}{6\eta} \quad \text{(19)}$$

Applying the Stokes – Einstein equation for Maxwell model we get

$$P = \frac{bl\pi NaD\tau\sigma_b^2}{k_bT} \quad \text{(20)}$$

where k_b is Boltzmann constant, T is temperature, N is number of segments of size a in the polymer chain, D is self-diffusion coefficient of the polymer segments. This equation does not take into account the distribution of relaxation times in polymers. Novikov et al[161] studied the response of adhesives after removal of bonding pressure, and showed two possible relaxation mode with times 10 – 70 s and 300 – 660 s respectively. These times were attributed to strain recovery modes on short and long time scales. The authors also observed that only the long-scale relaxation times changed by changing the composition of poly(vinyl pyrrole) (PVP)-based adhesives. Nevertheless, equation (20) tells us that a good adhesive should exhibit high molecular mobility (D), a long-scale chain relaxation time (τ), and high cohesive strength (σ_b). The molecular mobility of polymer is a function of its free volume described as follows.[162]

$$D = Aexp(-B/f_v) \quad \text{(21)}$$

Equations (20) and (21) suggest that a good PSA should have high cohesion strength and large free volume. However, cohesion strength in polymers is usually achieved by reducing the free volume. Thus, a balance between two competitive characteristics needs to be attained by altering molecular architecture of polymers and/or their blends. The high cohesive strength can be achieved by generating chemical or physical crosslinking. Addition of high-T_g materials (tackifiers) in the blends also improves cohesive strength of polymers. Low-T_g polymers have large free volume, and thus are widely used in PSA blends. In polyisobutylene (PIB) - based adhesives, chain entanglements of high molecular weight chains form physical crosslinks. In case of SIS-based adhesives, the microphase separated polystyrene domains act as physical crosslinks. The long isoprene chains exhibit low T_g thus increasing free volume of the adhesive. In case of acrylic-based adhesives containing carboxyl anions, the electrostatic repulsion increases the free volume.

2.5.2. Diffusion of polymer chains in PSAs

Voyutskii et al[163] developed another theory of adhesion which postulated that the adhesive polymer chains diffuse into the substrate in order to provide adhesion. The authors argued that self-diffusion coefficients for PSA polymers in the range of 10^{-9} to 10^{-14} cm^2/s should form a strong adhesive – substrate interface in the short contact times encountered during PSA application. Since the diffusion coefficient is an indicator of molecular mobility, a greater diffusion coefficient should lead to larger elongation at break as well as higher compliance. Indeed, self-diffusion coefficients on the order of 10^{-9} cm^2/s were observed in case of PVP-PEG adhesive blends assuming PVP segments diffusion.

Relaxation times also represent the mobility of polymer chains. Higher molecular mobility is associated with higher diffusion coefficients and shorter relaxation times. Since relaxation is the

material's response to external stimuli such as temperature change or mechanical stress, relaxation can be viewed as a driving force towards the equilibrium structure of the material. In the case of polymers, the long chains or their segments rearrange via several mechanisms including diffusion to attain the equilibrium structure.[164,165] The relaxation in elastomers, which form the main component of many PSAs has been well understood with respect to bonding time and adhesive strength.[166] Gunawan et al[167] showed that the relaxation in adhesives can be modeled using the theory of linear viscoelasticity. It was also shown that the memory effects in adhesives resulted in slower relaxation under cyclic load. However, the relaxation times and moduli of adhesives are different under compressive and debonding force. Thus, the experimental conditions need to be taken into account while establishing a relationship between relaxation times and adhesive strength.

The process of adhesive bonding and debonding can be expressed in three stages namely

1. Adhesive bonding with the substrate under compressive force
2. Relaxation of adhesive molecules after removal of compressive force
3. Adhesive debonding under tensile stress

Since PSAs are viscoelastic materials, the memory effect is likely to affect the adhesive strength. Also, the time of contact and applied force may also determine the strength of an adhesive joint.[168-170] Hence, it is important to understand the adhesive's response to conditions in each of the abovementioned steps. The probe tack test includes all the three steps mentioned previously, thus allowing the determination of relaxation properties and adhesive bond strength during a single experiment.

The relaxation behavior of three different classes of PSAs differs significantly. The PIB and silicone-based adhesives relax fully after removal of compressive force. However, in case of chemically or physically crosslinked materials such as SIS, a residual stress is observed.[172] However, the relaxation modulus of all adhesives could be expressed in terms of three exponents by the following equation.

$$G_t = G_{eq} + \sum_{i=1}^{n} G_i \exp(-t/\tau_i) \quad \text{..... (22)}$$

The relaxation behavior of PSAs after removal of the compressive force is considered as elastic recovery,[161] thus the material compliance and retardations times can be represented by following equation.

$$J = J_0 + \sum_{i=1}^{n} J_i (1 - e^{-t/\tau_i}) \quad \text{..... (23)}$$

where J_i and τ_i are compliance and retardation times of i^{th} element respectively. The stress relaxation curves of PSA materials could be described in terms of two elements, i.e. a shorter (τ_1) and longer (τ_2) retardation times.

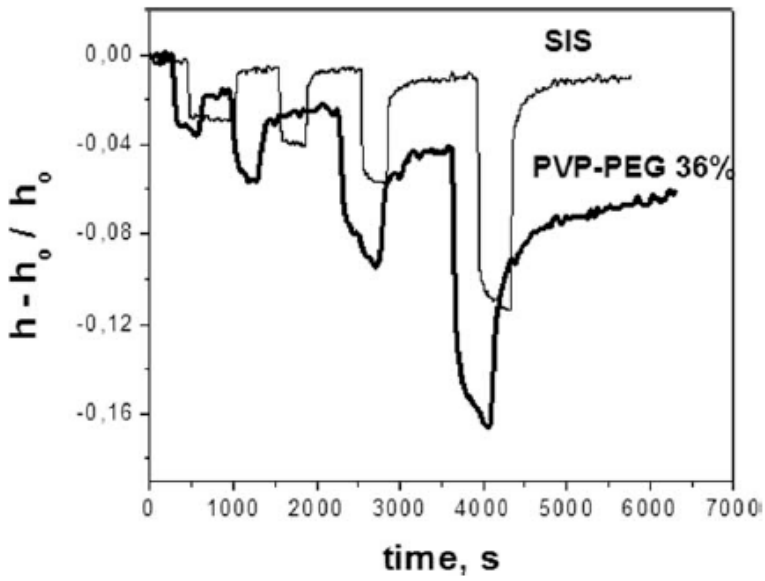

Figure 10: Squeeze-recoil profiles for SIS- and PVP-based PSAs under stepwise compressing force of 0.5, 1, 2 and 5N, respectively. Reprinted with permission from Novikov, M. B.; Borodulina, T. A.; Kotomin, S. V.; Kulichikhin, V. G.; Feldstein, M. M. *The Journal of Adhesion* **2005**, *81*, 77. Copyright 2005 Taylor and Francis.

It is evident from Figure 10 that PVP-based PSA sample is softer since it undergoes larger deformation ($h-h_0$) for a constant compressive force. Also, SIS-based adhesive shows a greater recovery upon stress relaxation indicating a greater viscous dissipation of applied force. To adjust the viscoelastic behavior of SIS-type elastomers, a low molecular weight resin (tackifier) and a plasticizer are often incorporated in PSA formulations. Addition of tackifier leads to an increase in T_g and decrease in the plateau modulus due to dilution of chain entanglements in the elastomer. Addition of a plasticizer also results in improved viscous response of the elastomer, but also causes a decrease in T_g of entangled chains. In terms of mechanical behavior, addition of tackifier and plasticizer leads to significant increase in long-scale retardation times, while shorter retardations times show little dependence.[161] The adhesive behavior at shorter time scales is dominated by elastic response, thus shorter retardation times are indicative of elastic behavior of the adhesive. The viscous behavior of a material requires a significantly longer time, thus the long-scale retardation time is indicative of the flow behavior of the adhesive.[160,162] Feldstein and Creton have

proposed that in order to be a good PSA, the material should have two relaxation times in the ranges 10-70 s and 300-660 s. Also, the corresponding relaxation moduli should be in ranges 0.70-2.20 MPa and 2.5-3.3 MPa, respectively.

2.5.3. Prediction of debonding mechanism from linear rheological studies

The debonding process in adhesives involves processes with a much more complex mechanism than simple linear rheological experiments. The debonding can take place via either interfacial failure followed by cavitation, or bulk fingering to fibrillation.[173] It is difficult to confirm what linear rheology can or cannot predict, but two criteria have been found to be important for the performance of adhesives. First is the Dahlquist criterion, which states that the elastic component of shear modulus of an adhesive should be less than 0.1 MPa at the debonding frequency, in order to achieve a good contact between the adhesive and substrate.[147] When the Dahlquist criterion is satisfied, both bulk and interfacial properties contribute to the debonding process. Two different mechanisms, namely interfacial crack growth and bulk deformation, govern the growth of defect at the interface. Interfacial crack growth depends on the critical energy release rate (G_c), and bulk deformation depends on the mechanical modulus of the material (E). The length scale of displacement during adhesive debonding within the viscoelastic framework should be compared with two length scales – size of the initial interface defect (r), and thickness of the adhesive layer (h). According to the theory predicted by Webber et al.[174], if G_c/E is smaller than r, debonding occurs via interfacial crack propagation and G_c is the limiting factor. For G_c/E values greater than h, debonding occurs primarily via bulk deformation, and fibrillar structure is observed. In the intermediate regime, both types of mechanisms can be observed,[175] while the dominant mechanism changes systematically with changing G_c/E ratio. This relationship assumes linear viscoelastic behavior of the adhesive layer, and that a very small volume around the crack

participates in the dissipation of energy. Both these assumption are not valid for soft and tacky adhesives. A correction to G_c can be written as following equation.

$$G_c = G_0\{1 + \phi(\alpha_T V)\} \quad \text{(24)}$$

Where, G_0 is crack propagation resistance at very low crack velocity, and $\phi(\alpha_T V)$ is called the dissipative factor. For elastomers and systems with weak adhesion due to van der Waal's forces, the dissipative factor is proposed as[153]

$$\phi(\alpha_T V) = k\tan\delta(\omega) \quad \text{(25)}$$

Thus, in a viscoelastic system, one can write

$$\frac{G_0}{E} \approx \frac{G_0\{1+\phi(\alpha_T V)\}}{G'(\omega)} = \frac{G_0\{1+k\tan\delta(\omega)\}}{G'(\omega)} \approx k\frac{G_0\tan\delta(\omega)}{G'(\omega)} \quad \text{(26)}$$

This approximation suggests that the ratio $\tan\delta(\omega)/G'(\omega)$ should function the same way as G_c/E within the viscoelastic framework. In probe tack tests, ω can be approximated to $2\pi V_{deb}/h_0$, where V_{deb} is probe velocity and h_0 is initial layer thickness. Thus, by performing a range of experiments at different V_{deb}, one can obtain a graph of $\tan\delta(\omega)/G'(\omega)$ vs G_0 showing a transition point between interfacial crack propagation and cavitation mechanisms of debonding. When $\tan\delta(\omega)/G'(\omega)$ values exceed a certain point, cavities are formed during the debonding process. At very large $\tan\delta(\omega)$, $G'(\omega)$ decreases and the adhesive becomes a viscous fluid, as has been observed experimentally.[176]

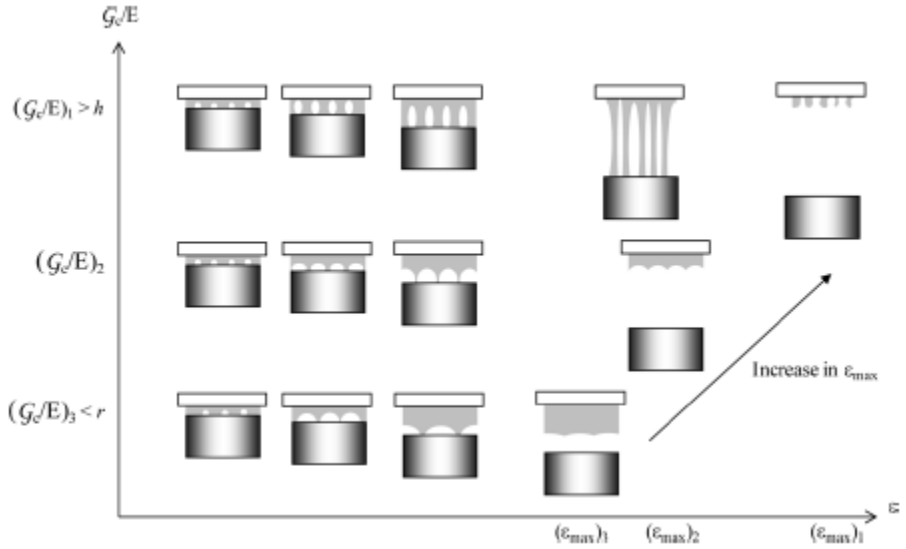

Figure 11: Adhesive behavior during a probe tack test depending on the value of G_c/E. Reprinted with permission from Deplace, F.; Carelli, C.; Mariot, S.; Retsos, H.; Chateauminois, A.; Ouzineb, K.; Creton, C. *The Journal of Adhesion* **2009**, *85*, 18. Copyright 2009 Taylor and Francis.

2.5.4. Prediction of debonding mechanisms from nonlinear rheological properties

At higher strains, the adhesive fibrils can undergo extension or detach themselves from the probe.[177] The fibril can undergo either strain hardening or cohesive failure. Such behavior can be observed in viscoelastic fluids at higher strains, when stress decreases with increasing strain. In a crosslinked network, a fraction of external work is stored in fibrils.[178] Adhesive failure is expected when either work stored in fibrils is greater than adhesion energy, or fibrillar stress is greater than surface forces. Thus, higher elongations can be achieved when fibrils can dissipate some of the external work, possibly through relaxation of polymer chains. Stress vs strain and reduced stress vs reduced strain curves are useful to study lightly entangled systems, since softening results in pronounced viscoelastic behavior of the materials under consideration.[177,179]

Non-linear behavior of PSAs can be described by Mooney stress, which is defined as,

$$\sigma_R = \frac{\sigma_N}{\lambda - {}^{1}/_{\lambda^2}} \quad \text{(27)}$$

where, σ_R is the reduced stress, σ_N is the nominal stress and λ is the extension ratio. Usually, σ_R is plotted against $1/\lambda$, to study the large strain behavior of PSAs. The absence of a minimum in Mooney-Rivlin plot is a signature for liquid-like behavior. Mooney-Rivlin model predicts the uniaxial strain by following equation

$$\sigma_N = 2(C_1 + \frac{C_2}{\lambda})(\lambda - \frac{1}{\lambda^2}) \quad \text{(28)}$$

C_1 and C_2 can be approximated to contribution from permanent and temporary crosslinks respectively.[180] Thus, low values of the ratio C_2/C_1 are result of highly crosslinked materials, while lightly crosslinked materials give higher values. $C_2/C_1 \sim 5$ was chosen to be optimum for acrylic adhesive synthesized via solution polymerization.[181] Very soft PSAs may have negative values of C_2/C_1. However, presence of a minimum in Mooney-Rivlin plot, and $C_2/C_1 > 5$ are reasonable criteria for PSAs.

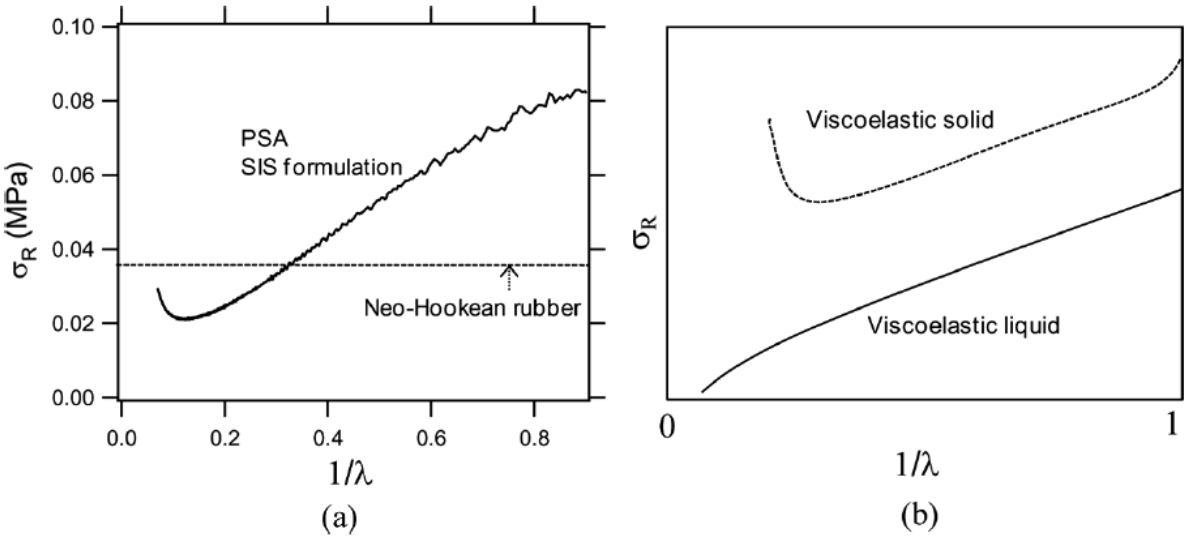

Figure 12: Mooney-Rivlin plots for (a) SIS triblock copolymer based PSA formulation and a neo-hookean rubber, (b) viscoelastic solid and viscoelastic liquid. Reprinted with permission from Deplace, F.; Carelli, C.; Mariot, S.; Retsos, H.; Chateauminois, A.; Ouzineb, K.; Creton, C. *The Journal of Adhesion* **2009**, *85*, 18. Copyright 2009 Taylor and Francis.

2.5.5. PSA behavior at large strains

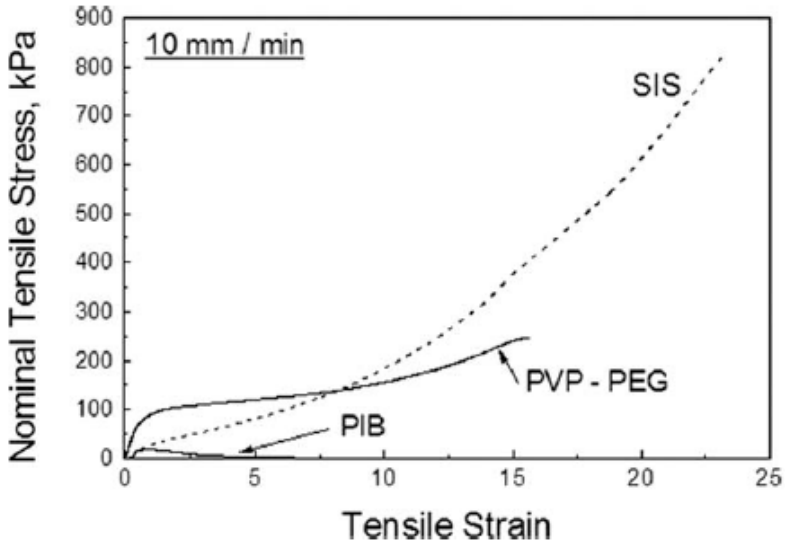

Figure 13: Stress-strain curves to break for PVP-PEG, PIB and SIS block copolymer (Duro-Tak® 34-4230) adhesives at 10 mm/min extension rate. Reprinted with permission from Novikov, M. B.; Roos, A.; Creton, C.; Feldstein, M. M. *Polymer* **2003**, *44*, 3561. Copyright 2003 Elsevier.

Based on the tensile analysis, pressure-sensitive adhesives can be classified into two categories (Figure 13). The first category consists of uncrosslinked adhesive such as PIB and acrylics. These adhesives are very soft and show very small values of ultimate tensile strength. They also show very low work of deformation and very high values of elongation at break. The uncrosslinked adhesive did not break under the experimental conditions. The second category consists of adhesives that behave like rubber networks.[173,180,183] The SIS and PVP-PEG adhesives are physically crosslinked materials and show much higher values of modulus and work of adhesion under the test conditions. Thus, the cohesive strength and elongation at break determined by such tests can be used only to compare adhesives from the same group. It is likely that the viscous and crosslinked adhesives have very different structures at large strains, hence inconclusive for a structure – property correlation.

The theory and analytical methods reviewed in this chapter attempt to provide a good understanding of the polymer physics involved in pressure-sensitive adhesives in general. It is also

apparent that a detailed kinetics study of block copolymer-based adhesives is necessary to understand the effect of various components of the adhesives on the evolution of the desired properties during melt processing. The need to understand the kinetics also requires an understanding of the phase behavior of adhesive materials, and the effect of adhesive composition on its properties at high temperatures. Thus, a systematic study of pressure-sensitive adhesive morphology under different conditions and at different compositions is envisioned to further improve our understanding of such systems.

2.6. References

(1) Haward, R. N. Y. R. J. *The Physics of glassy polymers*; Chapman & Hall: London, 1997.
(2) Leibler, L. *Macromolecules* **1980**, *13*, 1602.
(3) Gervais, M.; Gallot, B. *Die Makromolekulare Chemie* **1973**, *171*, 157.
(4) Gervais, M.; Gallot, B. *Die Makromolekulare Chemie* **1973**, *174*, 193.
(5) Inoue, T.; Soen, T.; Hashimoto, T.; Kawai, H. *Journal of Polymer Science Part A-2: Polymer Physics* **1969**, *7*, 1283.
(6) U.S.-Japan Seminar on the Polymer Solid State, G. P. H. B. E. W. Y.; M. Dekker: New York.
(7) Helfand, E. *Accounts of Chemical Research* **1975**, *8*, 295.
(8) Helfand, E.; Wasserman, Z. R. *Macromolecules* **1976**, *9*, 879.
(9) Helfand, E.; Wasserman, Z. R. *Macromolecules* **1978**, *11*, 960.
(10) Helfand, E.; Wasserman, Z. R. *Polymer Engineering & Science* **1977**, *17*, 582.
(11) Gennes, P.-G. d. *Scaling concepts in polymer physics*; Cornell University Press: Ithaca, N.Y., 1979.
(12) Helfand, E.; Wasserman, Z. *Macromolecules* **1980**, *13*, 994.
(13) Hashimoto, T.; Nagatoshi, K.; Todo, A.; Hasegawa, H.; Kawai, H. *Macromolecules* **1974**, *7*, 364.
(14) Hashimoto, T.; Todo, A.; Itoi, H.; Kawai, H. *Macromolecules* **1977**, *10*, 377.
(15) Hashimoto, T.; Shibayama, M.; Kawai, H. *Macromolecules* **1980**, *13*, 1237.
(16) Hashimoto, T.; Fujimura, M.; Kawai, H. *Macromolecules* **1980**, *13*, 1660.
(17) Bates, F. S.; Berney, C. V.; Cohen, R. E. *Macromolecules* **1983**, *16*, 1101.
(18) Bates, F. S.; Cohen, R. E.; Berney, C. V. *Macromolecules* **1982**, *15*, 589.
(19) Richards, R. W.; Thomason, J. L. *Macromolecules* **1983**, *16*, 982.
(20) Spontak, R. J.; Williams, M. C.; Agard, D. A. *Macromolecules* **1988**, *21*, 1377.
(21) Aggarwal, S. L. *Polymer* **1976**, *17*, 938.
(22) Alward, D. B.; Kinning, D. J.; Thomas, E. L.; Fetters, L. J. *Macromolecules* **1986**, *19*, 215.
(23) Kinning, D. J.; Thomas, E. L.; Alward, D. B.; Fetters, L. J.; Handlin, D. L. *Macromolecules* **1986**, *19*, 1288.
(24) Thomas, E. L.; Alward, D. B.; Kinning, D. J.; Martin, D. C.; Handlin, D. L.; Fetters, L. J. *Macromolecules* **1986**, *19*, 2197.

(25) Hasegawa, H.; Tanaka, H.; Yamasaki, K.; Hashimoto, T. *Macromolecules* **1987**, *20*, 1651.
(26) Thomas, E. L.; Anderson, D. M.; Henkee, C. S.; Hoffman, D. *Nature* **1988**, *334*, 598.
(27) Leary, D. F.; Williams, M. C. *Journal of Polymer Science Part B: Polymer Letters* **1970**, *8*, 335.
(28) Helfand, E. *Macromolecules* **1975**, *8*, 552.
(29) Semenov, A. N. *Macromolecules* **1989**, *22*, 2849.
(30) Mayes, A. M.; Olvera de la Cruz, M. *The Journal of Chemical Physics* **1989**, *91*, 7228.
(31) Fredrickson, G. H.; Leibler, L. *Macromolecules* **1989**, *22*, 1238.
(32) Olvera de la Cruz, M. *The Journal of Chemical Physics* **1989**, *90*, 1995.
(33) Hashimoto, T.; Shibayama, M.; Kawai, H. *Macromolecules* **1983**, *16*, 1093.
(34) Mori, K.; Hasegawa, H.; Hashimoto, T. *Polymer* **1985**, *17*, 799.
(35) Hashimoto, T.; Kowsaka, K.; Shibayama, M.; Kawai, H. *Macromolecules* **1986**, *19*, 754.
(36) Roe, R.-J.; Fishkis, M.; Chang, J. C. *Macromolecules* **1981**, *14*, 1091.
(37) Shibayama, M.; Hashimoto, T.; Kawai, H. *Macromolecules* **1983**, *16*, 1434.
(38) Shibayama, M.; Hashimoto, T.; Kawai, H. *Macromolecules* **1983**, *16*, 16.
(39) Kim, J.; Han, C. In *Polymer Materials*; Lee, K.-S., Kobayashi, S., Eds.; Springer Berlin Heidelberg: 2010; Vol. 231, p 77.
(40) Ijichi, Y.; Hashimoto, T.; Fetters, L. J. *Macromolecules* **1989**, *22*, 2817.
(41) Ogawa, T.; Sakamoto, N.; Hashimoto, T.; Han, C. D.; Baek, D. M. *Macromolecules* **1996**, *29*, 2113.
(42) Russell, T. P.; Hjelm, R. P.; Seeger, P. A. *Macromolecules* **1990**, *23*, 890.
(43) Sakamoto, N.; Hashimoto, T. *Macromolecules* **1995**, *28*, 6825.
(44) Sakurai, S.; Mori, K.; Okawara, A.; Kimishima, K.; Hashimoto, T. *Macromolecules* **1992**, *25*, 2679.
(45) Zha, W.; Han, C. D.; Lee, D. H.; Han, S. H.; Kim, J. K.; Kang, J. H.; Park, C. *Macromolecules* **2007**, *40*, 2109.
(46) Koga, T.; Koga, T.; Hashimoto, T. *The Journal of Chemical Physics* **1999**, *110*, 11076.
(47) Sakamoto, N.; Hashimoto, T. *Macromolecules* **1998**, *31*, 8493.
(48) Stühn, B. *Journal of Polymer Science Part B: Polymer Physics* **1992**, *30*, 1013.
(49) Adams, J. L.; Graessley, W. W.; Register, R. A. *Macromolecules* **1994**, *27*, 6026.
(50) Balsara, N. P.; Garetz, B. A.; Chang, M. Y.; Dai, H. J.; Newstein, M. C.; Goveas, J. L.; Krishnamoorti, R.; Rai, S. *Macromolecules* **1998**, *31*, 5309.
(51) Bates, F. S. *Macromolecules* **1984**, *17*, 2607.
(52) Bates, F. S.; Rosedale, J. H.; Fredrickson, G. H. *The Journal of Chemical Physics* **1990**, *92*, 6255.
(53) Floudas, G.; Hadjichristidis, N.; Iatrou, H.; Pakula, T.; Fischer, E. W. *Macromolecules* **1994**, *27*, 7735.
(54) Floudas, G.; Pispas, S.; Hadjichristidis, N.; Pakula, T.; Erukhimovich, I. *Macromolecules* **1996**, *29*, 4142.
(55) Gouinlock, E. V.; Porter, R. S. *Polymer Engineering & Science* **1977**, *17*, 535.
(56) Gehlsen, M. D.; Bates, F. S. *Macromolecules* **1993**, *26*, 4122.
(57) Modi, M. A.; Krishnamoorti, R.; Tse, M. F.; Wang, H. C. *Macromolecules* **1999**, *32*, 4088.
(58) Morrison, F. A.; Winter, H. H.; Gronski, W.; Barnes, J. D. *Macromolecules* **1990**, *23*, 4200.
(59) Patel, S. S.; Larson, R. G.; Winey, K. I.; Watanabe, H. *Macromolecules* **1995**, *28*, 4313.
(60) Phatak, A.; Macosko, C. W.; Bates, F. S.; Hahn, S. F. *Journal of Rheology (1978-present)* **2005**, *49*, 197.

(61) Rosedale, J. H.; Bates, F. S. *Macromolecules* **1990**, *23*, 2329.
(62) Wang, X.; Dormidontova, E. E.; Lodge, T. P. *Macromolecules* **2002**, *35*, 9687.
(63) Winey, K. I.; Gobran, D. A.; Xu, Z.; Fetters, L. J.; Thomas, E. L. *Macromolecules* **1994**, *27*, 2392.
(64) Winter, H. H.; Scott, D. B.; Gronski, W.; Okamoto, S.; Hashimoto, T. *Macromolecules* **1993**, *26*, 7236.
(65) Yurekli, K.; Krishnamoorti, R. *Macromolecules* **2002**, *35*, 4075.
(66) Han, C. D.; Baek, D. M.; Kim, J. K. *Macromolecules* **1990**, *23*, 561.
(67) Han, C. D.; Kim, J.; Kim, J. K. *Macromolecules* **1989**, *22*, 383.
(68) Han, C. D.; Baek, D. M.; Kim, J. K.; Ogawa, T.; Sakamoto, N.; Hashimoto, T. *Macromolecules* **1995**, *28*, 5043.
(69) Balsara, N. P.; Perahia, D.; Safinya, C. R.; Tirrell, M.; Lodge, T. P. *Macromolecules* **1992**, *25*, 3896.
(70) Ryu, C. Y.; Lodge, T. P. *Macromolecules* **1999**, *32*, 7190.
(71) Kasten, H.; Stuehn, B. *Macromolecules* **1995**, *28*, 4777.
(72) Stühn, B.; Mutter, R.; Albrecht, T. *EPL (Europhysics Letters)* **1992**, *18*, 427.
(73) Voronov, V. P.; Buleiko, V. M.; Podneks, V. E.; Hamley, I. W.; Fairclough, J. P. A.; Ryan, A. J.; Mai, S. M.; Liao, B. X.; Booth, C. *Macromolecules* **1997**, *30*, 6674.
(74) Ryu, D. Y.; Lee, D. J.; Kim, J. K.; Lavery, K. A.; Russell, T. P.; Han, Y. S.; Seong, B. S.; Lee, C. H.; Thiyagarajan, P. *Physical Review Letters* **2003**, *90*, 235501.
(75) Choi, S.; Vaidya, N. Y.; Han, C. D.; Sota, N.; Hashimoto, T. *Macromolecules* **2003**, *36*, 7707.
(76) Sakamoto, N.; Hashimoto, T.; Han, C. D.; Kim, D.; Vaidya, N. Y. *Macromolecules* **1997**, *30*, 1621.
(77) Han, C. D.; Vaidya, N. Y.; Kim, D.; Shin, G.; Yamaguchi, D.; Hashimoto, T. *Macromolecules* **2000**, *33*, 3767.
(78) Kim, J. K.; Lee, H. H.; Sakurai, S.; Aida, S.; Masamoto, J.; Nomura, S.; Kitagawa, Y.; Suda, Y. *Macromolecules* **1999**, *32*, 6707.
(79) Sakamoto, N.; Hashimoto, T. *Macromolecules* **1998**, *31*, 3292.
(80) Abuzaina, F. M.; Patel, A. J.; Mochrie, S.; Narayanan, S.; Sandy, A.; Garetz, B. A.; Balsara, N. P. *Macromolecules* **2005**, *38*, 7090.
(81) Han, C. D.; Jhon, M. S. *Journal of Applied Polymer Science* **1986**, *32*, 3809.
(82) Dae Han, C.; Kim, J. K. *Polymer* **1993**, *34*, 2533.
(83) Dormidontova, E. E.; Lodge, T. P. *Macromolecules* **2001**, *34*, 9143.
(84) Matsen, M. W. *Journal of Physics: Condensed Matter* **2002**, *14*, R21.
(85) Wang, J.; Wang, Z.-G.; Yang, Y. *Macromolecules* **2005**, *38*, 1979.
(86) Chaikin, P. M. L. T. C. *Principles of condensed matter physics*; Cambridge University Press: Cambridge; New York, NY, USA, 1995.
(87) Mandelkern, L. *Crystallization of polymers*; Cambridge University Press: Cambridge, UK; New York, 2002.
(88) Fredrickson, G. H.; Binder, K. *The Journal of Chemical Physics* **1989**, *91*, 7265.
(89) Avrami, M. *The Journal of Chemical Physics* **1939**, *7*, 1103.
(90) Avrami, M. *The Journal of Chemical Physics* **1940**, *8*, 212.
(91) Avrami, M. *The Journal of Chemical Physics* **1941**, *9*, 177.
(92) Young, R. J. L. P. A. *Introduction to polymers*; Chapman & Hall: London; New York, 1991.

(93) Floudas, G.; Fytas, G.; Hadjichristidis, N.; Pitsikalis, M. *Macromolecules* **1995**, *28*, 2359.
(94) Jones, R. A. L. *Soft condensed matter*; Oxford University Press: Oxford; New York, 2002.
(95) Hashimoto, T.; Shibayama, M.; Kawai, H.; Watanabe, H.; Kotaka, T. *Macromolecules* **1983**, *16*, 361.
(96) Harkless, C. R.; Singh, M. A.; Nagler, S. E.; Stephenson, G. B.; Jordan-Sweet, J. L. *Physical Review Letters* **1990**, *64*, 2285.
(97) Amundson, K.; Helfand, E.; Patel, S. S.; Quan, X.; Smith, S. D. *Macromolecules* **1992**, *25*, 1935.
(98) Balsara, N. P.; Garetz, B. A.; Dai, H. J. *Macromolecules* **1992**, *25*, 6072.
(99) Garetz, B. A.; Newstein, M. C.; Dai, H. J.; Jonnalagadda, S. V.; Balsara, N. P. *Macromolecules* **1993**, *26*, 3151.
(100) Jian, T.; Anastasiadis, S. H.; Fytas, G.; Adachi, K.; Kotaka, T. *Macromolecules* **1993**, *26*, 4706.
(101) Schuler, M.; Stuehn, B. *Macromolecules* **1993**, *26*, 112.
(102) Stuehn, B.; Vilesov, A.; Zachmann, H. G. *Macromolecules* **1994**, *27*, 3560.
(103) Adams, J. L.; Quiram, D. J.; Graessley, W. W.; Register, R. A.; Marchand, G. R. *Macromolecules* **1996**, *29*, 2929.
(104) Balsara, N. P.; Dai, H. J.; Watanabe, H.; Sato, T.; Osaki, K. *Macromolecules* **1996**, *29*, 3507.
(105) Balsara, N. P.; Dai, H. J. *The Journal of Chemical Physics* **1996**, *105*, 2942.
(106) Hashimoto, T.; Sakamoto, N.; Koga, T. *Physical Review E* **1996**, *54*, 5832.
(107) Soenen, H.; Berghmans, H.; Winter, H. H.; Overbergh, N. *Polymer* **1997**, *38*, 5653.
(108) Soenen, H.; Liskova, A.; Reynders, K.; Berghmans, H.; Winter, H. H.; Overbergh, N. *Polymer* **1997**, *38*, 5661.
(109) Hashimoto, T.; Ogawa, T.; Sakamoto, N.; Ichimiya, M.; Kim, J. K.; Han, C. D. *Polymer* **1998**, *39*, 1573.
(110) Nie, H.; Bansil, R.; Ludwig, K.; Steinhart, M.; Koňák, Č.; Bang, J. *Macromolecules* **2003**, *36*, 8097.
(111) Chastek, T. Q.; Lodge, T. P. *Macromolecules* **2003**, *36*, 7672.
(112) Liu, Z.; Shaw, M.; Hsiao, B. S. *Macromolecules* **2004**, *37*, 9880.
(113) Chastek, T. Q.; Lodge, T. P. *Journal of Polymer Science Part B: Polymer Physics* **2005**, *43*, 405.
(114) Yufa, N. A.; Li, J.; Sibener, S. J. *Macromolecules* **2009**, *42*, 2667.
(115) Chastek, T. Q.; Lodge, T. P. *Macromolecules* **2004**, *37*, 4891.
(116) Patel, A. J.; Mochrie, S.; Narayanan, S.; Sandy, A.; Watanabe, H.; Balsara, N. P. *Macromolecules* **2010**, *43*, 1515.
(117) Park, M. J.; Bang, J.; Harada, T.; Char, K.; Lodge, T. P. *Macromolecules* **2004**, *37*, 9064.
(118) Daniel, C.; Hamley, I. W.; Wilhelm, M.; Mingvanish, W. *Rheol. Acta* **2001**, *40*, 39.
(119) Schwab, M.; Stühn, B. *Journal of Molecular Structure* **1996**, *383*, 57.
(120) Floudas, G.; Pakula, T.; Fischer, E. W.; Hadjichristidis, N.; Pispas, S. *Acta Polymerica* **1994**, *45*, 176.
(121) Matsen, M. W. *Physical Review Letters* **1998**, *80*, 4470.
(122) Floudas, G.; Ulrich, R.; Wiesner, U. *Journal of Chemical Physics* **1999**, *110*, 652.
(123) Floudas, G.; Ulrich, R.; Wiesner, U.; Chu, B. *EPL (Europhysics Letters)* **2000**, *50*, 182.
(124) Wang, C.-Y.; Lodge, T. P. *Macromolecular Rapid Communications* **2002**, *23*, 49.
(125) Bang, J.; Lodge, T. P. *The Journal of Physical Chemistry B* **2003**, *107*, 12071.

(126) Kleppinger, R.; Reynders, K.; Mischenko, N.; Overbergh, N.; Koch, M. H. J.; Mortensen, K.; Reynaers, H. *Macromolecules* **1997**, *30*, 7008.
(127) Mortensen, K.; Pedersen, J. S. *Macromolecules* **1993**, *26*, 805.
(128) Balsara, N. P.; Tirrell, M.; Lodge, T. P. *Macromolecules* **1991**, *24*, 1975.
(129) Raspaud, E.; Lairez, D.; Adam, M.; Carton, J. P. *Macromolecules* **1994**, *27*, 2956.
(130) Raspaud, E.; Lairez, D.; Adam, M.; Carton, J.-P. *Macromolecules* **1996**, *29*, 1269.
(131) Singh, M. A.; Harkless, C. R.; Nagler, S. E.; Shannon, R. F.; Ghosh, S. S. *Physical Review B* **1993**, *47*, 8425.
(132) Hashimoto, T.; Sakamoto, N. *Macromolecules* **1995**, *28*, 4779.
(133) Inoue, T.; Moritani, M.; Hashimoto, T.; Kawai, H. *Macromolecules* **1971**, *4*, 500.
(134) Richards, R. W.; Thomason, J. L. *Polymer* **1981**, *22*, 581.
(135) Kinning, D. J.; Thomas, E. L. *Macromolecules* **1984**, *17*, 1712.
(136) Percus, J. K.; Yevick, G. J. *Physical Review* **1958**, *110*, 1.
(137) Berney, C. V.; Cohen, R. E.; Bates, F. S. *Polymer* **1982**, *23*, 1222.
(138) Schwab, M.; Stühn, B. *Physical Review Letters* **1996**, *76*, 924.
(139) Kleppinger, R.; van Es, M.; Mischenko, N.; Koch, M. H. J.; Reynaers, H. *Macromolecules* **1998**, *31*, 5805.
(140) Reynders, K.; Mischenko, N.; Kleppinger, R.; Reynaers, H.; Koch, M. H. J.; Mortensen, K. *Journal of Applied Crystallography* **1997**, *30*, 684.
(141) Binder, K. *Physica A: Statistical Mechanics and its Applications* **1995**, *213*, 118.
(142) Gupta, J. A.; Singh, M. A.; Salomons, G. J.; Foran, W. A.; Capel, M. S. *Macromolecules* **1998**, *31*, 3109.
(143) Pedersen, J. S. *Adv. Colloid Interface Sci.* **1997**, *70*, 171.
(144) Bansil, R.; Nie, H.; Li, Y.; Liao, G.; Ludwig, K.; Steinhart, M.; Koňák, Č.; Lal, J. *Macromolecular Symposia* **2002**, *190*, 161.
(145) Sato, T.; Han, C. C. *The Journal of Chemical Physics* **1988**, *88*, 2057.
(146) Kinloch, A. J. *Adhesion and adhesives : science and technology*; Chapman and Hall: London; New York, 1987.
(147) Patrick, R. L. *Treatise on adhesion and adhesives*; M. Dekker: New York, 1966.
(148) Gent, A. N.; Petrich, R. P. *Proceedings of the Royal Society of London. A. Mathematical and Physical Sciences* **1969**, *310*, 433.
(149) Gent, A. N.; Schultz, J. *The Journal of Adhesion* **1972**, *3*, 281.
(150) Derail, C.; Allal, A.; Marin, G.; Tordjeman, P. *The Journal of Adhesion* **1997**, *61*, 123.
(151) Derail, C.; Allal, A.; Marin, G.; Tordjeman, P. *The Journal of Adhesion* **1998**, *68*, 203.
(152) Gower, M. D.; Shanks, R. A. *Macromolecular Chemistry and Physics* **2004**, *205*, 2139.
(153) Maugis, D.; Barquins, M. *Journal of Physics D: Applied Physics* **1978**, *11*, 1989.
(154) Gdalin, B. E.; Bermesheva, E. V.; Shandryuk, G. A.; Feldstein, M. M. *The Journal of Adhesion* **2011**, *87*, 111.
(155) de Gennes, P. G. *Langmuir* **1996**, *12*, 4497.
(156) Benedek, I. *Pressure-sensitive design*; VSP: Leiden, 2006.
(157) Benedek, I. *Developments in pressure-sensitive products*; Taylor & Francis: Boca Raton, FL, 2006.
(158) Creton, C. *MRS Bulletin* **2003**, *28*, 434.
(159) Roos, A.; Creton, C.; Novikov, M. B.; Feldstein, M. M. *Journal of Polymer Science Part B: Polymer Physics* **2002**, *40*, 2395.

(160) Satas, D. *Handbook of pressure sensitive adhesive technology*; Satas & Associates: Warwick, RI, 1999.
(161) Novikov, M. B.; Borodulina, T. A.; Kotomin, S. V.; Kulichikhin, V. G.; Feldstein, M. M. *The Journal of Adhesion* **2005**, *81*, 77.
(162) Feldstein, M. M.; Siegel, R. A. *Journal of Polymer Science Part B: Polymer Physics* **2012**, *50*, 739.
(163) Voyutskii, S. S. *Autoadhesion and Adhesion of High Polymers*; Wiley Interscience: New York, 1963.
(164) Doi, M. E. S. F. *The theory of polymer dynamics*; Clarendon Press ; Oxford University Press: Oxford [Oxfordshire]; New York, 1987.
(165) Liao, Q.; Carrillo, J.-M. Y.; Dobrynin, A. V.; Rubinstein, M. *Macromolecules* **2007**, *40*, 7671.
(166) Creton, C.; Leibler, L. *Journal of Polymer Science Part B: Polymer Physics* **1996**, *34*, 545.
(167) Gunawan, M.; Wong, E. H.; Mhaisalkar, S. G.; Davila, L. T.; Hong, Y.; Caers, J. F. J. M.; Tsai, T. K. *Journal of Elec Materi* **2004**, *33*, 1041.
(168) Zosel, A. *International Journal of Adhesion and Adhesives* **1998**, *18*, 265.
(169) Zosel, A. *Journal of Adhesion Science and Technology* **1997**, *11*, 1447.
(170) *Advances in pressure sensitive adhesive technology*. **1992**.
(171) In *Fundamentals of Pressure Sensitivity*; Benedek, I. F., M;, Ed.; CRC-Taylor and Francis: Boca Raton, FL, 2009.
(172) Feldstein, M. M.; Kulichikhin, V. G.; Kotomin, S. V.; Borodulina, T. A.; Novikov, M. B.; Roos, A.; Creton, C. *Journal of Applied Polymer Science* **2006**, *100*, 522.
(173) Shull, K. R.; Creton, C. *Journal of Polymer Science Part B: Polymer Physics* **2004**, *42*, 4023.
(174) Webber, R. E.; Shull, K. R.; Roos, A.; Creton, C. *Physical Review E* **2003**, *68*, 021805.
(175) Nase, J.; Lindner, A.; Creton, C. *Physical Review Letters* **2008**, *101*, 074503.
(176) Deplace, F.; Carelli, C.; Mariot, S.; Retsos, H.; Chateauminois, A.; Ouzineb, K.; Creton, C. *The Journal of Adhesion* **2009**, *85*, 18.
(177) Glassmaker, N. J.; Hui, C. Y.; Yamaguchi, T.; Creton, C. *Eur. Phys. J. E* **2008**, *25*, 253.
(178) Possart, W. E. C. o. A. *Adhesion : current research and applications*; Wiley-VCH ; John Wiley distributor]: Weinheim; Chichester, 2005.
(179) Verdier, C.; Piau, J. M. *Journal of Polymer Science Part B: Polymer Physics* **2003**, *41*, 3139.
(180) Roos, A.; Creton, C. *Macromolecules* **2005**, *38*, 7807.
(181) Lindner, A.; Lestriez, B.; Mariot, S.; Creton, C.; Maevis, T.; Lühmann, B.; Brummer, R. *The Journal of Adhesion* **2006**, *82*, 267.
(182) Novikov, M. B.; Roos, A.; Creton, C.; Feldstein, M. M. *Polymer* **2003**, *44*, 3561.
(183) Rohn, C. L. *Analytical polymer rheology : structure-processing-property relationships*; Hanser ; Hanser/Gardner: Munich; New York; Cincinnati, 1995.

Chapter 3

Isothermal Microphase Separation Kinetics in Asymmetric Styrene – Isoprene Block Copolymers

Isothermal Microphase Separation Kinetics in Asymmetric Styrene – Isoprene Block Copolymers

Ninad Dixit[†], *Alicia Pape*[‡], *Lixia Rong*[‖§], *Eugene Joseph*[‡], *and Stephen M. Martin*[‡*]

[†]Department of Chemistry, Virginia Polytechnic Institute and State University, Blacksburg, Virginia 24061, United States

[‡]Department of Chemical Engineering, Virginia Polytechnic Institute and State University, Blacksburg, Virginia 24061, United States

[‖]Louisiana State University, Baton Rouge, Louisiana 70806, United States

3.1. Abstract

The microphase separation behavior of Kraton® D1161, a highly asymmetric styrene-isoprene triblock and diblock copolymer mixture often used as the base polymer in pressure-sensitive adhesives, was studied using time resolved small-angle X-ray scattering (SAXS) and oscillatory rheological analysis during temperature ramp and temperature quench experiments. The total scattering intensity obtained from SAXS was represented as a sum of the scattering from disordered and ordered polystyrene domains. A modified Percus – Yevick hard sphere model was used to describe the scattering from disordered spheres, while Gaussian functions were used to model scattering from ordered domains. The temperature and time dependent SAXS experiments suggest a sequence of 4 stages in the development of the copolymer morphology during the isothermal phase separation kinetics experiments. Avrami analysis of the shear modulus evolution following a temperature quench indicates that domain growth is preceded by nucleation process. The ordering polystyrene domains as observed during rheological and SAXS analysis is dominated by polymer chain mobility, which resulted in slower kinetics at lower temperatures.

3.2. Introduction

Block copolymers are commonly used as the base component of pressure-sensitive adhesive (PSA) formulations.[1] The most common applications of PSAs include tapes and labels, but they are also used in a variety of other areas[2,3] such as transdermal delivery systems.[4] One of the most commonly used systems is a mixture of SIS (styrene-isoprene-styrene) and SI (styrene-isoprene) block copolymers. These copolymers contain 15-25 % polystyrene (PS) and are blended with a high glass transition temperature (T_g), low molecular weight aliphatic resin known as a tackifier. At room temperature, the adhesive blend consists of PS spheres dispersed in a polyisoprene (PI)-rich matrix. The PS spheres act as physical crosslinks and fillers at service temperature, and the blend behaves as an elastomer.[5,6] The tackifier is selectively soluble in the PI-rich matrix, which leads to an increase in the T_g of the PI-rich phase and a decrease in the storage modulus of the blend at temperatures above T_g of PI-rich phase, as observed in oscillatory rheological analysis.[7] The microphase separation in the base block copolymer contributes to the mechanical and adhesive properties of the blend. Despite the strong relationship between morphology and adhesive properties, the microphase separation kinetics in adhesives and their base polymers have not been studied extensively. Herein we report on a combined small-angle X-ray scattering (SAXS) and rheological study aimed at understanding the microphase separation kinetics from the melt of a mixture of SIS and SI copolymers commonly used as the base component in commercially available adhesive formulations.

The morphology of ABA triblock copolymers is distinctly different from AB diblock copolymers due to the potential for tethering of both ends of the polymer. The two end-blocks can insert into the same or neighboring microdomains, giving rise to either looped or bridged morphologies. Bridging of polymer chains between microdomains leads to the formation physical

crosslinks (aggregates of end blocks) that enhance the mechanical properties of the ABA triblock compared to similar AB diblock copolymers. The blending of an AB diblock with an ABA triblock results in a net decrease in the number of physical crosslinks for two reasons: B-chains of the AB diblock are favored to be part of the B-rich phase in the blend; and long B-chains of the AB diblock force the B-chains from the ABA triblock away from the center of the interdomain region. Both factors hamper the process of midblock bridging. SAXS analysis of SIS/SI blends has shown an increase in the average spacing between PS domains with increasing SI fraction, supporting this argument.[8] This behavior is also similar to that of copolymer/homopolymer blends.[9]

The addition of AB diblock, and subsequent decrease in bridging, leads to a decrease in the storage modulus (*E'*) of the ABA triblock blend. The effect of diblock content on *E'* becomes less pronounced above 20% diblock content by weight.[8] Even though the number of free ends of B-chains increase with increasing diblock content, at high enough concentrations it is possible for the chains to form entanglements resulting in a smaller decrease in *E'*. Lovisi et al.[10] also reported a decrease in the elastic response of a styrene-butadiene-styrene (SBS) copolymer containing various amounts of uncoupled butadiene chains. The hardness and abrasion resistance also decreased as a result of styrene-butadiene (SB) diblock copolymer addition. At the same time, there was an increase in the viscous character of the blends and thus an improved melt flow rate. Improved melt processibility is a critical factor in the formulation of hot-melt pressure sensitive adhesives (HMPSAs). HMPSAs are coated on substrates in the melt state, and then cooled to a lower temperature for cutting and further processing.[11] Thus, the melt phase behavior of adhesives during processing can significantly affect the performance properties of HMPSAs. Melt processed adhesives are friendlier to the environment due to the lack of solvent or water use during processing. Although the rheological behavior, mechanical properties, and adhesive properties of

adhesive formulations have been reported in the past, little attention has been paid to their melt behavior – particularly in the case of block copolymer based HMPSAs.

Hashimoto et al[12] reported one of the earliest studies of ordering kinetics in block copolymers, and their methods have been followed by many researchers.[13-22] These studies involved quenching block copolymer samples from a disordered state to a metastable state. The ordering of block copolymer domains, a process that can take several hours, is observed using various techniques including SAXS and oscillatory rheology. A rise in the scattering intensity and shear modulus observed during the initial stages of the experiment is thought to be due to an incubation period, which accounts for the time taken for the growth of composition fluctuations from an undercooled disordered phase. The first step of the ordering process is a microphase separation of blocks, which occurs over several minutes. The second step is the evolution of a macrolattice at longer times, which may take place over several hours and accounts for the major increase in modulus and scattering intensity.[15,23] The ordering in block copolymers is observed to follow a sigmoidal trend, similar to that observed during the crystallization process. As a result, the Avrami model for crystallization kinetics has commonly been applied to these systems.[13,24,25]

3.3. Experimental

3.3.1. Materials and Sample Preparation. Commercially available PSA base component Kraton® D1161 (Kraton Polymers LLC), and antioxidant Irganox® 1010 (BASF SE) were used in this study. Kraton® D1161 is a mixture of SIS and SI block copolymers with 18 % SI content, and 15 % styrene content. Molecular weights of both blocks were obtained through Gel Permeation Chromatography (GPC) analysis using chloroform solvent and a polystyrene standard. The molecular weights and polydispersity of each block are given in Table 1.

Table 1. Molecular weight analysis of Kraton® D1161 by GPC equipped with refractive index detector

	M_n (kDa)	M_w (kDa)	PDI
SIS	144.3	146.5	1.015
SI	79.1	79.9	1.011

Solvent grade toluene was purchased from Sigma-Aldrich. 20 % (w/w) solutions were prepared by dissolving appropriate amounts of material in toluene, and pouring into casting blocks. The solutions were dried at room temperature for two weeks followed by vacuum drying at room temperature for two days. All dried samples were approximately 2 mm thick and contained 1 wt.% antioxidant.

3.3.2. Small-Angle X-ray Scattering (SAXS). SAXS measurements were performed on beamline X27C at the National Synchrotron Light Source (NSLS) at Brookhaven National Laboratory. The X-ray wavelength was 1.371 Å. SAXS data were acquired using a MAR-CCD detector. The acquisition time for each frame was 14 s. Silver Behenate standard was used to calibrate the scattering angle. The sample to detector distance was 1800 mm. The beamline was equipped with a heating/cooling stage capable of rapid quenches (HCS600V, Instec Inc.) Kapton tape was used to seal the samples in order to limit flow and deformation at higher temperatures. The samples were then sandwiched between two brass plates to ensure good heat transfer. All scattering signals were corrected for beam fluctuations and background scattering, before being subjected to further analysis.

3.3.3. Oscillatory Rheology. Rheological experiments were performed on a TA Instruments AR-G2 rheometer, equipped with 25 mm diameter steel plates. Nitrogen (N_2) gas was constantly circulated in the sealed furnace to maintain a neutral environment. Fast cooling during quench-isothermal experiments was achieved by using a liquid N_2 cooling system. At the beginning of each experiment, a thickness of 1000 μm was achieved by pressing the samples between the steel plates at 120 °C. In the case of temperature ramp experiments, the sample was pressed between the rheometer plates at 120 °C to achieve the desired thickness and establish good contact between the sample and plates. The temperature was then rapidly brought down to and equilibrated at 80 °C before subjecting it to temperature ramp. A strain of 0.5 % was used for temperature ramp and isothermal experiments. The strain value was confirmed to be within the linear viscoelastic regime at the lowest temperatures involved in the analysis. An oscillation frequency of 0.01 Hz was used during quench experiments to track the growth of microphase separated domains.

3.4. Modified Percus – Yevick Hard Sphere Model

SAXS profiles obtained during the temperature ramp and isothermal kinetics experiments show a broad primary maximum, which is an indication of a broad distribution of distances between PS domains. Moreover, many profiles also show two distinct maxima at smaller values of scattering vector (q) or scattering angle. These features can be seen in the example scattering profile shown in Figure 1 (arrows show positions of the two maxima). The PS chains can form only spherical microstructures due to the asymmetric composition of the copolymers.[26] Hence, we concluded that the two maxima correspond to PS spheres in a liquid-like disordered phase and PS spheres in a bcc-ordered structure.

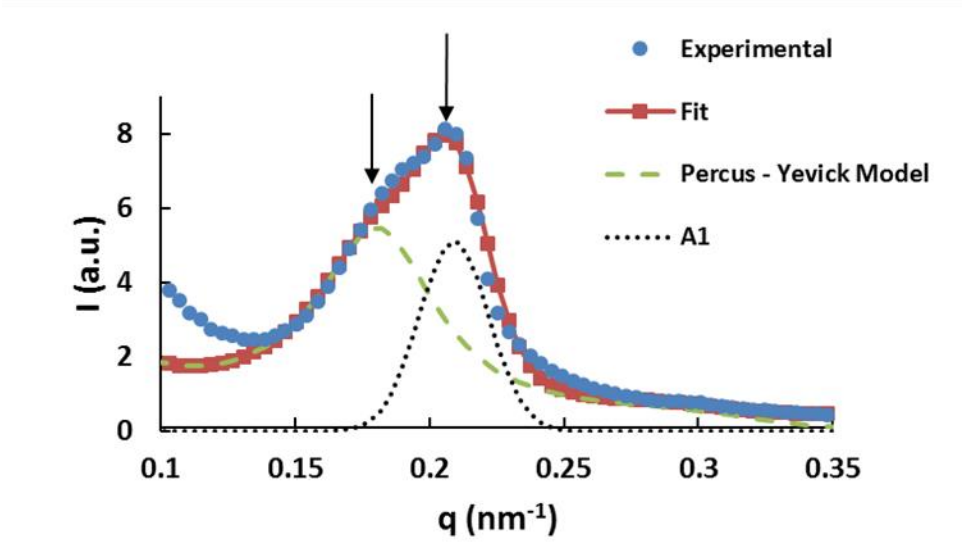

Figure 1. Experimental and modeled SAXS profiles of Kraton® D1161. The sample was quenched from 240 °C to 160 °C and held isothermal for 90 minutes. Arrows indicate the positions of the two maxima in the scattering profile. 'A1' corresponds to amplitude of the first Gaussian function that represents bcc-ordered polystyrene domains

Our assumption is further supported by the observation of two maxima, one at q_1 ~ 0.21 nm^{-1}, and the second at q_2 ~ 0.3 nm^{-1}. These relative positions are consistent with the scattering reflections from a bcc structure. The total scattering intensity is expressed as a sum of scattering from the liquid-like disordered domains and from the bcc-ordered domains. Scattering intensity from disordered monodisperse particles can be expressed using a modified Percus-Yevick hard sphere model[27,28] as follows,

$$I_s = KNP(q)S(q) \quad \text{(1)}$$

Where, K is the contrast factor, and N is the number density of scattering entities. The form factor for a PS sphere of radius (R_c) is expressed by the following equation,

$$P(q) = v_c^2 f^2(qR_c) \quad \text{(2)}$$

Where, $v_c = \frac{4}{3}\pi R_c^3$, is the PS sphere volume, and

$$f(x) = \frac{3}{x^3}(sinx - xcosx) \text{…….....} (3)$$

The structure factor for hard spheres comprised of PS spheres and a corona of PI chains can be described by following equation,

$$S(q) = \frac{1}{1+24\phi G(2qR_{hs})/(2qR_{hs})} \text{…..……..……} (4)$$

Where, R_{hs} is the radius of hard sphere, ϕ is the volume fraction of hard spheres, and

$$G(x) = \frac{\alpha}{x^2}(sinx - xcosx) + \frac{\beta}{x^3}[2xsinx + (2 - x^2)cosx - 2] + \frac{\gamma}{x^5}[-x^4cosx + 4\{(3x^2 - 6)cosx + (x^3 - 6x)sinx + 6\}] \text{……..……..…..…….. } (5)$$

Scattering from bcc-ordered spheres can be described as a sum of Gaussian functions.[13]

$$I_b = \sum_{i=1}^{n} A_i(t)\exp[-\frac{1}{2}\left(\frac{q-q_i}{\sigma_i}\right)^2] \text{…..……..…..} (6)$$

The total intensity (I_{tot}) can then be given as a sum of scattering from micelles in liquid-like order (I_s) and bcc-ordered structures (I_b).

$$I_{tot} = I_s + I_b \text{…….……..……} (7)$$

In order to fit the scattering profiles, a q range of 0.13 – 0.4 nm^{-1} was considered, which encompasses the primary maxima and the secondary maximum. For the purpose of this analysis, the intensity of the first Gaussian peak (i=1) has been considered and tracked as a function of either temperature or time. In several cases, a small tertiary peak is also observed, but not taken into consideration since it has minimal impact on the fitting procedure. At higher q, the hard sphere approximation does not fit well with the data, where the calculated structure factor reaches a sharp minimum. The experimentally observed broad minimum is an indication of a broad interface

between the polystyrene domains and the polyisoprene matrix, which the model does not take into account.

3.5. Results and Discussion

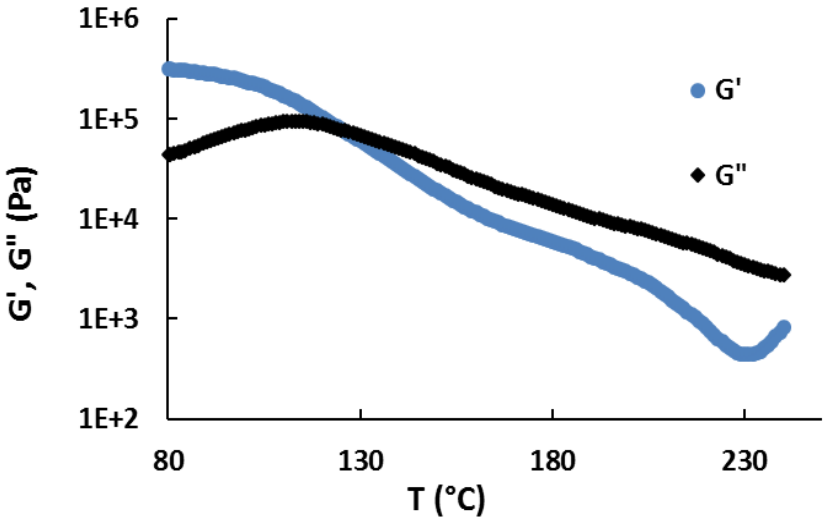

Figure 2. Thermal transitions in Kraton® D1161 sample during temperature ramp. Ramp rate: 1.5 °C/min, frequency: 1 Hz, strain: 0.5 %

3.5.1. Determination of phase transitions. The effect of temperature on the storage (*G'*) and loss (*G"*) modulus can be observed in Figure 2. *G'* monotonically decreases with increasing temperature, but shows the onset of a relatively sharp decrease at approximately 185 °C. This decrease is usually assigned to the order-disorder transition. Due to the highly asymmetric composition of Kraton® D1161 (15 % PS) we have followed the nomenclature proposed by Han et al.[29], and assigned this transition to the break-down of the bcc-ordered PS domains (Lattice Disordering/Ordering Transition – LDOT). SAXS data analysis (see below) supports this conclusion. The loss modulus (*G"*) does not drastically change during LDOT, but continues to decrease with increasing temperature.

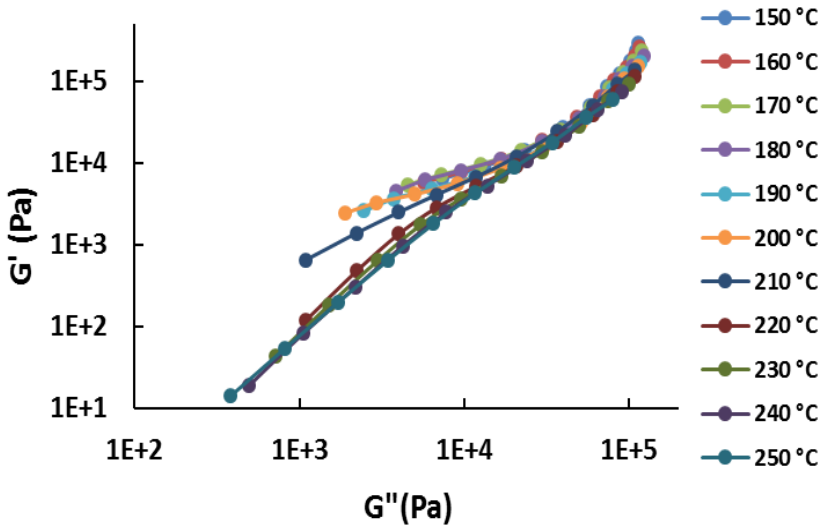

Figure 3. Han plots for Kraton® D1161. Collapse of *G'* vs *G"* plots indicate single-phase-like behavior.

Figure 3 shows Han plots (*G'* vs *G"* plots at various frequencies in the range 0.01-100 Hz) observed at temperatures ranging from 150 °C to 250 °C. Based on the slope in the terminal region, the Han plots can be divided into two regimes. At lower temperatures (150 °C – 200 °C), the plots show significantly lower slopes than those at higher temperatures (210 – 240 °C). In fact, plots at 220 °C, 230 °C and 240 °C seem to overlap. The deviation of the low temperature plots corresponds to rheological complexity induced by the microphase separated PS domains, which are in the liquid-like disordered state. The temperature 220 °C, where the plots begin to overlap, can be assigned to dissolution of the PS spheres in the PI matrix. This transition is designated as the 'Demicellization/Micellization Transition'(DMT) by Han et al.[29] However, the slopes of the *G'* vs *G"* plots in the terminal region for our material are much lower than 2, the number theoretically predicted for a monodisperse polymer.[30] The deviation is likely due to the binodal molecular weight distribution of Kraton® D1161.

Figure 4 shows changes in R_c and R_{hs} as the material is heated from 100 °C to 250 °C. R_{hs} begins to decrease at ~140 °C and continues to decrease throughout the temperature range; however, R_{hs} begins to decrease more rapidly at 180 °C corresponding to the LDOT observed in the rheological analysis. The lowest value (20.5 nm) is observed at 230 °C, above the DMT. R_c remains nearly constant up to a temperature of 220 °C, above which it begins to decrease dramatically. This behavior corresponds to the DMT observed in the frequency analysis. The monotonic decrease in R_{hs} is also consistent with the decrease in *G'* shown in Figure 3.

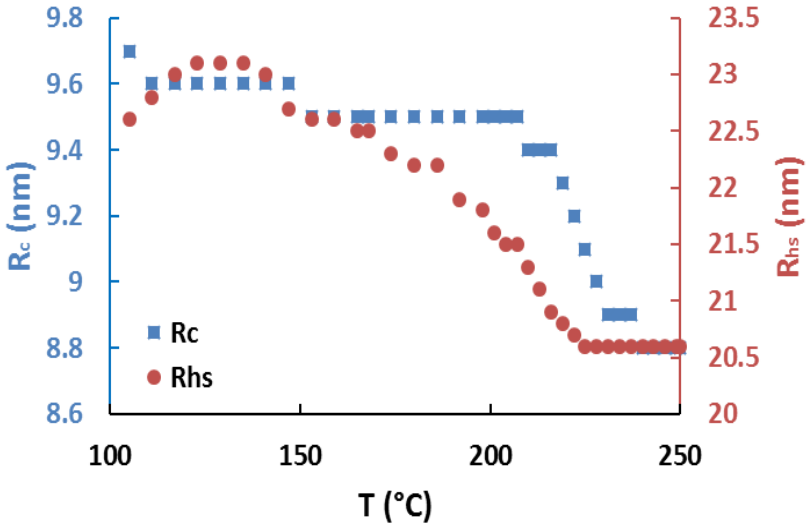

Figure 4. R_c and R_{hs} as a function of temperature for Kraton® D1161 sample during a stepwise heating experiment.

The correlation between R_{hs} and *G'* can be explained based on the microphase separated morphology in Kraton® D1161, wherein PS domains act as physical crosslinks. The SIS triblock copolymer shows the formation of a network structure when the PS end-blocks of the polymer chain become entangled in different PS domains. R_{hs} depends on the stiffness of the PI chains that surround the PS domains and on the size of the PS domains. *G'* also depends on the mobility (and

hence relaxation times) of PI and PS chains. Thus both R_{hs} and G' decrease with increasing temperatures when the mobility of the PI chains increases.

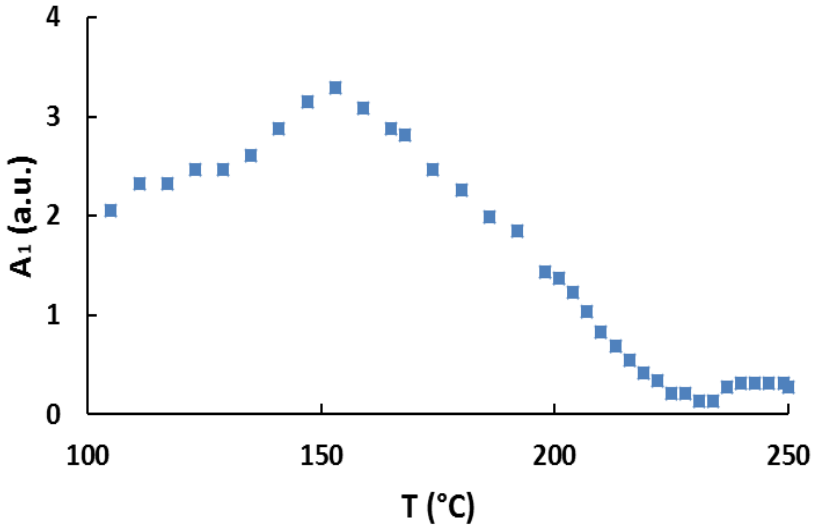

Figure 5. Intensity of primary Gaussian peak (bcc-ordered domains) – A_1 during a stepwise heating experiment.

The intensity of the primary Gaussian peak as a function of temperature during heating is shown in Figure 5. A_1 increases gradually as the material is heated above 100 °C (T_g of polystyrene), and begins to decrease monotonically above 150 °C. The initial increase in A_1 is due to improved ordering of PS domains. The samples subjected to heating experiments (in SAXS and rheology) are annealed only at room temperature after solvent is evaporated. Fast evaporation of a volatile solvent such as toluene can lead to trapping of PS domains in a disordered state. When the material is slowly heated above the polystyrene T_g, the PS chains have enough mobility to form a bcc-ordered microstructure in the bulk. The ordering process continues up to a temperature above which the disordering of bcc domains is favored as indicated by the gradual decrease in A_1. It is also important to note that the values of R_c, R_{hs}, and A_1 do not go to zero, but reach a low, finite value at temperature above DMT. Since ordered PS domains should not exist at such high

temperatures, the non-zero values of A_1 above the DMT are indication that the hard sphere model fails above DMT.

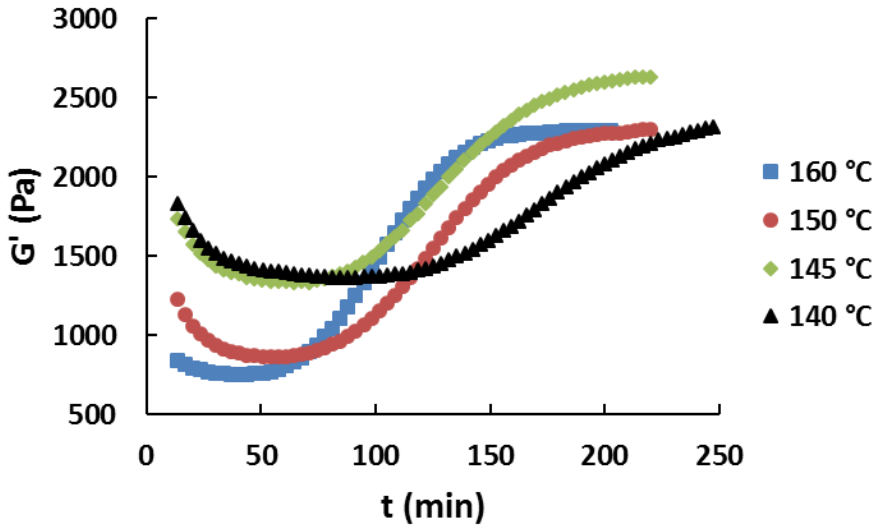

Figure 6. Effect of quench temperature on storage modulus (*G'*) of Kraton® D1161. Strain: 0.5 %, Frequency: 0.01 Hz

3.5.2. Isothermal microphase separation kinetics. Figure 2 shows an upturn in *G'* at temperatures above 230 °C during the temperature ramp experiment. This increase in *G'* is due to thermal degradation of the block copolymer. However, when Kraton® D1161 samples were heated to 240 °C (above the DMT), the modulus showed minimal change for 20 minutes (see supporting information). Thus, Kraton® D1161 samples were maintained at 240 °C for 10 minutes before rapidly quenching to temperatures below the DMT and LDOT. The time evolution of *G'* following the quench is shown in Figure 6 and provides insight into the microphase separation and ordering mechanism in the Kraton® D1161 melts. An initial decrease in *G'* is observed at short times following each quench. The decrease in *G'* is small when the material is quenched to 160 °C, and increases with decreasing quench temperature. This decrease takes place over a period of several minutes, and the duration is much longer than that required for samples to achieve thermal equilibrium. The molecular origins of this decrease will be discussed in section 7. The *G'* at short

times is higher for lower quench temperatures, but the growth of *G'* at longer times also becomes progressively slower with decreasing quench temperature. The time at which *G'* begins to increases becomes progressively longer with lower quench temperatures. The overall slowing down of ordering kinetics with decreasing quench temperature suggests that polymer chain mobility is the dominant factor during the ordering of PS domains.

The time evolution of *G"*, exhibited in Figure 7, exhibits a decrease at short times following the quench, followed by sigmoidal decrease due to the ordering process. Hence, rheological analysis suggests that the ordering process consists of two steps. To understand the trends in the moduli at shorter and longer times, one must consider mechanisms of microphase separation and ordering in an inhomogeneous system. Information obtained from SAXS analysis (R_c, A_1 peak intensity and R_{hs}) are helpful in understanding the evolution of the micro-phase separated morphology in block copolymer samples.

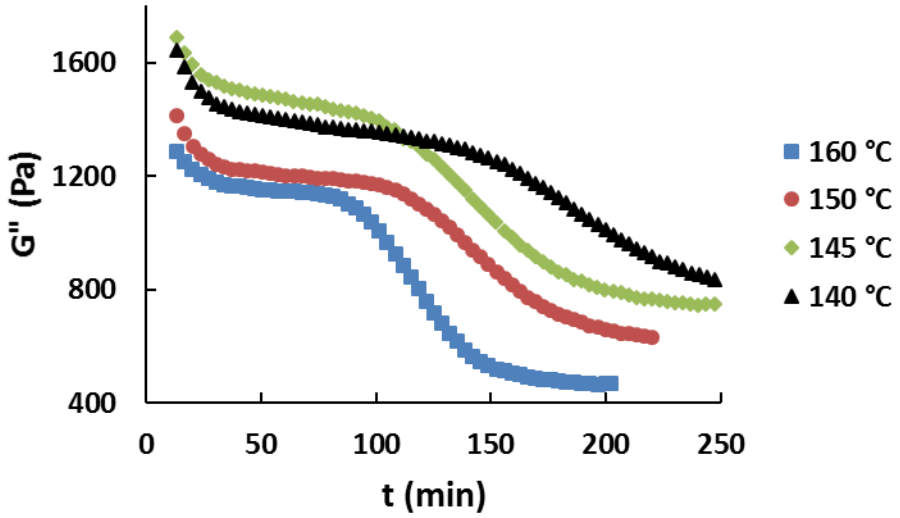

Figure 7. Evolution of loss modulus (*G"*) for Kraton® D1161 as a function of time when quenched to various temperatures.

Figure 8 shows the evolution of the polystyrene core radius (R_c) as function of time when Kraton® D1161 is quenched to different temperatures from the disordered melt. For temperatures

of 170 °C and 160 °C, R_c increases relatively quickly at shorter times, followed by slower growth at longer times. The rapid initial increase of R_c shows a significant temperature dependence. R_c begins to grow almost immediately at 170 °C and 160 °C, while at 150 °C the growth begins 10 minutes after reaching the desired temperature. The trend in R_c at times longer than 30 minutes is similar to rheological analysis, where the growth rate of both R_c and G' is slowest at 150 °C.

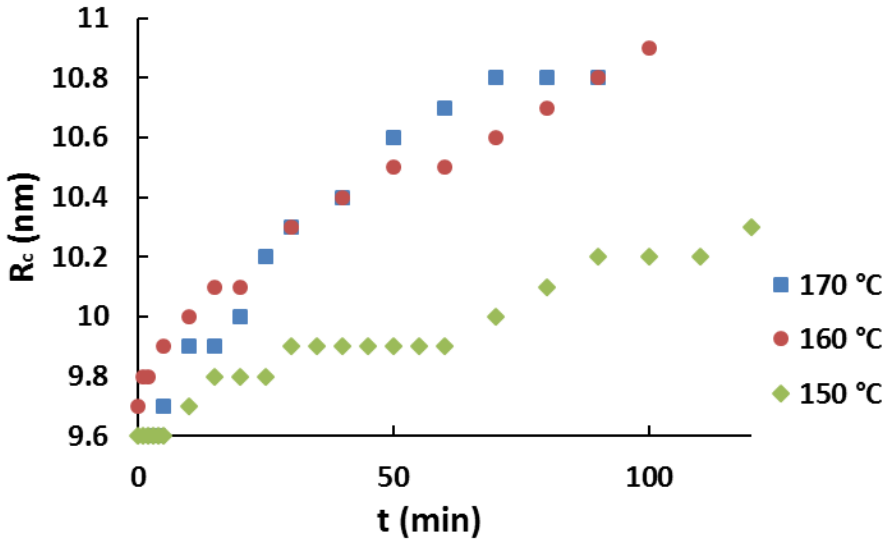

Fig. 8: Effect of quench temperature (quench depth) on evolution of R_c in Kraton® D1161

Figure 9 shows the evolution of hard sphere radius (R_{hs}) as function of time, when Kraton® D1161 is quenched to different temperatures from a disordered melt. Unlike R_c, the R_{hs} values do not show a systematic change with respect to quench temperature. R_{hs} values increase monotonically with time, and are very similar at longer times.

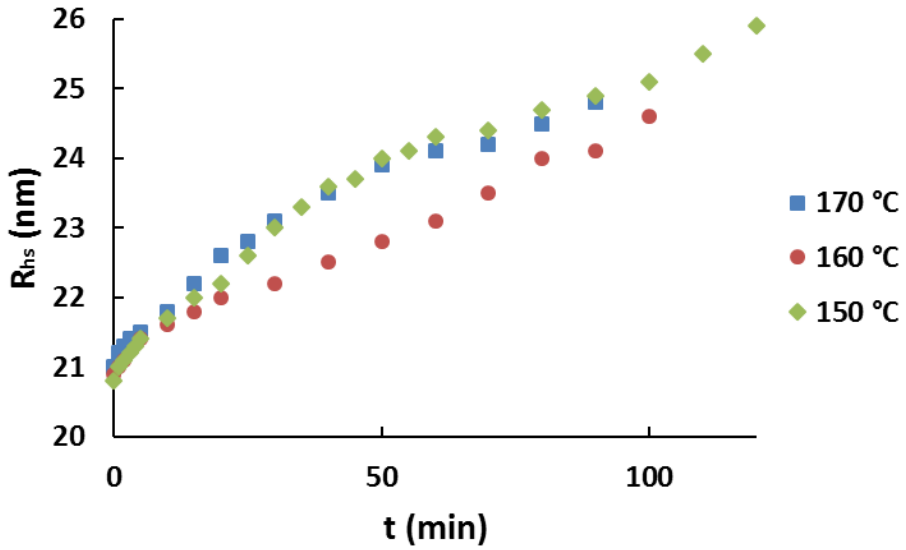

Figure 9: Effect of quench temperature (quench depth) on R_{hs} in Kraton® D1161

A_1 represents the extent of bcc-ordering of PS domains (Figure 10). The trends in A_1 are similar to the *G'* growth observed in isothermal experiments. The growth of A_1 begins at progressively earlier times with increasing quench temperature. The same trend can also been seen in the rheological analysis, where growth of *G'* in begins earlier for higher quench temperatures. The kinetics of intensity growth of the peak become progressively faster with increasing quench temperature, which is also consistent with the kinetics of *G'* growth.

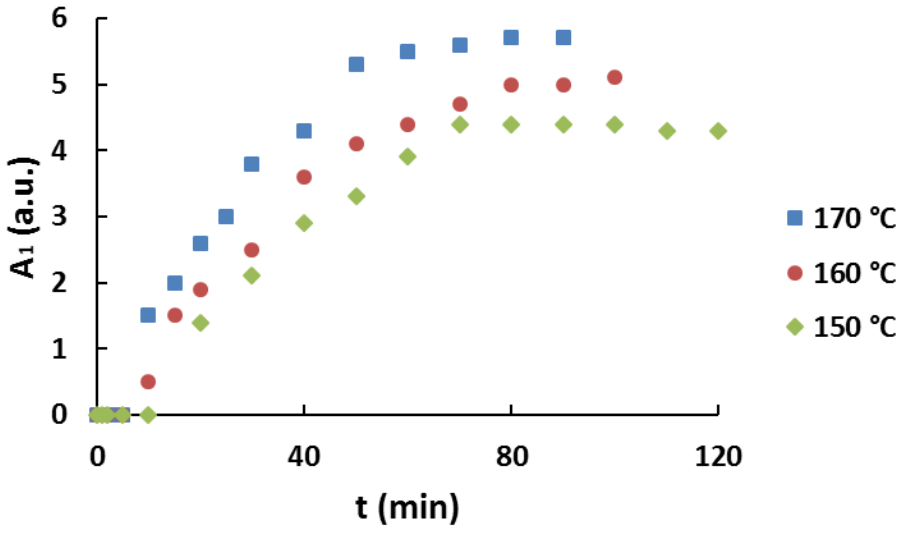

Figure 10. Effect of quench temperature (quench depth) on A_1 in Kraton® D1161

3.5.3. Ordering kinetics and the Avrami model. The fraction of ordered phase at a given time during the nucleation and growth process can be described using the following equation proposed by Avrami et al.[31]

$$X(t) = X_{\infty}\left(1 - e^{-k(t-t_0)^n}\right) \quad \text{..... (8)}$$

where *k* and *n* represent growth rate, and dimensionality of growth process. X_{∞} is the maximum possible ordered phase fraction. The term t_0 indicates the time at which the growth process begins, which is different from the time at which the quench temperature is achieved.

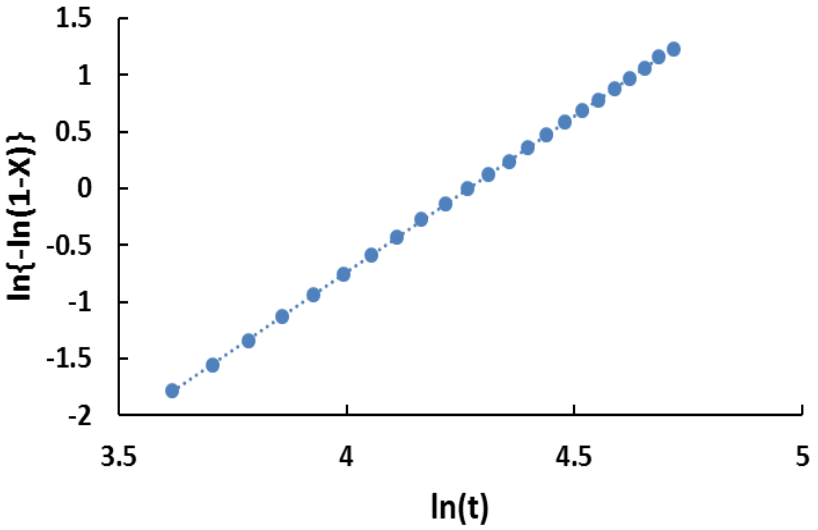

Figure 11. Avrami analysis of Kraton® D1161 quenched to 160 °C during rheology experiment.

$X = \frac{G'(t)-G'_0}{G'_{\infty}-G'_0}$, where *G'(t)* is storage modulus at time '*t*', G'_0 is storage modulus of the lower plateau (the beginning of ordering process) and G'_{∞} is the storage modulus of the higher plateau (the end of ordering process). A double-logarithmic plot of '*X*' should yield a linear fit from which *k* and *n* can be extracted, as shown in Figure 11 for Kraton® D1161 quenched to 160 °C. Table 2 lists *n* values determined for various quench temperatures obtained from rheological analysis.

Table 2. Avrami model parameters obtained from rheological analysis of Kraton® D1161 quenched at various temperatures

Quench Temperature (°C)	*n*	$t_{1/2}$ (min)
160	2.8	65
150	2.5	68
140	2.7	92

Rheological analysis yields values of *n* between 2 and 3. These values suggest that the nucleation sites are formed well before the growth occurs, and some of the nucleation sites are already saturated.[32] Table 2 also lists half-times of the growth process, and these increase with decreasing quench temperature. The growth rate is a function of two competing factors – the thermodynamic driving force, which is proportional to quench depth, and the mobility of polymer chains, which is inversely proportional to the quench depth. Thus, it is reasonable to conclude that the kinetics for deep temperature quenches are primarily limited by decreased chain mobility.

3.5.4. Morphological Model. Based on the SAXS and rheological analysis, we propose a morphological model for the Kraton® D1161 system. This model is an extension of the work of Gibert et al.[2], and is depicted in Figure 12. Microphase separation in the SIS triblock leads to the formation of a network structure, in which long PI chains (represented by red lines) connect spherical PS domains. However, some PI chains form loops (represented by the blue line) instead of forming a bridge between two polystyrene domains. This morphology is similar to that of bridged and looped micelles in block copolymer solutions.[33] Presence of SI diblocks leads to a few

PI chains with dangling ends that are not part of the network structure. These chains have shorter relaxation times compared to those bridging PS domains. It is likely that the relaxation time of PI chains from SI diblocks may vary depending upon whether they are part of a physical entanglement or not. Thus, presence of SI diblocks along with SIS triblocks should give rise to broad thermal transitions as confirmed in rheological analysis. In SAXS heating experiments, the intensity of the bcc-ordered peak (A_1) also begins to decrease monotonically above 150 °C, which is much lower than the observed LDOT. The results suggest that the presence of polyisoprene chains from SI diblocks has a significant effect on the ordering of PS domains in the SIS/SI mixture.

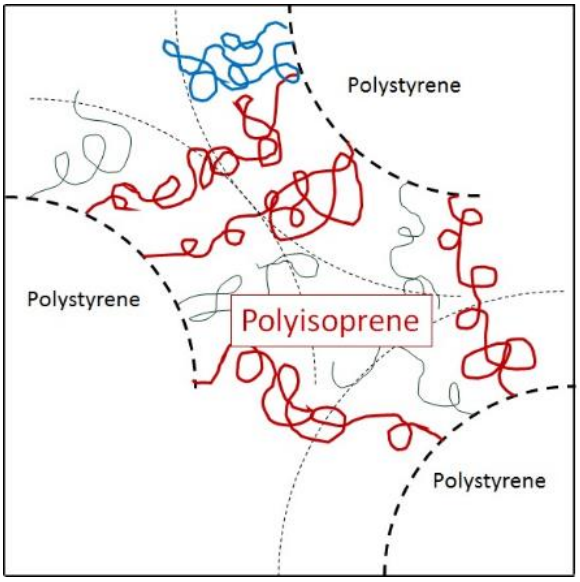

Figure 12: Morphological model for Kraton® D1161.

Scattering from disordered spheres can be adequately fit in the Percus-Yevick (PY) hard sphere model to yield morphological parameters such as R_c, and R_{hs}. R_c in the Kraton® D1161 samples corresponds to the radius of the PS cores, similar to that considered by Kinning and Thomas.[28] The hard sphere radius R_{hs} may be considered equivalent to that in block copolymer micelles, as it represents polyisoprene chain segments with decreased mobility due to the tethering of polystyrene chains at one or both ends. However, it is very important to realize that R_{hs} takes into account polyisoprene segments from both SIS triblock and SI diblock. Thus, R_{hs} may not have

a direct relationship with the average distance between two polystyrene domains. For example, at 250 °C, when only disordered spheres should be present in the melt, the R_{hs} is estimated to be 20.9 nm. The average interdomain spacing is calculated to be 29.4 nm based on SAXS data, although estimation of the interdomain spacing becomes difficult as the primary scattering maximum becomes broader at higher temperatures. Hence, Kraton® D1161 melts may not exhibit bridged micelle – like behavior in which the interdomain distance is roughly twice the R_{hs}.[34]

Microphase separation is generally believed to occur through concentration fluctuations via various mechanisms including nucleation, growth, coagulation, and diffusion. In Kraton® D1161, distinct steps of the process can be observed.

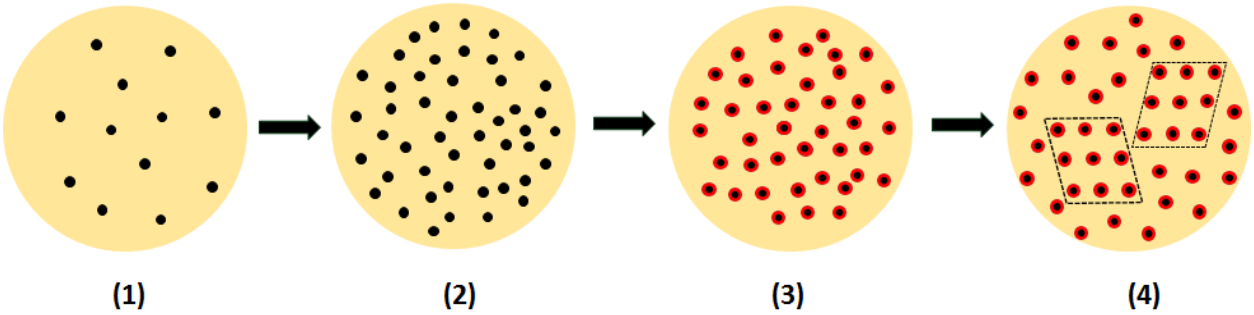

Figure 13. Stages of the microphase separation and ordering process in Kraton® D1161 melts.

The time evolution of the morphology in Kraton® D1161 melts is depicted schematically in Figure 13. At temperatures well above the DMT (~240 °C), significant mixing of the PS and PI chains occurs. However, a small but significant number of polystyrene domains may still exist in the melt (Stage 1 in Figure 13). The presence of a broad maximum in the SAXS profile collected at 250 °C supports our argument. The finite values of R_c, and R_{hs} above DMT (Figure 4) indicate the existence of PS domains in the melt before the quench process begins. After the sample is quenched to temperatures below the ODT, the morphology at short times is described by Stage 2. Microphase separation in the system results in an increased number of concentration fluctuations, which can be equivalent to small spherical domains rich with polystyrene. The existence of Stage

2 is supported by the relatively rapid growth of R_c and R_{hs} in the first 10-15 minutes (Figures 8 and 9). The formation of a larger number of physical crosslinks should result in an increase in G'; however, no such trend is observed in rheological quench analysis, possibly due to very long time required to begin data collection with a low oscillation frequency (0.01 Hz).

Stage 3 corresponds to concentration fluctuations existing at longer times. In early stages of the phase separation process, the modulus depends on the strength of concentration fluctuations. As time progresses, the system reaches a steady composition and concentration fluctuations are nearly saturated, and interfacial tension becomes the dominant factor. However, the modulus can still decrease with time due to coarsening of PS domains, which is observed in Figures 6 and 7. Coarsening of PS domains is also exhibited in Figure 8, which shows the continuous increase of the PS core radius R_c. The growth of some PS domains must come at the cost of other domains. Thus, the increase in the average PS domain size should result in fewer domains in the system. Since PS domains act as physical crosslinks that contribute to the mechanical modulus, the coarsening of PS domains results in a decrease in the modulus of Kraton® D1161 before the ordering process begins. Due to the increased strength of the concentration fluctuations, the storage modulus (G') increases with increasing quench depth. Since chain mobility decreases with decreasing temperatures, chain diffusion becomes slower at greater quench depths. As coarsening depends on PS chain diffusion, it should become slower with increased quench depth. A consistent decrease in R_c with respect to quench temperature (Figure 8) supports this argument. Hence, the time taken for G' and G'' to reach a plateau during Stage 3 should and does increase with decreasing quench temperature.

After concentration fluctuations are saturated, the ordering of the polystyrene domains begins, which is represented by stage 4 in Figure 13. During the ordering process, the primary scattering

maximum becomes broad or a distinct second peak emerges at $q \sim 0.21$ nm^{-1}. A peak fitting analysis reveals the presence of a second peak corresponding to a bcc microstructure of polystyrene domains. The emergence of the bcc peak corresponds to the increase in *G'* in rheological analysis, and can be fit using the Avrami equation.[31]

3.6. Conclusion

We have performed real-time SAXS and rheological analysis to understand the morphology and microphase separation kinetics of the base component of a widely used pressure-sensitive adhesive system. The presence of a small but finite number of polystyrene domains is observed at temperatures well above the lattice disordering transition temperature. The binodal molecular weight distribution obtained due to presences of SIS and SI led to broad thermal transitions and broad scattering patterns.

A morphological model has been proposed based on fitting of SAXS profiles using the Percus – Yevick hard sphere model. Even though there is no solvent present, the Kraton® D1161 melts show similar morphology to those of block copolymer solutions. The evolution of the morphology in Kraton® D1161 melts can be represented in 4 stages: 1. above the DMT, concentration fluctuations of PS exist at low concentrations in the melt; 2. at short times following a temperature quench, microphase separation takes place via enhanced concentration fluctuations of the polystyrene chains; 3. at longer times, coarsening of polystyrene domains occurs resulting in increased polystyrene domain size, but decreased numbers of polystyrene domains; 4. the domains slowly form a bcc-structure. The domain coarsening and ordering kinetics depend predominantly on quench depth, as they are limited by the mobility of the polymer chains and the ability of polystyrene blocks to diffuse through the polyisoprene matrix.

In this study, a model has been developed by performing a number of experiments on a SIS/SI block copolymer mixture. The experimental methods and model established in this paper can be used to study the effect of tackifier molecules on the morphology and microphase separation kinetics in pressure-sensitive adhesive blends containing a base copolymer and a tackifier.

AUTHOR INFORMATION

Corresponding Author

*Email: martinsm@vt.edu

Present Address

§Lixia Rong, Center for Advanced Microstructures & Devices, Louisiana State University, Baton Rouge, Louisiana 70806, United States

Author Contributions

The manuscript was written through contributions of all authors. All authors have given approval to the final version of the manuscript.

Notes

The authors declare no competing financial interest.

ACKNOWLEDGEMENT

Use of the National Synchrotron Light Source, Brookhaven National Laboratory, was supported by the U.S. Department of Energy, Office of Science, Office of Basic Energy Sciences, under Contract No. DE-AC02-98CH1088. The authors thank Dr. Richey Davis (Virginia Tech, Chemical Engineering) for access to the AR-G2 rheometer used in this work. The authors also thank 3M®

Corporation for providing the materials used in this work. One of the authors (Eugene Joseph) would like to thank 3M® Corporation for financial support. The authors would like to acknowledge Prof. Benjamin Hsiao (Stony Brook University) for his help in scheduling SAXS experiments at the Brookhaven National Laboratory.

3.7. References

(1) Ewins, E. E. S. C., D. J.; Erickson, J. R.; Korcz, W. H. *Handbook of Pressure-Sensitive-Adhesive technology*; 2nd ed.; Van Nostrand Reinhold: New York, 1989; Vol. 1.

(2) Gibert, F. X.; Marin, G.; Derail, C.; Allal, A.; Lechat, J. *The Journal of Adhesion* **2003**, *79*, 825.

(3) Satas, D. *Handbook of pressure sensitive adhesive technology*; Satas & Associates: Warwick, RI, 1999.

(4) Webster, I. *International Journal of Adhesion and Adhesives* **1997**, *17*, 69.

(5) Brown, K.; Hooker, J. C.; Creton, C. *Macromolecular Materials and Engineering* **2002**, *287*, 163.

(6) Nakajima, N.; Babrowicz, R.; Harrell, E. R. *Journal of Applied Polymer Science* **1992**, *44*, 1437.

(7) Kraus, G.; Jones, F. B.; Marrs, O. L.; Rollmann, K. W. *The Journal of Adhesion* **1976**, *8*, 235.

(8) Kane, L.; Norman, D. A.; White, S. A.; Matsen, M. W.; Satkowski, M. M.; Smith, S. D.; Spontak, R. J. *Macromolecular Rapid Communications* **2001**, *22*, 281.

(9) Lee, S.-H.; Koberstein, J. T.; Quan, X.; Gancarz, I.; Wignall, G. D.; Wilson, F. C. *Macromolecules* **1994**, *27*, 3199.

(10) Lovisi, H. R.; Nicolini, L. F.; Ferreira, A. A.; Martins, M. L. S. In *Applications of Anionic Polymerization Research*; American Chemical Society: 1998; Vol. 696, p 90.

(11) Derail, C.; Cazenave, M. N.; Gibert, F. X.; Marin, G.; Kappes, N.; Lechat, J. *The Journal of Adhesion* **2004**, *80*, 1131.

(12) Hashimoto, T.; Shibayama, M.; Kawai, H. *Macromolecules* **1983**, *16*, 1093.

(13) Harkless, C. R.; Singh, M. A.; Nagler, S. E.; Stephenson, G. B.; Jordan-Sweet, J. L. *Physical Review Letters* **1990**, *64*, 2285.

(14) Balsara, N. P.; Garetz, B. A.; Dai, H. J. *Macromolecules* **1992**, *25*, 6072.

(15) Winter, H. H.; Scott, D. B.; Gronski, W.; Okamoto, S.; Hashimoto, T. *Macromolecules* **1993**, *26*, 7236.

(16) Adams, J. L.; Quiram, D. J.; Graessley, W. W.; Register, R. A.; Marchand, G. R. *Macromolecules* **1996**, *29*, 2929.

(17) Hashimoto, T.; Sakamoto, N.; Koga, T. *Physical Review E* **1996**, *54*, 5832.

(18) Chastek, T. Q.; Lodge, T. P. *Macromolecules* **2003**, *36*, 7672.

(19) Liu, Z.; Shaw, M.; Hsiao, B. S. *Macromolecules* **2004**, *37*, 9880.

(20) Chastek, T. Q.; Lodge, T. P. *Macromolecules* **2004**, *37*, 4891.

(21) Chastek, T. Q.; Lodge, T. P. *Journal of Polymer Science Part B: Polymer Physics* **2005**, *43*, 405.

(22) Patel, A. J.; Mochrie, S.; Narayanan, S.; Sandy, A.; Watanabe, H.; Balsara, N. P. *Macromolecules* **2010**, *43*, 1515.

(23) Schuler, M.; Stuehn, B. *Macromolecules* **1993**, *26*, 112.

(24) Floudas, G.; Hadjichristidis, N.; Iatrou, H.; Pakula, T.; Fischer, E. W. *Macromolecules* **1994**, *27*, 7735.

(25) Floudas, G.; Fytas, G.; Hadjichristidis, N.; Pitsikalis, M. *Macromolecules* **1995**, *28*, 2359.

(26) Bates, F. S.; Fredrickson, G. H. *Annu. Rev. Phys. Chem.* **1990**, *41*, 525.

(27) Percus, J. K.; Yevick, G. J. *Physical Review* **1958**, *110*, 1.

(28) Kinning, D. J.; Thomas, E. L. *Macromolecules* **1984**, *17*, 1712.

(29) Han, C. D.; Vaidya, N. Y.; Kim, D.; Shin, G.; Yamaguchi, D.; Hashimoto, T. *Macromolecules* **2000**, *33*, 3767.

(30) Han, C. D.; Kim, J.; Kim, J. K. *Macromolecules* **1989**, *22*, 383.

(31) Hamley, I. W. *The physics of block copolymers*; Oxford University Press: Oxford; New York, 1998.

(32) Nie, H.; Bansil, R.; Ludwig, K.; Steinhart, M.; Koňák, Č.; Bang, J. *Macromolecules* **2003**, *36*, 8097.

(33) Winnik, M. A.; Yekta, A. *Current Opinion in Colloid & Interface Science* **1997**, *2*, 424.

(34) Bansil, R.; Nie, H.; Li, Y.; Liao, G.; Ludwig, K.; Steinhart, M.; Koňák, Č.; Lal, J. *Macromolecular Symposia* **2002**, *190*, 161.

Chapter 4

Isothermal Microphase Separation Kinetics in Styrene-Isoprene-Styrene Block Copolymer-based Hot-Melt Pressure-Sensitive Adhesives

Isothermal Microphase Separation Kinetics in Styrene-Isoprene-Styrene Block Copolymer-based Hot-Melt Pressure-Sensitive Adhesives

Ninad Dixit[†], Alicia Pape[‡], Lixia Rong[∥§], Eugene Joseph[‡], and Stephen M. Martin[‡]

[†]Department of Chemistry, Virginia Polytechnic Institute and State University, Blacksburg, Virginia 24061, United States

[‡]Department of Chemical Engineering, Virginia Polytechnic Institute and State University, Blacksburg, Virginia 24061, United States

[∥]Louisiana State University, Baton Rouge, Louisiana 70806, United States

4.1. Abstract

Pressure sensitive adhesives commonly consist of a base block copolymer to which a low molecular weight "tackifier" is added, altering both the mechanical properties and the phase behavior of the base block copolymer. Time-resolved small angle X-ray scattering (SAXS) and oscillatory rheology experiments were carried out to study the microphase separation kinetics of pressure-sensitive adhesive blends consisting of a commercially available styrene-isoprene block copolymer and a low molecular weight, high glass transition temperature (T_g) resin (tackifier). A modified Percus-Yevick hard-sphere model was used to determine morphological parameters from the SAXS analysis, and an Avrami kinetics model was used to characterize the growth kinetics of the ordered microphase. We observed that composition fluctuations drive the initial stage of microphase separation in the quenched adhesive melts. The addition of tackifier to the copolymer - tackifier blends led to a decrease in the extent of ordering of polystyrene domains. Polystyrene

domains exhibited no ordering and remained in a liquid-like disordered state for blends with tackifier content of 30 wt.% and above. In addition, increasing the amount of tackifier in the blend resulted in a shift in the microphase separation mechanism from a 'nucleation and growth' to a 'spinodal decomposition' process.

4.2. Introduction

Hot melt pressure-sensitive adhesives (HMPSAs) are a more environmentally friendly alternative to solvent- and water-borne adhesive systems. Block copolymers based on styrene and isoprene are one of the most commonly used materials in such adhesives. These block copolymers generally exhibit a microphase separated morphology at service temperatures resulting in the formation of physical crosslinks. The base component of the HMPSAs is often a mixture of a triblock (SIS) and diblock (SI) copolymer. The pure triblock (SIS) shows very low interfacial adhesion, and inclusion of the SI diblock in the base copolymer leads to improved tack[1] and modified mechanical and rheological behavior.[2,3] The base copolymer is blended with a low molecular weight resin, or tackifier, in order to achieve the desired adhesive properties. Although a variety of tackifiers are available commercially, compatibility with the base copolymer dictates the tackifier selection.[4] In the case of SIS-based adhesives, the tackifier is usually selectively miscible with the polyisoprene chains.

Several researchers have studied the effect of tackifier[5-9] and processing conditions on adhesive performance.[10] However, the phase structure of block copolymer based adhesives has not yet been conclusively identified. Several publications by Sasaki et al[1,4,11] argue that the tackifier forms a separate phase in the copolymer-tackifier blend above a certain concentration. Other researchers[12,13] have denied the formation of a separate phase and thus its effect on the adhesive properties of blends. In the case of HMPSAs, the blend components are mixed at high

temperatures, and the melt is applied to a substrate maintained at a lower temperature prior to further processing. Microphase separation in the block copolymer during the melt processing should significantly affect the resulting adhesive properties, since the formation of polystyrene (PS) domains (in the case of SIS based adhesives) enhances the mechanical strength of the blends. However, the kinetics of microphase separation in block copolymer based adhesives are not yet well understood.

The selective miscibility of tackifiers with one of the phases in a block copolymer suggests that they may be comparable to the blends containing other types of diluents. On the low end of the diluent molecular weight spectrum lie selective solvents, which lead to the formation of block copolymer micelles above a critical micelle concentration. Lodge and coworkers,[14,15] in particular, have established phase diagrams of styrene-isoprene diblock copolymer solutions with selective solvents. Homopolymers that are homologous with one of the blocks in the copolymer are high molecular weight diluents. Several studies[16-20] describe specific nanostructures formed by blending block copolymers with selectively miscible homopolymers. The enhanced viscoelastic loss in the rubbery plateau region of the SIS – polyisoprene blend[21] demonstrates a relationship between the blend composition and the resulting mechanical properties. Tackifiers, being intermediate molecular weight diluents, present an interesting scenario for the study of structure-property relationships in polymer blends. From an industrial perspective, understanding the evolution of the microphase separated morphology and the mechanical properties of the melts of HMPSA blends will aid in the optimization of adhesive formulation and processing.

In a previous paper,[22] we reported a study of the melt phase microphase separation kinetics of a commercially available styrene-isoprene based block copolymer (Kraton® D1161). Various morphological parameters (hard sphere radius, R_{hs}; polystyrene core radius, R_c) were obtained

from a small-angle X-ray scattering (SAXS) analysis by fitting the data to a modified Percus – Yevick hard-sphere model. The ordering kinetics of the microphase separated PS domains followed a nucleation and growth process, and were fitted using an Avrami model. A qualitative morphological model was proposed for the base copolymer (Kraton® D1161), which is a mixture of SIS and SI block copolymers. Herein we report on the microphase separation kinetics of blends of the same base block copolymer (Kraton® D1161) and a commercially available tackifier (Eastman Piccotac™ 1095). The effect of added tackifier on the thermal and morphological transitions in blends of different compositions is described using the morphological parameters established for the base block copolymer. The time evolution of the shear moduli is used to ascertain the ordering of PS domains in adhesive melts of different compositions. Finally, the role of tackifier on the microphase separation mechanism in quenched melts of copolymer-tackifier blends is discussed.

4.3. Experimental Section

Kraton® D1161 (base PSA copolymer), Eastman Piccotac™ 1095 (tackifier), and Irganox® 1010 (antioxidant) were used without further purification. Piccotac™ 1095 is a C_5 aliphatic resin with M_n ~ 800 g/mol, and M_w ~ 1700 g/mol. The glass transition temperature (T_g) of the tackifier is 43 °C, and the softening point is 94 °C. Details of Kraton® D1161, and the experimental methods for the SAXS and rheological measurements are described in a previous paper.[22]

Samples were prepared using the method similar to that described previously.[22] The block copolymer and tackifier were dissolved in toluene in various ratios by weight: 100/0, 90/10, 70/30, and 50/50 for Kraton® D1161 and Piccotac™ 1095 respectively. A small quantity of Irganox® 1010 was also added as an antioxidant. The solutions were placed in a covered well and the solvent was allowed to evaporate slowly. Residual solvent was then removed under vacuum.

4.4. SAXS Data Analysis

The scattering patterns obtained for the blend samples were similar to those obtained from disordered block copolymer micelles in a solvent. Hence, the Percus – Yevick model was used to model the scattering from the disordered PS domains as analogous to that from disordered micelles.[22] Assuming the monodispersity of scattering entities in the samples, the scattering intensity can be written as product of a function describing the shape of a single particle *P(q),* and a function corresponding to the interparticle interference *S(q),* also known as the structure factor:

$$I(q) = I_0 P(q) S(q) \quad \text{..... (1)}$$

where I_0 is a constant proportional to the number density of the scattering entities and the electron density difference between the two phases. We assumed PS spheres of radius R_c for fitting a spherical form factor approximation, and the Percus – Yevick structure factor to describe the interaction between hard-spheres of radius R_{hs}.[23] The scattering from ordered PS domains led to periodic but weak Bragg reflections in certain samples, which was represented by a sum of Gaussian functions $\sum A_i(t) e^{-(1/2)\{\frac{q-q_i}{\sigma_i}\}c^2}$, where A_i, q_i, and σ_i are the amplitude, position, and width of the i^{th} Bragg peak.[24] The position of the first Bragg peak was used as a fitting parameter during the analysis of scattering patterns. Subsequent peak positions were determined based on the Bragg reflections corresponding to a body-centered-cubic arrangement of PS spheres. The total scattering intensity (I_{tot}) was calculated as the sum of scattering from disordered (I_s) and bcc-ordered PS domains (I_b).

$$I_{tot} = I_s + I_b \quad \text{..... (2)}$$

A 'q' range of 0.13 – 0.4 nm^{-1} was considered for data fitting as it encompassed the primary and secondary scattering peaks. Gaussian functions corresponding to primary and secondary

ordered peaks were used when necessary. However, the secondary Gaussian had minimal impact on the fitting procedure, particularly in the case of quench-isothermal experiments.

4.5. Results and Discussion

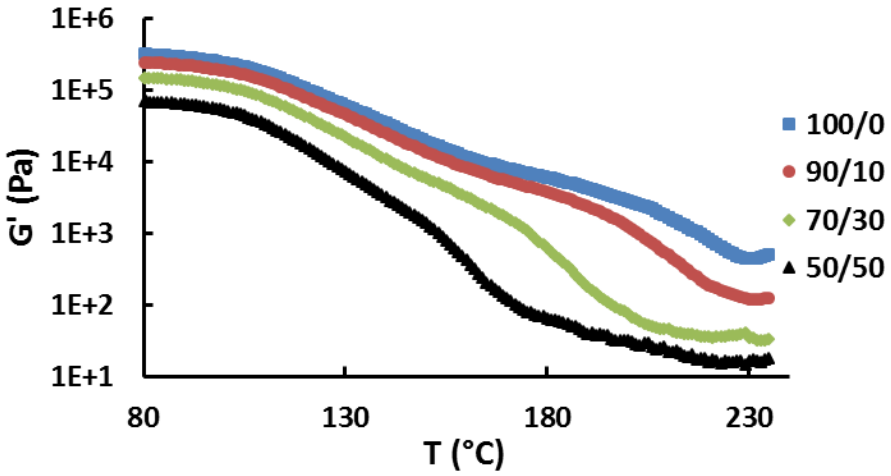

Figure 1. Thermal transitions in copolymer - tackifier blends with 0, 10, 30 and 50 wt. % tackifier are indicated by sharp decreases in the shear modulus during temperature ramp experiments. Ramp rate: 1.5 °C/min, frequency: 1 Hz, strain: 0.5 %.

4.5.1. Thermal and morphological transitions in blends. Copolymer - tackifier blends were subjected to slow temperature ramps during which the shear moduli were tracked. The temperature ramp experiments, shown in Figure 1, exhibit two prominent thermal transitions in which the shear storage modulus (*G'*) undergoes a significant decrease. The first transition occurs around 100 °C for all blend compositions, and corresponds to the T_g of polystyrene. The decrease in *G'* begins in a relatively narrow temperature range for all the blend compositions, which implies that inclusion of tackifier in the blends does not affect the T_g of PS chains significantly. Hence, it can be assumed that the tackifier is selectively soluble in the polyisoprene-rich phase with minimal partitioning across the styrene-isoprene phase boundary. The higher temperature transition is attributed to the disordering of PS domains and is termed the lattice disordering/ordering transition (LDOT). The LDOT in the blends is clearly a function of the blend composition, and decreases

with increasing tackifier content as shown in Table 1. Since the LDOT in the blends corresponds to the disordering of the bcc-ordered PS domains, it can be concluded that the presence of the polyisoprene-selective tackifier restricts the ordering of the PS domains. The shear storage modulus at a given temperature decreases with increasing tackifier content in the blend. This trend is consistent with the fact that the tackifier is a low molecular weight resin and has a softening temperature lower than the polystyrene T_g. Thus, the tackifier acts as a selective solvent at the temperatures under consideration.

Table 1. LDOT and DMT temperatures of the copolymer - tackifier blends as determined by rheological analysis

Blend Composition	**LDOT (°C)**	**DMT (°C)**
100/0	200	230
90/10	190	230
70/30	180	200
50/50	150	180

The demicellization-micellization transition (DMT) in the adhesive blends was determined by plotting *G'* against *G"* values obtained during multi-frequency analysis (0.01 – 100 Hz) at various temperatures (130 – 240 °C). In the case of multi-phase systems, the phase separation induces complexity in the rheological behavior of materials as indicated by variation in the slopes of the *G'* vs *G"* plots.[25] Thus, when the *G'* vs *G"* plots collapse, the system can be considered to behave like a single-phase system. The temperature at which this occurs is the DMT.[26] Table 1

shows DMT temperatures determined for each blend composition. (See Appendix B for rheological data). The DMT occurs at progressively lower temperatures as the tackifier content in the blend increases from 10 to 50 wt. %.

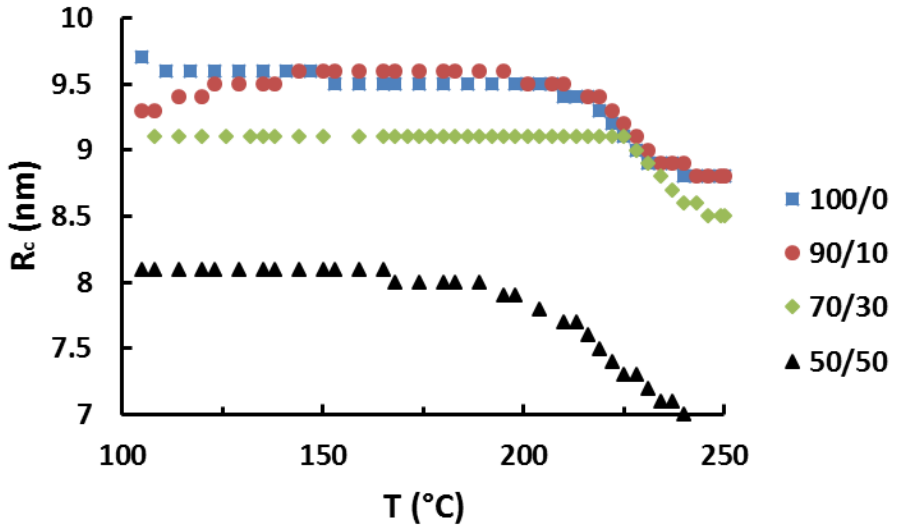

Figure 2. R_c as a function of temperature during a stepwise heating experiment.

Figure 2 shows the PS core radius, R_c, for various copolymer - tackifier blends, determined by fitting the scattering data to a modified Percus - Yevick hard-sphere model, as a function of temperature. The R_c values remain constant for a given sample up to about 200 °C, and begin to decrease in the temperature range corresponding to the DMT. The decrease in R_c indicates the mixing of PS chains into the polyisoprene matrix, and the DMT values determined by SAXS and rheology are consistent. There is little difference between the R_c of the 100/0 and 90/10 blend samples, however, a small decrease in R_c is observed for the 70/30 blends and a more significant decrease is observed for the 50/50 samples. The decrease in R_c with increasing tackifier content suggests that the tackifier serves to limit the polystyrene chain diffusion as the solvent evaporates from the solution cast sample, thereby inhibiting the growth of PS domains.

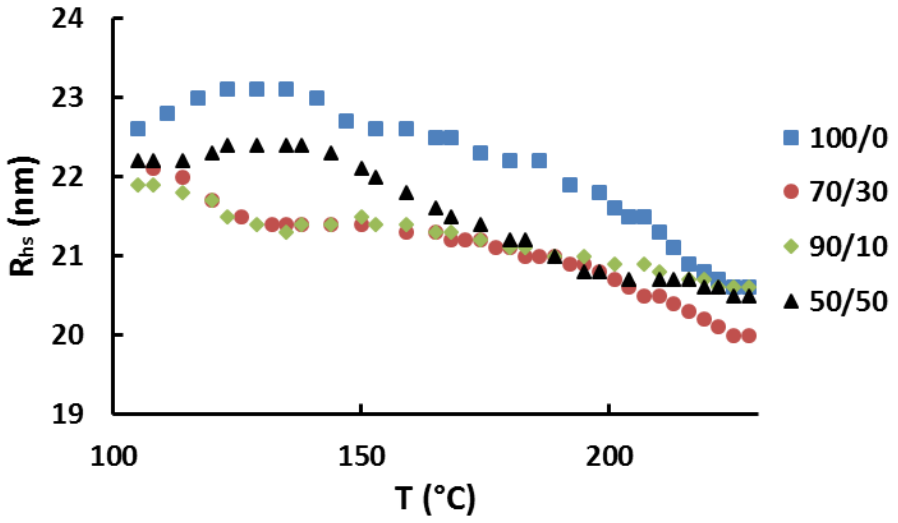

Figure 3. R_{hs} as a function of temperature during stepwise heating experiment.

The effect of blend composition on the hard-sphere radius (R_{hs}) is depicted in Figure 3. R_{hs} is influenced by the mobility of the polyisoprene chains and by the spacing between the micro-phase separated PS domains. R_{hs} generally decreases with increasing temperature for all blend compositions. The dependence of R_{hs} on concentration is more complex. The values decrease as the tackifier content in the blends increases from 0 to 10 wt.%. There is little difference between R_{hs} values in the 90/10 and 70/30 blends, but the 50/50 blend exhibits higher values at temperatures below the LDOT (150 °C.) This trend in R_{hs} can be explained on the basis of a morphological model as depicted in Figure 4. Since tackifier molecules act as selective solvent for the isoprene chains, they should reduce the number of entanglements. Consequently, the mobility of isoprene chains should increases and R_{hs} should decrease. This trend is observed in 90/10 and 70/30 blend samples. However, tackifier molecules may saturate the available free volume at high concentrations and begin to swell the polyisoprene-rich phase. Such swelling push the PS domains apart and thus result in higher R_{hs} values, which is observed in the case of 50/50 blend samples.

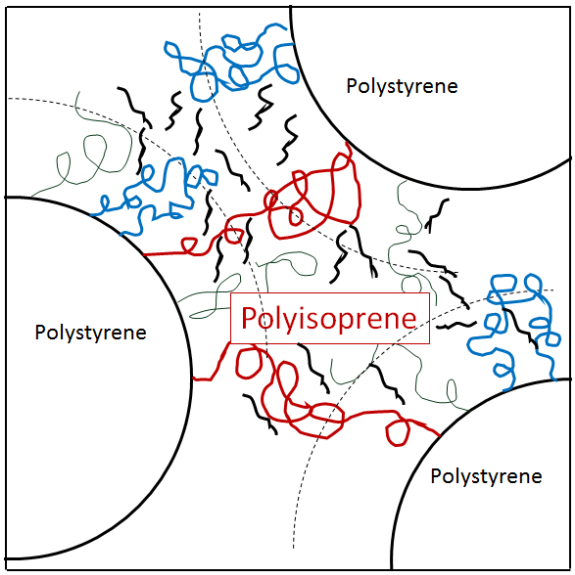

Figure 4. Morphological model for block copolymer – tackifier blends. Red, blue and green curves represent polyisoprene chain that connect two PS domains, form loops, and have one end in the polyisoprene phase respectively. Black segments represent tackifier molecules. Solid circles represent interface between polystyrene- and polyisoprene-rich phases. Dotted circles represent hard sphere radii.

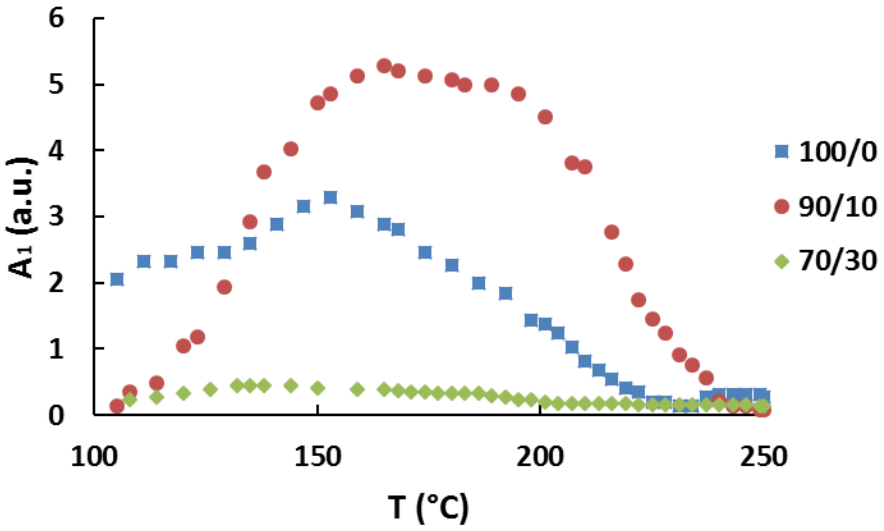

Figure 5. Intensity of primary Gaussian peak (A_1) during a stepwise heating experiment.

The intensity of the Gaussian peak corresponding to the bcc-ordered PS domains is plotted as a function of temperature in Figure 5. No bcc scattering peak was observed in the 50/50 blend, indicating that PS domains in the 50/50 blend remain in a disordered state. The initial increase in the intensity at low temperatures is attributed to ordering of the PS domains as the sample is heated

above the T_g of polystyrene. The increased mobility of the PS and polyisoprene chains allows better rearrangement of the domains and results in an increased fraction of bcc-ordered domains in the given sample volume. At temperatures higher than 150 °C, the peak intensity begins to decrease, indicating the disordering of the bcc-structure. This decrease takes place over a wide temperature range, which coincides with the decrease in *G'* observed in the rheological analysis (Figure 1).

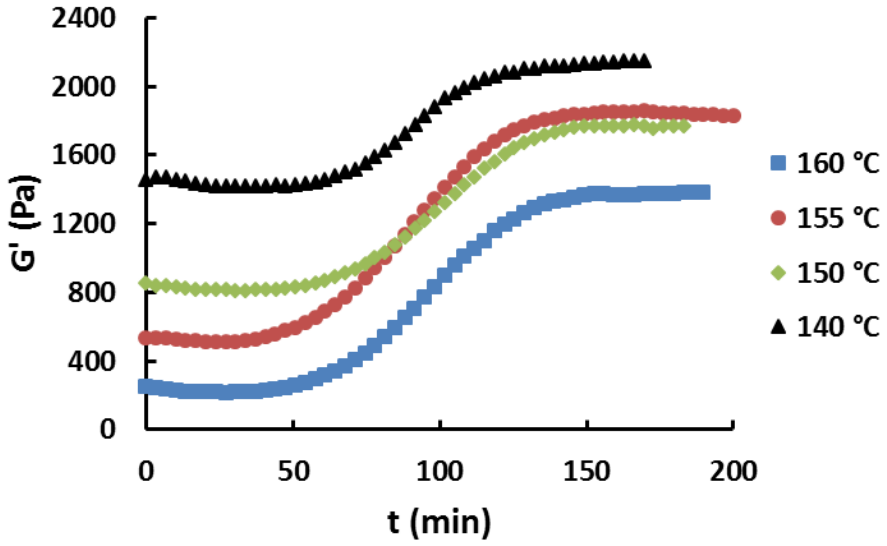

Figure 6. Effect of quench temperature on the storage modulus (*G'*) of 90/10 blend samples. Strain: 0.5 %, frequency: 0.01 Hz.

4.5.2. Isothermal microphase separation kinetics in blends. Figure 6 shows the evolution of the storage modulus (*G'*) of the 90/10 blend samples as they are quenched from 240 °C and held isothermally at four different temperatures. The *G'* profiles at all quench temperatures show sigmoidal behavior indicating a 'nucleation and growth' type mechanism for the ordering of microphase separated PS domains. The Avrami model[27,28] was used to extract kinetic parameters for the 90/10 blend samples:

$$X(t) = X_{\infty}(1 - e^{-k(t-t_0)^n}) \quad \text{.....(3)}$$

The Avrami coefficient, *n*, and half time of the ordering process, $t_{1/2}$, for the different quench temperatures are shown in Table 2. The Avrami coefficient varies between 4 and 5.8, and generally increases with increasing quench depth with respect to the LDOT temperature of the blend. The modulus at a given time during the quench experiment tends to increase with decreasing temperature (increasing quench depth.) In the case of quench temperatures of 150 °C and 155 °C there appears to be very little difference in *G'* at later stages of the ordering process. The ordering process is affected by two competitive forces: the thermodynamic driving force, which becomes greater with increasing quench depth; and the polymer chain mobility, which decreases with increasing quench depth. It is possible that over the temperature range between 150 and 155 °C the competitive effects strike a balance resulting in similar values of G' and similar kinetic parameters. The Avrami half-time shows little dependence on the quench temperature, indicating that chain mobility may not necessarily be the dominant factor in the ordering process in the temperature range under consideration.

Quench experiments were also performed on the 70/30 and 50/50 blends, the results of which are shown in Figure 7. These blends exhibited markedly different behavior than that observed for the 90/10 blend. The *G'* values for the 70/30 and 50/50 samples did not increase in a sigmoidal manner with time. In the case of the 70/30 blends, the samples quenched at 150 °C and 140 °C show a slight decrease at short times and almost no increase in *G'* at longer times. *G'* increases noticeably at longer times in the sample quenched to 160 °C, but the growth is slow, and may be due to crosslinking of the polymer.

Table 2. Avrami exponent '*n*' and ordering half-time '$t_{1/2}$' for 90/10 blend samples quenched at different temperatures. $\Delta T = T_{LDOT} - T_{quench}$ is the quench depth with respect to the LDOT.

Quench Temperature (°C)	**ΔT (°C)**	***n***	$t_{1/2}$ **(min)**
160	30	4.4	71
155	35	4	68
150	40	4.7	68
140	50	5.8	67

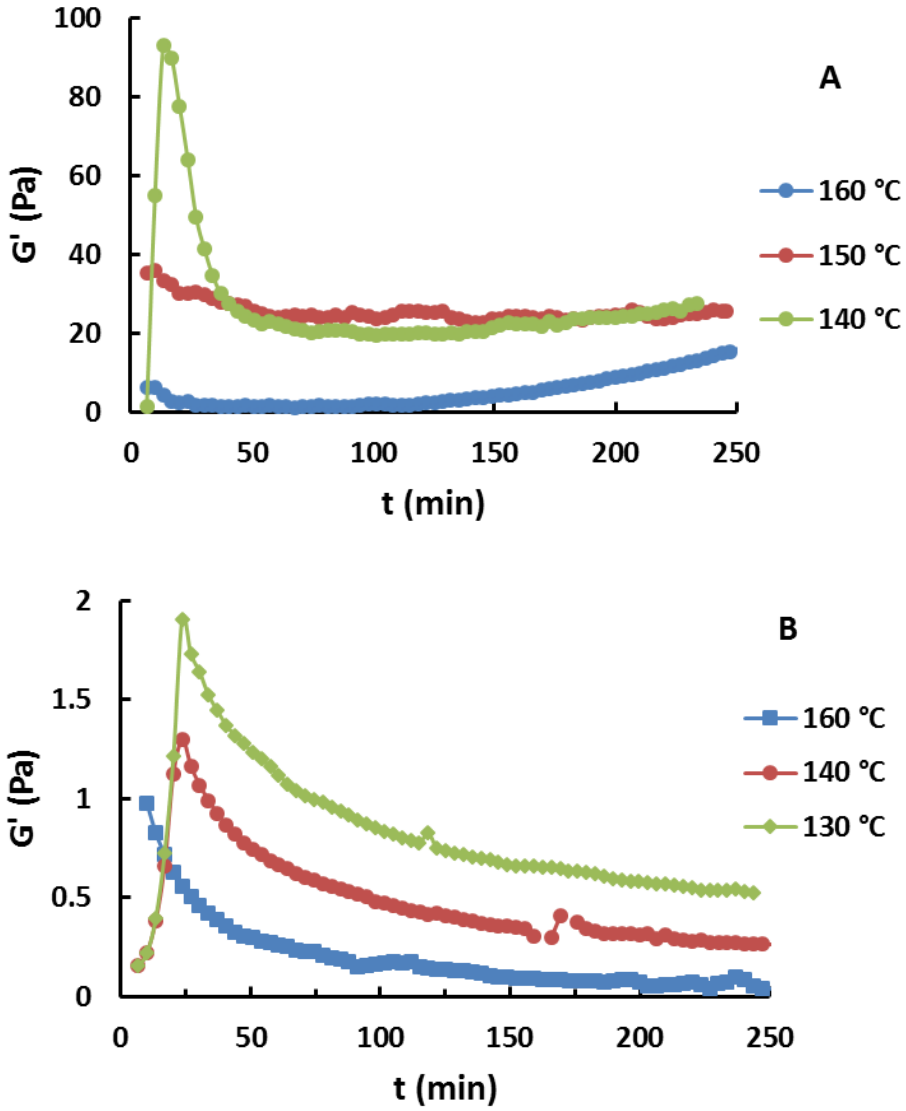

Figure 7. Evolution of shear storage modulus (*G'*) in (A) 70/30, and (B) 50/50 blend samples as a function of quench temperature. Strain: 0.5%, frequency: 0.01 Hz.

In the case of the 50/50 blends, the storage modulus increases sharply during the initial stage of microphase separation and then decreases consistently with time. The absence of growth at later stages of phase separation indicates a lack of ordering of the PS domains. It is interesting to note that the initial increase in *G'* becomes more prominent with decreasing quench temperature. This gradual change in the increase in *G'* will be discussed in the next section.

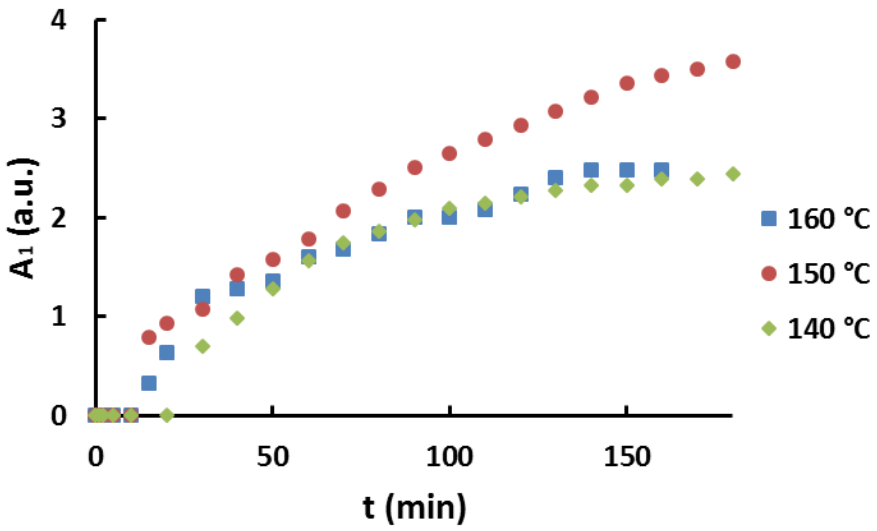

Figure 8. Evolution of the first Gaussian peak intensity (A_1) with time in 90/10 blend samples quenched to different temperatures.

The time evolution of the Gaussian peak intensity for the primary bcc peak (A_1) for 90/10 blends quenched from 240 °C to 160 °C, 150 °C, or 140 °C and then held isothermally is shown in Figure 8. The peak intensity begins to increase about 20 minutes after the quench, and the initial growth of A_1 is fastest in the sample quenched to 150 °C. The sample held at 150 °C also attains the highest final values of A_1, indicating that a greater fraction of the PS domains are arranged in a bcc-ordered morphology. The ordering process depends on two factors competing against each other: the thermodynamic driving force which is proportional to the quench depth relative to the LDOT (ΔT in table 2), and the polymer chain mobility, which decreases with decreasing quench temperature (or greater ΔT). Since the ordering process is fastest at 150 °C, compared to both higher and lower temperatures, and results in the highest degree of ordering, this temperature may be close to the optimum conditions for ordering.

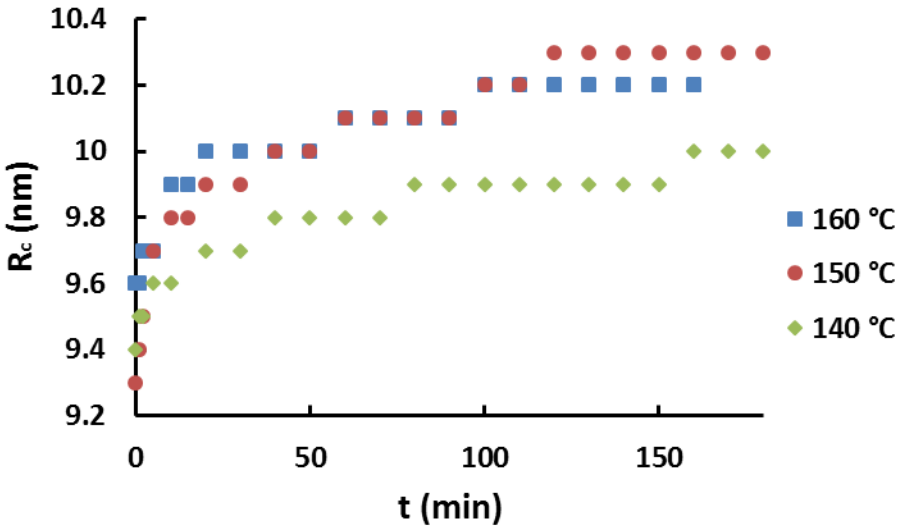

Figure 9. Evolution of PS core radius (R_c) with time in 90/10 blend samples quenched to different temperatures.

A plot of the PS core radius (R_c) as a function of time is depicted in Figure 9. R_c increases rapidly at short times (~30 minutes after quench) and then begins to plateau at longer times, and R_c values are higher for samples quenched at higher temperatures. For samples quenched to 160 °C and 150 °C, the maximum R_c values are 10.2 nm and 10.3 nm respectively. On the other hand, in the case of the sample quenched to 140 °C, the maximum R_c value is only 10 nm. It is likely that the size of the PS domains is dominated by the chain mobility, and as the quench temperature decreases, diffusion of the PS chains in the melt to form larger domains becomes more difficult. The R_c value determined at the end of quench experiment is slightly greater in the case of the sample quenched at 150 °C, again suggesting that this temperature is near the optimum value for growth of the ordered phase.

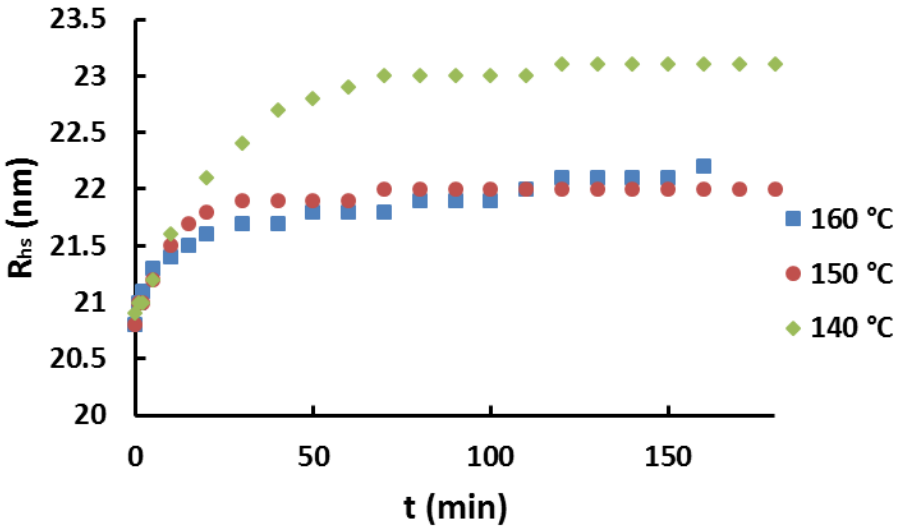

Figure 10. Evolution of hard-sphere radius (R_{hs}) with time in 90/10 blend samples quenched to different temperatures.

The hard-sphere radius (R_{hs}) values of 90/10 blend samples quenched to different temperatures (Figure 10) exhibits a sharp increase at short times (~30 minutes after quench), and a plateau at longer times. R_{hs} values for the sample quenched to 140 °C are significantly greater than those for samples quenched to higher temperatures. As the quench temperature decreases, the mobility of PS and polyisoprene chains decreases, which causes restricted polyisoprene chain mobility over a larger distance away from PS core. In the case of the samples quenched to 160 °C and 150 °C, the R_{hs} values reach a plateau about 30 minutes after the experiment begins. In the case of the sample quenched to 140 °C, the plateau is reached after about 70 minutes. Thus, lower quench temperatures lead to smaller PS domains (R_c), larger hard-sphere radii (R_{hs}), and slower kinetics the for 90/10 blends.

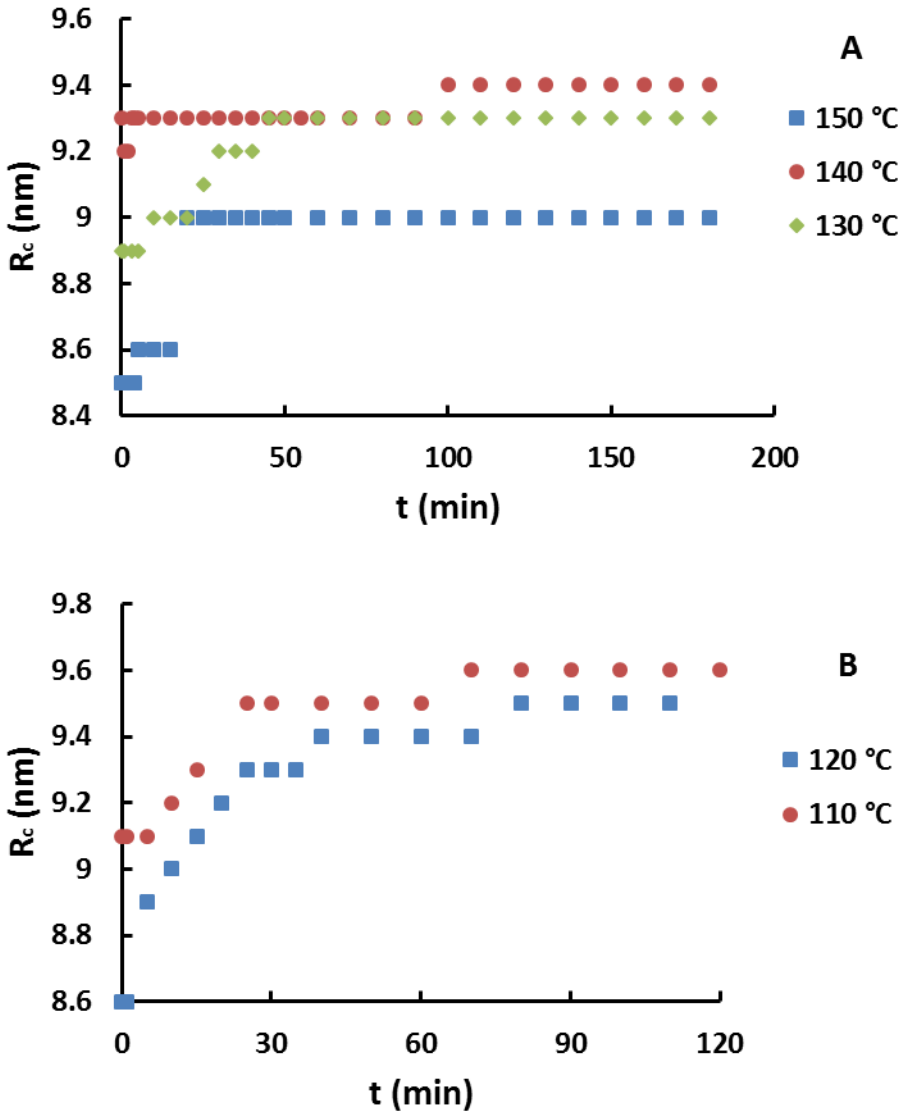

Figure 11. Evolution of PS core radius (R_c) in (A) 70/30 and (B) 50/50 blend samples quenched to various temperatures.

The evolution of R_c in the 70/30 and 50/50 blends (Figure 11) is slightly different than that observed in the 90/10 blend samples. The R_c values in the later stages of the quench experiments are lower in the 70/30 and 50/50 blends compared to the 90/10 blend samples. Also, the R_c values tend to increase in the 70/30 and 50/50 blend samples as quench temperature decreases, which is the opposite of the trend observed in the 90/10 blend samples. The lower values of R_c in the 70/30 and 50/50 blends indicate that the increased tackifier content in the blend hampers the growth of the PS domains. Since the T_g of the tackifier is much higher than that of the polyisoprene chains,

it is likely that tackifier molecules reduce the free volume of the isoprene matrix, making PS chain diffusion more difficult.

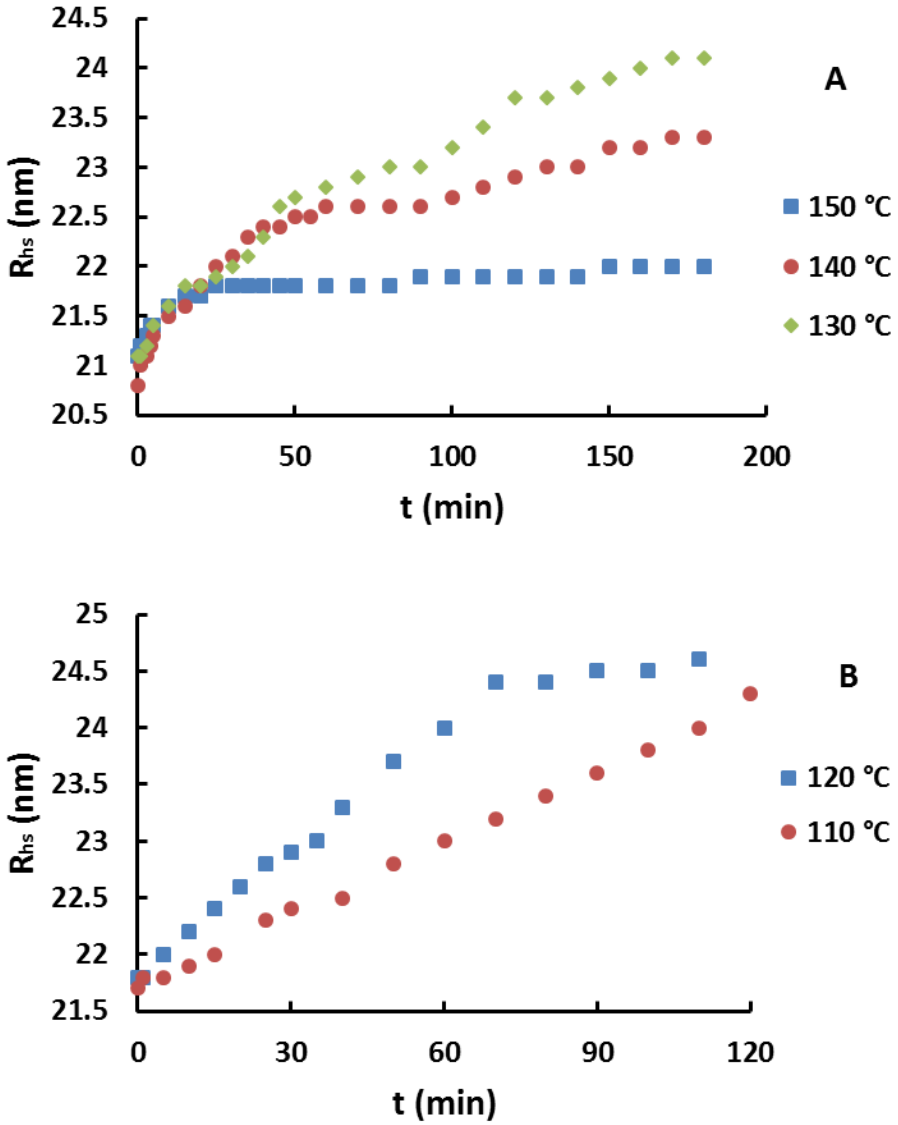

Figure 12. Evolution of hard-sphere radius (R_{hs}) in (A) 70/30 and (B) 50/50 blend samples quenched to various temperatures.

The time-evolution of hard-sphere radius (R_{hs}) in the 70/30 and 50/50 blends are shown in Figure 12. For the 70/30 sample quenched to 150 °C, there is little increase in R_{hs} over the experimental time-frame. On the other hand, R_{hs} values show significant increases at longer times for quench temperatures of 140 °C and 130 °C. The 70/30 blend sample quenched to lower

temperatures generally shows a greater R_{hs} at a given time, which is likely due to lower mobility of the polymer chains. R_{hs} values of the 70/30 blends 3 hours after the quench are close to those obtained for 90/10 blend samples after 3 hours. Since R_{hs} is also influenced by the average spacing between PS domains, this result indicates that increasing the amount of tackifier from 10 to 30 wt. % does not cause significant swelling of the polyisoprene phase under experimental conditions. The R_{hs} values for the 50/50 blend do not exhibit a sharp increase at shorter times, and at a quench temperature of 110 °C the R_{hs} values do not reach a plateau during the experimental time-frame. Since this temperature is very close to the T_g of PS chains, it is likely that the microphase separation process is slower due to the significantly lower mobility of the copolymer chains.

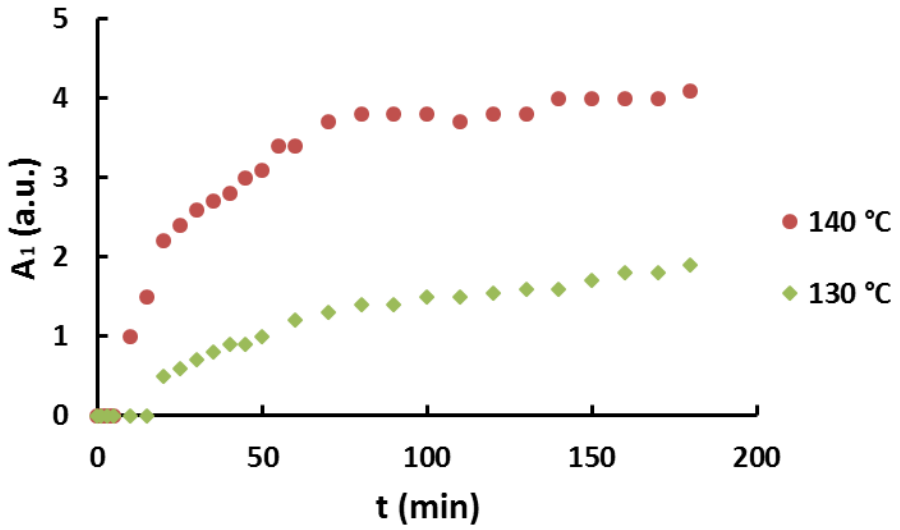

Figure 13. Evolution of A_1 with time in 70/30 blend samples quenched to different temperatures.

The evolution of A_1 following a quench from 240 °C is shown in Figure 13 for the 70/30 blend. The 70/30 sample exhibited no ordered peak when quenched to 150 °C, indicating this temperature was high enough to hamper the ordering of PS domains. 70/30 blends quenched to 140 °C and 130 °C do show the development of a Gaussian peak. The peak intensities are greater at 140 °C than at 130 °C, indicating increased ordering at the higher temperature. This suggests that the balance between thermodynamic driving force and polymer chain mobility occurs near

140 °C in the 70/30 blends, and that the optimum temperature for ordering decreases with increasing tackifier content.

4.5.3. Microphase separation mechanism. Microphase separation in block copolymer blends during quench experiments can proceed via a 'Nucleation and Growth' or 'Spinodal Decomposition' mechanism depending on the block copolymer and the experimental conditions. In nucleation and growth, large-scale composition fluctuations lead to the formation of nuclei, which then grow via a diffusion-controlled process. In the case of spinodal decomposition, phase separation occurs due to the spontaneous growth of small composition fluctuations. Often, spinodal decomposition leads initially to the formation of an interconnected morphology. However, the final morphology of the material may not be dictated by the mechanism during the early stages of phase separation, but by diffusion controlled coarsening and ripening of the microdomains.

Rheological analysis of the copolymer - tackifier blends under consideration sheds light on the possible microphase separation mechanism in the melt. In 90/10 blends (Figure 7), *G'* remains nearly constant during the initial stage of quench experiments, which resembles the incubation period of a nucleation and growth process. At later stages, *G'* grows in a sigmoidal manner, which is well fit by the Avrami model. The nucleation and growth mechanism is also confirmed in the SAXS analysis, especially in the development of an ordered Gaussian peak (Figure 9). The integrated peak area, A_1, begins to increase approximately 15 – 20 minutes after the samples are quenched to the desired temperatures, suggesting the existence of an incubation period. At longer times, the A_1 values reach a plateau indicating the completion of the growth of the ordered phase.

The 50/50 blends show significantly different patterns in both *G'* and the Percus-Yevick hard-sphere model parameters. *G'* increases sharply during the initial stage following the quench, indicating enhanced composition fluctuations due to quenching the material below the critical temperature. However, when composition fluctuations saturate at later times, *G'* decreases continually for all quench temperatures. This behavior indicates that the microphase separation in 50/50 blends occurs via rapid demixing of PS chains and subsequent domain, which is indicative of a spinodal decomposition mechanism. The 70/30 blends exhibited different behavior wherein G' remained nearly constant after an initial decrease, but began to increase at longer times. The change in the rheological behavior of blends with respect to their composition is shown in Figure 14.

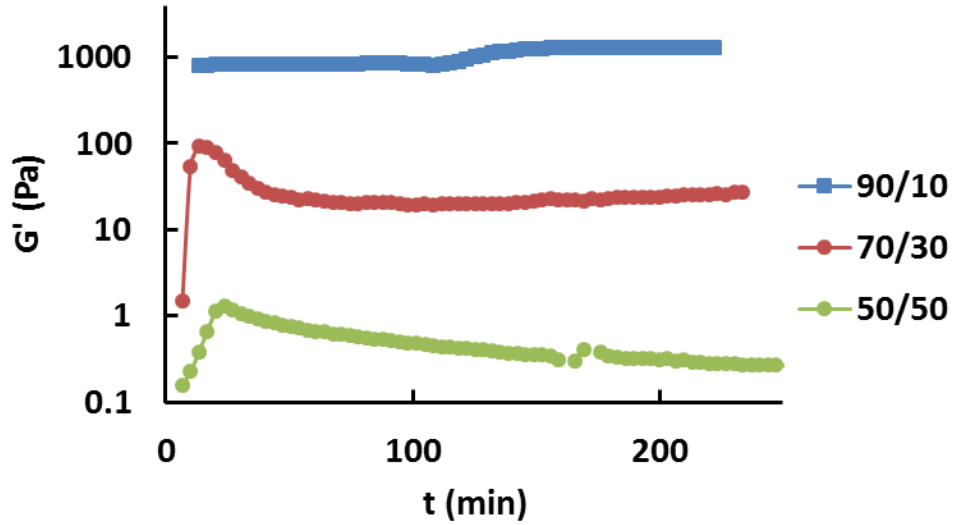

Figure 14. Evolution of *G'* in 90/10, 70/30 and 50/50 blend samples quenched to 140 °C.

The SAXS analysis of the 70/30 blends suggests a bcc-ordering of PS domains at 140 °C and 130 °C, but the rheological measurements do not show a sigmoidal growth pattern in the later stages of quench experiments. However, *G'* remains reasonably constant for different periods of time and then begins to increase slightly at longer times. Based on prior phase separation kinetics studies in polymer blends,[29] the absence of *G'* growth during a nucleation and growth type

microphase separation process in 70/30 blends can be justified. The initial growth in *G'* observed at 140 °C can be assigned to enhanced composition fluctuations during the early stages of phase separation.[30] Of the 70/30 blend samples, only the sample quenched to 140 °C shows an increase and subsequent decrease in *G'*. The frequency used in this analysis (0.01 Hz) is small enough so that the elastic response from the microphase separated domains can be considered negligible, so *G'* should primarily be a function of interfacial tension.[31] The interfacial tension depends on two factors – the interfacial area and domain deformability. If total interfacial area is the dominating factor, domain growth, which results in a decrease in area, should cause a decrease in *G'*. If domain deformability is the dominating factor, *G'* should increase with time. Since the SAXS data for the 70/30 blends indicates an increase in PS domain size (R_c) as well as the fraction of PS domains in the bcc-ordered morphology, it is likely that the total interfacial area is the factor dominating the rheological response in the blend following the initial formation of enhanced composition fluctuations. At longer times, bcc-ordered domains begin to grow causing the increase in *G'*. Hence, the initial phase separation in the 70/30 blends appears to follow a spinodal decomposition type process, followed by coarsening and the much slower nucleation and growth of the ordered phase.

The microphase separation mechanism changes based on the amount of tackifier in the blends. Thus, it is helpful to discuss the nucleation barrier (ΔF^*) in block copolymers near the spinodal boundary, which is related to the critical temperature (T_c) as follows:

$$\frac{\Delta F^*}{T_c} \propto N^{d/2-1}\left[1-\frac{T}{T_c}\right]^{2-d/2}\left[\frac{\psi-\psi_{sp}}{\psi_{coex}}\right]^{3-d/2} \quad \text{..... (4)}$$

where N is the degree of polymerization, d is the dimensionality of unit structure, ψ, ψ_{sp}, and ψ_{coex} are order parameters at temperature T, the spinodal, and the two-phase coexistence

respectively.[32] With respect to the block copolymer (Kraton® D1161), the addition of a low molecular weight resin (tackifier) leads to a decrease in N as well as in T_c, as both the LDOT and DMT occur at progressively lower temperatures with increasing tackifier content (Table 2). Thus, ΔF^* at a given temperature (T) should decrease with increasing tackifier content. As ΔF^* decreases, a shift from a nucleation and growth mechanism to a spinodal decomposition mechanism is expected.[32,33] This behavior is confirmed by the data for the block copolymer/tackifier system. The 90/10 blend has the highest LDOT and DMT, and exhibits a long incubation period followed by sigmoidal growth of shear storage modulus (G') at longer times. The 70/30 blend exhibits a decrease in LDOT as well as DMT, and little growth in G', which suggests spinodal decomposition followed by a very slow ordering process. In the case of the 50/50 blend, the G' indicates that the decrease in ΔF^* is large enough to drive the system out of the nucleation and growth regime, and into the spinodal decomposition regime where local composition fluctuations dominate the microphase separation process.

4.6. Conclusion

The morphology and microphase separation kinetics in the blends of a styrene-isoprene based block copolymer (Kraton® D1161) and a C_5 aliphatic tackifier resin (Piccotac™ 1095) were analyzed using a morphological model previously proposed[22] for Kraton® D1161. The correlation of SAXS and rheological analysis suggest that the copolymer - tackifier blends can be considered as concentrated solutions of the copolymer wherein the tackifier acts as a selective solvent for the polyisoprene chains. Variations in the morphological features of the blends, including the polystyrene core radius, polystyrene domain ordering, and hard-sphere radius can be explained on the basis of blend composition and quench temperature. Increasing the amount of tackifier in the blend reduces the LDOT and DMT, as observed in rheological and SAXS analysis. The

incompatibility of polystyrene and tackifier results in a gradual change in the microphase separation mechanism in quenched blend samples. As the tackifier content increases from 10 to 50 wt. %, the diffusion of polystyrene chains in the melt becomes more difficult. This leads to a smaller size and slower growth of bcc-ordered polystyrene domains, and eventually a shift in the microphase separation mechanism from 'nucleation and growth' for the 10 wt. % tackifier blends to 'spinodal decomposition' for the 50 wt. % tackifier blends, as indicated by the time-dependent rheological behavior. The temperature dependence of the phase separation and ordering kinetics clearly demonstrates the competition between thermodynamic driving force (i.e. quench depth) and decreasing chain mobility at lower temperatures, as the fastest kinetics were observed at an intermediate quench temperature. The impact of processing temperature and final blend morphology on the adhesive properties of the blends has not yet been studied.

AUTHOR INFORMATION

Corresponding Author

*Email: martinsm@vt.edu

Present Address

§Lixia Rong, Center for Advanced Microstructures & Devices, Louisiana State University, Baton Rouge, Louisiana 70806, United States

Author Contributions

The manuscript was written through contributions of all authors. All authors have given approval to the final version of the manuscript.

Notes

The authors declare no competing financial interest.

ACKNOWLEDGEMENT

Use of the National Synchrotron Light Source, Brookhaven National Laboratory, was supported by the U.S. Department of Energy, Office of Science, Office of Basic Energy Sciences, under Contract No. DE-AC02-98CH1088. The authors thank Dr. Richey Davis (Virginia Tech, Chemical Engineering) for access to the AR-G2 rheometer used in this work. The authors also thank 3M® Corporation for providing the materials used in this work. One of the authors (Eugene Joseph) would like to thank 3M® Corporation for financial support. The authors would like to acknowledge Prof. Benjamin Hsiao (Stony Brook University) for his help in scheduling SAXS experiments at the Brookhaven National Laboratory.

4.7. References

(1) Sasaki, M.; Adachi, M.; Kato, Y.; Fujii, S.; Nakamura, Y.; Urahama, Y.; Sakurai, S. *Journal of Applied Polymer Science* **2010**, *118*, 1766.

(2) Gibert, F. X.; Marin, G.; Derail, C.; Allal, A.; Lechat, J. *The Journal of Adhesion* **2003**, *79*, 825.

(3) Roos, A.; Creton, C. *Macromolecules* **2005**, *38*, 7807.

(4) Sasaki, M.; Nakamura, Y.; Fujita, K.; Kinugawa, Y.; Iida, T.; Urahama, Y. *Journal of Adhesion Science and Technology* **2005**, *19*, 1445.

(5) Kraus, G.; Rollmann, K. W.; Gray, R. A. *The Journal of Adhesion* **1979**, *10*, 221.

(6) Class, J. B.; Chu, S. G. *Journal of Applied Polymer Science* **1985**, *30*, 805.

(7) Hino, K.; Ito, T.; Toyama, M.; Hashimoto, H. *Journal of Applied Polymer Science* **1975**, *19*, 2879.

(8) Class, J. B.; Chu, S. G. *Journal of Applied Polymer Science* **1985**, *30*, 815.

(9) Class, J. B.; Chu, S. G. *Journal of Applied Polymer Science* **1985**, *30*, 825.

(10) O'Connor, A. E.; Macosko, C. W. *Journal of Applied Polymer Science* **2002**, *86*, 3355.

(11) Sasaki, M.; Fujita, K.; Adachi, M.; Fujii, S.; Nakamura, Y.; Urahama, Y. *International Journal of Adhesion and Adhesives* **2008**, *28*, 372.

(12) Aubrey, D. W. *Rubber Chemistry and Technology* **1988**, *61*, 448.

(13) Sherriff, M.; Knibbs, R. W.; Langley, P. G. *Journal of Applied Polymer Science* **1973**, *17*, 3423.

(14) Hanley, K. J.; Lodge, T. P.; Huang, C.-I. *Macromolecules* **2000**, *33*, 5918.

(15) Lodge, T. P.; Pudil, B.; Hanley, K. J. *Macromolecules* **2002**, *35*, 4707.

(16) Matsen, M. W. *Physical Review Letters* **1995**, *74*, 4225.

(17) Tanaka, H.; Hasegawa, H.; Hashimoto, T. *Macromolecules* **1991**, *24*, 240.

(18) Winey, K. I.; Thomas, E. L.; Fetters, L. J. *Macromolecules* **1992**, *25*, 2645.

(19) Lammertink, R. G. H.; Hempenius, M. A.; Thomas, E. L.; Vancso, G. J. *Journal of Polymer Science Part B: Polymer Physics* **1999**, *37*, 1009.

(20) Kane, L.; Norman, D. A.; White, S. A.; Matsen, M. W.; Satkowski, M. M.; Smith, S. D.; Spontak, R. J. *Macromolecular Rapid Communications* **2001**, *22*, 281.

(21) Berglund, C. A.; McKay, K. W. *Polymer Engineering & Science* **1993**, *33*, 1195.

(22) Dixit, N.; Pape, A.; Rong, L.; Joseph, E.; Martin, S. M. 2014.

(23) Kinning, D. J.; Thomas, E. L. *Macromolecules* **1984**, *17*, 1712.

(24) Harkless, C. R.; Singh, M. A.; Nagler, S. E.; Stephenson, G. B.; Jordan-Sweet, J. L. *Physical Review Letters* **1990**, *64*, 2285.

(25) Han, C. D.; Kim, J.; Kim, J. K. *Macromolecules* **1989**, *22*, 383.

(26) Han, C. D.; Vaidya, N. Y.; Kim, D.; Shin, G.; Yamaguchi, D.; Hashimoto, T. *Macromolecules* **2000**, *33*, 3767.

(27) Hamley, I. W. *The physics of block copolymers*; Oxford University Press: Oxford; New York, 1998.

(28) Avrami, M. *The Journal of Chemical Physics* **1940**, *8*, 212.

(29) Niu, Y.-H.; Wang, Z.-G. *Macromolecules* **2006**, *39*, 4175.

(30) Kapnistos, M.; Hinrichs, A.; Vlassopoulos, D.; Anastasiadis, S. H.; Stammer, A.; Wolf, B. A. *Macromolecules* **1996**, *29*, 7155.

(31) Palierne, J. F. *Rheol. Acta* **1990**, *29*, 204.

(32) Binder, K. *Physical Review A* **1984**, *29*, 341.

(33) Binder, K. *Physica A: Statistical Mechanics and its Applications* **1995**, *213*, 118.

Chapter 5

Thermal and Morphological Analysis of Styrene-(Isoprene-co-Butadiene)-Styrene Block Copolymer and its Pressure-Sensitive Adhesive Compositions

Thermal and Morphological Analysis of Styrene-(Isoprene-*co*-Butadiene)-Styrene Block copolymer and its Pressure-Sensitive Adhesive Compositions

Ninad Dixit[†], *Alicia Pape*[‡], *Sahel Aminian*[‡], *Byeongdu Lee*[|], *Eugene Joseph*[‡], *and Stephen M. Martin*[‡]

[†]Department of Chemistry, Virginia Polytechnic Institute and State University, Blacksburg, Virginia 24061, United States

[‡]Department of Chemical Engineering, Virginia Polytechnic Institute and State University, Blacksburg, Virginia 24061, United States

[|] X-ray Sciences Division, Advanced Photon Source, Argonne National Laboratory, 9700 S. Cass Ave., Argonne, Illinois 60439, United States

5.1. Abstract

The thermal and morphological behavior of a commercial styrene-(isoprene-co-butadiene)-styrene block copolymer (Kraton® D1171) and its blends with two low molecular resins (tackifiers) was studied using oscillatory shear rheology and time resolved small-angle X-ray scattering (SAXS) analysis. The compatibility of the tackifier with the polystyrene block has a significant impact on the phase behavior of the copolymer – tackifier blends, yielding different transition temperatures for the same blend composition containing different tackifiers. The order-disorder transition (ODT) temperature in Kraton® D1171 and the blends is characterized by changes in the shear storage modulus (*G'*) and peak intensity in the SAXS profiles, which decreases to differing extents depending on the tackifier compatibility with polystyrene. The microphase separation kinetics in

melts of Kraton® D1171 and its blends with each tackifier was studied using oscillatory shear rheology. The time-evolution of *G'* following a temperature quench indicate a strong dependence of the ordering process of microphase separated polystyrene domains on polymer chain mobility. The kinetics of ordering become much slower high tackifier content in the blends.

5.2. Introduction

Styrene-based block copolymers are commonly used in pressure-sensitive adhesives when blended with low molecular weight, high glass transition temperature (T_g) resins (tackifiers).[1] The microphase separated morphology of triblock copolymers leads to elastomeric behavior of the adhesive blends at service temperatures.[2] The tackifier adjusts the mechanical modulus of the adhesive composition as well as the T_g of the soft segments in the block copolymer (usually polyisoprene or other polydienes) so that the blend becomes tacky and has the desired mechanical strength. An analogous diblock copolymer is also added to the copolymer – tackifier blend to achieve the desired tack and mechanical properties.[3,4] In styrene-based block copolymer – tackifier blends, the tackifier is usually miscible with the soft block (i.e. polydienes).

Hot-melt pressure-sensitive adhesives (HMPSAs) are block copolymer – tackifier blends that are processed at high temperatures in a molten state, and do not require the use of volatile solvents or water. The molten adhesives are applied onto a substrate at high temperatures, and then rapidly cooled for the purpose of die-cutting or other processing steps.[3] Since the microphase separation in the block copolymer is responsible for the mechanical strength of adhesives, it is important to understand the effect of the tackifier and the adhesive processing temperature on the evolution of microphase separated morphologies in block copolymer – tackifier blends. Although a number of tackifiers are available commercially, their compatibility with the base block copolymer is the most important selection criterion.[5] Significant research has been reported on the effect of tackifier

structure[6], molecular weight[7], and concentration in the blend[8] on the morphology,[9] and viscoelastic as well as performance properties of the adhesives[2]. However, these studies are focused on the adhesive morphology at service temperature. We have previously reported on the microphase separation kinetics in the melts of a commercially available block copolymer (Kraton® D1161), as well as its blends with a commercially available tackifier (Piccotac™ 1095).[10,11] However, the effect of copolymer – tackifier compatibility on the kinetics of ordering and phase separation in adhesive blends has not previously been studied.

Herein we report the rheological and morphological analysis of a commercially available block copolymer Kraton® D1171, in which polystyrene (PS) chains form the end blocks, and the middle or soft (low T_g) block consists of isoprene as well as butadiene units (IB). Styrenic block copolymers with both isoprene and butadiene segments in the mid-block have attracted significant commercial interest and have been proposed as an alternative to the conventional styrene-isoprene block copolymers for adhesive formulations and film applications.[12] To date, the rheological and morphological behavior of Kraton® D1171 has not been reported. We also report on the thermal and morphological behavior of two series of adhesive compositions obtained by blending Kraton® D1171 with the commercially available tackifiers Sylvalite® RE 100L and Piccotac™ 1095. The effect of tackifier content and block copolymer – tackifier compatibility on the phase behavior and the adhesive blends is determined via analysis of the shear modulus and small-angle X-ray scattering (SAXS) measurements. The processing kinetics of the ordered structure in Kraton® D1171 is studied via the time-evolution of the shear modulus, and a possible ordering mechanism for the microphase separated polystyrene (PS) domains is discussed.

5.3. Experimental Sections

5.3.1. Materials and sample preparation. Kraton® D1171, Sylvalite® RE 100L, Piccotac™ 1095, and Irganox® 1010 were used without further purification. Kraton® D1171 is a mixture of diblock and triblock copolymers containing 19 % polystyrene. Sylvalite® RE 100L is a pentaerythritol - rosin ester with a softening point of 100 °C, whereas Piccotac™ 1095 is a C_5 aliphatic resin with a softening point of 94 °C. Gel permeation chromatography (GPC) analysis of Kraton® D1171 was carried out using chloroform solvent and a polystyrene standard. The molecular weights of the triblock and diblock copolymers are shown in Table 1.

Table 1. GPC (equipped with refractive index detector) analysis of Kraton® D1171

	M_n (kDa)	M_w (kDa)	PDI
Triblock	124.6	129.9	1.043
Diblock	65.0	65.4	1.006

Solvent grade toluene was used to prepare 20 % (w/w) solutions of copolymer – tackifier mixtures. For each tackifier, a series of four solutions was prepared with tackifier content of 0, 10, 30, and 50 wt. %, keeping the total solids content constant. The solutions were dried at room temperature for two weeks and then in vacuum at room temperature for two days. The final dried samples were approximately 2 mm thick.

5.3.2. Oscillatory Rheology. Rheological experiments were performed on a TA Instruments AR-G2 rheometer, equipped with 25 mm diameter steel plates. Nitrogen (N_2) gas was constantly circulated in the sealed furnace to maintain a neutral environment. Fast cooling during quench-isothermal experiments was achieved by using a liquid N_2 cooling system. At the beginning of

each experiment, a thickness of 1000 μm was achieved by pressing the samples between the steel plates at 120 °C. In the case of the temperature ramp experiments, the sample was pressed between the rheometer plates at 120 °C to achieve the desired thickness and establish good contact between the sample and plates. The temperature was then rapidly brought down to and equilibrated at 50 °C followed by the desired temperature ramp. A strain of 0.01 % for temperature ramp and 0.5 % for isothermal experiments was used. An oscillation frequency of 0.01 Hz was used during isothermal experiments to track the growth of the microphase separated domains.

5.3.3. Small angle X-ray scattering (SAXS). SAXS measurements were performed on beamline 12-ID-B at the Advanced Photon Source (APS) at Argonne National Laboratory. A 12 keV X-ray beam and Pilatus 2M detector was used to obtain the SAXS data. A Linkam TMS600 hot stage was used to control the sample temperature.

5.4. Results and Discussion

5.4.1. Determination of phase transitions. Temperature ramp experiments for 100/0 and 90/10 blends of Kraton® D1171 and Sylvalite® RE 100L show two thermal transitions (Figure 1) where *G'* exhibits a discernable response. The decrease in *G'* at lower temperatures (~100 °C) corresponds to the glass transition of the polystyrene (PS) chains in the triblock and diblock copolymers. The transition observed at higher temperatures (~200 °C) corresponds to the disordering of the PS domains. In the case of the 70/30 and 50/50 blends, only one broad transition is observed. The T_g of the blends decreases with increasing amount of tackifier in the blends, suggesting that the tackifier is compatible with PS chains. Thus, the decrease in *G'* observed for blends containing 30 and 50 wt. % tackifier might correspond to both the glass transition of the PS

chains and the mixing of the PS and IB blocks. As such, it appears that at 30 and 50 wt. % tackifier content, the tackifier acts as a solvent for both PS and IB blocks.

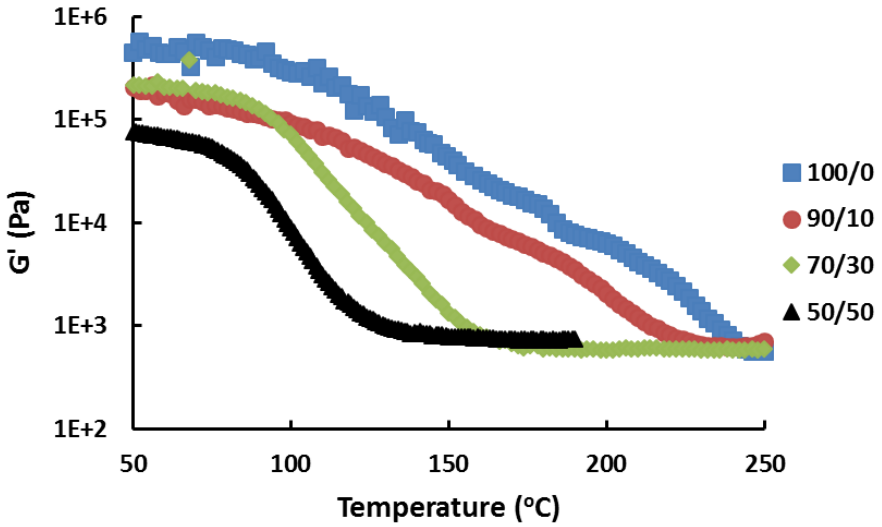

Figure 1. Temperature ramp analysis of Kraton® D1171 – Sylvalite® RE 100L blends. Ramp rate: 3 °C/min, frequency: 1Hz, strain: 0.01 %

Figure 2 shows the temperature ramp analysis of the Kraton® D1171 – Piccotac™ 1095 blends. All the blends show two prominent transitions characterized by a significant decrease in *G'*. The T_g of the PS chains is not significantly affected by the increasing tackifier content in these blends, which suggests that Piccotac™ 1095 is not compatible with the PS blocks. This analysis is consistent with our previous study involving another styrene-diene copolymer system.[11] The high temperature transition corresponds to the disordering of PS domains, which occurs at progressively lower temperatures as more tackifier is added in the blend. This trend suggests that Piccotac™ 1095 restricts the ordering of PS domains.

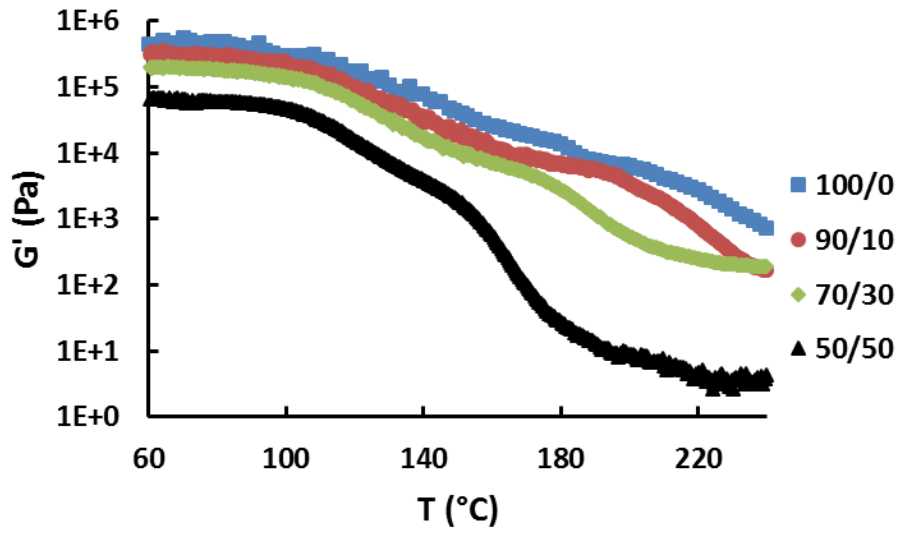

Figure 2. Temperature ramp analysis of Kraton® D1171 – Piccotac™ 1095 blends. Ramp rate: Ramp rate: 3 °C/min, frequency: 1Hz, strain: 0.01 %

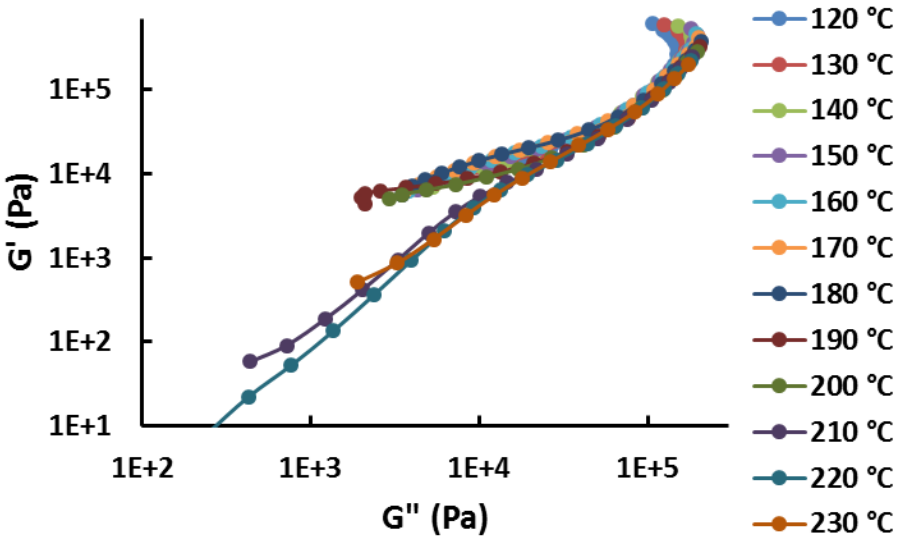

Figure 3. *G'* vs *G"* plots of Kraton® D1171

The molecular origins of the thermal transitions can be determined by multifrequency rheology analysis of the copolymer – tackifier blends. In these experiments, the *G'* values obtained at a fixed temperature over a range of frequencies are plotted against corresponding *G"* values to generate plots as shown in Figure 3. The slope of *G'* vs *G"* plots changes when a multi-phase system undergoes a phase transition[13], and the plots collapse at high temperatures indicating a single phase-like rheological behavior.[14] In Kraton® D1171, the *G'* vs *G"* plots change slope

between 200 °C and 210 °C, and the plots above 210 °C seem to collapse indicating single phase behavior. Since Kraton® D1171 contains 19% PS, the change in slope observed between 200 °C and 210 °C can be assigned to the disordering of hexagonally packed cylinders.[15]

Figure 4 shows the *G'* vs *G"* plots for blends of Kraton® D1171 and Sylvalite® RE 100L. The addition of tackifier results in a clear difference in rheological behavior. The slope of the plots for the 90/10 blend (Figure 4A) change over a wider temperature range compared to pure Kraton® D1171 (150 – 200 °C), and the plots begin to collapse at ~200 °C. In the case of the 70/30 blend (Figure 4B), the *G'* vs *G"* plots are parallel over a wide temperature range before collapsing onto each other. Han et al have attributed parallel *G'* vs *G"* plots to the presence of microphase separated disordered spheres in highly asymmetric block copolymers.[14] The PS content in the 70/30 blend is 13.3%, which makes the system highly asymmetric in composition. Hence, PS chains are likely to form spherical domains in the 70/30 and 50/50 blends as opposed to the cylindrical domains observed in pure Kraton® D1171. The presence of disordered spheres suggests that the collapse of the *G'* vs *G"* plots corresponds to the demicellization – micellization transition (DMT) observed in highly asymmetric block copolymers.[14] The *G'* vs *G"* plots in the 50/50 blend collapse at 90 °C, which means that the blend behaves as a single phase system at higher temperatures. In addition, the plots at 70 °C and 80 °C are parallel, also indicating the presence of disordered spheres.

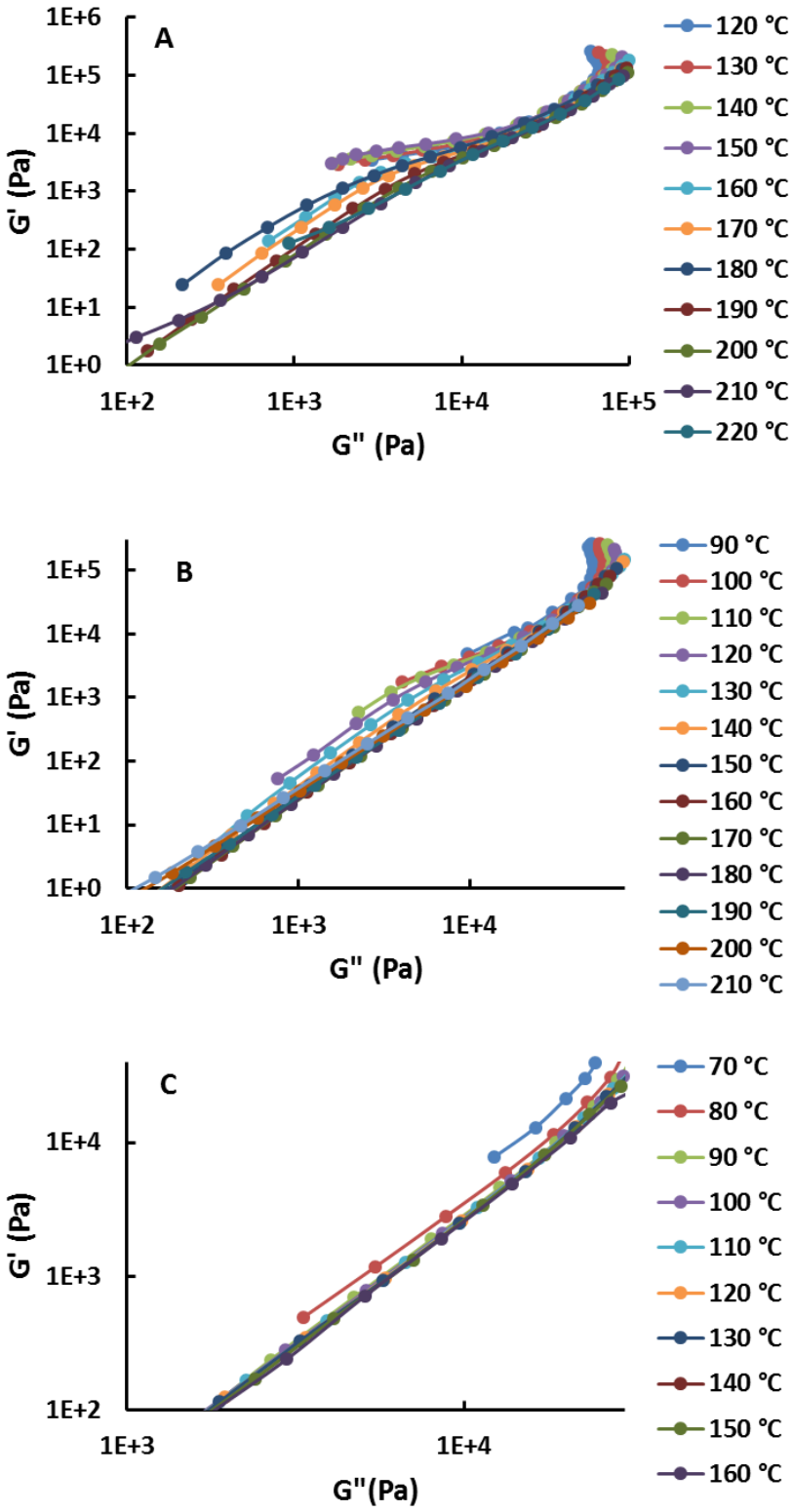

Figure 4. *G'* vs *G''* plots of (A) 90/10, (B) 70/30 and (C) 50/50 Kraton® D1171 - Sylvalite® RE 100L blends.

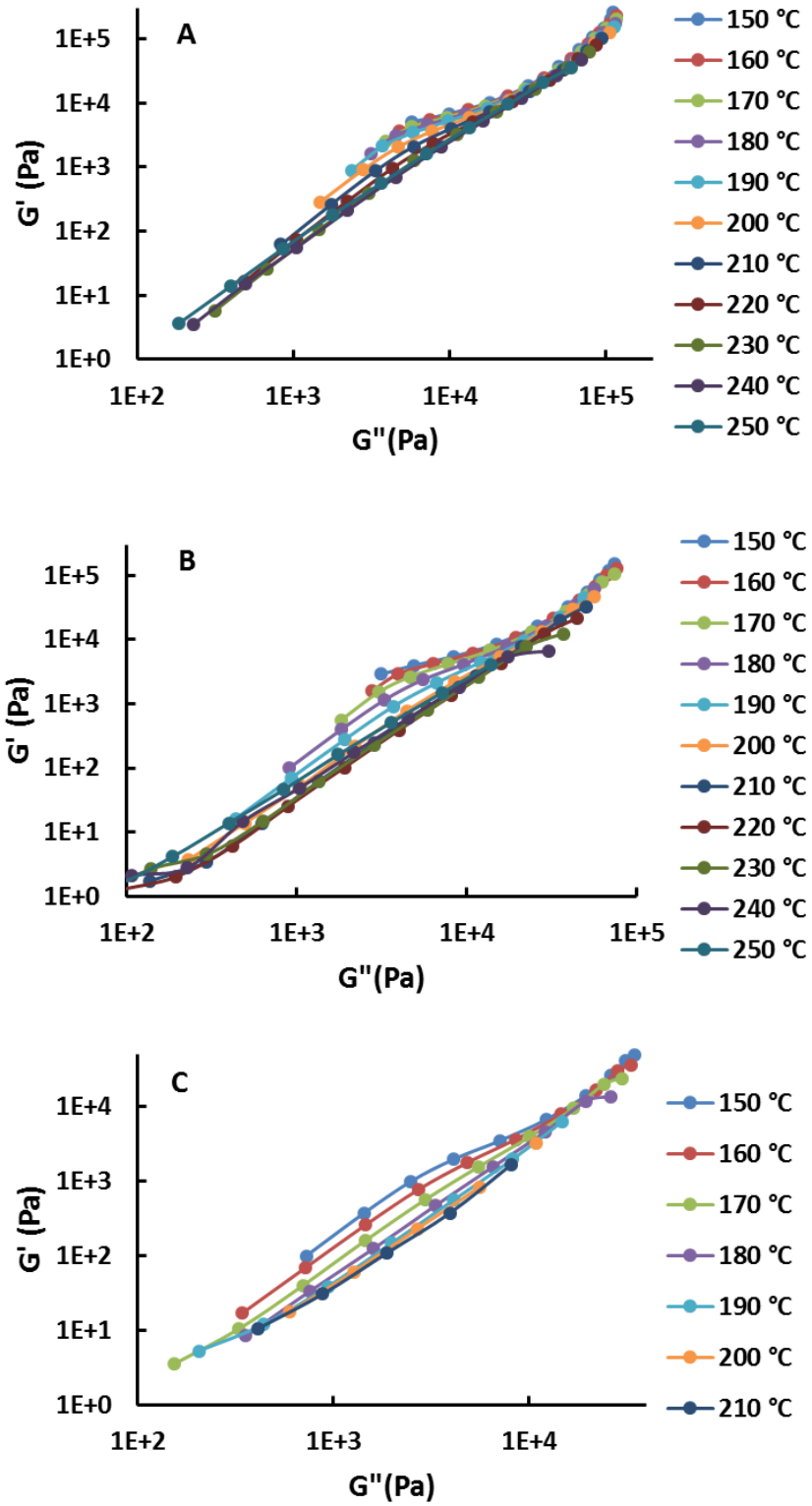

Figure 5. *G'* vs *G"* plots of (A) 90/10, (B) 70/30 and (C) 50/50 of Kraton® D1171 – Piccotac™ 1095 blends.

The rheological behavior of Kraton® D1171 – Piccotac™ 1095 blends is shown in Figure 5. The temperature at which the *G'* vs *G"* plots collapse decreases with increasing tackifier content in the blends. However, the change in the slope of plots is clearer in Piccotac™ 1095 blends as compared to Sylvalite® RE 100L blends. The temperature at which the *G'* vs *G"* plots collapse is consistently higher in the Kraton® D1171 – Piccotac™ 1095 blends for a given composition (Table 2). These results suggest that the Piccotac™ 1095 tackifier is less compatible with the PS blocks compared to Sylvalite® RE 100L. The microphase separated PS blocks form spherical domains upon addition of tackifier, due to the reduced PS fraction. The observed change in the microstructure is consistent with the theoretical predictions of Matsen and Bates.[16]

Table 2. ODT and DMT temperatures determined by the multifrequency analysis of Kraton D1171 blends as a function of blend composition

	ODT/DMT Temperature (°C)	
	Sylvalite® RE 100L	**Piccotac™ 1095**
100/0	210	210
90/10	190	210
70/30	150	200
50/50	90	180

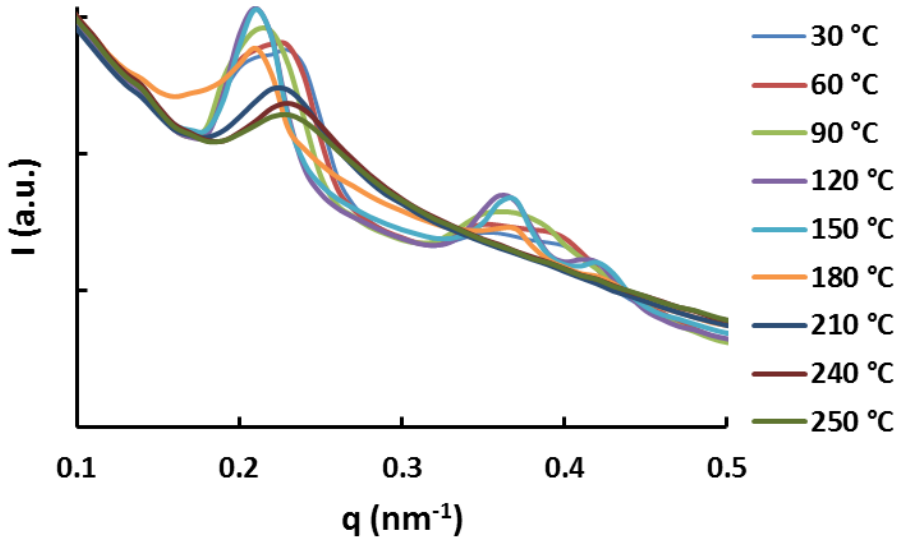

Figure 6. SAXS patterns of Kraton® D1171 at various temperatures during heating. Ramp rate 2 °C/min.

Blends of Kraton® D1171 were subjected to variable temperature SAXS analysis in order to identify the morphological transitions. Figure 6 shows SAXS profiles obtained at various temperatures in Kraton® D1171. The profiles show the primary scattering maximum (q_1) at $q \sim 0.23$ nm^{-1}, which shifts with temperature. The secondary peak appears at $q_2 \sim \sqrt{3}q_1$, and the tertiary peak at $q_3 \sim \sqrt{4}q_1$ indicating presence of hexagonally packed cylindrical (*hcp*) PS domains. The secondary and tertiary peaks are broad at lower temperatures, and become sharper at temperatures above 90 °C. This is an indication of reordering of the PS domains above the T_g of polystyrene. Since all the blends are solution cast and annealed at room temperature, it is likely that a significant fraction of the PS blocks are not initially part of the ordered structure. These blocks have enough mobility above the polystyrene T_g to form the *hcp* structure. The higher order peaks disappear between 180 °C and 210 °C, indicating a loss of *hcp* order. This agrees with rheological measurements in which *G'* begins to decrease sharply above 210 °C, which is also attributed to disordering of the *hcp* structure.

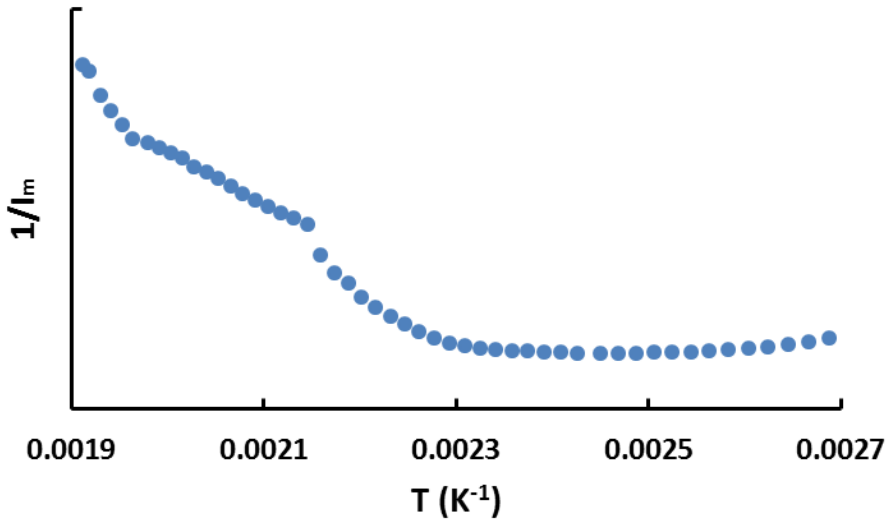

Figure 7. Variable temperature SAXS analysis of Kraton® D1171.

To determine the ODT correctly from SAXS analysis, the inverse of primary scattering maximum ($1/I_m$) was plotted against the inverse of absolute temperature ($1/T$) for all blends. Figure 7 shows such variable temperature SAXS analysis of Kraton® D1171, in which two prominent discontinuities in the plot are observed at ~ 190 °C and 230 °C (~ 0.00216 and 0.00199 K^{-1} respectively). The linear behavior of the plot above 230 °C indicates mean-field behavior in the block copolymer.[17,18] The discontinuity at ~190 °C is likely due to disordering of *hcp* domains of PS blocks. This result is consistent with the multifrequency rheological analysis in which the ODT was observed between 200 and 210 °C (Figure 3).

The 90/10 blend (Figure 8A) exhibits an ODT at ~ 160 °C and the onset of mean-field behavior at ~ 190 °C, in agreement with the multifrequency analysis. In the case of the 70/30 blend (Figure 8B), an ordered structure was not observed in SAXS analysis and the I_m^{-1} vs T^{-1} plot also shows only one transition at ~ 160 °C, which corresponds to the onset of mean field behavior. For highly asymmetric copolymers, this transition should correspond to the DMT as evident from multifrequency rheological analysis (Figure 4B). The intensity of the primary scattering maximum

was very low in the 50/50 blend, and the determination of the DMT from SAXS analysis was deemed unreliable.

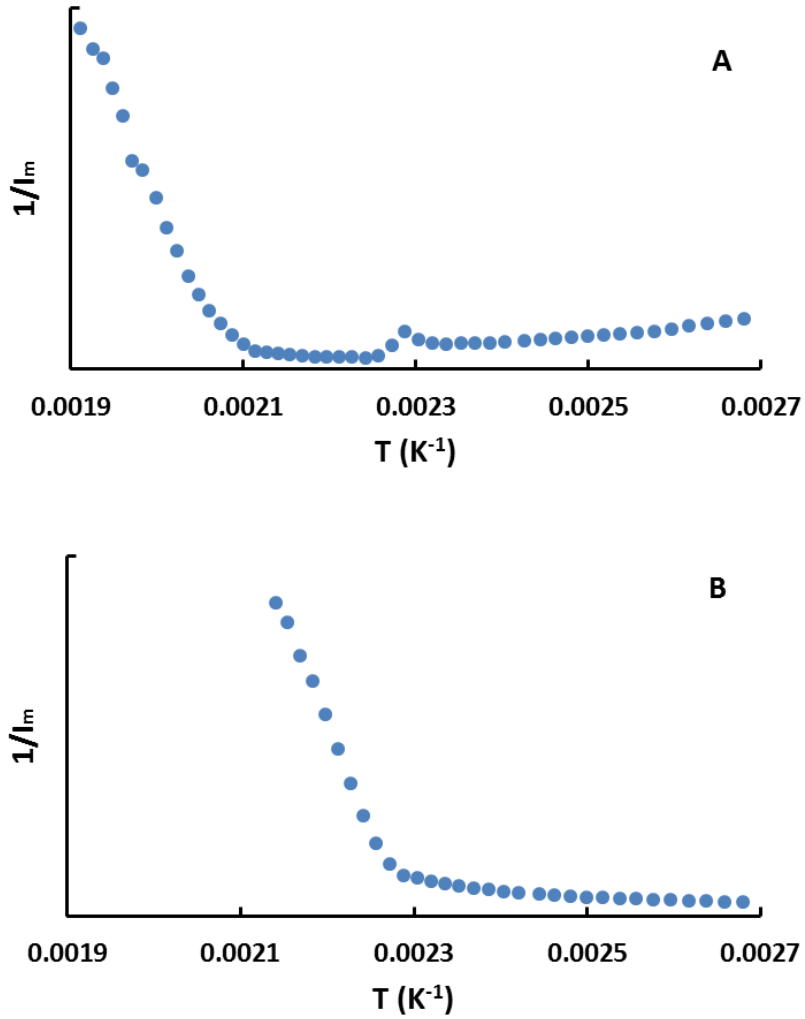

Figure 8. Variable temperature SAXS analysis of (A) 90/10 (B) 70/30 Kraton® D1171 – Sylvalite® RE 100L blends.

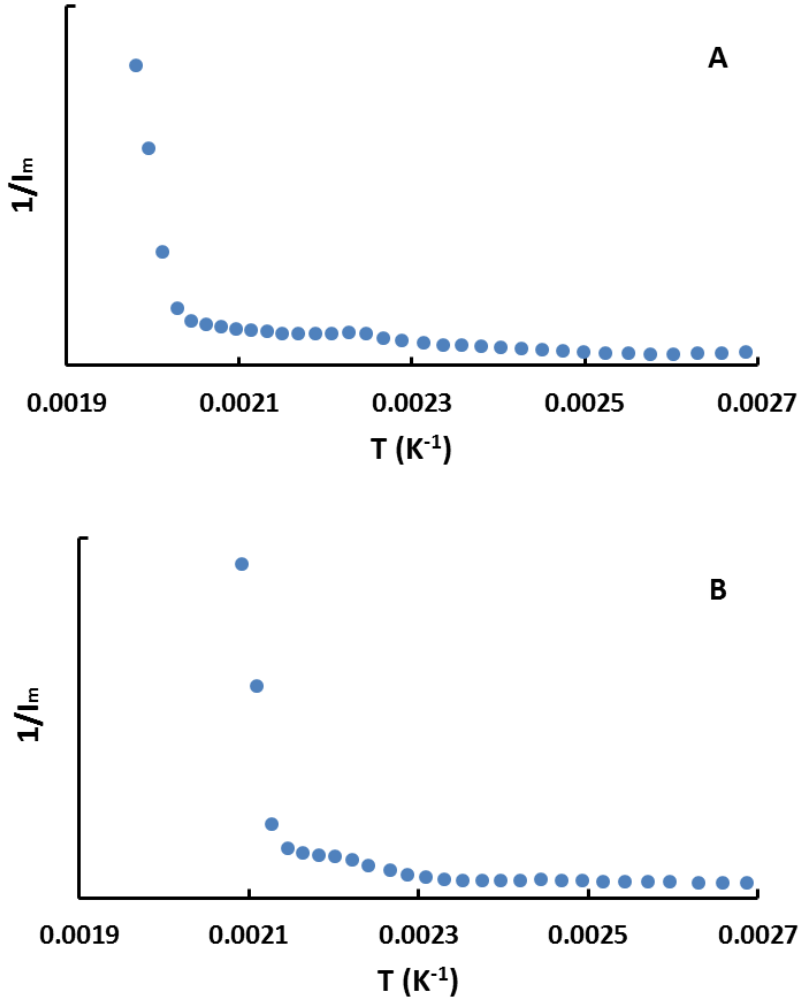

Figure 9. Variable temperature SAXS analysis of (A) 90/10 and (B) 70/30 Kraton® D1171 – Piccotac™ 1095 blends.

The SAXS analysis of blends containing Piccotac™ 1095 tackifier also exhibit a decrease in DMT with increasing tackifier content in the blend. However, the decrease is less drastic than in the Sylvalite® RE 100L blends (Table 3). The Piccotac™ 1095 blends also show a transition corresponding to disordering of ordered spheres at ~ 180 °C and ~ 170 °C for the 90/10 and 70/30 compositions respectively. The SAXS analysis of the 50/50 blend is not shown due to the low intensity of the primary scattering. The reduced intensity is an indication of the smaller electron density difference between the PS domains and the soft IB microphase that is rich with tackifier.

The ODT temperatures determined from SAXS analysis are consistently higher than those determined from rheological analysis. However, the values show the same trends with respect to composition and tackifier type.

Table 3. ODT determined by SAXS analysis of Kraton D1171 blends as a function of blend composition

	ODT / DMT Temperature (°C)	
	Sylvalite® RE 100L	**Piccotac™ 1095**
100/0	229	229
90/10	200	216
70/30	167	193

5.4.2. Isothermal microphase separation kinetics.

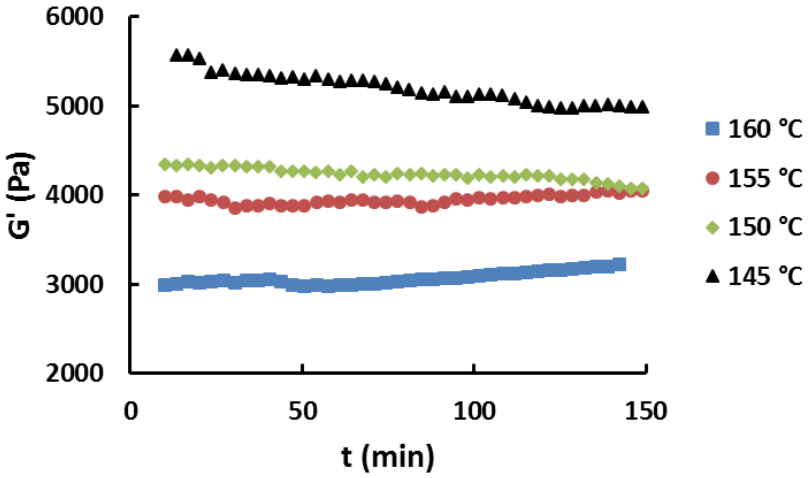

Figure 10. Evolution of storage modulus (G') of Kraton® D1171 quenched to various temperatures.

The time evolution of the shear storage modulus (*G'*) of Kraton® D1171 at various quench temperatures can be seen in Figure 10. All samples were maintained at 240 °C for 10 minutes before rapidly cooling to the desired temperature. *G'* increases as quench temperature is decreased, with the exception of samples held at 155 °C and 150 °C for long times. *G'* increases slowly with time at 160 °C and 155 °C, while it decreases slowly at 150 °C and 145 °C. Since SAXS analysis has confirmed the presence of hcp ordering in PS domains in Kraton® D1171, the ordering process is expected to take place in quenched samples resulting in a sigmoidal pattern of *G'* as a function of time. The absence of this behavior during the experiments could be due to a very slow ordering process and a very long incubation period.[19]

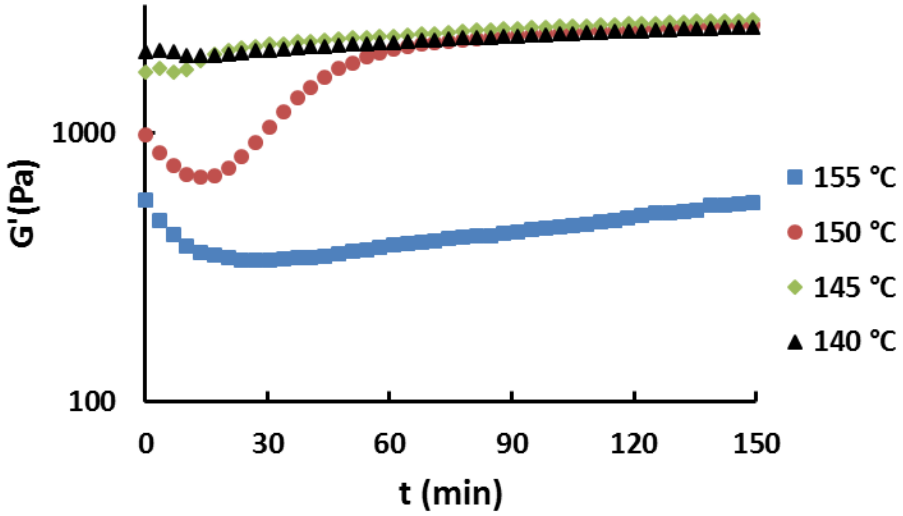

Figure 11. Evolution of *G'* of 90/10 copolymer – Sylvalite® RE 100L blend at various temperatures.

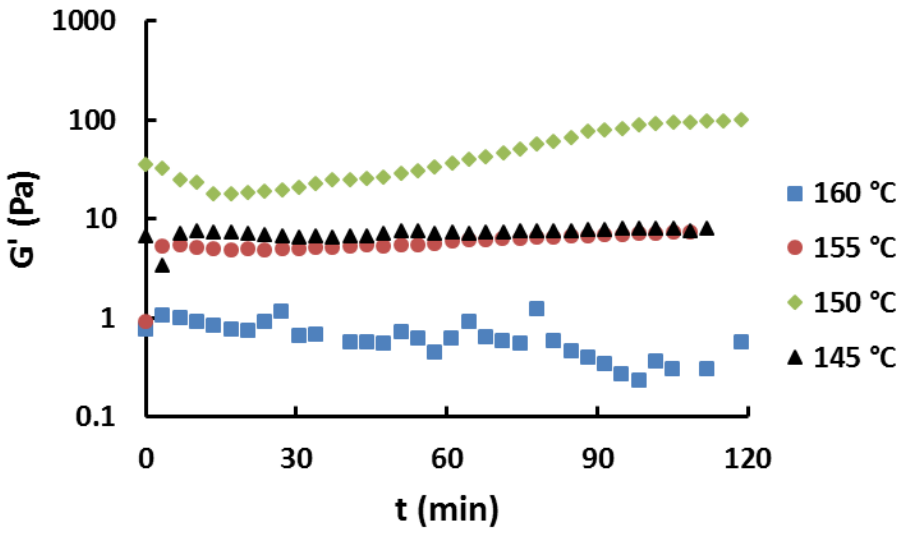

Figure 12. Evolution of *G'* of 70/30 copolymer – Sylvalite® RE 100L blend at various temperatures.

Figures 11 and 12 show the ordering kinetics in the melts of 90/10 and 70/30 blends of the copolymer and Sylvalite® RE 100L, in which sigmoidal growth of *G'* is observed in a very narrow range of temperatures. Even though the 70/30 blends did not show a transition corresponding to the disordering of PS domains in ramp experiments (SAXS and rheology), the growth of *G'* observed at 150 °C suggests a very weak ordering of PS domains in the 70/30 blend. The 90/10 blend quenched to 150 °C shows a much faster ordering process compared to the 70/30 blend. It appears that addition of Sylvalite® RE 100L in relatively small amount results in a faster ordering process in the copolymer – tackifier blends.

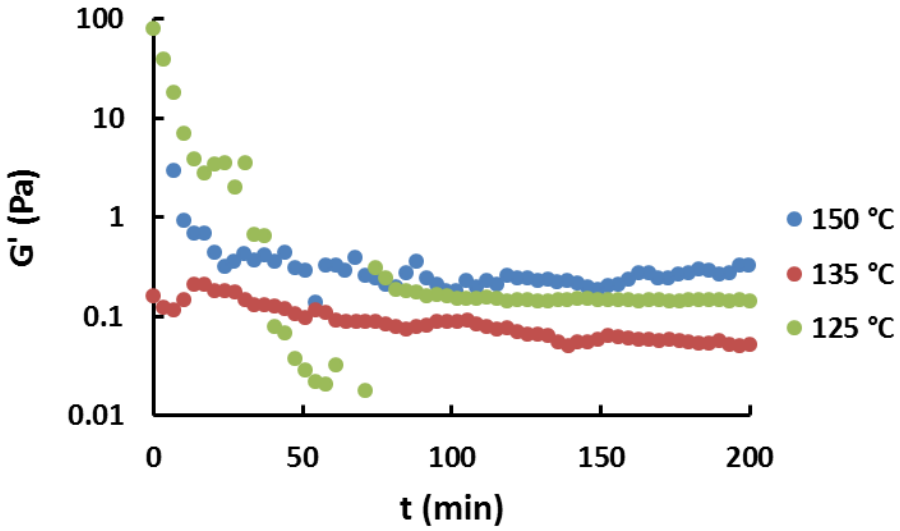

Figure 13. Evolution of storage modulus (*G'*) of 50/50 copolymer – Sylvalite® RE 100L blend at various temperatures.

The G' values observed for a 50/50 Sylvalite® RE 100L blend were extremely low as shown in Figure 13. G' remains reasonably constant when the blend is quenched to 150 °C and 135 °C. However, more interesting behavior is observed at 125 °C, where G' drastically decreases from ~ 100 Pa to ~ 0.01 Pa during the first 60 minutes of the experiment. This decrease is likely due to the saturation of concentration fluctuations, and is indicative of a microphase separation process driven by spinodal decomposition mechanism.[11]

The effect of Piccotac™ 1095 content in the copolymer – tackifier blends, can be observed in Figure 14. In contrast with the blends of Sylvalite® RE 100L, the Piccotac™ 1095 blends show sigmoidal behavior of *G'* over a much wider temperature range. As expected, the *G'* does not increase significantly at temperatures close the respective LDOT of each blends. However, the nucleation and growth mechanism in the blends can be seen even for quench depths (T_{LDOT} – T_{quench}) as large as 40 °C.

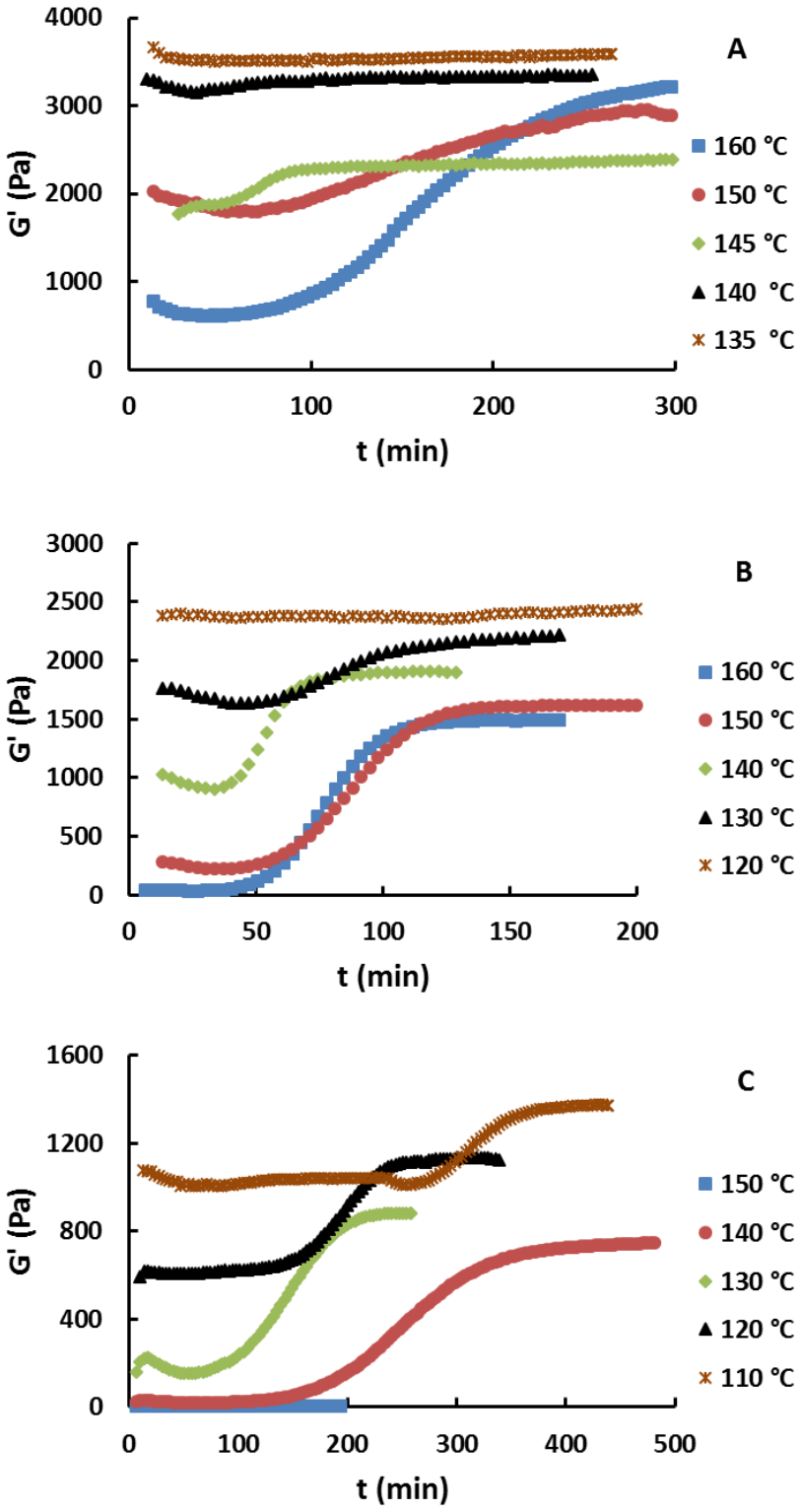

Figure 14. Evolution of *G'* of (A) 90/10, (B) 70/30, and (C) 50/50 copolymer – Piccotac™ 1095 blend at various temperatures.

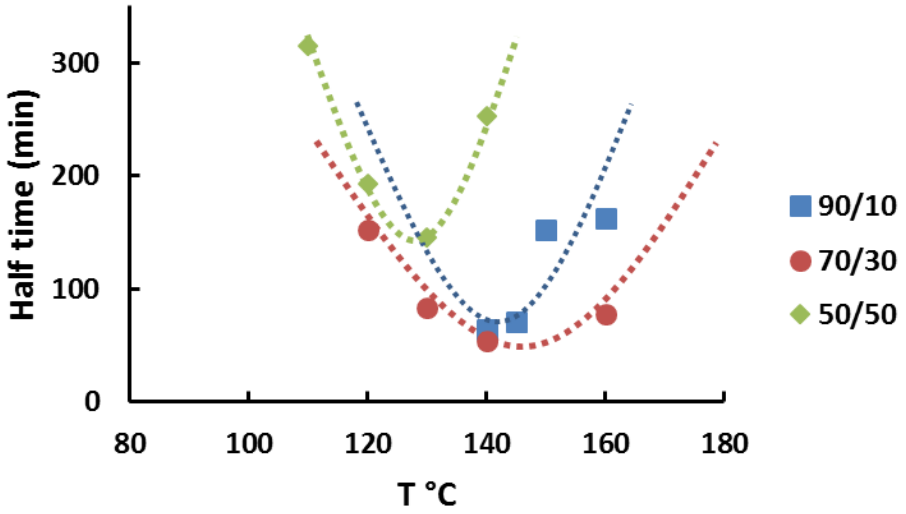

Figure 15. Effect of quench temperature and tackifier content on the ordering half-time in copolymer - Piccotac™ 1095 blends.

Figure 15 shows half-times calculated from G' values observed in isothermal rheological analysis. The 70/30 blend shows overall faster kinetics compared to 90/10 and 50/50 blends when quenched to the same temperatures. This trend is due to the Piccotac 1095™ molecules acting as selective solvent to IB blocks and thus increasing the mobility in IB-rich microphase. At higher tackifier content, the resistance to chain diffusion offered by high-T_g tackifier molecules becomes the dominant factor. Hence, the kinetics become slower. The ordering half-times of copolymer - Piccotac™ 1095 blends can be fit to a parabolic temperature dependence, which resembles that observed for polymer melt crystallization.[20] The slower ordering kinetics at temperatures near the LDOT are attributed to a smaller thermodynamic driving force resulting in a slower nucleation process. At temperatures closer to the T_g of the PS chains, the ordering process is dominated by chain diffusion and thus is slower at lower temperatures.[21,22] The competition between the thermodynamic driving force and chain diffusion leads to the parabolic behavior, and the minimum half-time is observed when these two opposing factors balance each other.

Tackifier compatibility with the block copolymer in an adhesive formulation has a significant impact on its phase structure and performance properties, such as peel adhesion. Nakamura and coworkers[23,24] have reported that compatible tackifier molecules form nanoscale domains and non-compatible molecules form micro-scale domains at room temperature in block copolymer-based pressure sensitive adhesives. In Kraton® D1171 – based adhesive blends, the tackifiers are differentiated based on their compatibility with the PS domains. The ordering kinetics in the blends tested here both slow down with increasing tackifiers content, but the cause of slower kinetics is different for each tackifier. Previously, we argued that the addition of a high-T_g and soft phase compatible tackifier led to slower ordering kinetics because the tackifier offered more resistance to the diffusion of polystyrene chains in the melt.[11] A similar trend is observed in the case of Kraton® D1171 - Piccotac™ 1095 blends. Since the tackifier does not change the T_g of the PS blocks, it is selectively miscible in the soft phase. Thus, the diffusion of PS chains in the melt dominates the ordering process. The isothermal rheological analysis shows that the kinetics get progressively slower with higher tackifier content in the blend. In contrast, Sylvalite® RE 100L tackifier is compatible with the PS blocks and reduces their T_g in the 70/30 and 50/50 copolymer – tackifier compositions. Thus, inclusion of Sylvalite® RE 100L results in a significant lowering of the shear modulus and morphological transition temperatures compared to the blends with Piccotac™ 1095 at the same composition. Thus, Sylvalite® RE 100L acts as a solvent and leads to a smaller thermodynamic driving force for microphase separation and ordering of the PS domains.

5.5. Conclusion

Morphological transitions and microphase separation kinetics in Kraton® D1171 and its blends with two tackifiers - Sylvalite® RE 100L and Piccotac™ 1095 - were studied using oscillatory rheology and small angle X-ray scattering. Kraton® D1171 forms hexagonally packed cylindrical

polystyrene domains as confirmed by SAXS analysis. However, its blends with tackifiers form spherical polystyrene-rich domains upon microphase separation. Sylvalite® RE 100L, a rosin ester based tackifier is miscible with both polystyrene and poly(isoprene-butadiene) blocks, and thus significantly lowers the critical temperature of the blends compared to the blends containing Piccotac™ 1095 (an aliphatic resin). Although both tackifiers slow down the ordering process of microphase separated polystyrene-rich domains, the difference in compatibility with the polystyrene blocks leads to different trends in the shear storage modulus of blends. This study thus concludes a simple rheological analysis testing the compatibility of the blend components can be correlated with the melt phase behavior of pressure sensitive adhesive blends.

AUTHOR INFORMATION

Corresponding Author

*Email: martinsm@vt.edu

Author Contributions

The manuscript was written through contributions of all authors. All authors have given approval to the final version of the manuscript.

Notes

The authors declare no competing financial interest.

ACKNOWLEDGEMENT

This research used resources of the Advanced Photon Source, a U.S. Department of Energy (DOE) Office of Science User Facility operated for the DOE Office of Science by Argonne National Laboratory under Contract No. DE-AC02-06CH11357. The authors thank Dr. Richey Davis

(Virginia Tech, Chemical Engineering) for access to the AR-G2 rheometer used in this work. The authors also thank 3M® Corporation for providing the materials used in this work.

5.6. References

(1) Satas, D. *Handbook of pressure sensitive adhesive technology*; Satas & Associates: Warwick, RI, 1999.

(2) Kraus, G.; Rollmann, K. W.; Gray, R. A. *The Journal of Adhesion* **1979**, *10*, 221.

(3) Gibert, F. X.; Marin, G.; Derail, C.; Allal, A.; Lechat, J. *The Journal of Adhesion* **2003**, *79*, 825.

(4) Roos, A.; Creton, C. *Macromolecules* **2005**, *38*, 7807.

(5) Sasaki, M.; Nakamura, Y.; Fujita, K.; Kinugawa, Y.; Iida, T.; Urahama, Y. *Journal of Adhesion Science and Technology* **2005**, *19*, 1445.

(6) Class, J. B.; Chu, S. G. *Journal of Applied Polymer Science* **1985**, *30*, 805.

(7) Class, J. B.; Chu, S. G. *Journal of Applied Polymer Science* **1985**, *30*, 815.

(8) Class, J. B.; Chu, S. G. *Journal of Applied Polymer Science* **1985**, *30*, 825.

(9) Hino, K.; Ito, T.; Toyama, M.; Hashimoto, H. *Journal of Applied Polymer Science* **1975**, *19*, 2879.

(10) Dixit, N.; Pape, A.; Rong, L.; Joseph, E.; Martin, S. M. 2014.

(11) Dixit, N.; Pape, A.; Rong, L.; Joseph, E.; Martin, S. M. 2014.

(12) Uzee, A. J. In *uspto.gov*; TSRC (USA) Investment Corporation: USA, 2014.

(13) Han, C. D.; Kim, J.; Kim, J. K. *Macromolecules* **1989**, *22*, 383.

(14) Han, C. D.; Vaidya, N. Y.; Kim, D.; Shin, G.; Yamaguchi, D.; Hashimoto, T. *Macromolecules* **2000**, *33*, 3767.

(15) Bates, F. S.; Fredrickson, G. H. *Annu. Rev. Phys. Chem.* **1990**, *41*, 525.

(16) Matsen, M. W.; Bates, F. S. *The Journal of Chemical Physics* **1997**, *106*, 2436.

(17) Leibler, L. *Macromolecules* **1980**, *13*, 1602.

(18) Hashimoto, T.; Kowsaka, K.; Shibayama, M.; Kawai, H. *Macromolecules* **1986**, *19*, 754.

(19) Liu, Z.; Shaw, M.; Hsiao, B. S. *Macromolecules* **2004**, *37*, 9880.

(20) Long, Y.; Shanks, R. A.; Stachurski, Z. H. *Progress in Polymer Science* **1995**, *20*, 651.

(21) Fredrickson, G. H.; Binder, K. *The Journal of Chemical Physics* **1989**, *91*, 7265.

(22) Binder, K. *Physica A: Statistical Mechanics and its Applications* **1995**, *213*, 118.

(23) Nakamura, Y.; Sakai, Y.; Adachi, M.; Fujii, S.; Sasaki, M.; Urahama, Y. *Journal of Adhesion Science and Technology* **2008**, *22*, 1313.

(24) Nakamura, Y.; Sakai, Y.; Imamura, K.; Ito, K.; Fujii, S.; Urahama, Y. *Journal of Applied Polymer Science* **2012**, *123*, 2883.

Chapter 6

Conclusions and Future Work

6.1. Conclusions

The following key conclusions are drawn from the work described in this dissertation and organized according to the objectives defined in the 'Introduction' chapter:

1. Real-time SAXS analysis and oscillatory rheological analysis can be used to study the morphology and microphase separation kinetics in pressure-sensitive adhesive blends. A modified Percus – Yevick hard sphere model can be used to determine morphological parameters such as polystyrene core radius and hard-sphere radius. The trends in these parameters with respect to temperature, composition and time correlate reasonably well with the trends in shear modulus obtained from rheological analysis.
2. The microphase separation in pressure-sensitive adhesive melts is a multi-step process, and is dominated by the polymer chain mobility. In general, slower ordering rates were observed in blends quenched to lower temperatures. The ordering of microphase separated polystyrene domains is also influenced by the tackifier content in the blend and its compatibility with polystyrene and polydiene blocks of the copolymer. At low concentrations, a polydiene - compatible tackifier (Piccotac 1095) accelerated the ordering process of polystyrene domains. At high concentrations, the tackifier offered resistance to chain diffusion and hampered the ordering process. The blends containing a polystyrene and polydiene – compatible tackifier (Sylvalite RE-100L) showed the growth of an ordered structure over a narrower temperature range compared to blends containing Piccotac 1095.
3. The isothermal rheological analysis showed that at high enough tackifier content, the mechanism of microphase separation shifted from 'nucleation and growth' to 'spinodal decomposition'. The same shift in the mechanism was also observed when the blends were

quenched to the temperatures near polystyrene T_g, again due to resistance to chain diffusion at lower temperatures.

6.2. Future Work

Although we have been successful in correlating the trends in morphological and rheological behavior in pressure-sensitive adhesive blends, additional analysis is required to fully understand the relationship between the morphology of adhesive blends and their performance properties.

6.2.1. Controlling the chemistry - determination of interaction parameters

Kraton® D1161 and 1171, the polymers used in this study, have a binodal molecular weight distribution, while the tackifiers have a molecular weight distribution of ~2. This complex distribution puts limits on the accurate determination of the change in the styrene – isoprene interaction parameter due to tackifier addition. Knowing the relationship between the interaction parameter and temperature would be very useful to ascertain the impact of tackifier on the microphase separation mechanism. E.g., the microstructure, ODT and resulting viscoelastic properties at a given temperature can be suitably modified in an adhesive blend by carefully controlling the tackifier compatibility with polystyrene and polydiene, if the effect of tackifier on the styrene – diene interaction parameter is known.

In order to determine the interaction parameter, synthesis of triblock and diblock copolymers with a narrow molecular weight distribution (1.2 or lower) is necessary.[1,2] These blocks could also be separated from the commercially available block copolymers used in this study by means of fractionation. For the tackifier, synthesis of small molecular weight resins seems to be the only viable option. The selection of monomers and the molecular weight of the resulting tackifier are a few parameters that may be varied to study their impact on the melt behavior of adhesive blends.

6.2.2. Imaging microphase separated domains

The SAXS and rheological analysis provide an indirect assessment of the microstructure in block copolymers. Hence, an imaging analysis of the block copolymers and their blends with tackifiers would help to support the conclusions drawn from this study. Transmission electron microscopy (TEM)[3] perhaps provides the most reliable analysis of the shape and size of microphase separated domains, as the osmium tetroxide (OsO_4) stained styrene – diene block copolymer provide a good contrast required for imaging. TEM also allows for analysis of the bulk of samples whereas other imaging techniques such as AFM and SEM are primarily surface analytical techniques.

The case of Kraton® D1171 and its blends is interesting in particular. Kraton® D1171 forms cylindrical domains, as suggested by SAXS patterns. However, as more tackifier is added, the secondary scattering peaks corresponding to the hexagonally packed cylindrical domains disappeared. The existence of disordered spheres was observed in the multifrequency rheological analysis. This transition from cylindrical to spherical domains could be confirmed by TEM. It is also important to determine the blend composition (or range) at which (or over which) this transition takes place.

6.2.3. Adhesive behavior analysis

In order to understand how the microphase separation kinetics in the melt affects adhesive performance, blend compositions processed isothermally at various temperatures should be subjected to adhesion tests. The probe tack test is one of the most widely used methods,[4] and generates a force – strain curve for each sample. The adhesive performance of each composition can be analyzed using the parameters (peak stress, work of adhesion etc.) obtained during the probe

tack test. 50/50 blends of the copolymer and tackifier in particular should be analyzed as this composition might be used commercially.[5]

6.2.4. Acrylic adhesives

It would be interesting to verify the conclusions of this study by analyzing other pressure – sensitive adhesive systems based on block copolymers. Poly(methyl methacrylate-co-butyl acrylate) copolymers are a suitable system for the microphase separation kinetics study. Acrylic copolymers offer the distinct advantage of relatively low ODT temperatures. Also, the absence of unsaturation (unlike diene units in styrene-diene block copolymers) leads to improved thermal stability. Various microstructures in acrylic adhesives can be obtained by varying the composition of the hard and soft segments in block copolymers. E.g. a gradual transition from a lamellar to a cylindrical or spherical microstructure is expected with the addition of a selectively soluble tackifier. This would help in understanding the relationship between the different microstructures and corresponding adhesive and rheological behavior of copolymer – tackifier blends. The lamellar and cylindrical structures can be also be studied by optical microscopy.

6.3. References

(1) Russell, T. P.; Hjelm, R. P.; Seeger, P. A. *Macromolecules* **1990**, *23*, 890.

(2) Sakurai, S.; Mori, K.; Okawara, A.; Kimishima, K.; Hashimoto, T. *Macromolecules* **1992**, *25*, 2679.

(3) Kim, J.; Han, C. In *Polymer Materials*; Lee, K.-S., Kobayashi, S., Eds.; Springer Berlin Heidelberg: 2010; Vol. 231, p 77.

(4) Feldstein, M. M.; Siegel, R. A. *Journal of Polymer Science Part B: Polymer Physics* **2012**, *50*, 739.

(5) Deplace, F.; Carelli, C.; Mariot, S.; Retsos, H.; Chateauminois, A.; Ouzineb, K.; Creton, C. *The Journal of Adhesion* **2009**, *85*, 18.

Appendix A: SAXS Data Fit and Thermal Stability of Kraton® D1161

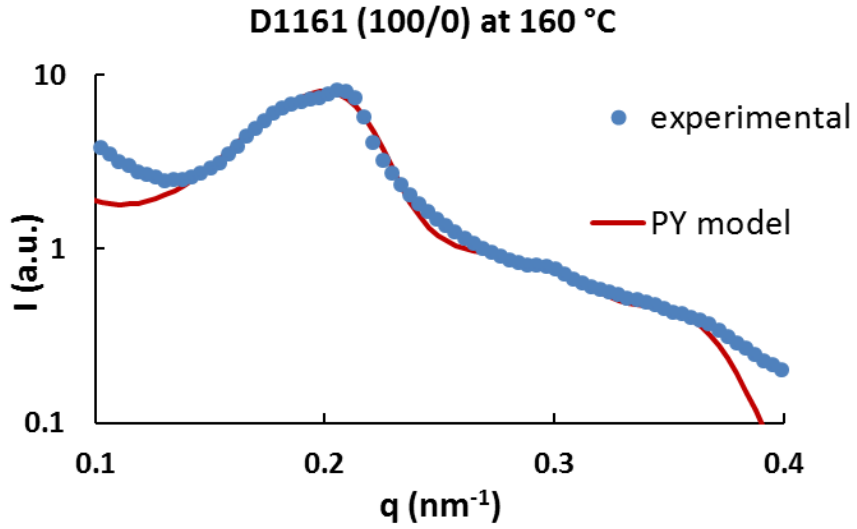

Figure A.1. SAXS data fit using the Percus – Yevick (PY) hard sphere model.

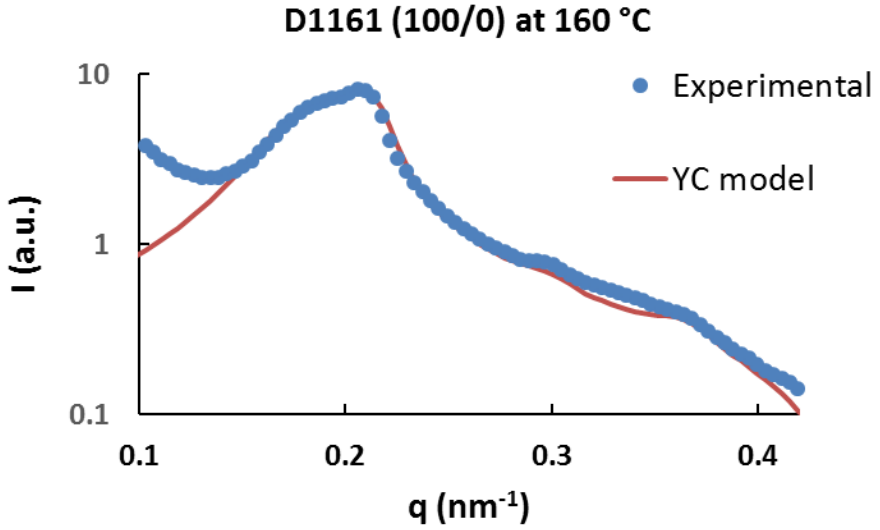

Figure A.2. SAXS data fit using Yarusso – Cooper (YC) model.

The use of an appropriate morphological model is necessary to interpret the small angle X-ray scattering data acquired for the pressure sensitive adhesive blends. Zernike and Prins[1] developed equations to describe the effect of interparticle interference on the scattering intensity. Debye[2] and Guinier[3] later modified these equations based on the hard sphere size and their concentration in solution. We believe that the Yarusso – Cooper model[4], which also assumes a core-shell structure of polymer micelles, requires some consideration along with the Percus – Yevick hard sphere model. We used these two models to fit the SAXS intensity profile (Figures A.1. and A.2.) to determine which model offered the best fit.

The scattering intensity in the YC model (for SIS block copolymers) is given by the following equation

$$I(q) = I_e(q)V\frac{1}{v_p}v_1^2\rho_1^2\Phi^2(qR_1)\frac{1}{1+\left(\frac{8v_{CA}}{v_p}\right)\epsilon\Phi(2qR_{CA})} \quad \text{..... (1)}$$

where R_1 is the polystyrene sphere radius, $2*R_{CA}$ is the distance of closest approach, i.e. the shortest possible distance between the two hard spheres (microphase separated polystyrene domains), V_p is the average volume of scattering particles, R_{av} is the average radius of scattering particles (which consists of a core of microphase separated polystyrene chains, and a corona of polyisoprene chains), and ρ is the electron density difference between styrene and isoprene-rich phases.

The function Φ is similar to the form factor for spherical particles and is described as follows

$$\Phi(x) = \frac{3(sinx - xcosx)}{x^3} \quad \text{..... (2)}$$

The morphological parameters obtained from the two models are shown in Table 1.

Table 1. Morphological parameters obtained from the Percus – Yevick and Yarusso – Cooper models for the Kraton® D1161 quenched to 160 ºC and held isothermal for 100 minutes.

Percus – Yevick Model			**Yarusso – Cooper Model**				
R_c **(nm)**	R_{hs} **(nm)**	A_1 **(a.u.)**	R_1 **(nm)**	R_{CA} **(nm)**	R_{av} **(nm)**	A_1 **(a.u.)**	ρ **(e^-/nm^3)**
10.9	24.6	4.8	8.8.	15.2	15.3	4.0	60

It appears that R_c from the PY model and R_1 from the YC model represent the size of polystyrene domains. While R_{CA} is the closest distance of approach, the average particle size R_{av} appears to be similar to R_{hs}, which depends on the separation between polystyrene domains due to polydiene corona. The difference between R_{CA} and R_{av} is very small, which suggests that the polystyrene domains have a nearly uniform distribution in the sample volume. The PY model predicts consistently higher numbers for the polystyrene core radius and the hard sphere radius. Even though both models offer good fits to the experimental data, the PY model is preferred as it has been applied to systems with higher concentrations (> 15 % by volume) of phase-separated entities.[5] Thomas et al.[6] have also studied the ordering of such micelles in cubic morphologies upon drying of the polymer solutions. Along with the studies performed by Bansil et al[7,8], this work serves as a valuable precedent for the application of the PY model to disordered polystyrene domains in our systems. The YC model is usually applied to much more dilute systems of ionomers (ion content < 15 mol %), thus its validity at the high volume fractions of the core-shell microphase separated structures is questionable.

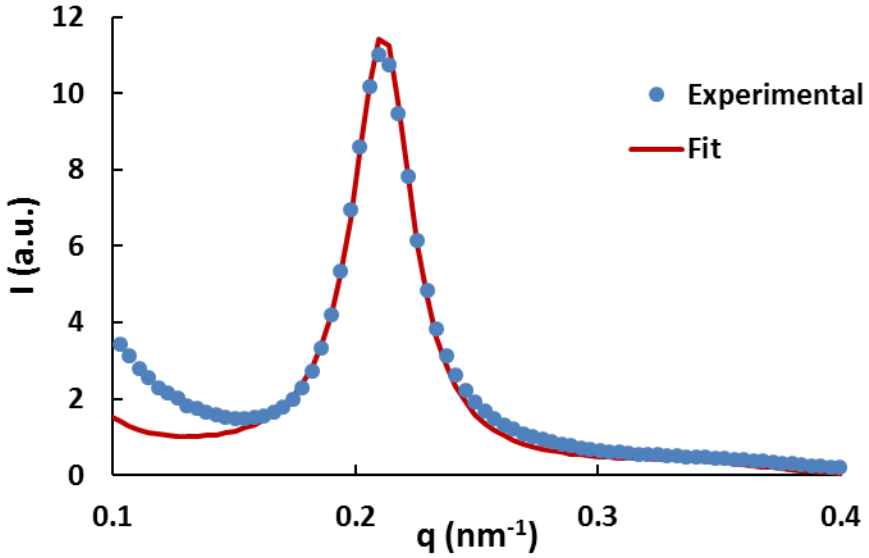

Figure A.3. Experimental and Percus-Yevick hard sphere model fit for the SAXS profile obtained 5 minutes after quenching the Kraton® D1161 from 240 °C to 160 °C.

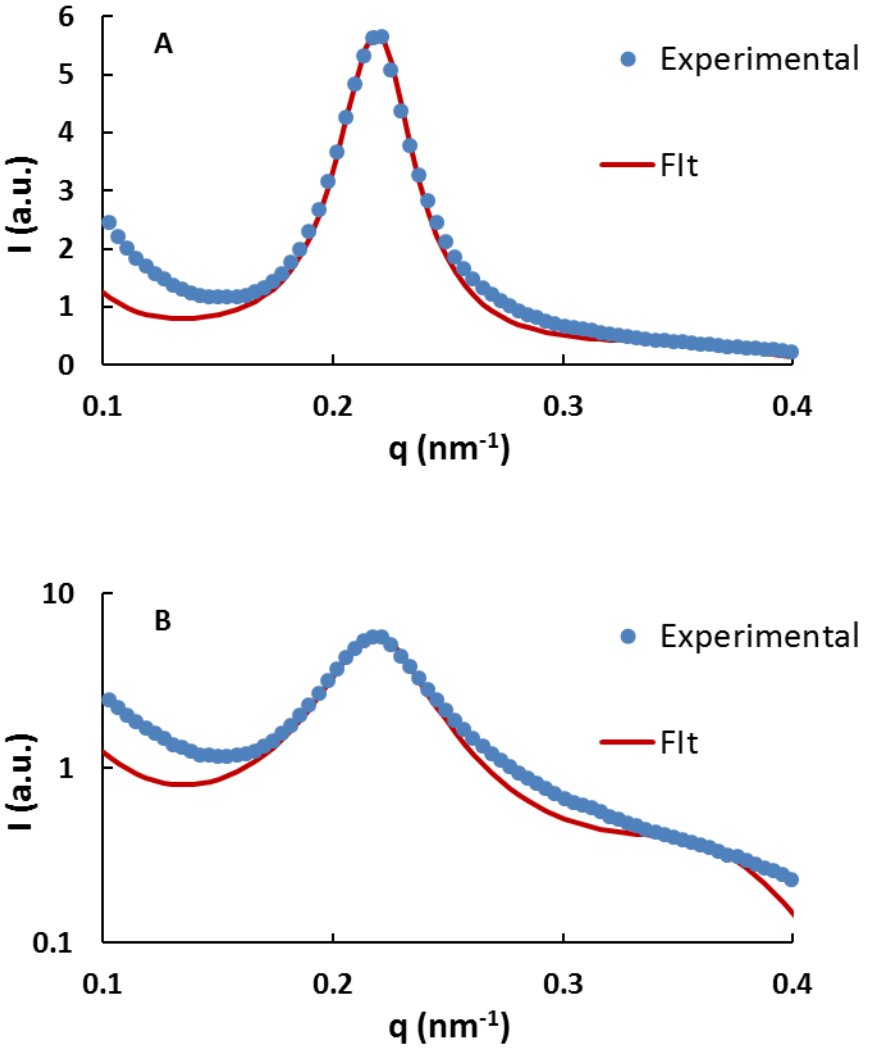

Figure A.4. Experimental and Percus-Yevick hard sphere model fit for Kraton® D1161 heated to 240 °C, where intensity I(q) is plotted on (A) linear scale and (B) log scale.

The Percus-Yevick hard sphere model fails at temperatures above DMT (230 °C). This is evident from the experimental SAXS profile obtained at 240 °C, which does not show the interference peak at $q \sim 0.35$ nm^{-1} that corresponds to packing of spheres. Thus, the scattering maximum at $q \sim 0.24$ nm^{-1} is due to the 'correlation hole' effect.

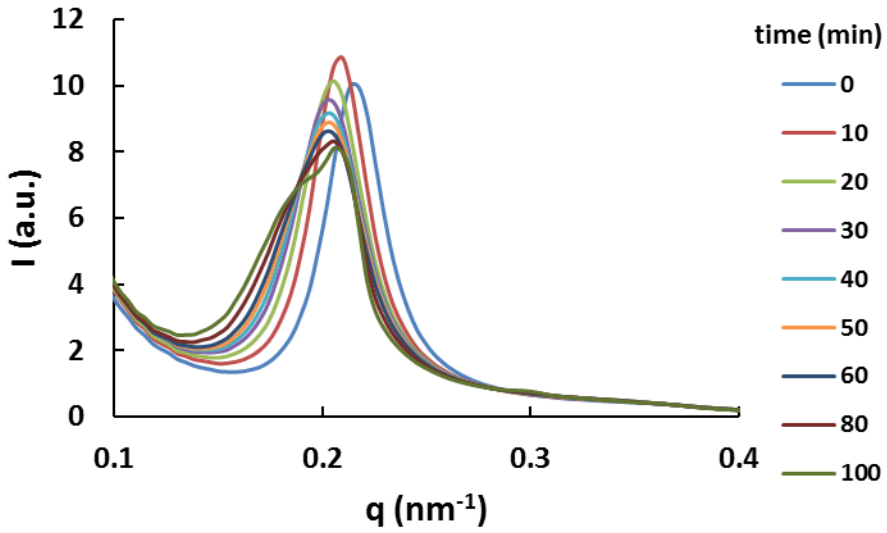

Figure A.5. Development of SAXS pattern as a function of time (in minutes) in Kraton® D1161 sample quenched from 240 °C to 160 °C.

The *I(q) vs q* patterns become broader as time progresses in quench experiments. In the case of sample quenched to 160 °C, the second scattering maximum is clearly visible at 80 minutes of isothermal hold. The gradual shift of SAXS profiles to lower q suggests increased spacing between microphase-separated domains, which correlates well with increase in R_c and R_{hs} values with time.

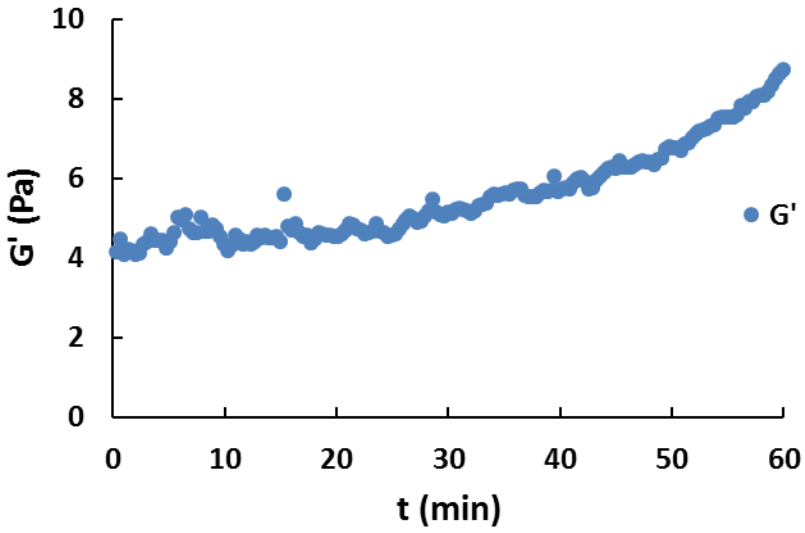

Figure A.6. Thermal stability of Kraton D1161 at 240 C. G' observed as a function of time.

Figure 4 shows that the block copolymer does not undergo significant crosslinking at 240 °C for ~ 20 minutes. Thus, all samples were maintained at 240 °C for 10 minutes before quenching to the desired temperatures.

References:

(1) Zernike, F. t.; Prins, J. Zeitschrift für Physik 1927, 41, 184.
(2) Debye, P. Zeitschrift für Physik 1959, 156, 256.
(3) Guinier, A.; Fournet, G. Small-angle scattering of X-rays; John Wiley: New York, 1955.
(4) Yarusso, D. J.; Cooper, S. L. Macromolecules 1983, 16, 1871.
(5) Mortensen, K. EPL (Europhysics Letters) 1992, 19, 599.
(6) Thomas, E. L.; Kinning, D. J.; Alward, D. B.; Henkee, C. S. Macromolecules 1987, 20, 2934.
(7) Bansil, R.; Nie, H.; Li, Y.; Liao, G.; Ludwig, K.; Steinhart, M.; Koňák, Č.; Lal, J. Macromolecular Symposia 2002, 190, 161.
(8) Nie, H.; Bansil, R.; Ludwig, K.; Steinhart, M.; Koňák, Č.; Bang, J. Macromolecules 2003, 36, 8097.

Appendix B: Oscillatory Rheology Data

B.1. Kraton® D1161 – Rheology temperature ramp

Ramp rate: 1.5 °C/min, frequency: 1 Hz, strain: 0.5 %

Temperature	G'	G''
°C	Pa	Pa
80.2	3.13E+05	43380
80.5	3.13E+05	43810
81.5	3.11E+05	44960
82.6	3.09E+05	46390
83.5	3.06E+05	47290
84.4	3.04E+05	48660
85.5	3.00E+05	50540
86.8	2.96E+05	52520
87.9	2.93E+05	54640
89	2.89E+05	56500
90.1	2.85E+05	58480
91	2.81E+05	60170
92	2.77E+05	62110
92.9	2.73E+05	63900
93.9	2.69E+05	65780
94.9	2.64E+05	67830
95.9	2.59E+05	69830
97	2.54E+05	71770
98	2.49E+05	73920
99	2.43E+05	75890
100	2.38E+05	77890
101	2.32E+05	79830
102	2.26E+05	81700
103	2.20E+05	83560
104	2.13E+05	85430
105	2.07E+05	87150
106	2.00E+05	88710
107	1.93E+05	90190
108	1.87E+05	91530
109	1.80E+05	92680
110	1.72E+05	93520
111	1.65E+05	94340
112	1.58E+05	94740
113	1.51E+05	95090
114	1.43E+05	94960

115	1.36E+05	94550
116	1.29E+05	93750
117	1.22E+05	92790
118	1.16E+05	91440
119	1.09E+05	89920
120	1.03E+05	88130
121	97840	86180
122	92500	84220
123	87550	82130
124	82990	80110
125	78570	78070
126	74490	76050
127	70600	74100
128	66970	72140
129	63410	70330
130	60060	68480
131	56890	66660
132	53890	64830
133	50920	63080
134	48100	61340
135	45420	59570
136	42900	57850
137	40480	56140
138	38150	54440
139	35930	52780
140	33950	51110
141	32010	49510
142	30130	47900
143	28440	46320
144	26800	44800
145	25320	43320
146	23930	41860
147	22540	40370
148	21320	38970
149	20100	37550
150	19060	36220
151	18050	34910
152	17120	33660
153	16180	32390
154	15400	31240
155	14640	30100

156	13930	29010
157	13280	27970
158	12680	26970
159	12070	26000
160	11580	25120
161	11100	24300
162	10650	23500
163	10230	22750
164	9836	22030
165	9480	21360
166	9148	20720
167	8822	20090
168	8536	19520
169	8266	18960
170	7988	18390
171	7743	17890
172	7510	17390
173	7296	16930
174	7091	16480
175	6882	16030
176	6695	15620
177	6509	15190
178	6323	14780
179	6147	14390
180	5971	14000
181	5818	13620
182	5621	13230
183	5446	12860
184	5282	12500
185	5097	12140
186	4920	11800
187	4756	11470
188	4572	11140
189	4389	10810
190	4224	10530
191	4046	10230
192	3889	9974
193	3742	9734
194	3598	9506
195	3461	9291
196	3329	9093

197	3212	8915
198	3089	8728
199	2976	8563
200	2863	8401
201	2743	8229
202	2632	8081
203	2526	7939
204	2413	7770
205	2294	7581
206	2161	7355
207	2030	7132
208	1905	6897
209	1780	6663
210	1656	6440
211	1551	6252
212	1447	6078
213	1353	5927
214	1270	5809
215	1189	5678
216	1112	5557
217	1038	5441
218	968.1	5320
219	897.6	5188
220	829.4	5027
221	760.7	4840
222	696.3	4644
223	640.5	4460
224	589.4	4285
225	548.3	4129
226	515.7	3994
227	485.8	3862
228	463.3	3742
229	447.9	3627
230	439.5	3520
231	438.2	3416
232	442.3	3319
233	456.2	3222
234	477.6	3137
235	508.6	3052
236	549.5	2975
237	601.8	2908

238	664	2845
239	740.5	2787
240	829	2738

B.2. Kraton® D1161 – multifrequency analysis

Temperature range: 150 – 270 °C, Frequency range: 0.1 – 100 Hz, Strain: 0.05

	Frequency (Hz)									
G'	**0.1**	**0.2154**	**0.4642**	**1**	**2.154**	**4.642**	**10**	**21.54**	**46.42**	**100**
150 °C	6417	8925	14160	26580	50440	83970	1.24E+05	1.73E+05	2.31E+05	2.88E+05
160 °C	5709	7770	11120	18710	35890	65080	1.02E+05	1.47E+05	2.01E+05	2.56E+05
170 °C	5434	7186	9563	14280	25410	48480	83200	1.25E+05	1.76E+05	2.30E+05
180 °C	4551	6157	8077	11200	18130	34660	64900	1.05E+05	1.54E+05	2.06E+05
190 °C	2574	3666	4826	6743	10760	20670	42930	79130	1.23E+05	1.69E+05
200 °C	2434	3255	4121	5613	8548	15280	31540	63000	1.06E+05	1.49E+05
210 °C	652.5	1388	2491	4087	6685	11870	24030	50440	92030	1.35E+05
220 °C	119.6	477	1351	2839	5098	9141	17970	38060	74380	1.14E+05
230 °C	42.85	183.2	641.9	1746	3638	6912	13490	28210	57630	92370
240 °C	18.78	81.78	301.3	972.5	2486	5267	10560	21630	44640	73820
250 °C	14.19	54.06	195.7	644.8	1808	4251	8877	17830	35730	58870
260 °C	19.73	68.57	218.6	619.6	1644	3884	8144	15860	30040	47020
270 °C	51.96	152.1	396.3	920.4	2048	4277	8324	15190	26560	37720

	Frequency (Hz)									
G"	**0.1**	**0.2154**	**0.4642**	**1**	**2.154**	**4.642**	**10**	**21.54**	**46.42**	**100**
150 °C	7374	13130	23410	39460	57870	73640	88340	1.02E+05	1.11E+05	1.13E+05

160 °C	5665	9569	16940	29930	48250	66320	81550	96260	1.09E+05	1.17E+05
170 °C	4574	7309	12510	22330	38610	58660	76390	92050	1.07E+05	1.20E+05
180 °C	3886	5775	9530	16700	29840	49710	70660	88240	1.05E+05	1.23E+05
190 °C	2464	3763	6395	11520	21120	37600	59700	80080	97220	1.17E+05
200 °C	1897	2938	5033	9038	16560	30190	51170	74330	93550	1.15E+05
210 °C	1699	2944	4798	8054	14150	25450	44540	69590	92510	1.15E+05
220 °C	1096	2225	4015	6804	11740	20770	36660	60260	85200	1.09E+05
230 °C	716.2	1511	2998	5459	9543	16750	29530	50040	75140	99840
240 °C	492.4	1051	2182	4261	7797	13780	24110	41210	64730	90090
250 °C	382.2	816.8	1706	3441	6528	11700	20270	34300	54910	79640
260 °C	347.3	734.3	1511	3003	5695	10200	17400	28740	45780	68160
270 °C	396.4	805.2	1562	2932	5277	9094	14980	23820	36910	55230

B.3. Kraton® D1161 Isothermal Microphase Separation Kinetics Analysis – Shear Storage Modulus (G')

Quench Temperatures – 160, 150, 145, 140 °C. Frequency: 0.01 Hz, Strain: .005

160 °C		**150 °C**		**145 °C**		**140 °C**	
time	**G'**	**time**	**G'**	**time**	**G'**	**time**	**G'**
min	**Pa**	**min**	**Pa**	**min**	**Pa**	**min**	**Pa**
13.389	844.5	13.3885	1231	13.389	1735	13.38983	1837
16.78	818.9	16.78	1132	16.775	1654	16.78167	1745
20.16667	797	20.17167	1063	20.16167	1578	20.16833	1662
23.55667	783.6	23.55833	1014	23.55	1519	23.55833	1598
26.945	771	26.94667	970.5	26.935	1475	26.94667	1554
30.335	762.3	30.33667	938	30.32333	1442	30.335	1519
33.725	757.2	33.725	914.8	33.71	1416	33.725	1489
37.11167	754.8	37.11167	899.6	37.09667	1397	37.11333	1469
40.5	753	40.5	889.5	40.48333	1387	40.50167	1454
43.89	754.4	43.885	876.3	43.87167	1367	43.89	1439

47.27667	758.2	47.275	875.6	47.26	1358	47.28	1426
50.66667	764.7	50.66	869.8	50.645	1351	50.66667	1413
54.055	771.7	54.04833	866	54.03333	1343	54.05333	1410
57.44333	789.2	57.43833	864.8	57.42167	1341	57.44167	1403
60.83167	806.5	60.825	867	60.80833	1339	60.83	1395
64.21833	832.1	64.215	873.3	64.195	1332	64.21667	1390
67.60833	860.9	67.60167	881.1	67.58333	1340	67.605	1382
70.99833	900.2	70.98833	893.4	70.97	1337	70.99333	1381
74.38667	941.7	74.37667	905.6	74.35833	1348	74.38333	1374
77.77333	991.2	77.76333	923.7	77.745	1357	77.77167	1372
81.165	1047	81.15167	947.6	81.13167	1370	81.15833	1367
84.55167	1107	84.54	966.4	84.52	1387	84.55	1363
87.94	1179	87.92833	995.1	87.905	1408	87.93833	1368
91.32833	1252	91.31667	1027	91.29167	1432	91.325	1368
94.715	1331	94.705	1065	94.67833	1463	94.715	1372
98.105	1411	98.09333	1107	98.06667	1497	98.10333	1373
101.4917	1491	101.4833	1156	101.4533	1535	101.4917	1377
104.8817	1573	104.8717	1202	104.8417	1582	104.8817	1380
108.2683	1652	108.26	1251	108.2267	1627	108.2683	1388
111.6567	1726	111.6483	1308	111.615	1663	111.6583	1394
115.045	1798	115.0367	1366	115.0033	1729	115.0483	1400
118.4333	1864	118.4233	1425	118.3917	1773	118.4383	1414
121.82	1930	121.8133	1484	121.7783	1837	121.825	1424
125.2117	1986	125.2	1553	125.1667	1886	125.2133	1441
128.5983	2039	128.59	1617	128.5517	1942	128.6033	1458
131.9867	2083	131.9767	1681	131.9383	2000	131.9917	1477
135.375	2123	135.3633	1744	135.3317	2053	135.38	1501
138.765	2158	138.75	1802	138.7183	2107	138.77	1520
142.1533	2186	142.14	1855	142.1067	2154	142.1583	1546
145.5417	2211	145.5267	1904	145.4933	2204	145.5483	1575
148.93	2232	148.915	1954	148.8817	2248	148.935	1603
152.3183	2246	152.3033	1999	152.2683	2286	152.325	1632
155.705	2258	155.69	2040	155.6567	2323	155.7133	1664
159.095	2260	159.08	2079	159.0417	2361	159.1	1690
162.4817	2272	162.4667	2106	162.4317	2395	162.4883	1723
165.8683	2276	165.8533	2134	165.8183	2425	165.8783	1764
169.25	2273	169.25	2157	169.2	2454	169.2667	1794
172.65	2275	172.6333	2182	172.6	2480	172.65	1831
176.0333	2284	176.0167	2202	175.9833	2494	176.05	1867
179.4167	2289	179.4	2214	179.3667	2518	179.4333	1904
182.8167	2290	182.8	2228	182.75	2536	182.8167	1937

186.2	2290	186.1833	2241	186.15	2555	186.2167	1967
189.5833	2292	189.5667	2250	189.5333	2568	189.6	2002
192.9833	2295	192.9667	2260	192.9167	2582	192.9833	2031
196.3667	2296	196.35	2266	196.3	2594	196.3833	2063
199.75	2295	199.7333	2274	199.6833	2600	199.7667	2087
202.4167	2295	203.1333	2280	203.0833	2608	203.15	2111
		206.5167	2281	206.4667	2614	206.55	2135
		209.9	2284	209.85	2621	209.9333	2157
		213.3	2293	213.2333	2629	213.3167	2178
		216.6833	2299	216.6167	2635	216.7167	2196
		220.0667	2303	220.0167	2633	220.1	2213
		223.4667	2304	223.4	2639	223.4833	2234
		226.85	2301	226.7833	2641	226.8667	2244
		230.2333	2302	230.1667	2646	230.2667	2256
		233.6333	2306	233.5667	2653	233.65	2269
		237.0167	2304	236.95	2657	237.05	2284
		240.4	2307	240.3333	2664	240.4333	2291
		243.7833	2310	243.7167	2666	243.8167	2306
		247.1833	2316	247.1167	2670	247.2167	2314
		250.5667	2322	250.5	2672	250.6	2322

B.4. Kraton® D1161 Isothermal Microphase Separation Kinetics Analysis – Shear Loss Modulus (G'')

Quench Temperatures – 160, 150, 145, 140 °C. Frequency: 0.01 Hz, Strain: .005

160 °C		**150 °C**		**145 °C**		**140 °C**	
time	**G''**	**time**	**G''**	**time**	**G''**	**time**	**G''**
min	**Pa**	**min**	**Pa**	**min**	**Pa**	**min**	**Pa**
13.389	1289	13.3885	1415	13.389	1690	13.38983	1644
16.78	1249	16.78	1351	16.775	1636	16.78167	1583
20.16667	1222	20.17167	1305	20.16167	1592	20.16833	1532
23.55667	1204	23.55833	1277	23.55	1559	23.55833	1500
26.945	1190	26.94667	1260	26.935	1541	26.94667	1475
30.335	1179	30.33667	1241	30.32333	1529	30.335	1456
33.725	1171	33.725	1231	33.71	1516	33.725	1445
37.11167	1167	37.11167	1226	37.09667	1507	37.11333	1438
40.5	1163	40.5	1225	40.48333	1505	40.50167	1428
43.89	1159	43.885	1220	43.87167	1495	43.89	1423
47.27667	1156	47.275	1219	47.26	1490	47.28	1418
50.66667	1150	50.66	1213	50.645	1485	50.66667	1414

54.055	1150	54.04833	1210	54.03333	1480	54.05333	1407
57.44333	1147	57.43833	1205	57.42167	1475	57.44167	1404
60.83167	1147	60.825	1202	60.80833	1472	60.83	1399
64.21833	1146	64.215	1200	64.195	1464	64.21667	1394
67.60833	1143	67.60167	1199	67.58333	1460	67.605	1391
70.99833	1142	70.98833	1195	70.97	1453	70.99333	1385
74.38667	1140	74.37667	1194	74.35833	1453	74.38333	1380
77.77333	1134	77.76333	1191	77.745	1445	77.77167	1374
81.165	1127	81.15167	1190	81.13167	1438	81.15833	1371
84.55167	1118	84.54	1188	84.52	1433	84.55	1367
87.94	1104	87.92833	1185	87.905	1428	87.93833	1365
91.32833	1087	91.31667	1183	91.29167	1422	91.325	1365
94.715	1065	94.705	1180	94.67833	1413	94.715	1360
98.105	1039	98.09333	1174	98.06667	1404	98.10333	1358
101.4917	1007	101.4833	1170	101.4533	1394	101.4917	1354
104.8817	968.1	104.8717	1159	104.8417	1372	104.8817	1349
108.2683	927.1	108.26	1150	108.2267	1362	108.2683	1345
111.6567	886.4	111.6483	1137	111.615	1334	111.6583	1339
115.045	844.2	115.0367	1121	115.0033	1322	115.0483	1336
118.4333	801.7	118.4233	1104	118.3917	1307	118.4383	1331
121.82	757.1	121.8133	1086	121.7783	1276	121.825	1325
125.2117	717.1	125.2	1066	125.1667	1258	125.2133	1321
128.5983	680.1	128.59	1044	128.5517	1234	128.6033	1313
131.9867	644.8	131.9767	1021	131.9383	1205	131.9917	1310
135.375	617.4	135.3633	994.4	135.3317	1177	135.38	1302
138.765	588.8	138.75	968.2	138.7183	1151	138.77	1294
142.1533	563.8	142.14	941.5	142.1067	1120	142.1583	1284
145.5417	548.5	145.5267	916.3	145.4933	1092	145.5483	1274
148.93	533.7	148.915	888.2	148.8817	1067	148.935	1265
152.3183	520.3	152.3033	860.9	152.2683	1037	152.325	1252
155.705	513.4	155.69	838.4	155.6567	1009	155.7133	1241
159.095	505	159.08	815.2	159.0417	983.6	159.1	1226
162.4817	503	162.4667	795	162.4317	958.2	162.4883	1211
165.8683	491.6	165.8533	772	165.8183	938.1	165.8783	1191
169.25	487.8	169.25	758.4	169.2	918.6	169.2667	1176
172.65	483.3	172.6333	742.7	172.6	897.8	172.65	1159
176.0333	481.1	176.0167	727	175.9833	880.5	176.05	1142
179.4167	478.1	179.4	715.4	179.3667	862.2	179.4333	1125
182.8167	475.5	182.8	702.6	182.75	853	182.8167	1105
186.2	473.6	186.1833	693.5	186.15	837.5	186.2167	1086
189.5833	471.7	189.5667	685.2	189.5333	828.9	189.6	1067

192.9833	469.9	192.9667	673.8	192.9167	816.6	192.9833	1047
196.3667	464.8	196.35	669	196.3	806.4	196.3833	1030
199.75	469.3	199.7333	661.6	199.6833	799.5	199.7667	1010
202.4167	469.3	203.1333	655.5	203.0833	793.4	203.15	993.5
		206.5167	648	206.4667	789.5	206.55	976.2
		209.9	645.4	209.85	780	209.9333	961.5
		213.3	641.5	213.2333	774.2	213.3167	944.2
		216.6833	638.4	216.6167	769.7	216.7167	929.2
		220.0667	632	220.0167	766.6	220.1	918.6
		223.4667	628.6	223.4	761.4	223.4833	898.8
		226.85	625.7	226.7833	759.6	226.8667	892.4
		230.2333	624.7	230.1667	756.4	230.2667	880
		233.6333	618.5	233.5667	753.5	233.65	869.6
		237.0167	618.2	236.95	751.1	237.05	859.8
		240.4	612.8	240.3333	746.6	240.4333	854.6
		243.7833	606.9	243.7167	748.2	243.8167	846.3
		247.1833	607.6	247.1167	747.8	247.2167	835.3
		250.5667	604.4	250.5	746.8	250.6	831.9

B.5. Kraton® D1161 Avrami Kinetics Analysis

B.5.1. T = 160 °C, $= \frac{G't - G'_0}{G'_\infty - G'_0}$, where G'_0 = 753 Pa, G'_∞ = 2296 Pa.

ln (t)	ln{-ln(1-X)}
1.220829921	-7.00455778
1.913485339	-5.69113783
2.319114395	-4.87809166
2.606755483	-4.40686988
2.829874443	-3.74057803
3.012179605	-3.34421004
3.166248307	-2.94457413
3.299841184	-2.62425092
3.417672037	-2.29998003
3.523021623	-2.03681235
3.618278147	-1.78570503
3.705367772	-1.55407254
3.785363187	-1.34470739
3.859465755	-1.12984895
3.928453942	-0.93989441
3.992957623	-0.75639427
4.053609369	-0.58717368

4.110737243	-0.42979636
4.164828913	-0.27697344
4.216095026	-0.13492078
4.264884019	-0.00416115
4.31140297	0.122999429
4.35585376	0.241422088
4.398391989	0.363844544
4.439253333	0.473068649
4.478453615	0.583559837
4.516193242	0.683193651
4.552560236	0.78307575
4.587667911	0.881380465
4.621568332	0.971158953
4.654357097	1.064308103
4.686104803	1.157698714
4.716875531	1.232403061
4.74671315	1.309385696
4.775714327	1.323877565
4.80387076	1.426339259
4.831256071	1.469198719
4.85787254	1.436509613
4.883937641	1.457908125
4.909217613	1.58033391
4.933874233	1.685578933
4.958054622	1.713748266
4.981549713	1.713748266
5.004505434	1.784263023
5.0270553	1.993540982
5.049000941	#NUM!
5.070475294	1.993540982
5.0870818	1.993540982

B.5.2. T = 150 °C, $= \frac{G'_t - G'_0}{G'_\infty - G'_0}$, where G'_0 = 864.8 Pa, G'_∞ = 2366 Pa.

ln (t)	**ln{-ln(1-X)}**
5.314191	-6.50735
6.00783	-5.15359
6.413131	-4.49983
6.700731	-3.93337
6.923924	-3.57388
7.106196	-3.2004

7.260382	-2.85138
7.39394	-2.64004
7.511743	-2.38083
7.61712	-2.15004
7.712444	-1.92519
7.799466	-1.71845
7.879556	-1.5146
7.95367	-1.34892
8.022667	-1.19226
8.08721	-1.02919
8.147838	-0.87915
8.204972	-0.73893
8.25907	-0.60829
8.310341	-0.4647
8.359158	-0.33808
8.405658	-0.21589
8.450091	-0.09838
8.492634	0.008653
8.53348	0.10652
8.572685	0.197954
8.610428	0.2932
8.646799	0.381627
8.681877	0.465472
8.715798	0.549293
8.748575	0.610433
8.780311	0.67736
8.81116	0.735758
8.840971	0.803773
8.869918	0.862593
8.898051	0.90027
8.925547	0.947033
8.952178	0.993781
8.978118	1.028454
9.003525	1.069706
9.028183	1.096104
9.052247	1.133624
9.07586	1.163839
9.098816	1.169074
9.121258	1.185156
9.143313	1.237331
9.164788	1.276194

9.185812	1.304442
9.206503	1.311848
9.226676	1.290055
9.24645	1.29718
9.265936	1.327125
9.284956	1.311848
9.303621	1.335012
9.321944	1.359784
9.340026	1.415488
9.357699	1.483007
9.375066	1.538477
9.392137	1.629108
9.409003	1.677216
9.425508	1.677216
9.441746	1.738202

B.5.3. T = 145 °C, $X = \frac{G't - G'_0}{G'_\infty - G'_0}$, where G'_0 = 1332 Pa, G'_∞ = 2674 Pa.

ln (t)	**ln{-ln(1-X)}**
5.314683	-5.12023
6.007584	-5.59136
6.413131	-4.42409
6.700731	-3.9744
6.923825	-3.55076
7.106196	-3.17449
7.260241	-2.84294
7.393755	-2.55905
7.511525	-2.27659
7.616923	-2.03189
7.71222	-1.80864
7.799261	-1.57998
7.879254	-1.39424
7.953389	-1.26239
8.022405	-1.04863
8.086964	-0.92119
8.147578	-0.75153
8.204754	-0.63131
8.258785	-0.50168

8.310071	-0.37404
8.358947	-0.26173
8.405457	-0.1502
8.44992	-0.05455
8.49247	0.046696
8.533303	0.13617
8.572514	0.214371
8.610265	0.291945
8.646606	0.373815
8.681724	0.449719
8.715618	0.519508
8.748353	0.590283
8.780219	0.657345
8.810952	0.695227
8.840768	0.763799
8.869722	0.818981
8.897997	0.881769
8.925361	0.928153
8.951997	0.982102
8.977942	1.032548
9.00323	1.059585
9.028015	1.097935
9.052083	1.128749
9.075585	1.167416
9.098548	1.216105
9.120995	1.256693
9.143057	1.24271
9.164537	1.286237
9.185566	1.301907
9.206162	1.344265
9.22644	1.413817
9.246219	1.461469
9.265614	1.569608
9.28464	1.610525
9.303403	1.721556
9.32173	1.808952
9.339727	1.974451
9.357406	1.974451
9.374863	1.633783
9.391937	1.808952

B.5.4. T = 140 °C, = $\frac{G\prime_t - G\prime_0}{G\prime_\infty - G\prime_0}$, where G'$_0$ = 1363 Pa, G'$_\infty$ = 2364 Pa.

ln (t)	ln{-ln(1-X)}
5.3146827	-5.2806603
6.0075839	-5.2806603
6.413295	-4.690831
6.7009771	-4.5849588
6.9241206	-4.2464353
7.1065242	-4.0507361
7.2605929	-3.6609392
7.3941857	-3.4427081
7.5120166	-3.2626412
7.6174154	-2.9343512
7.7126674	-2.7499733
7.7996713	-2.4949668
7.8797456	-2.2884832
7.9538454	-2.0955737
8.0228313	-1.8908666
8.0873944	-1.7508374
8.1480118	-1.5821485
8.2051911	-1.4173204
8.2592252	-1.2756213
8.310538	-1.142685
8.3593223	-1.0087248
8.4058146	-0.9077357
8.4502625	-0.7876997
8.492839	-0.6486698
8.5336569	-0.5525561
8.5728171	-0.4391272
8.6106835	-0.3329942
8.6469926	-0.2271301
8.6820294	-0.1346195
8.7160441	-0.0514593
8.748781	0.04516729
8.7804801	0.12552179
8.8113542	0.21523432
8.841159	0.28376534
8.870101	0.35387809
8.8983656	0.42614936
8.9257203	0.49492074
8.9523465	0.56351856

8.9784083	0.62527571
9.0036851	0.68681058
9.0283388	0.76846019
9.0523992	0.81015247
9.0760087	0.86324983
9.0989618	0.92552548
9.1215092	1.00567742
9.1434524	1.04717526
9.1649245	1.14897963
9.1860477	1.21380861
9.2066335	1.29048396
9.2268041	1.38686167
9.2466723	1.48336095
9.2660589	1.50290924
9.2850767	1.59872705

B.6. Kraton® D1161 – Piccotac™ 1095 Blends Rheology temperature ramp

Ramp rate: 1.5 °C/min, frequency: 1 Hz, strain: 0.5 %

90/10		70/30		50/50	
Temperature	**G'**	**Temperature**	**G'**	**Temperature**	**G'**
°C	**Pa**	**°C**	**Pa**	**°C**	**Pa**
80.2	2.41E+05	80.2	1.47E+05	80.2	68240
80.5	2.41E+05	80.4	1.47E+05	80.5	68270
81.6	2.39E+05	81.4	1.46E+05	81.5	67900
82.7	2.38E+05	82.4	1.46E+05	82.6	67480
83.7	2.36E+05	83.4	1.45E+05	83.5	67160
84.5	2.34E+05	84.5	1.44E+05	84.5	66680
85.5	2.33E+05	85.7	1.42E+05	85.6	66130
86.6	2.30E+05	86.9	1.41E+05	86.8	65470
87.8	2.27E+05	88.1	1.39E+05	88	64840
89	2.24E+05	89.1	1.37E+05	89.1	64070
90.1	2.21E+05	90	1.36E+05	90.1	63400
91.1	2.19E+05	91	1.34E+05	91	62570
92	2.16E+05	91.9	1.32E+05	92	61740
93	2.12E+05	92.9	1.30E+05	92.9	60800
93.9	2.09E+05	93.9	1.28E+05	93.9	59770
94.9	2.06E+05	94.9	1.26E+05	94.9	58720
95.9	2.02E+05	95.9	1.23E+05	95.9	57500

96.9	1.98E+05	97	1.21E+05	97	56260
98	1.94E+05	98	1.18E+05	98	54900
99	1.90E+05	99	1.15E+05	99	53540
100	1.85E+05	100	1.12E+05	100	52040
101	1.81E+05	101	1.09E+05	101	50440
102	1.77E+05	102	1.06E+05	102	48840
103	1.72E+05	103	1.03E+05	103	47090
104	1.67E+05	104	99410	104	45260
105	1.62E+05	105	95790	105	43390
106	1.56E+05	106	92230	106	41460
107	1.51E+05	107	88460	107	39500
108	1.45E+05	108	84740	108	37490
109	1.40E+05	109	80860	109	35450
110	1.34E+05	110	76910	110	33460
111	1.28E+05	111	73100	111	31470
112	1.22E+05	112	69230	112	29510
113	1.16E+05	113	65420	113	27560
114	1.11E+05	114	61680	114	25760
115	1.05E+05	115	58140	115	23980
116	99440	116	54670	116	22270
117	94070	117	51470	117	20680
118	88830	118	48390	118	19150
119	84000	119	45450	119	17740
120	79400	120	42680	120	16400
121	74990	121	40050	121	15110
122	70940	122	37590	122	13940
123	67040	123	35250	123	12830
124	63490	124	33000	124	11810
125	59990	125	30870	125	10880
126	56760	126	28880	126	10010
127	53710	127	26970	127	9210
128	50740	128	25180	128	8475
129	47900	129	23500	129	7780
130	45250	130	21920	130	7163
131	42710	131	20410	131	6607
132	40090	132	19010	132	6090
133	38010	133	17730	133	5607
134	35780	134	16530	134	5170
135	33670	135	15380	135	4753
136	31680	136	14330	136	4378
137	29800	137	13360	137	4023

138	27980	138	12470	138	3703
139	26320	139	11640	139	3395
140	24760	140	10850	140	3129
141	23270	141	10150	141	2877
142	21840	142	9480	142	2658
143	20610	143	8869	143	2454
144	19410	144	8293	144	2269
145	18270	145	7797	145	2100
146	17180	146	7337	146	1944
147	16240	147	6907	147	1801
148	15300	148	6509	148	1668
149	14490	149	6157	149	1532
150	13710	150	5822	150	1392
151	12970	151	5508	151	1257
152	12260	152	5213	152	1131
153	11620	153	4938	153	1001
154	11020	154	4678	154	889.7
155	10470	155	4417	155	789.3
156	9959	156	4174	156	698.9
157	9465	157	3913	157	617.9
158	9030	158	3674	158	545.4
159	8604	159	3450	159	480
160	8203	160	3230	160	420.8
161	7823	161	3016	161	364.2
162	7477	162	2813	162	314.1
163	7141	163	2633	163	270.7
164	6836	164	2464	164	238.5
165	6551	165	2310	165	207.5
166	6276	166	2167	166	187.4
167	6011	167	2033	167	165.9
168	5776	168	1903	168	151.3
169	5575	169	1780	169	136.2
170	5369	170	1659	170	124.6
171	5182	171	1541	171	113.2
172	4994	172	1427	172	102.1
173	4839	173	1309	173	94.55
174	4672	174	1191	174	87.31
175	4519	175	1077	175	80.1
176	4359	176	965.8	176	80.46
177	4207	177	861.6	177	73.5
178	4057	178	770.2	178	70.44

179	3921	179	689	179	69.7
180	3784	180	615.9	180	64.99
181	3642	181	552.5	181	62.65
182	3508	182	490.6	182	61.31
183	3351	183	437.1	183	58.94
184	3200	184	388.5	184	56.41
185	3050	185	343.4	185	55.72
186	2902	186	301.4	186	50.24
187	2750	187	264	187	49.41
188	2611	188	229.6	188	47.04
189	2475	189	203	189	43
190	2348	190	179.8	190	39.75
191	2225	191	160.4	191	40.38
192	2101	192	144.4	192	38.17
193	1996	193	130	193	38.89
194	1890	194	118.2	194	37.53
195	1781	195	111.1	195	37.03
196	1679	196	102.1	196	33.24
197	1575	197	93.57	197	32.39
198	1470	198	84.35	198	32.51
199	1361	199	81.05	199	31.53
200	1260	200	76.78	200	32.14
201	1143	201	66.77	201	30.95
202	1044	202	63.22	202	28.31
203	950.2	203	59.52	203	27.06
204	864.1	204	55.21	204	29.73
205	789.8	205	52.41	205	28.99
206	719.7	206	50.18	206	26.1
207	656.6	207	47.71	207	24.05
208	600.1	208	46.61	208	24.76
209	547.3	209	46.25	209	25.92
210	496.4	210	45.93	210	22.2
211	451.4	211	43	211	21.86
212	409.6	212	41.23	212	22.83
213	370.5	213	40.68	213	21.39
214	333	214	39.83	214	19.67
215	301.4	215	39.64	215	19.06
216	271.2	216	39.57	216	20.71
217	245.2	217	37.67	217	17.13
218	223.2	218	36.63	218	17.96
219	205.9	219	36.57	219	18.25

220	191.1	220	36	220	15.91
221	179.2	221	35.03	221	17.57
222	169.4	222	36.12	222	16.81
223	159.1	223	35.76	223	15.33
224	151	224	36.89	224	16.34
225	144.3	225	38.14	225	15.88
226	138.9	226	36.99	226	16.18
227	133	227	37.8	227	16.88
228	127.9	228	39.58	228	16.77
229	123.8	229	40.47	229	14.57
230	120.4	230	35.32	230	16.28
231	118.7	231	34.56	231	17.13
232	118.5	232	32.05	232	16.68
233	119.8	233	32.29	233	16.11
234	122.9	234	32.43	234	17.09
235	125.6	235	32.88	235	17.76
236	130.1				
237	136.9				
238	145.6				
239	156.3				
240	170.3				

B.7. Kraton® D1161 – Piccotac™ 1095 blend multifrequency analysis

B.7.1. Blend: 90/10, Temperature range: 150 – 270 °C, Frequency range: 0.1 – 100 Hz, Strain: 0.05

G'	**0.1**	**0.2154**	**0.4642**	**1**	**2.154**	**4.642**	**10**	**21.54**	**46.42**	**100**
150 °C	3280	4678	7868	15750	31270	53040	79860	1.12E+05	1.49E+05	1.84E+05
160 °C	2211	3516	5491	10140	21030	40600	66500	97280	1.34E+05	1.72E+05
170 °C	1530	2686	3965	6736	13610	28830	52860	82590	1.18E+05	1.58E+05
180 °C	884.7	1873	2902	4754	8925	19390	40040	68780	1.03E+05	1.43E+05
190 °C	371.4	1084	1994	3368	6117	12890	28780	55330	88370	1.27E+05
200 °C	110.5	420.3	1125	2194	4101	8504	19630	42120	73570	1.10E+05
210 °C	28.6	125.7	439.6	1197	2605	5576	12970	30360	58970	93120

220 °C	7.62	29.98	133.7	497.5	1412	3452	8343	20670	44680	75460
230 °C	3.068	10.83	43.17	182.7	649.8	1956	5230	13600	32220	59080
240 °C	2.048	5.074	22.45	89.22	320.5	1072	3239	8870	22370	44940
250 °C	1.944	5.858	13.1	50.6	187.3	657.1	2000	5620	14490	31070
260 °C	2.779	7.072	12.49	33.59	113.2	384.6	1181	3292	8359	17260
270 °C	3.401	3.979	6.04	15.69	48.39	159.7	498.3	1406	3630	5203

G"	**0.1**	**0.2154**	**0.4642**	**1**	**2.154**	**4.642**	**10**	**21.54**	**46.42**	**100**
150 °C	4644	8264	14940	25450	37510	48070	57100	64660	68160	64600
160 °C	3517	5980	10810	19440	32080	44920	55630	64960	72390	74030
170 °C	2800	4452	7874	14360	25520	39970	52960	63600	73300	78930
180 °C	2210	3509	5952	10750	19660	33540	49090	61810	73050	82100
190 °C	1574	2773	4645	8221	15080	27090	43540	58890	71520	83000
200 °C	983.6	1968	3568	6329	11510	21210	36640	54110	68680	81630
210 °C	597.7	1259	2534	4771	8810	16370	29610	47610	64370	78320
220 °C	365.8	785.2	1655	3405	6607	12490	23140	39750	58010	73060
230 °C	238.5	512.3	1096	2320	4762	9405	17810	31990	50380	66920
240 °C	167.3	359.6	764	1633	3416	6957	13600	25170	42260	60320
250 °C	120.6	258.8	543.1	1157	2436	4999	9936	18790	33040	50950
260 °C	83.07	174	366.9	773.5	1616	3326	6628	12660	22840	37340
270 °C	46.5	93.95	194.9	407.7	849.6	1742	3493	6773	12480	20960

B.7.2. Blend: 70/30, Temperature range: 150 – 270 °C, Frequency range: 0.1 – 100 Hz, Strain: 0.05

G'	**0.1**	**0.2154**	**0.4642**	**1**	**2.154**	**4.642**	**10**	**21.54**	**46.42**	**100**
150 °C	1744	2638	4074	7524	15760	31230	52240	77490	1.06E+05	1.31E+05
160 °C	729.8	1650	2694	4626	9282	20150	38400	61780	89410	1.14E+05
170 °C	196.9	678.6	1499	2785	5397	11820	25690	46600	72090	95290
180 °C	36.17	160	548.2	1397	2974	6583	15480	32310	54920	74870
190 °C	6.201	29.17	128.6	481.2	1389	3497	8743	20790	40150	57160
200 °C	1.967	7.882	31.1	132.1	505.8	1644	4722	12650	28410	43040
210 °C	1.216	3.845	11.71	47.11	185.1	700	2390	7278	18960	31130
220 °C	0.7581	2.844	5.855	21.78	87.32	339.8	1230	4066	11930	20760
230 °C	1.3	1.799	3.585	13.42	48.52	189.7	699.9	2359	7375	12580
240 °C	1.536	3.265	3.585	8.585	28.66	113.2	418.4	1411	4570	6323
250 °C	1.57	2.112	3.003	5.724	18.29	65.14	238.5	790.8	2695	1355
260 °C	3.695	3.846	4.886	6.114	11.28	31.74	107.1	347.4	1408	2221
270 °C	3.223	3.149	4.15	4.603	6.072	11.44	33.37	74.73	544.4	4205

G"	**0.1**	**0.2154**	**0.4642**	**1**	**2.154**	**4.642**	**10**	**21.54**	**46.42**	**100**
150 °C	2864	4677	8264	14950	24970	35750	44380	51090	54880	55580
160 °C	2089	3420	5765	10360	18530	29770	40500	48910	55300	59470
170 °C	1232	2344	4067	7139	12970	22730	34660	44900	52990	59900
180 °C	631.8	1331	2635	4849	8852	16130	27170	38800	48130	56830
190 °C	332.6	717.7	1518	3098	5983	11220	20130	31920	42570	52240

200 °C	196.8	419.8	892.4	1894	3925	7791	14700	25460	37300	47840
210 °C	124.2	266	564.2	1201	2552	5292	10550	19570	31580	43170
220 °C	84.29	180.1	380.5	809.5	1721	3625	7443	14520	25440	37830
230 °C	61.31	128.2	267	570.1	1214	2558	5309	10620	19680	31700
240 °C	45.57	92.53	191.8	403.4	855	1808	3769	7639	14600	24870
250 °C	30.96	62.97	129.1	270.4	571.6	1206	2517	5139	9977	17800
260 °C	23.2	40.1	79.67	160.4	332.8	694.8	1447	2970	5825	10820
270 °C	14.44	21.17	38.83	74.27	149.4	308	639.3	1327	2595	5473

B.7.3. Blend: 50/50, Temperature range: 130 – 240 °C, Frequency range: 0.1 – 100 Hz, Strain: 0.05

G'	**0.1**	**0.2154**	**0.4642**	**1**	**2.154**	**4.642**	**10**	**21.54**	**46.42**	**100**
130 °C	1400	2229	3909	7776	14750	24270	35280	46750	57780	63520
140 °C	694.9	1351	2266	4226	8684	16620	27330	39780	53050	61180
150 °C	158.3	506.1	1117	2138	4346	9392	18220	29940	43650	53370
160 °C	21.2	86.96	324.6	889.7	2026	4675	10600	20370	33030	42940
170 °C	4.662	13.68	54.93	216.3	728	2033	5291	12250	22970	32030
180 °C	2.447	5.228	14.84	47.99	192.8	720.4	2344	6597	14950	22540
190 °C	2.013	3.743	6.904	18.22	65.09	253.9	965.9	3248	9079	14780
200 °C	1.994	3.681	5.968	11.62	32	114.7	442.8	1592	5219	8808
210 °C	2.225	3.694	6.157	9.687	20.13	62.23	232.4	848.7	3011	4564
220 °C	2.536	4.205	6.376	9.444	16.28	41	141.6	498.8	1882	1855
230 °C	2.458	4.142	6.82	9.81	14.83	29.65	91.42	300.4	1192	27.24

240 °C	2.825	4.253	6.9	10.19	13.94	24	62.23	184.7	766.4	1168

G"	**0.1**	**0.2154**	**0.4642**	**1**	**2.154**	**4.642**	**10**	**21.54**	**46.42**	**100**
130 °C	2337	3951	6881	11230	15800	19220	21050	21310	20590	19840
140 °C	1666	2679	4561	7962	12910	18000	21850	24130	24800	24530
150 °C	900.9	1681	2897	5055	8887	14340	19800	23980	26610	27950
160 °C	392.4	833	1677	3143	5699	10090	15980	21570	25900	28850
170 °C	182.1	392.1	835	1747	3469	6531	11520	17680	23210	27450
180 °C	96.36	205.3	437.3	936.1	1974	4041	7775	13460	19720	24820
190 °C	57.93	122.3	258.4	550.6	1174	2476	5067	9665	15960	21650
200 °C	39.11	80.21	166	352	751.8	1595	3335	6707	12210	18100
210 °C	28.26	56.54	114.5	240	509.5	1083	2283	4704	9055	14660
220 °C	22.09	42.68	84.9	174.3	365.2	775	1642	3424	6784	11410
230 °C	17.81	32.76	63.17	127.1	264	559.2	1184	2485	5002	8801
240 °C	15.58	25.47	47.54	92.28	188.1	392.6	829.8	1743	3521	6339

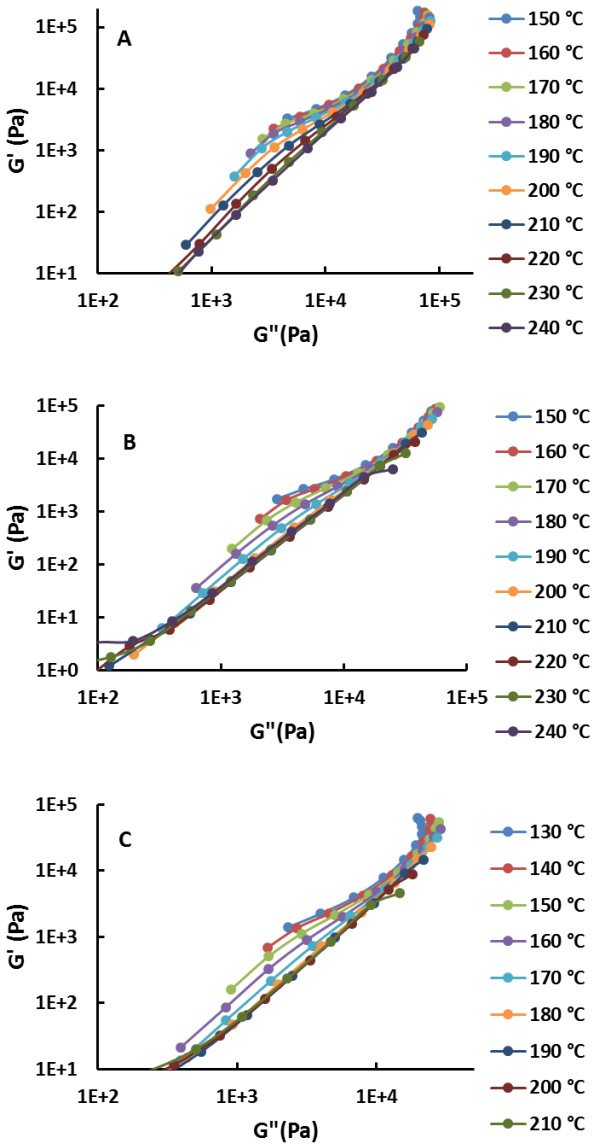

Figure B.1. *G'* vs *G"* plots of (A) 90/10, (B) 70/30, and (C) 50/50 Kraton® D1161 – Piccotac™ 1095 blends.

The temperature over which the slope of the *G'* vs *G"* plots changes corresponds to the LDOT, or the disordering of the PS domains. The LDOT occurs at temperatures significantly lower than the DMT, and the plots are parallel over a certain temperature range before they collapse above the DMT. These region of parallel slopes are an indication of the presence of equilibrium disordered PS domains in the blends at temperatures between the LDOT and DMT.[1]

(1) Han, C. D.; Vaidya, N. Y.; Kim, D.; Shin, G.; Yamaguchi, D.; Hashimoto, T. *Macromolecules* **2000**, *33*, 3767.

B.8. Kraton® D1161 – Piccotac 1095 Blends Isothermal Microphase Separation Kinetics Analysis – Shear Storage Modulus (G')

B.8.1. Blend: 90/10, Quench Temperatures – 160, 155, 150, 140 °C. Frequency: 0.01 Hz, Strain: .005

160 °C		155 °C		150 °C		140 °C	
time	G'	time	G'	time	G'	time	G'
min	Pa	min	Pa	min	Pa	min	Pa
13.38383	252.3	13.39267	537.4	10.04117	853.5	14.225	1460
16.76833	242.8	16.78	537.4	13.42967	844.5	14.075	1473
20.15333	235	20.16667	534.8	16.82	841.2	14.02	1471
23.54167	229.2	23.555	527.6	20.21	835	13.91667	1461
26.93	226.4	26.94167	524.4	23.59833	827.1	13.785	1448
30.315	223.1	30.33	518.8	26.985	818.5	13.64167	1438
33.70167	220.5	33.71833	514.5	30.37333	820	13.66667	1431
37.08667	219.9	37.105	513.3	33.76167	818.4	13.64	1419
40.475	218.7	40.49167	513.7	37.15	817.3	13.62167	1424
43.86	219.6	43.88	513.6	40.54	813	13.55	1421
47.24667	221.8	47.26833	522.4	43.92667	813.1	13.55167	1422
50.63333	225.1	50.655	531.2	47.31667	815.2	13.58667	1423
54.02	231.5	54.04333	542.1	50.70333	818.6	13.64333	1420
57.405	238.6	57.43	556.9	54.09167	821.6	13.69333	1425
60.79	249	60.81833	577.7	57.48	825.2	13.75333	1423
64.175	262.4	64.205	596.3	60.86667	830.8	13.84667	1431
67.565	277.5	67.59333	626.9	64.255	841.4	14.02333	1439
70.95333	296.1	70.97833	655.6	67.64167	856.5	14.275	1447
74.34167	316.9	74.36667	693.8	71.03333	872.6	14.54333	1460
77.72833	343.7	77.75833	730.9	74.42167	890.9	14.84833	1480
81.11667	373.3	81.145	777	77.80833	913.4	15.22333	1501
84.505	408.9	84.53	828.6	81.19667	937.7	15.62833	1517
87.89167	448.7	87.92	884.4	84.58333	970.4	16.17333	1553
91.28	493.4	91.30667	941.6	87.97333	1003	16.71667	1591
94.66833	543.4	94.695	1008	91.36333	1036	17.26667	1633
98.05667	594.9	98.085	1073	94.75	1080	18	1675
101.445	652.3	101.4733	1142	98.13667	1124	18.73333	1728
104.8333	710.3	104.8617	1214	101.525	1173	19.55	1779
108.2217	771.8	108.25	1278	104.915	1221	20.35	1832
111.61	836.2	111.6383	1348	108.305	1274	21.23333	1880
114.9967	898.7	115.03	1414	111.695	1324	22.06667	1931
118.385	959.3	118.4167	1475	115.08	1377	22.95	1964

121.7733	1014	121.8033	1532	118.4717	1425	23.75	1997
125.1617	1060	125.1933	1589	121.8583	1473	24.55	2022
128.5517	1101	128.58	1636	125.2483	1522	25.36667	2046
131.94	1159	131.9667	1682	128.6367	1562	26.03333	2064
135.3283	1197	135.355	1716	132.025	1605	26.75	2082
138.7183	1230	138.745	1749	135.415	1646	27.43333	2086
142.105	1267	142.1333	1773	138.805	1675	27.91667	2104
145.4933	1296	145.52	1793	142.1933	1698	28.3	2106
148.8817	1319	148.9083	1809	145.5833	1720	28.66667	2117
152.27	1333	152.2983	1815	148.9733	1737	28.95	2122
155.6567	1342	155.6867	1828	152.36	1751	29.18333	2119
159.045	1354	159.075	1835	155.7483	1762	29.36667	2131
162.435	1372	162.4633	1841	159.1383	1769	29.48333	2132
165.8233	1378	165.85	1848	162.525	1772	29.53333	2136
169.2167	1375	169.2333	1852	165.9133	1774	29.56667	2142
172.6	1369	172.6333	1851	169.3	1771	29.51667	2144
175.9833	1369	176.0167	1853	172.7	1773	29.55	2147
179.3833	1372	179.4	1856	176.0833	1779	29.65	2150
182.7667	1377	182.8	1857	179.4667	1773	29.55	2150
186.1667	1377	186.1833	1855	182.8667	1759	29.31667	
189.55	1379	189.5667	1849	186.25	1768	29.46667	
192.9333	1379	192.95	1846	189.65	1768	29.46667	
196.3167	1381	196.35	1847	193.0333	1771	29.51667	
199.7167	1382	199.7333	1839				
203.1	1382	203.1167	1839				
206.4833	1383	206.5167	1837				
209.8833	1383	209.9	1833				
213.2667	1383	213.2833	1833				
216.65	1382	216.6833	1831				
220.05	1381	220.0667	1824				
223.4333	1379	223.45	1822				
226.8167	1374						
230.2	1374						
233.6	1370						
236.9833	1370						
240.3667	1369						
243.7667	1370						
247.15	1368						
250.5333	1366						
253.9333	1364						
257.3167	1360						

B.8.2. Avrami Kinetics Analysis – 160 °C

$X = \frac{G'_t - G'_0}{G'_\infty - G'_0}$, where G'_0 = 1363 Pa, G'_∞ = 2364 Pa.

ln (t)	ln{-ln(1-X)}
-6.755737	7.711983
-5.106453	7.799003
-4.407316	7.879015
-3.825446	7.953097
-3.346056	8.022067
-2.975359	8.086678
-2.677356	8.147337
-2.401011	8.204527
-2.148092	8.258596
-1.930414	8.309916
-1.707163	8.35873
-1.502327	8.405249
-1.300626	8.449721
-1.112241	8.4923
-0.949479	8.533139
-0.779586	8.572376
-0.620057	8.610131
-0.465856	8.646513
-0.30808	8.681617
-0.160089	8.715514
-0.020429	8.748316
0.1060866	8.780076
0.2098347	8.810858
0.3079107	8.840735
0.4730113	8.869731
0.5897776	8.897911
0.711374	8.925331
0.8493374	8.951993
0.9813795	8.977976
1.0941909	9.0033
1.1846948	9.027999
1.2255735	9.052091
1.3288492	9.075628
1.6654203	9.098634

B.8.3. Avrami Kinetics Analysis – 155 °C

$X = \frac{G't - G'_0}{G'_\infty - G'_0}$, where G'_0 = 1363 Pa, G'_∞ = 2364 Pa.

ln (t)	ln{-ln(1-X)}
7.393841	-8.11932
7.511656	-8.40704
7.617042	-4.99151
7.712328	-4.31168
7.79936	-3.83199
7.879382	-3.41168
7.953508	-3.01361
8.022484	-2.75263
8.087038	-2.42666
8.147618	-2.1898
8.204792	-1.93619
8.258925	-1.73349
8.310203	-1.52113
8.358957	-1.31892
8.405511	-1.12945
8.44995	-0.95758
8.492519	-0.77844
8.53337	-0.61846
8.572598	-0.46061
8.610345	-0.30512
8.646719	-0.17212
8.681816	-0.0297
8.715755	0.104011
8.748533	0.229334
8.780271	0.350204
8.811062	0.477597
8.840904	0.590571
8.869882	0.712163
8.898057	0.812894
8.925473	0.924676
8.952145	1.019701
8.978111	1.113271
9.003432	1.203567
9.02814	1.242861
9.05224	1.344401
9.075773	1.413944
9.098765	1.488534

9.121229	1.610629
9.143179	1.721649
9.164761	1.688512
9.185785	1.760765
9.206377	1.974523

B.8.4. Avrami Kinetics Analysis – 150 °C

$X = \frac{G't - G'_0}{G'_\infty - G'_0}$, where G'_0 = 1363 Pa, G'_∞ = 2364 Pa.

ln (t)	**ln{-ln(1-X)}**
7.617332	-9.1757
7.712681	-6.08357
7.799643	-5.14749
7.879681	-4.71693
7.953786	-4.36538
8.022743	-3.98468
8.087281	-3.51189
8.147876	-3.07745
8.20509	-2.75384
8.259155	-2.47599
8.310422	-2.20963
8.359212	-1.97894
8.40571	-1.72676
8.450183	-1.51863
8.492763	-1.33763
8.533564	-1.12852
8.572766	-0.94539
8.610507	-0.76296
8.646893	-0.60001
8.682001	-0.43293
8.715918	-0.28387
8.748675	-0.13158
8.780454	0.003859
8.81121	0.139396
8.841077	0.280724
8.870063	0.400966
8.898233	0.538893
8.925645	0.684517
8.952325	0.801451
8.978299	0.90774

9.003627	1.028056
9.02833	1.142787
9.052414	1.264398
9.075943	1.396232
9.098943	1.51964
9.121403	1.594782
9.143381	1.660839
9.164875	1.567307
9.186	1.625588

B.8.5. Avrami Kinetics Analysis – 140 °C

$X = \frac{G\prime_t - G\prime_0}{G\prime_\infty - G\prime_0}$, where G'_0 = 1363 Pa, G'_∞ = 2364 Pa.

ln (t)	**ln{-ln(1-X)}**
7.394106	-4.98155
7.512	-5.8999
7.617302	-5.49375
7.712609	-5.20538
7.799618	-6.59373
7.879696	-4.79854
7.9538	-5.20538
8.022789	-4.10124
8.087324	-3.58484
8.147945	-3.24274
8.205128	-2.85212
8.259192	-2.44029
8.310506	-2.12879
8.359245	-1.93834
8.405763	-1.59703
8.450213	-1.31578
8.492771	-1.06025
8.533612	-0.84142
8.57283	-0.59891
8.610569	-0.3883
8.646935	-0.18349
8.682007	-0.00402
8.715924	0.186763
8.748697	0.313837
8.78046	0.447231
8.811201	0.555254

8.841053	0.667841
8.870041	0.760837
8.898211	0.864958
8.925623	0.890165
8.952278	1.01732
8.978241	1.033264
9.003546	1.130726
9.028227	1.182405
9.052325	1.150707
9.075868	1.29472
9.098835	1.309425
9.12132	1.375071
9.143289	1.507399
9.164754	1.569169
9.185881	1.703984

B.8.6.. Blend: 70/30, Quench Temperatures – 160, 150, 140 °C. Frequency: 0.01 Hz, Strain: .005

160 °C		**150 °C**		**140 °C**	
time	**G'**	**time**	**G'**	**time**	**G'**
min	**Pa**	**min**	**Pa**	**min**	**Pa**
6.690667	6.158	6.689333	35.21	6.688	1.506
10.07733	6.168	10.07633	35.92	10.0765	54.84
13.46217	4.172	13.4625	33.25	13.46167	92.83
16.84833	2.603	16.85	32.19	16.84833	89.75
20.235	2.42	20.23667	30.21	20.235	77.37
23.62	2.523	23.62333	30.09	23.62167	63.85
27.00833	1.758	27.00833	30.42	27.00833	49.48
30.395	1.803	30.395	29.82	30.395	41.37
33.78167	1.603	33.78333	28.72	33.78333	34.69
37.17	1.309	37.16833	27.79	37.17	30.02
40.555	1.424	40.555	27.48	40.555	27.47
43.94	1.363	43.94333	27.31	43.94	25.43
47.33	1.554	47.33	26.74	47.32667	24.18
50.715	1.252	50.71667	25.51	50.71333	23.38
54.10167	1.285	54.10167	25.02	54.1	22.36
57.48833	1.544	57.49	24.32	57.485	22.99
60.875	1.37	60.88	24.08	60.87333	22.18
64.26	1.391	64.26667	24.24	64.26167	21.53
67.64667	1.135	67.65167	24.69	67.65	21.05
71.03333	1.349	71.04	24.18	71.03667	20.73

74.42167	1.394	74.425	24.46	74.42333	19.93
77.80833	1.646	77.81333	24.07	77.81	20.33
81.19333	1.484	81.19833	23.94	81.19667	20.81
84.58	1.488	84.58667	24.46	84.585	20.71
87.96667	1.476	87.97333	23.93	87.97	20.74
91.35333	1.45	91.36	25.24	91.35667	20.5
94.74	1.731	94.74667	24.51	94.745	19.85
98.125	1.863	98.13333	24.13	98.13	19.64
101.5117	1.957	101.5217	23.66	101.5183	19.5
104.8983	1.956	104.9083	23.82	104.905	19.88
108.2833	1.797	108.295	24.6	108.2933	19.62
111.6717	1.77	111.6817	25.52	111.68	19.75
115.0567	1.813	115.0683	25.47	115.0667	19.74
118.4433	2.063	118.455	25.71	118.455	20.13
121.83	2.36	121.8417	25.3	121.8417	20.14
125.2167	2.419	125.23	25.24	125.23	19.84
128.6033	2.565	128.6167	25.4	128.6183	19.76
131.99	2.828	132.0017	23.98	132.005	19.95
135.375	2.978	135.3883	23.57	135.3933	19.83
138.7617	3.32	138.775	22.93	138.7817	20.29
142.15	3.549	142.1633	22.65	142.1683	20.44
145.5383	3.745	145.55	22.55	145.555	20.42
148.925	4.076	148.9367	23.53	148.945	21.27
152.3117	4.308	152.3233	23.68	152.33	22.04
155.6967	4.396	155.71	24.11	155.7183	22.73
159.0833	4.63	159.0967	24.15	159.1067	22.43
162.4717	4.837	162.4833	24.25	162.4933	22.42
165.8583	5.064	165.87	23.89	165.8817	22.19
169.25	5.474	169.25	23.72	169.2667	21.71
172.6333	5.853	172.65	24.19	172.6667	22.82
176.0167	6.181	176.0333	24.03	176.05	22.17
179.4167	6.607	179.4167	23.34	179.4333	22.62
182.8	6.882	182.8	23.76	182.8167	23.52
186.1833	7.243	186.1833	23.44	186.2	23.78
189.5667	7.524	189.5833	23.9	189.6	23.87
192.9667	7.904	192.9667	24.22	192.9833	23.94
196.35	8.306	196.35	24.34	196.3667	23.92
199.7333	8.661	199.7333	24.64	199.75	23.92
203.1167	9.071	203.1333	24.68	203.15	24.18
206.5167	9.457	206.5167	25.73	206.5333	24.37
209.9	9.829	209.9	25.19	209.9167	25.04

213.2833	10.26	213.2833	24.11	213.3	25.02
216.6667	10.68	216.6667	23.51	216.6833	25.2
220.0667	11.14	220.0667	23.7	220.0833	25.77
223.45	11.6	223.45	23.86	223.4667	26.25
226.8333	12.12	226.8333	24.49	226.8667	25.68
230.2167	12.64	230.2167	24.83	230.25	27.23
233.6167	13.14	233.6167	25.04	233.6333	27.65
237	13.71	237	25.23		
240.3833	14.26	240.3833	25.98		

B.8.7. Blend: 50/50, Quench Temperatures – 160, 140, 130 °C. Frequency: 0.01 Hz, Strain: .005

160 °C		**140 °C**		**130 °C**	
time	**G'**	**time**	**G'**	**time**	**G'**
min	**Pa**	**min**	**Pa**	**min**	**Pa**
6.689	1.128	6.689	0.155	6.688333	0.1557
10.07733	0.9771	10.07817	0.2241	10.07717	0.2199
13.464	0.8277	13.46583	0.3851	13.462	0.3983
16.85	0.7204	16.85333	0.6644	16.85	0.7254
20.23667	0.6284	20.24167	1.128	20.23667	1.213
23.62333	0.5599	23.63	1.301	23.62167	1.905
27.01167	0.5044	27.01667	1.165	27.00667	1.732
30.39833	0.4606	30.40333	1.07	30.395	1.64
33.78667	0.4231	33.79167	0.993	33.78333	1.524
37.17333	0.389	37.17833	0.928	37.16833	1.447
40.55833	0.3598	40.56667	0.8699	40.555	1.373
43.94667	0.3254	43.95333	0.8223	43.94167	1.321
47.33333	0.3075	47.34	0.7801	47.32833	1.28
50.72	0.2972	50.72833	0.7453	50.715	1.236
54.105	0.2835	54.11667	0.7181	54.10333	1.203
57.49167	0.2723	57.505	0.6878	57.49	1.164
60.88	0.2608	60.89167	0.6653	60.875	1.118
64.26667	0.2516	64.28	0.6474	64.26333	1.076
67.655	0.2381	67.66833	0.6222	67.65167	1.042
71.04167	0.23	71.05333	0.6029	71.03833	1.017
74.43	0.2265	74.44167	0.5916	74.42667	0.9962
77.81667	0.2072	77.83	0.5697	77.81167	0.9812
81.20167	0.1983	81.21667	0.5604	81.19833	0.9611
84.59167	0.1906	84.60333	0.5438	84.58333	0.9402
87.97667	0.1799	87.99	0.5306	87.97	0.9171

91.36833	0.1484	91.37833	0.5183	91.35667	0.8937
94.755	0.1591	94.765	0.5051	94.745	0.8717
98.14	0.1638	98.15333	0.4819	98.13167	0.8579
101.5267	0.1724	101.54	0.4773	101.5183	0.8342
104.9133	0.1767	104.9283	0.4596	104.9067	0.8203
108.3	0.1734	108.315	0.4462	108.2933	0.8027
111.6867	0.1774	111.7033	0.4376	111.6817	0.7876
115.075	0.1528	115.0917	0.4286	115.0667	0.7766
118.46	0.1468	118.4783	0.4191	118.455	0.8259
121.8483	0.1413	121.8667	0.4199	121.8417	0.7489
125.2367	0.1394	125.2533	0.4094	125.23	0.738
128.6233	0.1321	128.6383	0.4019	128.615	0.7261
132.01	0.1291	132.0267	0.3897	132	0.7172
135.3983	0.1243	135.415	0.3823	135.3867	0.7089
138.785	0.1195	138.8033	0.371	138.7733	0.7013
142.1733	0.1075	142.19	0.3637	142.1617	0.6937
145.56	0.1028	145.5783	0.3589	145.5467	0.6781
148.9483	0.1002	148.9633	0.3554	148.9333	0.6685
152.335	0.09473	152.3483	0.3522	152.32	0.6589
155.7233	0.09228	155.7383	0.342	155.7067	0.6582
159.1083	0.09381	159.1267	0.3081	159.0933	0.6581
162.4933	0.08885	162.5133	0.3052	162.4783	0.6528
165.8817	0.08555	165.9033	0.3001	165.8667	0.6525
169.2667	0.08454	169.2833	0.4076	169.25	0.6487
172.6667	0.08312	172.6833	0.3977	172.6333	0.6377
176.05	0.07975	176.0667	0.3788	176.0333	0.6325
179.4333	0.07828	179.45	0.3468	179.4167	0.6263
182.8167	0.07872	182.85	0.3311	182.8	0.6199
186.2167	0.07677	186.2333	0.3215	186.1833	0.6099
189.6	0.07807	189.6167	0.3199	189.5833	0.5991
192.9833	0.08568	193	0.322	192.9667	0.5917
196.3667	0.08727	196.4	0.3164	196.35	0.5822
199.7667	0.0767	199.7833	0.3142	199.7333	0.5806
203.15	0.05361	203.1667	0.3175	203.1333	0.5769
206.5333	0.05323	206.55	0.2963	206.5167	0.5719
209.9167	0.06368	209.95	0.313	209.9	0.5709
213.3167	0.06398	213.3333	0.2912	213.2833	0.5647
216.7	0.06848	216.7167	0.2886	216.6667	0.5577
220.0833	0.07266	220.1	0.2833	220.05	0.5511
223.4667	0.06423	223.4833	0.2841	223.45	0.5413
226.8667	0.04248	226.8833	0.2768	226.8333	0.5418

230.25	0.06466	230.2667	0.2755	230.2167	0.5375
233.6333	0.07474	233.65	0.2741	233.6	0.5354
237.0167	0.09975	237.05	0.272	236.9833	0.5432
240.4167	0.08915	240.4333	0.2707	240.3833	0.5345

B.9. Kraton® D1171 – Sylvalite® RE 100L Blends Rheology temperature ramp

Ramp rate: 3 °C/min, frequency: 1 Hz, strain: 0.01 %

D1171		**90/10**		**70/30**		**50/50**	
Temp	**G'**	**Temp**	**G'**	**Temp**	**G'**	**Temp**	**G'**
°C	**Pa**	**°C**	**Pa**	**°C**	**Pa**	**°C**	**Pa**
30.7	572000	30.7	160900	30	141100	30	73950
31.4	528200	31.4	168700	31.3	157800	30.8	93860
34.4	539000	33.7	173000	33.5	170700	31.9	92190
36.2	524200	35.6	177900	35.4	200100	32.9	92030
38	519600	37.3	173700	37.2	230000	33.9	91050
40	520200	39	172100	38.7	232700	34.9	90130
42	516700	41	174900	40.6	229500	35.8	88990
44	542200	43.4	177100	43.3	225500	36.9	87400
46	520300	45.8	175800	45.7	224100	37.9	86550
48	556400	48.1	201700	47.9	221200	38.8	87040
50	445400	50.3	205500	50.3	218700	39.9	84380
52	577000	52.2	190700	52.1	215300	40.8	85610
54	484800	54.1	193100	53.9	213700	41.7	86290
56	520000	56	218600	56	213000	42.8	80980
58	454300	57.9	168300	57.8	235100	43.5	82230
60	440200	59.9	182500	59.7	208700	44.3	80540
62	443700	61.9	177500	61.6	206200	45.3	80120
64	511400	63.9	156100	63.9	203700	46.6	78700
66	462700	66	135100	65.9	201300	47.8	78170
68	330900	68	158000	67.7	376600	48.9	77550
70	565800	70	157600	70	192100	50.1	75990
72	510100	72	151300	71.9	188100	51	75750
74	470100	74	138100	73.8	182900	51.9	74460
76	413600	76	141000	76	181000	53	73610
78	496500	78	135100	77.9	173400	53.9	72470
80	486900	80	130300	79.8	167800	54.8	72520
82	476100	82	127200	81.7	162300	55.9	71340

84	443500	84	121400	83.9	153100	56.9	70400
86	429100	86	116100	85.8	145800	57.8	70440
88	385400	88	114700	87.7	137900	59	69000
90	395500	90	112000	89.9	127700	59.9	68000
92	464300	92	107500	91.8	115500	60.9	67960
94	357100	94	103000	93.7	105800	61.8	67050
96	323000	96	99950	95.9	93380	62.9	66630
98	301900	98	99310	97.9	80920	63.9	65760
100	292200	100	92830	99.8	71780	64.8	64710
102	284300	102	87860	102	60710	65.9	63430
104	297300	104	86100	103.9	51780	66.9	62930
106	262600	106	79500	105.8	44570	67.8	61610
108	317400	108	79540	107.7	37530	69	60550
110	228900	110	69700	109.9	31220	69.9	60290
112	262500	112	70360	111.9	26300	70.9	59240
114	208400	114	66860	113.7	22350	72	57180
116	219200	116	62330	116	18900	72.9	56690
118	177600	118	53100	117.9	16080	73.9	55060
120	122600	120	53810	119.8	13840	75	53610
122	175300	122	50140	121.7	11680	75.9	51900
124	136100	124	46670	123.9	10050	76.9	50160
126	121300	126	43100	125.8	8495	78	48220
128	140900	128	40190	127.8	7555	78.9	46230
130	107600	130	37760	130	6336	79.9	44460
132	84380	132	35780	131.9	5588	80.8	42980
133.9	72070	134	32420	133.8	4724	82	40460
135.9	100300	136	30370	136	3951	82.9	38390
137.9	78240	138	27900	137.9	3442	83.9	36770
139.9	76880	140	25550	139.8	2999	85	34190
141.9	64860	142	23970	141.7	2563	85.9	32230
143.4	59380	144	21160	144	2097	86.9	30060
145	58880	146	20300	145.9	1802	88	27610
147.6	48120	148	18880	147.8	1627	88.9	25810
149.2	44300	150	16850	150	1352	89.9	23950
151.1	40010	152	15040	151.9	1208	91	21680
152.6	36860	154	13020	153.8	1071	91.9	19960
155	32080	156	11740	155.7	985.6	92.9	18260
157.7	28520	158	10940	157.9	882.5	93.9	16820
160.1	25840	160	9707	159.9	819.7	95	14860
162.2	24320	162	8913	161.8	783.1	95.9	13580
164.1	22600	164	8409	164	751.5	96.9	12290

166	21110	166	7893	165.9	704	98	10780
167.9	20030	168	7440	167.8	732.7	98.9	9818
169.9	18590	170	7058	169.7	681.7	99.9	9017
171.9	17940	172	6617	171.9	645.8	100.8	8156
174	16750	174	6255	173.8	620.9	101.9	7195
176	15670	176	5899	175.7	648.3	102.9	6424
178	15170	178	5494	178	639.1	103.9	5815
180	13810	180	5164	179.9	604.5	105	5241
182	12200	182	4831	181.8	608.9	105.9	4748
184	10140	184	4478	184	604.1	106.9	4304
186	8810	186	4171	185.9	596.8	108	3792
188	8068	188	3816	187.8	596.4	108.9	3426
190	7723	190	3501	190	597.1	109.9	3122
192	7387	192	3172	191.9	591.6	110.9	2873
194	7143	194	2851	193.8	592.7	112	2641
196	6874	196	2563	195.7	593.7	112.9	2402
198	6602	198	2316	198	587.3	113.9	2228
200	6329	200	2064	199.9	582.1	115	2013
202	5992	202	1834	201.8	587	115.9	1940
204	5558	204	1641	204	600.9	116.9	1768
206	5133	206	1473	205.9	613.7	118	1691
208	4628	208	1335	207.8	601.1	118.9	1615
210	4220	210	1208	209.7	603.8	119.9	1511
212	3876	212	1092	211.9	607.7	120.9	1434
214	3606	214	1005	213.8	610.4	122	1328
216	3277	216	940.1	215.7	612.7	122.9	1294
218	3022	218	871.1	218	598.3	123.9	1210
220	2744	220	813.7	219.9	598.8	125	1187
222	2465	222	772.4	221.8	604.3	125.9	1155
224	2163	224	740.2	224	599.6	126.9	1099
226	1871	226	713.4	225.9	592.8	127.8	1079
228	1593	228	679.9	227.8	595.5	129	1022
230	1389	230	662.2	229.7	589.5	129.9	998.7
232	1195	232	639.8	231.9	589.4	130.9	969.9
234	1070	234	636.8	233.9	590.8	132	955.5
236	934.4	236	639.6	235.8	588.5	132.9	937.3
238	830.3	238	635	238	594.6	133.9	917.7
240	723.8	240	628.4	239.9	583.3	135	896
242	639.1	242	630.3	241.8	590	136	877.5
244	603.5	244	637.2	243.7	587.5	136.9	874.4
246	575.5	246	647.8	245.9	594.8	137.8	843.4

248	565.8	248	677.4	247.9	578.2	139	858.3
250	563.9	250	704.8	249.7	598.2	139.9	843.1
						140.9	874.3
						142	843
						142.9	836.2
						143.9	834
						144.8	802.9
						146	818.1
						146.9	816.7
						147.9	813.6
						149	803.3
						149.9	786
						150.9	781.9
						152	780.1
						153	775.6
						153.9	786.9
						154.9	788.2
						156	781.8
						156.9	773.8
						157.9	765.1
						159	775.2
						159.9	757.6
						160.9	759.6
						161.9	757.6
						163	764.1
						163.9	759.2
						164.9	744.9
						166	742.3
						166.9	751.3
						167.9	747
						169	749.9
						170	743.2
						170.9	740
						171.9	735
						173	744.7
						173.9	739.6
						174.9	735.1
						176	739.7
						176.9	737.7
						177.9	735.2
						179	744.6

						180	740.9
						180.9	731
						181.9	736.4
						183	739.8
						183.9	734.8
						184.9	736.3
						186	739.8
						186.9	736.8
						187.9	741.1
						189	744
						190	739.4

B.10. Kraton® D1171 – Piccotac™ 1095 Blends Rheology temperature ramp

Ramp rate: 3 °C/min, frequency: 1 Hz, strain: 0.01 %

90/10		70/30		50/50	
Temperature	G'	Temperature	G'	Temperature	G'
°C	Pa	°C	Pa	°C	Pa
60.5	3.17E+05	60.5	1.96E+05	60.5	66650
60.9	3.34E+05	60.9	1.95E+05	60.9	66730
61.3	3.44E+05	61.3	1.97E+05	61.3	69760
61.7	3.21E+05	61.7	2.02E+05	61.7	67100
62.1	3.19E+05	62.1	2.00E+05	62.1	66830
62.6	3.14E+05	62.5	1.98E+05	62.6	69110
63.2	3.23E+05	62.9	1.96E+05	63.1	65460
63.7	3.17E+05	63.3	2.01E+05	63.5	68360
64.3	3.53E+05	63.8	1.95E+05	64.1	68250
64.9	2.97E+05	64.3	1.95E+05	64.7	63290
65.6	3.31E+05	64.9	1.98E+05	65.4	63440
66.2	3.04E+05	65.5	2.07E+05	65.9	68660
66.7	3.19E+05	66.1	1.98E+05	66.5	63420
67.3	3.21E+05	66.7	1.98E+05	67	60720
67.9	3.11E+05	67.3	1.99E+05	67.4	66350
68.4	3.05E+05	67.9	2.00E+05	67.8	63860
69	3.04E+05	68.5	1.96E+05	68.1	67610
69.5	3.07E+05	69.1	1.91E+05	68.5	63450
70	3.08E+05	69.6	1.99E+05	68.9	61200
70.4	2.99E+05	70.2	1.99E+05	69.3	61510

70.9	3.10E+05	70.7	1.92E+05	69.8	64130
71.3	3.04E+05	71.3	1.91E+05	70.3	65920
71.8	2.90E+05	71.8	1.93E+05	70.8	57050
72.2	2.92E+05	72.2	1.94E+05	71.4	62860
72.6	3.11E+05	72.7	1.94E+05	72	57440
73	3.09E+05	73.2	1.91E+05	72.7	62140
73.4	2.99E+05	73.6	1.92E+05	73.2	58530
73.9	3.29E+05	74.1	1.91E+05	73.7	58190
74.3	3.01E+05	74.5	1.92E+05	74.2	59380
74.7	3.09E+05	74.9	1.92E+05	74.7	63290
75.1	3.09E+05	75.3	1.91E+05	75.2	62250
75.6	2.89E+05	75.8	1.89E+05	75.7	62970
76	2.97E+05	76.2	1.84E+05	76.2	61580
76.5	3.04E+05	76.6	1.94E+05	76.7	61600
76.9	3.14E+05	77.1	1.88E+05	77.2	60710
77.4	2.98E+05	77.6	1.88E+05	77.7	61010
77.9	3.07E+05	78	1.88E+05	78.1	62260
78.4	2.85E+05	78.5	1.84E+05	78.6	59900
78.8	2.88E+05	78.9	1.86E+05	79.1	60360
79.3	2.91E+05	79.4	1.84E+05	79.6	61110
79.8	3.02E+05	79.8	1.92E+05	80	60890
80.2	2.90E+05	80.3	1.80E+05	80.5	60310
80.7	2.96E+05	80.8	1.83E+05	80.9	60480
81.2	2.87E+05	81.3	1.81E+05	81.4	60450
81.7	2.98E+05	81.7	1.84E+05	81.9	60170
82.1	2.85E+05	82.2	1.78E+05	82.3	59450
82.6	3.07E+05	82.7	1.77E+05	82.8	59930
83.1	2.95E+05	83.2	1.78E+05	83.3	59720
83.6	2.84E+05	83.7	1.86E+05	83.8	59210
84	2.52E+05	84.1	1.78E+05	84.2	59010
84.5	2.96E+05	84.6	1.75E+05	84.7	59460
85	2.88E+05	85.1	1.83E+05	85.2	58870
85.4	2.79E+05	85.6	1.70E+05	85.6	58590
85.9	2.75E+05	86	1.72E+05	86.1	58450
86.3	2.82E+05	86.5	1.78E+05	86.6	58860
86.8	2.81E+05	87	1.75E+05	87.1	57660
87.3	2.64E+05	87.4	1.72E+05	87.5	57220
87.7	2.56E+05	87.9	1.71E+05	88	57370
88.2	2.67E+05	88.4	1.70E+05	88.4	56770
88.6	2.77E+05	88.8	1.71E+05	89	56660
89.1	2.58E+05	89.3	1.67E+05	89.4	56100

89.6	2.67E+05	89.8	1.64E+05	89.9	56140
90	2.77E+05	90.2	1.70E+05	90.4	55850
90.5	2.63E+05	90.7	1.67E+05	90.9	55270
90.9	2.55E+05	91.1	1.61E+05	91.4	55540
91.4	2.62E+05	91.6	1.64E+05	92	54410
91.9	2.54E+05	92.1	1.62E+05	92.5	54430
92.3	2.50E+05	92.6	1.61E+05	93	53900
92.8	2.30E+05	93.1	1.60E+05	93.5	53620
93.3	2.31E+05	93.5	1.53E+05	94	53180
93.7	2.51E+05	94	1.59E+05	94.5	52800
94.2	2.37E+05	94.5	1.50E+05	95	52560
94.6	2.53E+05	94.9	1.49E+05	95.4	52110
95.1	2.17E+05	95.3	1.52E+05	95.9	52030
95.6	2.46E+05	95.8	1.51E+05	96.4	51220
96.1	2.31E+05	96.3	1.52E+05	96.8	50780
96.6	2.45E+05	96.7	1.51E+05	97.2	50610
97.1	2.46E+05	97.2	1.49E+05	97.6	50100
97.5	2.15E+05	97.6	1.53E+05	98.1	49400
98	2.20E+05	98.1	1.42E+05	98.5	48820
98.5	2.20E+05	98.6	1.47E+05	98.9	48590
98.9	1.97E+05	99.1	1.40E+05	99.3	47910
99.4	2.46E+05	99.5	1.48E+05	99.7	47630
99.9	2.04E+05	100	1.43E+05	100.1	46890
100.3	2.24E+05	100.4	1.39E+05	100.5	46380
100.8	2.21E+05	100.9	1.39E+05	101	46300
101.3	1.99E+05	101.4	1.36E+05	101.4	45220
101.8	2.09E+05	101.8	1.38E+05	101.8	45130
102.2	1.95E+05	102.3	1.29E+05	102.3	44230
102.7	1.94E+05	102.8	1.32E+05	102.8	43470
103.1	1.87E+05	103.2	1.36E+05	103.2	42500
103.6	2.09E+05	103.7	1.29E+05	103.7	42200
104.1	1.96E+05	104.2	1.35E+05	104.2	41040
104.6	2.00E+05	104.6	1.25E+05	104.7	40300
105	1.94E+05	105.1	1.22E+05	105.2	39210
105.5	1.93E+05	105.6	1.24E+05	105.7	38620
105.9	1.75E+05	106	1.24E+05	106.2	37770
106.4	2.02E+05	106.5	1.20E+05	106.8	36760
106.9	1.77E+05	106.9	1.17E+05	107.3	35990
107.4	1.77E+05	107.4	1.15E+05	107.9	34760
107.8	1.92E+05	107.9	1.16E+05	108.4	33820
108.3	1.73E+05	108.4	1.11E+05	109	32780

108.8	1.59E+05	108.8	1.15E+05	109.5	31870
109.2	1.72E+05	109.3	1.08E+05	110.1	30920
109.7	1.70E+05	109.7	1.02E+05	110.6	30110
110.1	1.69E+05	110.2	1.01E+05	111.1	28860
110.6	1.63E+05	110.7	1.03E+05	111.6	28020
111.1	1.61E+05	111.1	97710	112.1	27180
111.6	1.49E+05	111.6	95510	112.6	27100
112	1.51E+05	112	92680	113	25800
112.5	1.35E+05	112.5	92610	113.5	25580
112.9	1.58E+05	112.9	91350	114	24470
113.4	1.34E+05	113.4	89870	114.4	23670
113.9	1.38E+05	113.9	88920	114.9	23170
114.4	1.29E+05	114.4	83120	115.3	22390
114.9	1.25E+05	114.8	83740	115.8	21590
115.3	1.31E+05	115.3	82140	116.2	21120
115.8	1.33E+05	115.8	80150	116.6	20110
116.2	1.25E+05	116.3	74380	117.1	19480
116.7	1.07E+05	116.7	76150	117.5	18740
117.1	1.24E+05	117.2	74050	118	18000
117.6	1.13E+05	117.7	72030	118.4	17340
118.1	1.09E+05	118.1	70240	118.9	16990
118.6	1.03E+05	118.6	65130	119.4	16410
119.1	1.04E+05	119	62840	119.8	15820
119.5	86450	119.5	62200	120.3	15150
120	1.04E+05	120	61400	120.8	14670
120.5	97580	120.4	59780	121.2	14160
120.9	93800	120.9	58660	121.7	13600
121.4	93580	121.4	52940	122.2	13130
121.8	91310	121.9	54900	122.7	12550
122.3	81810	122.4	54130	123.2	12210
122.8	77690	122.9	48280	123.7	11790
123.3	82010	123.4	48500	124.2	11300
123.7	88100	123.9	49090	124.7	10900
124.2	83900	124.4	45290	125.1	10620
124.7	74650	124.8	44120	125.6	10180
125.1	68900	125.3	43710	126.1	9877
125.6	72710	125.8	43060	126.6	9551
126	69530	126.3	41880	127	9207
126.5	69260	126.8	40280	127.5	8985
127	55630	127.2	37100	127.9	8646
127.4	68360	127.7	35760	128.4	8353

127.9	66340	128.2	36700	128.8	8056
128.4	63110	128.6	35360	129.3	7784
128.8	59400	129.1	35030	129.8	7580
129.3	50810	129.6	32690	130.2	7342
129.8	58500	130	31210	130.7	7072
130.2	57170	130.5	31640	131.1	6804
130.7	60530	131	27230	131.6	6683
131.2	52440	131.4	32260	132	6459
131.6	51360	131.9	29750	132.5	6272
132.1	49900	132.4	27730	132.9	6094
132.6	46970	132.8	27680	133.4	5931
133	47840	133.3	27830	133.8	5735
133.5	55480	133.8	24030	134.3	5585
134	45990	134.3	24960	134.7	5438
134.5	44570	134.8	23570	135.2	5268
134.9	43780	135.3	23740	135.6	5102
135.4	45070	135.7	24110	136.1	4975
135.9	44710	136.2	20230	136.5	4831
136.3	41040	136.7	20440	136.9	4684
136.8	45330	137.1	21900	137.4	4544
137.3	42700	137.6	19140	137.9	4414
137.8	35690	138.1	18570	138.3	4309
138.3	37850	138.6	18730	138.8	4189
138.7	31110	139.1	17890	139.2	4067
139.2	27900	139.6	17250	139.7	3943
139.7	37240	140	17050	140.1	3840
140.1	33180	140.5	15540	140.6	3736
140.6	28760	141	17140	141.1	3620
141	34730	141.4	15010	141.5	3517
141.5	34410	141.9	15120	142	3414
142	32490	142.4	15160	142.4	3324
142.4	30920	142.9	15740	142.9	3219
142.9	27860	143.3	14440	143.3	3148
143.4	29560	143.8	14290	143.8	3038
143.8	27990	144.3	13980	144.3	2944
144.3	27160	144.7	14450	144.7	2866
144.8	24590	145.2	12450	145.2	2775
145.2	23410	145.7	11770	145.7	2690
145.7	22530	146.1	12060	146.1	2598
146.2	21130	146.6	12000	146.6	2526
146.6	24950	147	12560	147	2443

147.1	21300	147.5	11660	147.5	2356
147.6	25330	148	11410	148	2262
148.1	18900	148.4	10970	148.4	2189
148.6	19050	148.9	11140	148.9	2112
149	18450	149.3	11030	149.3	2037
149.5	20200	149.8	10760	149.8	1952
149.9	21910	150.3	10100	150.3	1874
150.4	20200	150.8	10110	150.7	1806
150.8	22220	151.2	10210	151.1	1737
151.3	16910	151.7	8896	151.6	1656
151.7	18850	152.2	9890	152.1	1585
152.2	16270	152.6	9264	152.5	1512
152.7	17190	153.1	9437	153	1444
153.2	19090	153.5	9186	153.5	1366
153.6	17620	154	9495	153.9	1297
154.1	15580	154.4	8806	154.4	1230
154.6	17840	154.9	8553	154.8	1162
155	13790	155.4	8189	155.3	1103
155.5	14710	155.8	8085	155.7	1041
156	16590	156.3	8395	156.2	975.3
156.4	13740	156.7	8282	156.6	917.7
156.9	13880	157.2	7993	157.1	860.2
157.4	14980	157.7	7787	157.6	805.8
157.9	15660	158.1	7624	158	757.8
158.3	14000	158.6	7616	158.5	707.1
158.8	14180	159	7245	159	657.4
159.3	10700	159.5	7174	159.4	612.1
159.7	12250	159.9	7150	159.9	570
160.2	10590	160.4	7158	160.4	526.9
160.7	11210	160.9	6802	160.8	490
161.1	12260	161.3	6963	161.3	453.6
161.6	11520	161.8	6686	161.7	416.9
162	11320	162.2	6674	162.2	385.6
162.5	10880	162.7	6418	162.7	356
162.9	11480	163.1	6430	163.2	326.4
163.4	10730	163.6	6426	163.6	302.4
163.9	11170	164.1	6299	164.1	280
164.4	9750	164.6	6026	164.6	259.3
164.8	9920	165	6038	165	239.9
165.3	9711	165.5	5859	165.5	218.9
165.8	9389	165.9	5891	165.9	202.3

166.2	9235	166.4	5693	166.4	185
166.7	9284	166.8	5760	166.9	170.4
167.2	8970	167.3	5553	167.3	155.7
167.7	8733	167.7	5454	167.8	146.4
168.1	9827	168.2	5384	168.2	134.5
168.6	9369	168.6	5444	168.7	124.4
169.1	9283	169.1	5279	169.1	113.6
169.5	9049	169.5	5242	169.6	105.5
170	9561	170	4995	170.1	98.68
170.5	7661	170.4	4845	170.5	91.21
170.9	8273	170.9	4751	171	84.43
171.4	8962	171.3	4580	171.4	79.83
171.9	8498	171.8	4587	171.9	73.91
172.4	7910	172.3	4496	172.4	68.61
172.8	8163	172.7	4442	172.8	64.01
173.3	7850	173.2	4240	173.3	59.38
173.7	8249	173.7	4208	173.7	55.83
174.2	7667	174.1	4069	174.2	51.93
174.7	7977	174.6	3905	174.7	47.89
175.1	7267	175	3890	175.1	47.11
175.6	7935	175.5	3758	175.6	43.53
176	7608	176	3668	176	41.01
176.5	7336	176.4	3561	176.5	37.2
177	6773	176.9	3507	177	36.22
177.4	7220	177.3	3366	177.4	35.17
177.9	7072	177.8	3251	177.9	34.25
178.4	6881	178.2	3180	178.3	31.24
178.8	7205	178.7	3039	178.8	29.6
179.3	6972	179.2	3008	179.3	29.65
179.7	7208	179.6	2894	179.7	29.68
180.2	7089	180.1	2804	180.2	27.32
180.7	6586	180.6	2693	180.6	25.92
181.1	6568	181	2621	181.1	25.35
181.6	6441	181.5	2521	181.5	24.04
182.1	6676	182	2436	182	22.52
182.6	6191	182.4	2359	182.5	22.72
183	6313	182.9	2240	183	21.46
183.5	6352	183.3	2156	183.4	21.11
183.9	6408	183.8	2110	183.9	18.55
184.4	6205	184.2	2003	184.3	18.69
184.9	6344	184.7	1909	184.8	17.18

185.3	6216	185.2	1833	185.3	18.03
185.8	5995	185.6	1756	185.7	18.02
186.2	6110	186.1	1688	186.2	17.3
186.7	6068	186.6	1616	186.7	16.47
187.1	5850	187.1	1555	187.1	15.48
187.6	5826	187.5	1479	187.6	15.89
188	5514	188	1424	188	14.68
188.5	5622	188.5	1346	188.5	14.59
188.9	5905	189	1291	188.9	14.58
189.4	5778	189.5	1243	189.4	14.25
189.9	5631	189.9	1196	189.9	13.12
190.3	5729	190.4	1142	190.3	12.46
190.8	5371	190.8	1105	190.8	12.44
191.2	5389	191.3	1066	191.3	11.33
191.7	5298	191.7	1017	191.7	10.62
192.2	5183	192.2	973.5	192.2	11.03
192.6	5138	192.6	947.9	192.7	10.54
193.1	4990	193	899.6	193.1	11.02
193.5	4950	193.4	880.9	193.6	10.9
194	4949	193.9	841.6	194.1	10.67
194.5	4796	194.3	818.3	194.5	9.557
194.9	4662	194.7	786	195	9.262
195.4	4629	195.2	764.1	195.4	9.421
195.9	4623	195.6	733.7	195.9	9.25
196.3	4407	196	715.9	196.3	9.137
196.8	4502	196.5	694.5	196.8	8.175
197.2	4249	196.9	672.3	197.3	9.373
197.7	4025	197.3	651.7	197.7	9.211
198.1	4035	197.8	639	198.2	10.15
198.6	3849	198.2	617.4	198.7	9.66
199.1	3792	198.6	606.8	199.1	9.848
199.5	3557	198.9	594	199.6	8.622
200	3514	199.3	578.9	200.1	8.72
200.4	3383	199.8	558.2	200.5	8.645
200.9	3253	200.2	541.8	201	8.635
201.4	3135	200.7	524.2	201.5	8.365
201.8	3076	201.2	508.4	201.9	8.251
202.3	3080	201.8	493.3	202.4	7.478
202.7	2892	202.3	477.3	202.9	7.651
203.2	2806	202.9	458.4	203.3	8.931
203.7	2748	203.5	439.2	203.8	8.339

204.1	2630	204	427.5	204.2	8.307
204.6	2621	204.5	418.5	204.7	8.508
205	2524	205	405.9	205.2	7.999
205.4	2499	205.5	393.8	205.6	7.103
205.9	2452	206	388.8	206.1	6.831
206.4	2368	206.4	383.5	206.6	6.872
206.8	2282	206.9	375.5	207	7
207.3	2204	207.4	372.6	207.5	6.775
207.8	2127	207.8	366.3	207.9	6.761
208.2	2103	208.3	360.4	208.4	6.916
208.7	2074	208.8	352.6	208.9	6.962
209.1	1994	209.3	343.7	209.3	6.899
209.6	1929	209.8	336.9	209.8	7.888
210	1850	210.3	328.7	210.2	5.795
210.5	1814	211	317.8	210.7	5.243
210.9	1749	211.5	312.7	211.2	6.183
211.4	1673	212	313.9	211.6	6.698
211.9	1615	212.4	308.5	212.1	6.101
212.3	1585	212.9	301.2	212.6	5.48
212.8	1519	213.4	298.5	213	5.81
213.2	1448	213.9	296.4	213.5	6.05
213.7	1402	214.3	294.6	213.9	5.642
214.1	1368	214.7	290.6	214.4	5.76
214.6	1302	215	289.2	214.9	5.586
215.1	1245	215.4	286.1	215.4	5.187
215.5	1203	215.8	279.3	215.8	5.652
216	1140	216.4	273.4	216.3	5.388
216.4	1134	217	268.5	216.7	4.443
216.9	1076	217.4	267.7	217.2	4.498
217.4	1033	217.8	265.6	217.7	4.907
217.9	985	218.4	259.9	218.1	4.48
218.3	943.1	219.1	256.1	218.6	3.86
218.7	906.2	219.6	253.2	219	4.113
219.2	868.6	220	250.2	219.5	4.577
219.7	821.1	220.5	247.2	220	4.786
220.1	794.3	221	242.8	220.4	4.104
220.6	765.8	221.5	239.1	220.9	4.502
221.1	732.6	221.9	237.9	221.4	5.072
221.5	679.3	222.4	237.7	221.8	4.492
222	663.8	222.9	234.7	222.3	3.539
222.4	640.5	223.4	231.2	222.8	4.044

222.9	610.8	223.8	229.4	223.2	3.985
223.3	576	224.2	224.5	223.7	3.555
223.8	557.2	224.7	221.5	224.1	2.655
224.2	523.9	225.2	215.4	224.6	3.184
224.7	505.9	225.7	216.6	225.1	4.039
225.2	480.3	226.1	217.4	225.5	3.787
225.6	468.2	226.5	215.5	226	3.36
226.1	438.3	227	212.2	226.5	4.31
226.6	421.9	227.4	210.5	226.9	4.455
227.1	400.4	227.8	211	227.4	3.719
227.5	385.8	228	210.1	227.8	3.614
228	372.7	228.3	209	228.3	3.83
228.4	358.3	228.7	208	228.8	3.206
228.9	338.2	229.1	209.6	229.2	2.952
229.3	331.7	229.4	206.9	229.7	3.646
229.8	311.8	229.8	207.8	230.1	2.633
230.2	298.4	230.1	205.7	230.6	3.766
230.7	280.1	230.6	204.8	231.1	3.913
231.1	276.3	231	205.7	231.5	3.78
231.6	264.9	231.5	203.8	232	3.685
232.1	251.8	231.9	201.3	232.4	4.502
232.5	246.7	232.4	202.6	232.9	3.551
233	235.9	232.9	201.6	233.4	3.212
233.4	229.4	233.4	199	233.8	4.491
233.9	221.5	233.9	199.3	234.3	3.833
234.3	213.5	234.4	197.7	234.8	3.224
234.8	209.2	234.8	196.1	235.2	3.585
235.3	199.7	235.3	195.3	235.7	3.322
235.8	201.3	235.8	194.4	236.1	3.257
236.2	191.6	236.3	192.3	236.6	3.561
236.7	186.7	236.7	189.9	237.1	4.001
237.2	182.2	237.2	191.8	237.5	3.352
237.6	179.5	237.7	190.3	238	3.552
238.1	179.2	238.1	188.5	238.5	4.052
238.5	171	238.6	188.6	238.9	3.099
239	170.1	239	189.9	239.4	3.846
239.4	167.1	239.4	188.1	239.8	4.328
239.9	165.1	239.9	188.2	240.3	3.948
240.3	162.6	240.3	186.1		

B.11. Kraton® D1171 multifrequency analysis

Temperature range: 120 – 230 °C, Frequency range: 0.01 – 100 Hz, Strain: 0.001

G'	120 °C	130 °C	140 °C	150 °C	160 °C	170 °C	180 °C	190 °C	200 °C	210 °C	220 °C	230 °C
0.01	10970	8908	7028	6457	6216	6165	5687	4439	1755	58.39	7.273	154.5
0.01778	13880	11280	9272	8245	7676	7539	7121	5333	3068	91.05	22.26	230
0.03162	19050	14280	11700	10330	9483	9141	8585	5869	4201	187.4	52.95	292.6
0.05623	25970	18060	14710	13070	11790	11030	10190	6313	5045	421.5	135.5	369.3
0.1	39600	24490	18640	16240	14520	13350	12100	6852	5717	956.8	362.6	517.3
0.1778	64320	35550	24300	20060	17700	15980	14400	7616	6456	1989	936.6	867.7
0.3162	1.01E+05	55740	34540	25790	21580	19100	17090	8801	7504	3516	2113	1672
0.5623	1.47E+05	86290	52840	36070	27640	23280	20350	10580	9054	5438	3991	3218
1	2.04E+05	1.27E+05	82290	54930	38650	29990	25060	13450	11460	7900	6513	5598
1.778	2.65E+05	1.77E+05	1.22E+05	85290	59150	42450	33090	18410	15320	11390	9749	8990
3.162	3.24E+05	2.37E+05	1.69E+05	1.26E+05	91220	65310	48520	27940	22350	17010	14670	13960
5.623	3.81E+05	3.05E+05	2.23E+05	1.73E+05	1.34E+05	1.01E+05	76190	46760	35650	26630	22710	21690
10	4.32E+05	3.74E+05	2.88E+05	2.30E+05	1.84E+05	1.46E+05	1.17E+05	80040	60800	44530	36710	33770
17.78	4.81E+05	4.40E+05	3.61E+05	2.93E+05	2.41E+05	1.99E+05	1.68E+05	1.27E+05	1.01E+05	76160	61200	54090
31.62	5.26E+05	5.00E+05	4.40E+05	3.68E+05	3.09E+05	2.62E+05	2.26E+05	1.84E+05	1.53E+05	1.23E+05	1.02E+05	88790

56.23	5.73 E+05	5.55 E+05	5.09 E+05	4.44 E+05	3.83 E+05	3.32 E+05	2.94 E+05	2.45 E+05	2.14 E+05	1.80 E+05	1.56 E+05	1.38 E+05
100	6.15 E+05	6.05 E+05	5.75 E+05	5.27 E+05	4.70 E+05	4.19 E+05	3.78 E+05	3.23 E+05	2.86 E+05	2.50 E+05	2.21 E+05	1.99 E+05

G"	**120 °C**	**130 °C**	**140 °C**	**150 °C**	**160 °C**	**170 °C**	**180 °C**	**190 °C**	**200 °C**	**210 °C**	**220 °C**	**230 °C**
0.01	11950	7745	5331	4323	3827	3634	3510	2116	2270	440.4	228.9	198.6
0.01778	17370	10870	7730	6171	5093	4388	4010	1982	2638	720.1	427.4	352.4
0.03162	26370	15490	10680	8288	6696	5553	4780	2091	2738	1217	767.9	619.2
0.05623	39770	22750	14930	11190	8876	7130	5962	2603	2911	2039	1364	1088
0.1	59190	34400	21440	15420	11770	9278	7634	3666	3518	3303	2371	1900
0.1778	81800	51500	32110	22090	16110	12390	10020	5532	4868	5021	3963	3254
0.3162	1.07 E+05	73030	48290	32880	23210	17250	13640	8568	7257	7201	6232	5354
0.5623	1.28 E+05	96440	69420	49340	34860	25360	19560	13400	11110	10180	9261	8324
1	1.43 E+05	1.19 E+05	92550	71170	52380	38450	29350	21080	17210	14720	13450	12340
1.778	1.49 E+05	1.40 E+05	1.15 E+05	94890	75550	57930	44870	33210	26800	21930	19450	18010
3.162	1.48 E+05	1.59 E+05	1.35 E+05	1.17 E+05	1.00 E+05	82600	67130	51680	41710	33430	28840	26460
5.623	1.43 E+05	1.69 E+05	1.55 E+05	1.37 E+05	1.23 E+05	1.08 E+05	94310	77090	63160	50800	43580	39030
10	1.36 E+05	1.68 E+05	1.73 E+05	1.57 E+05	1.42 E+05	1.30 E+05	1.21 E+05	1.07 E+05	91920	75340	64840	57560
17.78	1.28 E+05	1.62 E+05	1.83 E+05	1.74 E+05	1.62 E+05	1.52 E+05	1.44 E+05	1.34 E+05	1.22 E+05	1.05 E+05	93230	83280

31.62	1.23 E+05	1.51 E+05	1.81 E+05	1.87 E+05	1.81 E+05	1.74 E+05	1.67 E+05	1.57 E+05	1.49 E+05	1.34 E+05	1.25 E+05	1.14 E+05
56.23	1.28 E+05	1.50 E+05	1.78 E+05	1.96 E+05	1.97 E+05	1.94 E+05	1.91 E+05	1.81 E+05	1.72 E+05	1.58 E+05	1.52 E+05	1.45 E+05
100	1.07 E+05	1.25 E+05	1.51 E+05	1.80 E+05	1.94 E+05	2.02 E+05	2.08 E+05	2.05 E+05	1.99 E+05	1.84 E+05	1.80 E+05	1.76 E+05

B.12. Kraton® D1171 – Sylvalite® RE 100L Blends multifrequency analysis

B.12.1. Blend: 90/10, Temperature range: 120 – 230 °C, Frequency range: 0.01 – 100 Hz, Strain: 0.001

G'	**120 °C**	**130 °C**	**140 °C**	**150 °C**	**160 °C**	**170 °C**	**180 °C**	**190 °C**	**200 °C**	**210 °C**	**220 °C**	**230 °C**
0.01	3485	2936	3056	3026	138.2	24.24	6.262	1.798	0.6874	1.424	27.51	220.4
0.01778	4166	3470	3596	3644	357.7	84.04	20.96	6.3	2.334	2.974	38.77	277.4
0.03162	5060	4179	4213	4225	779.7	235.6	65.69	20.09	6.817	6.014	49.23	318.6
0.05623	6712	5057	5004	4861	1398	573.2	194.9	62.79	20.59	13.03	61.36	354.7
0.1	10090	6464	6003	5655	2123	1138	506.4	186.1	62.72	32.79	81.89	397.3
0.1778	15520	8853	7338	6554	2953	1885	1087	497.3	185.2	88.25	127.9	469.4
0.3162	25540	13290	9626	7925	3987	2780	1910	1103	498.3	238.7	239.1	607.8
0.5623	41060	21660	13960	10260	5464	3942	2969	2009	1145	608	503.3	886.3
1	61420	34600	22180	14780	8045	5695	4445	3215	2219	1389	1099	1444
1.778	85350	52030	35240	23310	13010	8837	6795	4930	3829	2743	2258	2501
3.162	1.12 E+05	73380	52750	37060	22360	14910	11020	7796	6222	4896	4219	4358
5.623	1.38 E+05	99010	73860	55130	37510	26160	19210	13240	10470	8263	7349	7355
10	1.63 E+05	1.28 E+05	99040	76860	57700	44010	33930	23730	18390	14320	12410	12110
17.78	1.88 E+05	1.60 E+05	1.28 E+05	1.03 E+05	81440	66990	55670	41390	32680	25360	21480	19670

31.62	2.11 E+05	1.90 E+05	1.63 E+05	1.34 E+05	1.10 E+05	94130	82680	66100	55690	44020	36380	32080
56.23	2.34 E+05	2.18 E+05	1.98 E+05	1.69 E+05	1.44 E+05	1.26 E+05	1.12 E+05	96140	83460	70270	59190	51550
100	2.56 E+05	2.45 E+05	2.33 E+05	2.10 E+05	1.86 E+05	1.64 E+05	1.44 E+05	1.32 E+05	1.13 E+05	99400	85470	76400

G"	120 °C	130 °C	140 °C	150 °C	160 °C	170 °C	180 °C	190 °C	200 °C	210° C	220° C	230° C
0.01	2917	1840	1694	1665	702.1	352	214.3	133.2	86.17	61.67	55.11	77.63
0.01778	4405	2632	2181	1938	1163	639.3	388.2	243.6	156.5	112.9	97.38	126.7
0.03162	6836	3882	2923	2345	1752	1094	688.3	437.9	279.9	203.2	171.3	201.9
0.05623	10740	5817	4071	3073	2438	1742	1189	777	498.8	361.9	302.1	327.7
0.1	16810	9026	5970	4206	3301	2569	1947	1349	883.4	639.8	532.3	542.8
0.1778	25030	13990	9016	6113	4599	3642	2981	2248	1545	1123	934	911.5
0.3162	35130	21350	13890	9283	6718	5223	4374	3514	2616	1939	1626	1534
0.5623	45880	30810	21300	14420	10190	7759	6449	5243	4224	3260	2780	2559
1	55190	41200	30960	22100	15790	11910	9786	7797	6589	5332	4644	4194
1.778	62070	51080	41500	32230	24270	18570	15220	11780	10140	8460	7466	6682
3.162	65790	60600	51610	43260	35500	28460	23640	18140	15560	13190	11560	10290
5.623	66540	68960	61060	53560	47600	41150	35780	27890	24100	20130	17530	15560
10	64990	74400	70610	63230	58690	54250	50290	41170	36220	30200	26350	22830
17.78	62450	75060	78570	73330	69270	66040	64440	56120	52040	44340	38650	32770
31.62	61150	72890	83560	82210	79990	77420	77340	70180	68230	60760	54180	46470
56.23	60560	71390	83470	89010	91060	89450	89960	82150	82220	76480	70510	62370
100	59250	65890	78680	90510	99940	1.02E+05	1.04E+05	96700	97450	91950	87160	78740

B.12.2. Blend: 70/30, Temperature range: 90 – 210 °C, Frequency range: 0.01 – 100 Hz, Strain: 0.001

G'	90 °C	100 °C	110 °C	120 °C	130 °C	140 °C	150 °C	160 °C	170 °C	180 °C	190 °C	200 °C	210 °C
0.01	4758	1752	575.6	52.84	3.302	0.6385	0.06705	0.062	0.02458	0.0182	0.01405	0.4744	0.8962
0.01778	10710	3112	1234	124.9	13.93	2.088	0.4526	0.142	0.06125	0.03269	0.03276	0.3203	0.4826
0.03162	12190	4331	2086	384.8	45.45	6.987	1.384	0.3715	0.1631	0.08511	0.08311	0.2917	0.341
0.05623	21660	6481	3279	915	134.4	21.62	4.315	1.121	0.4789	0.2498	0.2324	0.3806	0.3594
0.1	35510	10820	5053	1762	371.6	66.1	13.4	3.404	1.475	0.7672	0.6271	0.731	0.6625
0.1778	52950	19360	8524	2991	901	195.6	41.04	10.46	4.544	2.322	1.797	1.751	1.495
0.3162	72930	33510	15300	4991	1875	531.6	122.5	32.02	13.78	7.037	5.047	4.639	3.752
0.5623	93530	53010	27870	8914	3543	1265	347	94.35	41.12	21.05	14.45	12.56	9.716
1	1.14E+05	75430	47330	16490	6672	2695	937.3	268.4	119.6	61.57	40.94	34.6	26.34
1.778	1.34E+05	98920	70470	29700	12850	5490	2292	745.7	332.6	174.4	112.6	94	70.56
3.162	1.53E+05	1.23E+05	96150	48340	24110	11140	5081	1900	909.3	454.5	303.3	245.5	186.6
5.623	1.72E+05	1.46E+05	1.22E+05	71020	40710	21470	10970	4674	2289	1243	806.7	627.3	472.2
10	1.91E+05	1.68E+05	1.49E+05	96950	61140	36990	21870	10540	5694	3119	2025	1517	1144
17.78	2.09E+05	1.90E+05	1.75E+05	1.26E+05	85620	56360	37370	21830	13100	7575	4946	3690	2787
31.62	2.29E+05	2.12E+05	2.01E+05	1.55E+05	1.14E+05	79160	57170	38920	26480	16800	11740	8439	6444

56.23	2.46E+05	2.34E+05	2.25E+05	1.85E+05	1.45E+05	1.06E+05	79900	59540	44660	31750	25270	18080	14830
100	2.66E+05	2.57E+05	2.51E+05	2.15E+05	1.76E+05	1.37E+05	1.07E+05	80820	60700	44080	41620	30230	28250

G"	**90 °C**	**100 °C**	**110 °C**	**120 °C**	**130 °C**	**140 °C**	**150 °C**	**160 °C**	**170 °C**	**180 °C**	**190 °C**	**200 °C**	**210 °C**
0.01	9699	4058	2234	761.1	268.2	127.8	65.19	36.2	23.59	16.44	12.56	10.52	8.625
0.01778	18100	6866	3486	1232	501.6	229.8	117.2	63.91	41.82	29.13	22.29	18.68	15.13
0.03162	21720	9978	5226	2187	889.1	409.9	209	113.4	74.3	51.69	39.56	32.95	26.5
0.05623	30520	14790	8029	3549	1549	727	372.7	201.7	132	91.78	70.24	58.34	46.75
0.1	39370	22320	12460	5519	2649	1289	661.2	358	234.8	163.1	124.7	103.5	82.77
0.1778	46340	32340	19540	8458	4382	2264	1173	635.5	417	289.6	221.6	183.5	146.7
0.3162	50590	42960	29620	13210	7042	3879	2068	1128	739.5	514.2	393.5	325.6	260.2
0.5623	52570	51690	41390	20520	11160	6384	3581	1991	1311	912.6	697.7	577	461.1
1	52980	57240	52490	30560	17610	10270	6238	3481	2312	1612	1236	1020	815.8
1.778	52620	60030	60810	42020	26880	16280	10520	6171	4032	2834	2177	1795	1436
3.162	52010	60970	65550	52630	38170	25020	16740	10260	7134	4937	3827	3137	2511
5.623	51640	60890	67870	61510	48990	35570	25560	17170	12180	8473	6658	5432	4357
10	50650	59930	68290	68040	58450	45720	36690	26330	19890	14070	11150	9463	7495
17.78	50590	58300	66950	72020	67340	54720	46170	37610	30690	23050	18380	15470	12110
31.62	49170	57370	65630	72670	75060	63410	54440	47980	43010	35780	28500	24990	19830
56.23	50730	57020	64280	70700	79400	71620	62140	56270	53040	48120	40960	37530	30580
100	51750	56830	63380	69240	80900	79040	71460	65440	62460	58630	53190	50210	43060

B.12.3. Blend: 50/50, Temperature range: 70 – 190 °C, Frequency range: 0.01 – 100 Hz, Strain: 0.001

G'	70 °C	80 °C	90 °C	100 °C	110 °C	120 °C	130 °C	140 °C	150 °C	160 °C	170 °C	180 °C	190 °C
0.01	7821	494.8	29.88	3.669	0.7315	0.1897	0.09402	0.07861	0.05497	0.06058	0.06496	0.04835	0.04371
0.01778	12950	1177	67.9	11.65	2.363	0.8106	0.35 61	0.1983	0.1158	0.114	0.1053	0.09173	0.07488
0.03162	21460	2790	236.8	33.12	6.699	1.953	0.7237	0.3552	0.1993	0.2065	0.1562	0.1543	0.1321
0.05623	30150	5891	698.3	94.44	19.77	5.196	1.746	0.8112	0.3974	0.3681	0.257	0.238	0.2271
0.1	39660	11540	1884	277.9	57.2	14.67	4.784	1.927	0.9339	0.6757	0.4553	0.3743	0.3591
0.17778	49970	19890	4581	784.7	165.4	42.75	13.59	5.284	2.45	1.423	0.9305	0.6731	0.5904
0.31622	59410	30990	9929	2095	463.8	123.5	39.74	15.32	6.858	3.624	2.156	1.462	1.125
0.56223	68440	41850	18580	5146	1261	349.4	115.2	44.59	19.78	10.23	5.853	3.628	2.547
1	77840	53310	29600	11170	3259	969	329.5	130.3	58.74	29.73	16.63	10.19	6.771
1.778	87060	64890	41750	20220	7639	2582	926.2	367.4	170.3	86.98	48.83	29.58	19.23
3.162	96800	76600	54540	31320	15180	6325	2490	1022	483.9	239.7	130.2	77.77	55.66
5.623	1.07E+05	88460	67690	43760	25100	13160	6085	2673	1329	708	378.2	249.5	163
10	1.17E+05	99970	80720	57290	36650	22820	12850	6641	3425	1912	1084	716.2	429.4
17.78	1.26E+05	1.12E+05	94300	71630	49960	33980	22130	13740	8111	4898	3008	1918	1185
31.62	1.36E+05	1.24E+05	1.07E+05	86390	65290	46940	32880	23270	16170	10870	7426	4706	3294
56.23	1.47E+05	1.34E+05	1.19E+05	1.01E+05	81510	61690	45230	34040	26200	19720	15730	9973	8876
100	1.56E+05	1.43E+05	1.29E+05	1.14E+05	95970	73320	56060	42960	31520	24750	23420	13720	16340

G"	70 °C	80 °C	90 °C	100 °C	110 °C	120 °C	130 °C	140 °C	150 °C	160 °C	170 °C	180 °C	190 °C
0.01	12320	3343	772.3	258.1	114.8	58.03	32.8	20.07	13.45	9.612	7.183	5.55	4.412
0.01778	16290	5464	1408	509.8	218.7	108.8	59.86	36.29	24.13	17.18	12.79	9.868	7.82
0.03162	20120	8815	2667	924.8	400.9	195.9	107	64.59	42.89	30.53	22.7	17.49	13.85
0.05623	22890	13230	4727	1663	723.3	350.4	190.7	115	76.27	54.19	40.3	30.98	24.56
0.1	24530	18490	8025	2956	1288	623.4	338.9	204.6	135.6	96.23	71.54	55.01	43.55
0.1778	24440	23280	12780	5132	2264	1110	602.8	363.6	241	171	127.1	97.69	77.39
0.3162	24800	27180	18680	8657	3933	1951	1069	645	427.6	303.7	225.6	173.6	137.3
0.5623	25470	29080	24360	13740	6697	3384	1882	1146	760.2	537.8	400.8	308.4	244
1	25570	29860	28600	19830	10980	5845	3267	2031	1342	955.1	712	547.6	433.5
1.778	25920	30750	31390	25380	16730	9843	5750	3485	2393	1687	1261	970.4	769.1
3.162	26520	31270	33350	29720	22660	15480	9719	6054	4115	2982	2251	1730	1363
5.623	27220	31640	34560	33110	27640	21590	15190	10100	7062	5072	3899	3007	2393
10	27850	31550	34790	35600	31940	26870	21280	15910	11390	8566	6749	5163	4223
17.78	29380	31920	34840	36880	35690	31510	26540	22100	17400	13940	11000	8844	7325
31.62	31270	31880	34040	36880	38510	36190	31070	27300	23660	20730	17110	14520	12010
56.23	34190	33510	34750	36210	38970	39670	35510	31820	29180	27180	24050	22080	18390
100	39780	36610	35920	36470	39270	41930	39600	36780	34580	32450	29980	28740	25140

B.13. Kraton® D1171 – Piccotac™ Blends multifrequency analysis

B.13.1. Blend: 90/10, Temperature range: 150 – 250 °C, Frequency range: 0.1 – 100 Hz, Strain: 0.05

	Frequency (Hz)									
G'	**0.1**	**0.2154**	**0.4642**	**1**	**2.154**	**4.642**	**10**	**21.54**	**46.42**	**100**
150 °C	5113	6865	10320	18820	37440	67520	1.05E+05	1.51E+05	2.07E+05	2.66E+05
160 °C	3708	5464	7832	12890	25080	49510	84420	1.26E+05	1.77E+05	2.35E+05
170 °C	2593	4284	6019	9160	16470	33560	63930	1.03E+05	1.50E+05	2.03E+05
180 °C	1607	3169	4630	6856	11400	22560	46480	83130	1.27E+05	1.76E+05
190 °C	892.2	2123	3463	5242	8378	15570	32820	64970	1.07E+05	1.53E+05
200 °C	286.3	914.9	2043	3642	6041	10880	22540	47940	86940	1.28E+05
210 °C	61.62	261	869.4	2109	4022	7406	15060	33120	65820	1.01E+05
220 °C	16.45	74.85	290.4	959.8	2391	5018	10380	23030	49200	79990
230 °C	5.777	25.43	105.1	389.4	1250	3226	7255	16300	36300	62350
240 °C	3.492	15.22	56.13	209.9	704.1	2058	5187	12020	27170	48070
250 °C	3.651	14.06	52.81	181.3	556.8	1603	4136	9589	21050	36160

	Frequency (Hz)									
G"	**0.1**	**0.2154**	**0.4642**	**1**	**2.154**	**4.642**	**10**	**21.54**	**46.42**	**100**
150 °C	5685	9928	17930	31710	50010	67450	82570	97230	1.08E+05	1.11E+05
160 °C	4746	7416	13100	23530	40180	59590	76210	91300	1.05E+05	1.16E+05
170 °C	3889	5692	9514	16940	30260	49520	69030	85070	1.00E+05	1.16E+05
180 °C	3130	4510	7254	12550	22660	39600	61070	79850	95970	1.15E+05
190 °C	2345	3721	5813	9718	17340	31180	52050	73970	91780	1.12E+05

200 °C	1483	2787	4643	7683	13380	24070	42120	65050	85020	1.05E+05
210 °C	831.8	1738	3327	5855	10160	18130	32330	53360	74800	94090
220 °C	488.4	1050	2194	4282	7819	14060	25280	43540	65610	85730
230 °C	315.4	680.2	1452	3013	5938	11060	20060	35280	56450	77800
240 °C	229.1	495.3	1052	2207	4506	8780	16250	28920	48090	69880
250 °C	185	400.4	848.5	1777	3620	7089	13250	23530	39580	59680

B.13.2. Blend: 70/30, Temperature range: 150 – 250 °C, Frequency range: 0.1 – 100 Hz, Strain: 0.05

	Frequency (Hz)									
G'	**0.1**	**0.2154**	**0.4642**	**1**	**2.154**	**4.642**	**10**	**21.54**	**46.42**	**100**
150 °C	2875	3941	5450	8596	16220	31940	55490	84270	1.19E+05	1.51E+05
160 °C	1609	2916	4169	6189	10670	21400	41320	68040	1.00E+05	1.30E+05
170 °C	558.2	1506	2628	4143	6761	13010	27250	50670	79970	1.07E+05
180 °C	100.7	397.3	1145	2346	4112	7702	16460	34580	60660	
190 °C	16.15	70.42	277.7	906.2	2139	4416	9596	21950	43810	
200 °C	3.652	13.8	51.74	219.5	777.2	2186	5362	13190	30050	46180
210 °C	1.74	3.485	13.82	62.09	241.4	881.2	2746	7680	19780	32780
220 °C	1.254	2.002	5.961	25.43	101.3	388.9	1360	4299	12370	21290
230 °C	1.067	2.656	4.457	14.63	60.71	228	797.8	2557	7712	12380
240 °C	1.126	2.083	2.774	14.77	48.22	175.2	589.8	1812	5290	6595
250 °C	1.236	1.556	4.139	13.84	45.94	161.6	510.8	1474	4053	

	Frequency (Hz)									
G"	**0.1**	**0.2154**	**0.4642**	**1**	**2.154**	**4.642**	**10**	**21.54**	**46.42**	**100**
150 °C	3149	4859	8311	14900	25830	39200	50810	60570	68460	74080
160 °C	2789	3963	6300	10910	19460	32360	45970	57080	66780	76420
170 °C	1829	3019	4644	7720	13670	24140	38370	51550	62370	74340
180 °C	909.8	1832	3281	5490	9526	17070	29410	43930	56070	68630
190 °C	436.6	934.1	1920	3692	6686	12040	21560	35410	49110	62060
200 °C	230.1	493.6	1052	2208	4441	8476	15650	27460	42000	55820
210 °C	137.6	296.3	628.8	1348	2845	5834	11420	21140	35350	50500
220 °C	90.8	194.7	417.5	893.5	1904	3994	8162	15890	28620	44430
230 °C	65.36	139	297	631.9	1353	2856	5905	11780	22310	37100
240 °C	50.84	107.7	228.1	485.3	1035	2180	4497	8988	17360	30200
250 °C	42.46	88.64	186.4	398.9	842	1761	3601	7135	13800	24030

B.13.3. Blend: 50/50, Temperature range: 150 – 250 °C, Frequency range: 0.1 – 100 Hz, Strain: 0.05

	Frequency (Hz)									
G'	**0.1**	**0.2154**	**0.4642**	**1**	**2.154**	**4.642**	**10**	**21.54**	**46.42**	**100**
150 °C	98.74	369.4	985.6	1949	3439	6697	13920	26040	41300	49200
160 °C	16.75	67.9	256.4	766.7	1753	3601	7863	16680	29860	35880
170 °C	3.569	10.44	39.52	160	555.1	1555	3875	9334	19660	23500
180 °C	2.028	4.148	8.346	33.36	124.3	468.7	1561	4558	11670	13370
190 °C	1.938	3.829	5.279	11.87	38.24	146.4	559.4	1948	6253	
200 °C	2.335	2.974	4.077	7.164	17.34	60.36	228.4	826.5	3223	

210 °C	5.569	2.93	3.714	5.414	10.57	30.51	108	372.2	1662	

	Frequency (Hz)									
G"	**0.1**	**0.2154**	**0.4642**	**1**	**2.154**	**4.642**	**10**	**21.54**	**46.42**	**100**
150 °C	724.9	1431	2490	4123	7065	12310	19540	26300	31200	34580
160 °C	340.4	715.6	1457	2722	4821	8521	14610	22050	28360	33230
170 °C	154.5	329.5	696.7	1462	2930	5539	10050	16850	24090	29760
180 °C	79.4	168.1	356.9	758.2	1608	3329	6575	12090	19480	26020
190 °C	47.16	98.3	205.5	438.1	933.5	1982	4128	8222	14790	21700
200 °C	31.24	62.91	131.6	280.5	595.6	1269	2685	5552	10830	17230
210 °C	24.71	44.54	92.16	194	413.1	882.7	1878	3945	8132	13520

B.14. Kraton® D1171 Isothermal Microphase Separation Kinetics Analysis – Shear Storage Modulus (G')

Quench Temperatures – 160, 155, 150, 145 °C. Frequency: 0.01 Hz, Strain: .005

160 °C		**155 °C**		**150 °C**		**140 °C**	
time	**G'**	**time**	**G'**	**time**	**G'**	**time**	**G'**
min	**Pa**	**min**	**Pa**	**min**	**Pa**	**min**	**Pa**
10.04733	2993	10.04667	3983	10.04133	4347	13.39167	5571
13.4385	3011	13.43467	3991	13.42883	4337	16.78333	5570
16.83	3029	16.825	3945	16.81667	4342	20.17	5536
20.21833	3023	20.21333	3979	20.205	4337	23.56	5385
23.60667	3033	23.60333	3941	23.59	4314	26.945	5410
26.99333	3037	26.99	3922	26.97833	4330	30.33333	5370
30.38167	3020	30.37667	3857	30.365	4339	33.72	5359
33.76833	3038	33.76333	3888	33.755	4316	37.10667	5356
37.15667	3039	37.15167	3888	37.14	4315	40.495	5345
40.545	3052	40.54	3908	40.52833	4318	43.88167	5313
43.93333	3032	43.92833	3883	43.91667	4266	47.26833	5324
47.32167	2998	47.31333	3880	47.305	4265	50.65667	5296
50.71	2982	50.70167	3877	50.69	4268	54.04167	5341

54.09667	2990	54.08833	3917	54.07833	4261	57.43167	5301
57.485	2984	57.47833	3934	57.46667	4267	60.81833	5281
60.87333	2992	60.86333	3922	60.855	4226	64.20667	5291
64.26333	2996	64.25333	3950	64.24167	4264	67.59167	5289
67.65	3000	67.64167	3946	67.63	4201	70.97833	5277
71.035	3003	71.02833	3926	71.01833	4229	74.36667	5245
74.42333	3021	74.415	3916	74.40667	4199	77.75333	5215
77.81333	3030	77.80333	3930	77.79667	4237	81.14167	5187
81.2	3040	81.19	3916	81.185	4231	84.52833	5148
84.59	3050	84.57833	3863	84.57333	4247	87.915	5129
87.975	3052	87.96833	3881	87.96167	4222	91.30333	5154
91.36667	3064	91.35833	3915	91.35	4230	94.69167	5113
94.755	3073	94.745	3958	94.73833	4224	98.07833	5108
98.14167	3084	98.135	3951	98.125	4194	101.4667	5129
101.53	3096	101.5233	3966	101.5133	4234	104.855	5138
104.92	3114	104.9083	3961	104.9017	4206	108.2433	5122
108.3083	3115	108.2983	3970	108.29	4221	111.6317	5083
111.7	3118	111.685	3974	111.6767	4203	115.0183	5042
115.0867	3134	115.07	3986	115.0683	4226	118.4067	5006
118.475	3146	118.4583	3999	118.4583	4211	121.795	4992
121.865	3159	121.845	4007	121.8483	4211	125.185	4985
125.2517	3164	125.235	3982	125.235	4185	128.5733	4983
128.6383	3169	128.63	3995	128.6233	4179	131.9617	5010
132.0267	3184	132.02	3999	132.01	4176	135.3483	5010
135.415	3198	135.41	4032	135.3983	4143	138.7367	5016
138.8033	3197	138.8	4051	138.7867	4125	142.1233	5010
142.1933	3220	142.1883	4022	142.175	4095	145.51	4986
145.5833	3403	145.575	4047	145.5633	4076	148.9	4993
148.98	3556	148.9633	4051	148.9533	4080	152.2867	4933
152.37	3605	152.3517	4040	152.3417	4050	155.675	4955
155.76	3454	155.74	4062	155.7283	4050	159.0633	4972
159.1483	3406	159.1283	4079	159.1183	4043	162.4517	5034

B.15. Kraton® D1171 – Sylvalite® RE 100L Blends Isothermal Microphase Separation Kinetics Analysis – Shear Storage Modulus (G')

B.15.1. Blend: 90/10, Quench Temperatures – 155, 150, 145, 140°C. Frequency: 0.01 Hz, Strain: .005

155 °C		150 °C		145 °C		140 °C	
time	G'	time	G'	time	G'	time	G'
min	Pa	min	Pa	min	Pa	min	Pa
13.39733	561.2	13.3945	984.6	13.39317	1694	13.38717	2018
16.785	471.7	16.78167	848	16.78333	1737	16.77667	2044
20.17167	421.4	20.16833	760	20.17167	1691	20.165	2024
23.55833	381.3	23.55667	705.7	23.55833	1736	23.55167	1951
26.94667	358.6	26.945	684.8	26.94667	1855	26.94	1938
30.335	350.3	30.33333	696.7	30.33333	1969	30.33	1952
33.72333	343.6	33.72	739	33.72	2039	33.71667	1975
37.11167	336.4	37.10833	816.1	37.10667	2081	37.10333	1999
40.49667	338.2	40.49667	923	40.495	2112	40.49	2028
43.88667	337.4	43.885	1053	43.88167	2145	43.88	2041
47.27333	339.2	47.27167	1202	47.27	2159	47.265	2062
50.66167	342.8	50.66167	1351	50.65833	2189	50.655	2082
54.05	345	54.05	1487	54.04667	2200	54.04333	2100
57.43833	348.9	57.43833	1614	57.435	2227	57.43333	2113
60.82667	356.6	60.82833	1739	60.82333	2242	60.81833	2126
64.215	362.3	64.215	1834	64.215	2273	64.20667	2144
67.60333	368.7	67.60667	1917	67.60333	2284	67.59667	2157
70.99	374.3	70.99333	1994	70.99	2291	70.98333	2179
74.37833	383.3	74.38333	2054	74.37667	2306	74.37333	2186
77.76333	387.2	77.77	2103	77.765	2324	77.76333	2205
81.15167	394.6	81.15667	2140	81.15333	2339	81.15	2216
84.53667	396.1	84.54333	2178	84.54	2358	84.53833	2227
87.92667	404.5	87.93167	2207	87.92833	2370	87.92667	2244
91.315	410.6	91.32167	2231	91.31833	2401	91.315	2260
94.70167	415.9	94.71	2256	94.705	2416	94.70333	2271
98.08667	416.3	98.09833	2278	98.095	2423	98.09167	2284
101.475	424.4	101.4867	2297	101.485	2441	101.4817	2294
104.8633	427.3	104.875	2312	104.8717	2449	104.8717	2307
108.2517	439.4	108.2633	2327	108.2617	2474	108.2583	2322
111.64	444.1	111.6533	2346	111.6533	2483	111.6483	2330
115.0283	449.1	115.0417	2359	115.0417	2496	115.035	2344
118.4167	452.7	118.43	2371	118.43	2510	118.4233	2359

121.8033	459.6	121.8167	2388	121.82	2516	121.81	2364
125.1933	469.1	125.2067	2399	125.2083	2531	125.2	2379
128.58	475.7	128.5967	2412	128.5983	2538	128.585	2390
131.97	482.8	131.9867	2430	131.9867	2551	131.9733	2396
135.3567	492.1	135.375	2444	135.3733	2555	135.3617	2411
138.745	502.9	138.765	2459	138.7633	2572	138.75	2415
142.13	506.6	142.15	2474	142.1517	2587	142.1367	2435
145.52	511	145.54	2483	145.54	2600	145.525	2441
148.9083	516.5	148.9267	2502	148.9317	2607	148.9133	2452
152.2967	537.6	152.3183	2509	152.32	2618	152.3017	2466
155.6833	542.4	155.7067	2522	155.7083	2625	155.6883	2472
159.0733	544	159.095	2534	159.1	2634	159.0767	2478
162.4633	553.9	162.4833	2544	162.49	2643	162.465	2481
165.8517	566.9	165.8717	2556	165.8783	2655	165.8517	2493
169.2333	574.5	169.2667	2572	169.2667	2657	169.2333	2502
172.6333	586.6	172.65	2585	172.65	2668	172.6333	2510
176.0167	592	176.0333	2595	176.05	2678	176.0167	2522
179.4	612.7	179.4333	2610	179.4333	2691	179.4	2531
182.8	631.7	179.5167	2610	182.8167	2690	182.8	2538

B.15.2. Blend: 70/30, Quench Temperatures – 160, 155, 150, 145 °C. Frequency: 0.01 Hz, Strain: .005

160 °C		**155 °C**		**150 °C**		**145 °C**	
time	**G'**	**time**	**G'**	**time**	**G'**	**time**	**G'**
min	**Pa**	**min**	**Pa**	**min**	**Pa**	**min**	**Pa**
6.689333	0.7711	6.6985	0.9128	6.690333	35.76	6.694333	6.763
10.07583	1.075	10.086	5.26	10.082	32.68	10.08467	3.423
13.4575	1.004	13.47217	5.419	13.46983	24.99	13.47033	7.146
16.84167	0.921	16.85667	5.124	16.85833	23.45	16.85667	7.719
20.22667	0.8549	20.24333	4.992	20.24333	18.18	20.24333	7.401
23.61167	0.7739	23.63	4.926	23.62833	18.27	23.63167	7.29
26.99667	0.7548	27.01667	4.975	27.01333	18.8	27.01833	7.217
30.38333	0.932	30.40333	4.917	30.4	19.21	30.405	7.061
33.77	1.183	33.79	4.982	33.785	19.96	33.79167	6.75
37.15667	0.6758	37.175	5.025	37.17167	21	37.18	6.617
40.54167	0.6828	40.56333	5.103	40.55833	23.08	40.56667	6.725
43.92667	0.06728	43.95	5.218	43.94667	25.03	43.955	6.615
47.31167	0.5801	47.33667	5.319	47.335	25.28	47.34	6.707
50.69667	0.5709	50.72333	5.457	50.72167	25.82	50.72833	6.782

54.08333	0.5584	54.11167	5.376	54.11	26.67	54.115	7.269
57.46833	0.728	57.49667	5.516	57.49333	28.94	57.50167	7.716
60.855	0.6222	60.88667	5.571	60.88167	30.72	60.88833	7.547
64.24167	0.4528	64.27167	5.689	64.26833	33.49	64.275	7.122
67.62833	0.6306	67.66	5.953	67.65833	36.86	67.66333	7.347
71.01333	0.9217	71.04667	6.127	71.04333	39.92	71.05167	7.118
74.4	0.6484	74.43167	6.237	74.43	43.17	74.43667	7.328
77.78667	0.597	77.81833	6.324	77.81667	46.65	77.82333	7.386
81.17	0.5541	81.205	6.455	81.20333	51.09	81.21	7.558
84.55667	1.261	84.595	6.554	84.59	56.85	84.595	7.58
87.94333	0.5868	87.98167	6.543	87.97667	61.66	87.985	7.685
91.32833	0.473	91.36833	6.715	91.36333	66.24	91.37167	7.618
94.715	0.3994	94.755	6.853	94.75167	76.28	94.76	7.775
98.1	0.3503	98.14333	6.885	98.13833	80.34	98.14833	7.91
101.485	0.276	101.5333	7.063	101.5267	82.59	101.5333	8.006
104.8717	0.2387	104.9217	7.155	104.9167	88.55	104.9217	8.024
108.2567	0.3673	108.3083	7.272	108.3033	92.97	108.3083	8.014
111.6433	0.3087	111.6967	7.341	111.6917	95.12	111.6983	8.058
115.0283		115.0833	7.44	115.08	95.91	115.0867	7.725
118.4133				118.4683	97.57	118.4733	7.983

B.15.3. Blend: 50/50, Quench Temperatures – 150, 135, 125 °C. Frequency: 0.01 Hz, Strain: .005

150 °C		**135 °C**		**125 °C**	
time	**G'**	**time**	**G'**	**time**	**G'**
min	**Pa**	**min**	**Pa**	**min**	**Pa**
6.692	2.994	6.689	0.1634	6.690667	80.64
10.08017	0.9487	10.07833	0.123	10.07717	40.16
13.46717	0.6915	13.46567	0.1158	13.46167	18.37
16.85333	0.7027	16.85167	0.1473	16.845	7.104
20.23833	0.4522	20.24	0.2097	20.23	3.92
23.62667	0.3263	23.62667	0.2101	23.61667	2.791
27.01333	0.3612	27.01333	0.1827	27.00167	3.46
30.4	0.4326	30.40167	0.1849	30.38833	3.601
33.78833	0.3774	33.78833	0.1769	33.775	2.025
37.17667	0.4213	37.17667	0.1499	37.16167	3.622
40.56	0.3629	40.56167	0.1342	40.54667	0.6734
43.94833	0.4463	43.95	0.1326	43.935	0.6618
47.33333	0.3097	47.33833	0.1271	47.31833	0.08058

50.72167	0.2947	50.72667	0.1207	50.70833	0.06802
54.10833	0.139	54.11667	0.1079	54.095	0.0375
57.495	0.3334	57.50333	0.09972	57.48167	0.02908
60.88	0.3364	60.89	0.1184	60.86833	0.02194
64.27	0.2945	64.275	0.1122	64.25333	0.02103
67.65667	0.4013	67.66333	0.0939	67.64333	0.03242
71.04333	0.2637	71.05	0.08873	71.02833	0.001464
74.43	0.2446	74.43833	0.08877	74.41333	-0.1139
77.81667	0.2131	77.825	0.0911	77.8	0.01794
81.205	0.2035	81.21333	0.08921	81.18667	0.3103
84.59	0.2798	84.6	0.08502	84.57333	0.246
87.97667	0.3684	87.99	0.08082	87.96167	0.1873
91.36333	0.2463	91.37667	0.07503	91.34833	0.1817
94.75167	0.2114	94.765	0.07956	94.73667	0.1785
98.14	0.1823	98.15167	0.08194	98.12167	0.1633
101.525	0.1844	101.54	0.09126	101.5117	0.1689
104.9133	0.233	104.9283	0.08866	104.9	0.1605
108.3017	0.199	108.315	0.08881	108.2883	0.1554
111.6867	0.2309	111.7033	0.09274	111.675	0.1532
115.0733	0.2102	115.0883	0.08477	115.0633	0.1523
118.4617	0.2608	118.4767	0.08056	118.45	0.156
121.8483	0.2488	121.8633	0.07583	121.8367	0.1545
125.2367	0.2448	125.2517	0.07665	125.2267	0.1452
128.6233	0.2307	128.64	0.07099	128.6133	0.1492
132.01	0.2398	132.0283	0.06734	132.0017	0.1487
135.3967	0.2283	135.4167	0.06704	135.39	0.1456
138.785	0.2329	138.8033	0.06425	138.7767	0.1433
142.1733	0.2223	142.19	0.05524	142.165	0.1474
145.5583	0.1995	145.5783	0.0517	145.5517	0.1484
148.9467	0.1917	148.965	0.05626	148.94	0.1526
152.3333	0.2044	152.355	0.05559	152.3267	0.1513
155.7217	0.2149	155.7417	0.06019	155.7167	0.1511
159.11	0.2392	159.13	0.06434	159.1033	0.1504
162.4967	0.2746	162.5167	0.06305	162.4917	0.1489
165.8833	0.2775	165.905	0.06135	165.8833	0.1476
169.2667	0.2461	169.3	0.05964	169.2833	0.1433
172.6667	0.2449	172.6833	0.05944	172.6667	0.1478
176.05	0.2715	176.0667	0.05742	176.05	0.1485
179.4333	0.2772	179.45	0.05918	179.4333	0.1443
182.8167	0.3014	182.85	0.05767	182.8333	0.1452
186.2	0.2931	186.2333	0.0565	186.2167	0.1498

189.6	0.2702	189.6167	0.05459	189.6	0.1496
192.9833	0.2784	193	0.05422	192.9833	0.1476
196.3667	0.3301	196.4	0.05721	196.3833	0.1474
199.6333	0.3301	199.7833	0.05246	199.7667	0.1468

B.16. Kraton® D1171 – Piccotac™ 1095 Blends Isothermal Microphase Separation Kinetics Analysis – Shear Storage Modulus (G')

B.16.1. Blend: 90/10, Quench Temperatures – 160, 150, 145, 140, 135 °C. Frequency: 0.01 Hz, Strain: .005

160 °C		**150 °C**		**145 °C**		**140 °C**		**135 °C**	
time	**G'**	**time**	**G'**	**time**	**G'**	**time**	**G'**	**time**	**G'**
min	**Pa**	**min**	**Pa**	**min**	**Pa**	**min**	**Pa**	**min**	**Pa**
13.38483	774.6	13.38417	2022	6.691333		10.04017	3310	13.39383	3669
16.775	717	16.77333	1980	10.07767		13.42867	3294	16.78167	3598
20.16167	679.8	20.16167	1963	13.46883		16.815	3260	20.17	3544
23.55	661.7	23.54833	1940	16.85833		20.20167	3220	23.55667	3546
26.93833	635.4	26.93667	1919	20.24833		23.59	3211	26.945	3543
30.325	630	30.32667	1911	23.63667		26.97833	3185	30.33167	3526
33.71167	621.1	33.715	1882	27.02167	1763	30.36667	3179	33.71667	3524
37.10167	615.8	37.105	1897	30.41	1810	33.75333	3158	37.105	3516
40.48667	611.9	40.49167	1859	33.79667	1849	37.14	3156	40.49167	3518
43.87333	610.6	43.88167	1842	37.185	1862	40.53	3172	43.88	3518
47.26167	615.3	47.27	1819	40.57333	1866	43.91667	3182	47.26667	3503
50.64833	613.9	50.655	1811	43.96167	1869	47.305	3190	50.65333	3509
54.03667	615.9	54.04333	1798	47.35	1877	50.695	3198	54.04	3523
57.42167	620.9	57.43333	1802	50.73833	1888	54.08167	3207	57.42667	3507
60.81167	632.1	60.82167	1799	54.125	1900	57.47167	3222	60.81333	3505

64.2	638.9	64.21	1806	57.5133 3	1920	60.8583 3	3228	64.2	3511
67.5866 7	642.2	67.5983 3	1800	60.9016 7	1951	64.2466 7	3257	67.5866 7	3513
70.9733 3	655.1	70.9883 3	1800	64.29	1984	67.6333 3	3255	70.9716 7	3518
74.3633 3	670.3	74.3766 7	1818	67.6783 3	2026	71.0216 7	3260	74.36	3512
77.75	687.1	77.765	1830	71.0666 7	2071	74.41	3262	77.745	3516
81.1383 3	702.2	81.155	1830	74.455	2121	77.7983 3	3274	81.1316 7	3524
84.525	724.4	84.5416 7	1865	77.8433 3	2162	81.1833 3	3283	84.5183 3	3508
87.9116 7	746.5	87.93	1861	81.2316 7	2199	84.5733 3	3290	87.905	3506
91.3	772.9	91.32	1891	84.6183 3	2227	87.9616 7	3277	91.295	3523
94.6883 3	798.5	94.7083 3	1903	88.0066 7	2244	91.35	3274	94.6816 7	3511
98.0766 7	825.9	98.0966 7	1922	91.3966 7	2259	94.7366 7	3285	98.0683 3	3502
101.465	859.9	101.486 7	1949	94.785	2267	98.1266 7	3282	101.455	3532
104.853 3	896.9	104.873 3	1978	98.175	2275	101.518 3	3301	104.841 7	3541
108.241 7	930.7	108.261 7	1997	101.563 3	2281	104.906 7	3302	108.23	3519
111.628 3	975.4	111.65	2024	104.953 3	2287	108.295	3316	111.618 3	3514
115.016 7	1017	115.038 3	2058	108.341 7	2291	111.683 3	3293	115.006 7	3524
118.405	1066	118.425	2070	111.728 3	2294	115.07	3307	118.391 7	3528
121.793 3	1113	121.813 3	2103	115.116 7	2301	118.456 7	3308	121.78	3531
125.181 7	1162	125.2	2130	118.505	2302	121.843 3	3315	125.168 3	3532
128.57	1216	128.59	2144	121.893 3	2306	125.23	3311	128.553 3	3518
131.96	1278	131.976 7	2183	125.281 7	2310	128.616 7	3313	131.94	3519
135.348 3	1342	135.365	2211	128.67	2309	132.006 7	3324	135.325	3526
138.736 7	1408	138.753 3	2233	132.058 3	2309	135.393 3	3312	138.713 3	3534

142.1233	1470	142.1417	2273	135.4467	2313	138.78	3323	142.1	3524
145.5117	1576	145.53	2302	138.8333	2313	142.1667	3333	145.4883	3539
148.9	1655	148.9167	2322	142.22	2315	145.5567	3331	148.8733	3540
152.29	1720	152.305	2357	145.6083	2312	148.9467	3331	152.2617	3541
155.68	1789	155.6917	2364	148.9983	2314	152.335	3319	155.6467	3555
159.0683	1847	159.0817	2402	152.3867	2318	155.7233	3333	159.035	3538
162.4567	1911	162.47	2425	155.7767	2320	159.11	3322	162.4233	3544
165.845	1972	165.8567	2443	159.1633	2316	162.4983	3340	165.8117	3545
169.2333	2036	169.25	2477	162.5533	2323	165.8867	3330	169.2	3548
172.6167	2090	172.6333	2488	165.94	2324	169.2667	3331	172.5833	3553
176	2153	176.0167	2514	169.3333	2327	172.6667	3314	175.9667	3556
179.4	2214	179.4167	2532	172.7167	2330	176.05	3335	179.3667	3566
182.7833	2264	182.8	2560	176.1	2333	179.4333	3336	182.75	3562
186.1667	2320	186.1833	2578	179.5	2327	182.8333	3324	186.1333	3562
189.5667	2374	189.5667	2601	182.8833	2336	186.2167	3324	189.5167	3565
192.95	2427	192.9667	2625	186.2667	2331	189.6	3336	192.9	3556
196.3333	2479	196.35	2641	189.6667	2345	192.9833	3326	196.3	3546
199.7167	2527	199.7333	2663	193.05	2339	196.3833	3331	199.6833	3562
203.1167	2568	203.1333	2679	196.4333	2340	199.7667	3344	203.0667	3567
206.5	2617	206.5167	2709	199.8333	2341	203.15	3324	206.4667	3555
209.8833	2659	209.9	2700	203.2167	2348	206.55	3335	209.85	3551
213.2667	2698	213.2833	2707	206.6	2343	209.9333	3340	213.2333	3576
216.6667	2729	216.6833	2738	209.9833	2342	213.3167	3330	216.6167	3575

220.05	2767	220.0667	2727	213.3833	2342	216.7	3347	220.0167	3552
223.4333	2802	223.45	2746	216.7667	2343	220.1	3348	223.4	3570
226.8333	2839	226.8333	2774	220.15	2347	223.4833	3324	226.7833	3567
230.2167	2870	230.2333	2753	223.55	2343	226.8667	3332	230.1667	3570
233.6	2894	233.6167	2762	226.9333	2345	230.2667	3351	233.5667	3572
236.9833	2926	237	2805	230.3167	2343	233.65	3351	236.95	3572
240.3833	2958	240.4	2809	233.7167	2348	237.0333	3349	240.3333	3573
243.7667	2985	243.7833	2839	237.1	2347	240.4333	3347	243.7167	3571
247.15	3006	247.1667	2855	240.4833	2352	243.8167	3346	247.1167	3589
250.55	3029	250.5667	2885	243.8833	2357	247.2	3343	250.5	3583
253.9333	3048	253.95	2890	247.2667	2362	250.5833	3348	253.8833	3579
257.3167	3066	257.3333	2896	250.65	2361	253.9833	3358	257.2667	3585
260.7	3087	260.7167	2910	254.0333	2362			260.65	3584
264.1	3103	264.1167	2910	257.4333	2366			264.05	3584
267.4833	3115	267.5	2918	260.8167	2368			264.7167	3584
270.8667	3131	270.9	2940	264.2	2371				
274.25	3140	274.2833	2949	267.6	2370				
277.65	3153	277.6667	2930	270.9833	2371				
281.0333	3162	281.0667	2960	274.3667	2376				
284.4167	3181	284.45	2953	277.7667	2374				
287.8167	3183	287.8333	2931	281.15	2377				
291.2	3203	291.2333	2904	284.5333	2382				
294.5833	3212	294.6167	2892	287.9167	2379				

297.9833	3216	298.0167	2887	291.3167	2386				
301.3667	3237	301.4	2911	294.7	2386				

B.16.2. Blend: 70/30, Quench Temperatures – 160, 150, 140, 130, 120 °C. Frequency: 0.01 Hz, Strain: .005

160 °C		**150 °C**		**140 °C**		**130 °C**		**120 °C**	
time	**G'**	**time**	**G'**	**time**	**G'**	**time**	**G'**	**time**	**G'**
min	**Pa**	**min**	**Pa**	**min**	**Pa**	**min**	**Pa**	**min**	**Pa**
6.688333	39	13.38617	285.1	13.39633	1029	13.3935	1764	13.39733	2383
10.07583	41.52	16.775	271.4	16.78333	997.1	16.78333	1767	16.78833	2397
13.46283	40.77	20.16167	261.5	20.17333	962.6	20.17167	1740	20.17667	2398
16.85	38.47	23.54833	246.8	23.56	938.4	23.56	1722	23.565	2381
20.23667	36.74	26.935	237.5	26.95	917.9	26.94833	1699	26.95333	2397
23.62333	35.34	30.32	226.1	30.33667	908.4	30.33833	1685	30.34333	2382
27.01167	35.16	33.705	223.6	33.725	906.3	33.72333	1673	33.73167	2373
30.39667	36.44	37.09167	227.3	37.11333	924.5	37.11167	1647	37.12	2372
33.78333	39.39	40.47667	227.6	40.5	963.3	40.49833	1640	40.50833	2363
37.17	44.82	43.86333	232.7	43.88833	1020	43.88833	1641	43.89333	2364
40.55667	53.52	47.25	240.8	47.275	1117	47.27667	1636	47.28	2371
43.94333	66.79	50.63667	259	50.66333	1243	50.66667	1651	50.66833	2377
47.33	85.91	54.02167	281.7	54.05167	1385	54.055	1655	54.05333	2376
50.71667	114.5	57.40833	313.5	57.44	1530	57.44333	1670	57.44333	2378
54.10333	153	60.795	346.3	60.82667	1649	60.83	1693	60.83333	2387
57.49	204.3	64.18167	393.5	64.21667	1731	64.21833	1713	64.22	2379

60.87667	272	67.56833	444.2	67.60333	1785	67.60667	1738	67.61	2371
64.26333	352.5	70.955	504.6	70.99167	1819	70.99333	1778	70.99833	2380
67.65	446.7	74.345	576.1	74.38	1841	74.38167	1813	74.39167	2383
71.03833	556.4	77.73333	652.2	77.76667	1853	77.76833	1848	77.77833	2379
74.425	671.9	81.12167	737.7	81.155	1862	81.15667	1891	81.165	2370
77.81333	782.9	84.51	824.6	84.54333	1872	84.54333	1926	84.555	2368
81.20167	898.4	87.89667	913.7	87.93333	1879	87.93	1964	87.94167	2380
84.59167	1001	91.28833	1005	91.32	1884	91.31833	1996	91.33167	2371
87.98	1095	94.67667	1088	94.70833	1890	94.70667	2026	94.71833	2371
91.37333	1180	98.06333	1170	98.095	1895	98.09333	2049	98.10667	2379
94.76167	1250	101.4517	1243	101.485	1898	101.4817	2071	101.4983	2365
98.15	1307	104.84	1313	104.875	1901	104.87	2086	104.8883	2378
101.54	1353	108.2283	1371	108.2617	1902	108.255	2101	108.2767	2372
104.9267	1389	111.6183	1422	111.65	1904	111.6433	2116	111.665	2367
108.315	1417	115.005	1464	115.0383	1904	115.03	2121	115.055	2368
111.705	1436	118.3933	1496	118.4267	1904	118.4183	2135	118.4417	2360
115.0933	1452	121.7817	1526	121.8167	1905	121.8067	2145	121.8317	2352
118.4833	1464	125.17	1547	125.205	1903	125.1917	2150	125.22	2356
121.8717	1471	128.5583	1564	128.5917	1895	128.58	2157	128.6067	2363
125.2617	1476	131.945	1577			131.9667	2164	131.995	2359
128.6467	1480	135.335	1588			135.355	2175	135.3833	2375
132.0367	1483	138.7217	1595			138.7417	2175	138.7717	2386
135.4217	1486	142.1083	1600			142.1283	2180	142.16	2393

138.8117	1488	145.495	1605			145.5167	2191	145.55	2401
142.2	1488	148.885	1607			148.9017	2190	148.9383	2399
145.5883	1490	152.2717	1611			152.29	2200	152.325	2402
148.9767	1489	155.6617	1611			155.6767	2193	155.7133	2410
152.365	1486	159.0483	1613			159.0667	2209	159.1	2411
155.7533	1488	162.435	1615			162.4517	2213	162.4883	2405
159.1417	1490	165.825	1616			165.8417	2211	165.8767	2401
162.53	1489	169.2167	1618			169.2333	2216	169.2667	2413
165.9167	1490	172.6	1617			169.35	2216	172.65	2415
169.3167	1490	175.9833	1618					176.0333	2421

B.16.3. Blend: 50/50, Quench Temperatures – 150, 140, 130, 120, 110 °C. Frequency: 0.01 Hz, Strain: .005

150 °C		**140 °C**		**130 °C**		**120 °C**		**110 °C**	
time	**G'**	**time**	**G'**	**time**	**G'**	**time**	**G'**	**time**	**G'**
min	**Pa**	**min**	**Pa**	**min**	**Pa**	**min**	**Pa**	**min**	**Pa**
6.690167	4.477	6.688333	24.87	6.690833	160.4	10.0385	593.9	13.382	1077
10.0765	5.015	10.07467	29.82	10.07633	207.6	13.42883	617.4	16.77167	1074
13.4615	4.666	13.462	29.81	13.462	223.4	16.81667	617.1	20.16167	1071
16.84667	4.327	16.85	29.24	16.84833	226.7	20.205	614.6	23.54667	1059
20.235	4.098	20.235	28.32	20.235	214.5	23.59333	613.3	26.93667	1051
23.62167	3.845	23.62167	26.98	23.62	205.3	26.98	611.9	30.32333	1043
27.00667	3.51	27.01	25.67	27.00667	194.1	30.36667	610.4	33.71333	1037
30.39333	3.526	30.39667	24.58	30.39333	185.1	33.755	608.2	37.1	1031

33.78	3.57	33.78333	23.56	33.77833	178.5	37.14333	608.2	40.49	1026
37.16667	3.487	37.16833	22.78	37.16667	167.2	40.53167	607.8	43.87667	1026
40.555	3.443	40.55333	21.98	40.55333	162.8	43.91833	607.4	47.26667	1006
43.94	3.549	43.94167	21.35	43.93833	158.8	47.30833	608.3	50.65333	1018
47.32667	3.452	47.32667	20.75	47.32667	156.2	50.69333	609	54.04167	1014
50.71333	3.461	50.715	20.43	50.71167	154.7	54.08167	608.2	57.43	1008
54.1	3.244	54.1	20.25	54.09833	153.8	57.47	608.2	60.82	1007
57.48833	3.076	57.48667	20	57.48667	154	60.85833	608.6	64.20833	1007
60.87667	3.317	60.875	19.9	60.87333	155.7	64.24667	610.3	67.59667	1010
64.26333	3.203	64.26167	20.2	64.26333	158.5	67.63333	613.8	70.98667	1016
67.64833	3.325	67.65	20.23	67.65	160.4	71.02	612.6	74.37667	1011
71.03667	3.278	71.035	20.24	71.03667	163.9	74.40833	615	77.76667	1004
74.42333	3.237	74.42333	20.3	74.42167	171.3	77.80167	616	81.155	1006
77.81	3.207	77.81	20.48	77.81	179.2	81.18833	617.2	84.545	1006
81.19667	3.183	81.195	20.81	81.19667	186.5	84.575	619.5	87.93333	1012
84.58333	3.39	84.58	21.21	84.58333	192.9	87.96333	622	91.32333	1011
87.97167	3.543	87.96833	21.63	87.97167	199.3	91.35167	620.7	94.71333	1012
91.35667	3.137	91.35333	22.15	91.35833	206.8	94.73833	622.1	98.10167	1016
94.74833	3.165	94.74167	22.8	94.74667	216.3	98.12667	623.9	101.4917	1017
98.13667	3.223	98.12667	23.73	98.13333	227.5	101.5133	624.4	104.8817	1020
101.525	3.164	101.5133	24.3	101.5217	239.5	104.9	625	108.27	1021
104.9117	3.243	104.9017	25.44	104.9067	253.7	108.2883	626.3	111.6583	1022
108.3	3.207	108.2867	26.27	108.295	269.4	111.675	627.1	115.0467	1025

111.6883	3.117	111.675	27.22	111.6833	286	115.0617	628.6	118.4383	1027
115.075	3.259	115.0617	28.25	115.07	304.9	118.4517	630.4	121.8283	1030
118.4617	3.192	118.4483	29.53	118.46	324	121.84	632	125.2167	1031
121.8467	3.517	121.8367	30.79	121.8467	346.6	125.2267	634.4	128.605	1033
125.2333	3.463	125.2233	32.51	125.2367	367.8	128.6167	637.3	131.9967	1035
128.6217	3.245	128.61	34.44	128.625	389.8	132.0067	641.2	135.385	1036
132.0067	3.159	131.995	36.68	132.0117	414.2	135.395	644.5	138.775	1036
135.3967	3.199	135.3833	38.98	135.3983	439.8	138.7817	650.1	142.165	1037
138.785	3.04	138.7683	41.58	138.7867	463.9	142.17	655.9	145.5533	1038
142.1717	3.265	142.1567	44.57	142.1767	490.6	145.56	662.5	148.9433	1037
145.5583	3	145.545	47.92	145.565	516	148.95	670.1	152.3317	1038
148.9467	2.936	148.93	51.06	148.9517	542.3	152.3383	677.2	155.72	1037
152.3333	3.055	152.3167	54.59	152.34	566.6	155.73	687.6	159.11	1038
155.7217	2.958	155.7033	59.39	155.7283	592.1	159.1183	698.2	162.4983	1040
159.11	2.975	159.09	64.42	159.115	618.1	162.5067	709	165.8883	1042
162.4983	2.917	162.4767	69.85	162.5033	641	165.895	722.6	169.2833	1043
165.8833	2.846	165.8633	75.59	165.8917	663.7	169.2833	736.7	172.6667	1043
169.2667	2.895	169.25	81.71	169.2833	685.6	172.6667	753.8	176.05	1043
172.6667	3.016	172.6333	88.05	172.6667	707.4	176.0667	771.3	179.45	1041
176.05	3.03	176.0167	95.59	176.05	728	179.45	789.2	182.8333	1040
179.4333	3.211	179.4167	102.5	179.45	745.2	182.8333	808.1	186.2333	1038
182.8167	3.147	182.8	111.6	182.8333	763.4	186.2167	829.8	189.6167	1042
186.2167	3.072	186.1833	119.2	186.2167	780.2	189.6167	850.4	193	1042

189.6	3.344	189.5667	128.2	189.6167	793.9	193	870.8	196.3833	1044
192.9833	3.021	192.95	138.1	193	808	196.3833	893.3	199.7833	1044
193.2833	3.021	196.35	148.2	196.3833	820.1	199.7833	915.6	203.1667	1044
		199.7333	157.6	199.7833	831	203.1667	937.4	206.5667	1042
		203.1167	168.4	203.1667	840.8	206.55	959.2	209.95	1040
		206.5	180.5	206.55	847.7	209.95	978.8	213.3333	1042
		209.9	192.5	209.95	855.1	213.3333	996.9	216.7333	1041
		213.2833	204.8	213.3333	860.8	216.7167	1015	220.1167	1041
		216.6667	217.9	216.7167	864.7	220.1167	1031	223.5167	1041
		220.05	231.9	220.1167	869.9	223.5	1047	226.9	1045
		223.45	245.9	223.5	872.5	226.8833	1059	230.2833	1043
		226.8333	261.5	226.8833	876.8	230.2833	1071	233.6833	1044
		230.2167	275.1	230.2833	877.5	233.6667	1082	237.0667	1044
		233.6167	291.3	233.6667	879.3	237.05	1091	240.45	1033
		237	307.1	237.05	879.3	240.45	1099	243.85	1019
		240.3833	323	240.45	880.5	243.8333	1104	247.2333	1015
		243.7667	338.4	243.8333	882	247.2167	1109	250.6333	1011
		247.1667	353.7	247.2167	881.6	250.6	1113	254.0167	1010
		250.55	369.1	250.6167	880.4	254	1115	257.4	1013
		253.9333	385.2	254	879.9	257.3833	1116	260.8	1015
		257.3167	401.1	257.3833	880.8	260.7667	1118	264.1833	1019
		260.7167	416	257.5333	880.8	264.1667	1117	267.5667	1023
		264.1	429.6			267.55	1118	270.9667	1027

		267.4833	446.7			270.9333	1116	274.35	1033
		270.8667	461.4			274.3333	1122	277.7333	1041
		274.2667	475.8			277.7167	1125	281.1333	1051
		277.65	489.6			281.1	1127	284.5167	1062
		281.0333	502.5			284.5	1128	287.9	1074
		284.4167	517.1			287.8833	1129	291.3	1084
		287.8167	529.5			291.2667	1130	294.6833	1098
		291.2	542.4			294.6667	1130	298.0833	1113
		294.5833	554.2			298.05	1130	301.4667	1127
		297.9667	564.5			301.45	1133	304.85	1141
		301.3667	577.3			304.8333	1133	308.25	1158
		304.75	586.3			308.2167	1134	311.6333	1172
		308.1333	596			311.6167	1135	315.0167	1189
		311.5167	606.5			315	1137	318.4167	1206
		314.9167	615.9			318.3833	1137	321.8	1221
		318.3	624.3			321.7833	1137	325.1833	1235
		321.6833	632.9			325.1667	1136	328.5833	1248
		325.0667	640			328.5667	1136	331.9667	1262
		328.4667	648.4			331.95	1132	335.3667	1270
		331.85	654.1			335.3333	1127	338.75	1284
		335.2333	660.2			338.7333	1126	342.1333	1295
		338.6333	667.2					345.5333	1303
		342.0167	673					348.9167	1312

		345.4	677.9					352.3167	1320
		348.7833	683.4					355.7	1326
		352.1833	687					359.0833	1331
		355.5667	691.4					362.4833	1337
		358.95	695.6					365.8667	1342
		362.35	698.7					369.25	1347
		365.7333	702.9					372.65	1350
		369.1167	706					376.0333	1355
		372.5	708.7					379.4167	1357
		375.9	711.4					382.8167	1358
		379.2833	713.7					386.2	1361
		382.6667	716.3					389.5833	1363
		386.0667	717.7					392.9833	1364
		389.45	720.2					396.3667	1366
		392.8333	721.8					399.75	1367
		396.2333	722.7					403.15	1369
		399.6167	724.9					406.5333	1371
		403	726.4					409.9333	1371
		406.4	728					413.3167	1371
		409.7833	729.1					416.7	1373
		413.1667	730.1					420.1	1374
		416.55	731.2					423.4833	1374
		419.95	731.9					426.8667	1375

		423.3333	733.5					430.2667	1375
		426.7167	735					433.65	1375
		430.1167	736					437.0333	1374
		433.5	736.3					438.1	1374
		436.8833	737.1						
		440.2833	738.3						
		443.6667	739.7						
		447.05	740						
		450.45	741.3						
		453.8333	742.1						
		457.2167	741.5						
		460.6167	742.7						
		464	744.7						
		467.3833	744.2						
		470.7833	745.2						
		474.1667	745.6						
		477.5667	746.5						
		480.95	746.9						

B.17. Kraton® D1171 – Piccotac™ 1095 50/50 Blends Isothermal Microphase Separation Kinetics Analysis – Half times of ordering (min)

Blend	Temperature (°C)	Half time (min)
D1171-Piccotac 90/10	160	162
	150	152
	145	71
	140	64
	135	162
D1171-Piccotac 70/30	160	78
	140	54
	130	84
	120	152
D1171-Piccotac 50/50	140	253
	130	145
	120	193
	110	315

Appendix C: Small Angle X-ray Scattering Data

C.1. Modified Percus – Yevick Hard Sphere Model Fit

Kraton® D1161 quenched to 160 C and held isothermal for 90 minutes

q (nm^{-1})	**I_{exp} (a.u.)**	**I_{model} (a.u.)**		
0.134525	2.349557	2.026722	**K**	2.40E-07
0.138481	2.354276	2.150088	**V_c (nm^3)**	5276.669
0.142438	2.436282	2.303147	**R_c (nm)**	10.8
0.146395	2.525341	2.490152	**R_{hs} (nm)**	24.1
0.150351	2.689413	2.715819	**A_1 (a.u.)**	5.0
0.154308	2.915193	2.98484	**b (nm^{-1})**	0.209
0.158264	3.257517	3.300988	**c (nm^{-1})**	0.013
0.162221	3.645766	3.665681		
0.166177	4.117991	4.076105		
0.170134	4.640785	4.523387		
0.17409	5.188363	4.992255		
0.178047	5.788072	5.464514		
0.182004	6.280603	5.92787		
0.18596	6.692334	6.385967		
0.189917	7.083391	6.856909		
0.193873	7.332658	7.349176		
0.19783	7.59323	7.825049		
0.201786	7.881895	8.183233		
0.205743	8.191727	8.285263		
0.209699	8.006021	8.017427		
0.213656	7.317193	7.35178		
0.217612	5.806895	6.368691		
0.221569	4.275565	5.228082		
0.225525	3.351558	4.107993		
0.229482	2.811169	3.145305		
0.233439	2.403268	2.405753		
0.237395	2.108135	1.8885		
0.241352	1.881395	1.551886		
0.245308	1.66637	1.341837		
0.249265	1.507072	1.210935		
0.253221	1.367832	1.125729		
0.257177	1.261495	1.065998		
0.261134	1.162263	1.02081		
0.26509	1.082481	0.984604		
0.269047	1.00374	0.954491		

0.273003	0.95043	0.928771		
0.27696	0.904364	0.90622		
0.280916	0.858029	0.8858		
0.284873	0.819369	0.866544		
0.288829	0.792637	0.847525		
0.292786	0.777004	0.827855		
0.296742	0.770583	0.806722		
0.300699	0.741988	0.783437		
0.304655	0.703871	0.757501		
0.308611	0.662404	0.728679		
0.312568	0.62879	0.697046		
0.316524	0.598643	0.662998		
0.320481	0.575357	0.627216		
0.324437	0.560066	0.590573		
0.328393	0.539477	0.554007		
0.33235	0.519987	0.518406		
0.336306	0.501955	0.484499		
0.340263	0.486041	0.452806		
0.344219	0.473274	0.423624		
0.348175	0.451557	0.397049		
0.352132	0.433636	0.37302		
0.356088	0.415461	0.351369		
0.360044	0.394714	0.331858		
0.364001	0.382656	0.314227		
0.367957	0.363905	0.298211		
0.371913	0.345134	0.283561		
0.37587	0.315093	0.270055		
0.379826	0.289045	0.257501		
0.383782	0.269443	0.24574		
0.387739	0.249578	0.234646		
0.391695	0.233924	0.224121		
0.395651	0.215375	0.214091		
0.399608	0.202234	0.204509		

C.2. Kraton® D1161 – Stepwise Heating Experiment

T (°C)	K	Rc (nm)	Rhs (nm)	Φ	A (a.u.)	b (nm^{-1})	c
250	4.2E-07	8.8	20.6	0.395	0.4	0.21	0.03
249	4.2E-07	8.8	20.6	0.396	0.45	0.21	0.03
246	4.2E-07	8.8	20.6	0.397	0.45	0.21	0.03
243	4.2E-07	8.8	20.6	0.398	0.45	0.21	0.03
240	4.2E-07	8.8	20.6	0.4	0.45	0.215	0.03
237	4.2E-07	8.9	20.6	0.401	0.4	0.22	0.03
234	4.2E-07	8.9	20.6	0.403	0.2	0.22	0.025
231	4.2E-07	8.9	20.6	0.403	0.2	0.22	0.025
228	4E-07	9	20.6	0.404	0.3	0.215	0.025
225	4E-07	9.1	20.6	0.403	0.3	0.215	0.025
222	3.9E-07	9.2	20.7	0.402	0.5	0.212	0.025
219	3.9E-07	9.3	20.8	0.4	0.6	0.21	0.025
216	3.8E-07	9.4	20.9	0.398	0.8	0.205	0.025
213	3.8E-07	9.4	21.1	0.397	1	0.19	0.025
210	3.8E-07	9.4	21.3	0.396	1.2	0.186	0.025
207	3.7E-07	9.5	21.5	0.393	1.5	0.187	0.025
204	3.7E-07	9.5	21.5	0.392	1.8	0.188	0.024
201	3.6E-07	9.5	21.6	0.391	2	0.189	0.024
198	3.6E-07	9.5	21.8	0.391	2.1	0.189	0.024
195							
192	3.5E-07	9.5	21.9	0.39	2.7	0.19	0.023
189							
186	3.4E-07	9.5	22.2	0.389	2.9	0.193	0.023
183							
180	3.4E-07	9.5	22.2	0.389	3.3	0.193	0.023
177							
174	3.3E-07	9.5	22.3	0.389	3.6	0.195	0.023
171							
168	3.3E-07	9.5	22.5	0.389	4.1	0.198	0.02
165	3.3E-07	9.5	22.5	0.391	4.2	0.198	0.019
162							
159	3.5E-07	9.5	22.6	0.391	4.5	0.2	0.017
156							
153	3.4E-07	9.5	22.6	0.393	4.8	0.2	0.016
150							
147	3.3E-07	9.6	22.7	0.396	4.6	0.2	0.015
144							
141	3.3E-07	9.6	23	0.399	4.2	0.202	0.015

138							
135	3.4E-07	9.6	23.1	0.401	3.8	0.203	0.015
132							
129	3.5E-07	9.6	23.1	0.402	3.6	0.203	0.015
126							
123	3.5E-07	9.6	23.1	0.403	3.6	0.203	0.014
120							
117	3.3E-07	9.6	23	0.405	3.4	0.203	0.015
114							
111	3.2E-07	9.6	22.8	0.406	3.4	0.202	0.016
108							
105	3.2E-07	9.7	22.6	0.406	3	0.202	0.017

C.3. Kraton® D1161 – Piccotac™ 1095 Blends Stepwise Heating Experiment

C.3.1. Blend: 90/10

T (°C)	K	Rc (nm)	Rhs (nm)	Φ	A (a.u.)	b (nm^{-1})	c
250	3.7E-07	8.8	20.4	0.39	0.12	0.21	0.02
249	3.75E-07	8.8	20.4	0.391	0.12	0.21	0.02
246	3.75E-07	8.8	20.5	0.392	0.2	0.217	0.02
243	3.75E-07	8.8	20.5	0.394	0.2	0.215	0.02
240	3.8E-07	8.9	20.5	0.394	0.3	0.215	0.01
237	3.7E-07	8.9	20.5	0.395	0.8	0.217	0.01
234	3.6E-07	8.9	20.5	0.396	1.1	0.217	0.01
231	3.5E-07	9	20.6	0.398	1.3	0.217	0.008
228	3.4E-07	9.1	20.6	0.4	1.8	0.217	0.008
225	3.15E-07	9.2	20.6	0.401	2.1	0.217	0.007
222	3.1E-07	9.3	20.6	0.4	2.5	0.217	0.007
219	3E-07	9.4	20.7	0.4	3.3	0.216	0.007
216	2.9E-07	9.4	20.7	0.4	4	0.217	0.008
213							
210	2.7E-07	9.5	20.8	0.399	5.4	0.216	0.007
207	2.9E-07	9.5	20.9	0.4	5.5	0.217	0.008
204							
201	2.8E-07	9.5	20.9	0.4	6.5	0.215	0.008
198							
195	2.6E-07	9.6	21	0.398	7	0.214	0.007
192							
189	2.6E-07	9.6	21	0.398	7.2	0.213	0.007
186							

183	2.6E-07	9.6	21.1	0.397	7.2	0.213	0.007
180	2.6E-07	9.6	21.1	0.396	7.3	0.212	0.007
177							
174	2.6E-07	9.6	21.2	0.393	7.4	0.212	0.008
171							
168	2.6E-07	9.6	21.3	0.39	7.5	0.212	0.008
165	2.6E-07	9.6	21.3	0.385	7.6	0.212	0.009
162							
159	2.6E-07	9.6	21.4	0.387	7.4	0.213	0.009
156							
153	2.6E-07	9.6	21.4	0.389	7	0.213	0.01
150	2.65E-07	9.6	21.5	0.391	6.8	0.214	0.01
147							
144	2.65E-07	9.6	21.4	0.398	5.8	0.214	0.01
141							
138	2.75E-07	9.5	21.4	0.401	5.3	0.214	0.01
135	2.75E-07	9.5	21.3	0.405	4.2	0.214	0.01
132							
129	2.8E-07	9.5	21.4	0.408	2.8	0.214	0.01
126							
123	2.85E-07	9.5	21.5	0.41	1.7	0.213	0.01
120	2.85E-07	9.4	21.7	0.411	1.5	0.213	0.01
117							
114	2.85E-07	9.4	21.8	0.413	0.7	0.21	0.01
111							
108	2.9E-07	9.3	21.9	0.414	0.5	0.2	0.008
105	2.85E-07	9.3	21.9	0.415	0.2	0.2	0.008

C.3.2. Blend: 70/30

T (°C)	**K**	**Rc (nm)**	**Rhs (nm)**	**Φ**	**A (a.u.)**	**b (nm^{-1})**	**c**
250	1.25E-07	8.5	19.3	0.325	0.2	0.21	0.03
249	1.35E-07	8.5	19.2	0.33	0.2	0.21	0.03
246	1.40E-07	8.5	19.3	0.335	0.24	0.21	0.027
243	1.45E-07	8.6	19.4	0.34	0.24	0.21	0.027
240	1.55E-07	8.6	19.6	0.35	0.24	0.21	0.026
237	1.6E-07	8.7	19.7	0.355	0.24	0.21	0.026
234	1.6E-07	8.8	19.8	0.36	0.24	0.21	0.021
231	1.62E-07	8.9	19.9	0.366	0.24	0.21	0.021
228	1.62E-07	9	20	0.368	0.24	0.215	0.02

225	1.62E-07	9.1	20	0.371	0.24	0.215	0.02
222	1.63E-07	9.1	20.1	0.378	0.24	0.21	0.02
219	1.65E-07	9.1	20.2	0.38	0.26	0.21	0.02
216	1.68E-07	9.1	20.3	0.383	0.26	0.216	0.02
213	1.68E-07	9.1	20.4	0.387	0.26	0.216	0.02
210	1.7E-07	9.1	20.5	0.389	0.26	0.216	0.02
207	1.72E-07	9.1	20.5	0.391	0.26	0.216	0.02
204	1.75E-07	9.1	20.6	0.392	0.26	0.216	0.02
201	1.77E-07	9.1	20.7	0.393	0.31	0.22	0.02
198	1.78E-07	9.1	20.8	0.394	0.37	0.22	0.02
195	1.8E-07	9.1	20.9	0.396	0.37	0.22	0.02
192	1.8E-07	9.1	20.9	0.397	0.42	0.22	0.02
189	1.8E-07	9.1	21	0.399	0.44	0.215	0.025
186	1.8E-07	9.1	21	0.4	0.5	0.215	0.025
183	1.8E-07	9.1	21	0.402	0.5	0.214	0.025
180	1.8E-07	9.1	21.1	0.403	0.5	0.213	0.025
177	1.8E-07	9.1	21.1	0.405	0.52	0.21	0.025
174	1.8E-07	9.1	21.2	0.405	0.54	0.21	0.025
171	1.8E-07	9.1	21.2	0.406	0.54	0.21	0.025
168	1.8E-07	9.1	21.2	0.408	0.56	0.21	0.025
165	1.8E-07	9.1	21.3	0.408	0.6	0.21	0.025
162							
159	1.8E-07	9.1	21.3	0.408	0.6	0.21	0.025
156							
153							
150	1.8E-07	9.1	21.4	0.408	0.63	0.21	0.027
147							
144	1.8E-07	9.1	21.4	0.408	0.7	0.21	0.025
141							
138	1.8E-07	9.1	21.4	0.408	0.7	0.21	0.026
135	1.8E-07	9.1	21.4	0.4085	0.7	0.22	0.03
132	1.8E-07	9.1	21.4	0.409	0.7	0.215	0.027
129							
126	1.8E-07	9.1	21.5	0.409	0.6	0.225	0.03
123							
120	1.8E-07	9.1	21.7	0.4095	0.5	0.232	0.032
117							
114	1.8E-07	9.1	22	0.41	0.42	0.24	0.032
111							
108	1.85E-07	9.1	22.1	0.411	0.35	0.25	0.037

C.3.3. Blend: 50/50

T (°C)	K	Rc (nm)	Rhs (nm)	Φ	A (a.u.)	b (nm^{-1})	c
250							
249	1.2E-07	6.7	20.5	0.28	0		
246	1.3E-07	6.8	20.5	0.3	0		
243	1.4E-07	6.8	20.5	0.31	0		
240	1.4E-07	7	20.5	0.32	0		
237	1.4E-07	7.1	20.5	0.32	0		
234	1.45E-07	7.1	20.5	0.324	0		
231	1.45E-07	7.2	20.5	0.33	0		
228	1.5E-07	7.3	20.5	0.34	0		
225	1.55E-07	7.3	20.5	0.344	0		
222	1.6E-07	7.4	20.6	0.348	0		
219	1.6E-07	7.5	20.6	0.35	0		
216	1.6E-07	7.6	20.7	0.355	0		
213	1.65E-07	7.7	20.7	0.36	0		
210	1.65E-07	7.7	20.7	0.364	0		
207							
204	1.7E-07	7.8	20.7	0.371	0		
201							
198	1.75E-07	7.9	20.8	0.375	0		
195	1.75E-07	7.9	20.8	0.38	0		
192							
189	1.78E-07	8	21	0.384	0		
186							
183	1.78E-07	8	21.2	0.389	0		
180	1.8E-07	8	21.2	0.392	0		
177							
174	1.85E-07	8	21.4	0.395	0		
171							
168	1.92E-07	8	21.5	0.397	0		
165	1.9E-07	8.1	21.6	0.397	0		
162							
159	1.9E-07	8.1	21.8	0.4	0		
156							
153	1.9E-07	8.1	22	0.402	0		
150	1.9E-07	8.1	22.1	0.403	0		
147							
144	1.95E-07	8.1	22.3	0.404	0		
141							

138	1.95E-07	8.1	22.4	0.404	0.1	0.2	0.01
135	1.95E-07	8.1	22.4	0.404	0.2	0.2	0.01
132							
129	1.9E-07	8.1	22.4	0.404	0.3	0.2	0.01
126							
123	1.9E-07	8.1	22.4	0.403	0.4	0.2	0.01
120	1.9E-07	8.1	22.3	0.403	0.5	0.195	0.008
117							
114	1.9E-07	8.1	22.2	0.404	0.6	0.19	0.008
111							
108	1.9E-07	8.1	22.2	0.4	0.6	0.19	0.01
105	1.9E-07	8.1	22.2	0.398	0.7	0.19	0.01

C.4. Kraton® D1161 – Isothermal Microphase Separation Kinetics

C.4.1. *T* = 160 °C

Time (min)	**K**	**Rc (nm)**	**Rhs (nm)**	**Φ**	**A (a.u.)**	**b (nm^{-1})**	**c**
0	3.8E-07	9.7	20.9	0.406	0		
1	3.7E-07	9.8	21	0.407	0		
2	3.6E-07	9.8	21.1	0.408	0		
3							
4							
5	3.4E-07	9.9	21.4	0.408	0		
10	3.3E-07	10	21.6	0.406	0.5	0.2	0.025
15	3E-07	10.1	21.8	0.404	1.5	0.208	0.02
20	2.9E-07	10.1	22	0.403	1.9	0.21	0.02
25							
30	2.7E-07	10.3	22.2	0.399	2.5	0.207	0.02
35							
40	2.6E-07	10.4	22.5	0.392	3.6	0.207	0.016
45							
50	2.5E-07	10.5	22.8	0.386	4.1	0.207	0.016
55							
60	2.5E-07	10.5	23.1	0.381	4.4	0.207	0.016
70	2.4E-07	10.6	23.5	0.378	4.7	0.208	0.016
80	2.3E-07	10.7	24	0.375	5	0.207	0.015
90	2.4E-07	10.8	24.1	0.378	5	0.209	0.013
100	2.3E-07	10.9	24.6	0.378	5.1	0.209	0.013

C.4.2. *T* = 170 °C

Time (min)	K	Rc (nm)	Rhs (nm)	Φ	A (a.u.)	b (nm^{-1})	c
0	6.9E-07	9.5	21	0.404	0		
1	6.9E-07	9.4	21.2	0.406	0		
2	6.9E-07	9.5	21.3	0.405	0		
3	6.8E-07	9.6	21.4	0.405	0		
4	6.7E-07	9.6	21.4	0.405	0		
5	6.7E-07	9.7	21.5	0.404	0		
10	6.2E-07	9.9	21.8	0.4	1.5	0.211	0.016
15	5.9E-07	9.9	22.2	0.399	2	0.211	0.016
20	5.50E-07	10	22.6	0.397	2.6	0.211	0.016
25	5.2E-07	10.2	22.8	0.394	3	0.21	0.016
30	5E-07	10.3	23.1	0.39	3.8	0.21	0.016
35							
40	4.9E-07	10.4	23.5	0.386	4.3	0.211	0.015
45							
50	4.5E-07	10.6	23.9	0.383	5.3	0.21	0.013
55							
60	4.5E-07	10.7	24.1	0.379	5.5	0.209	0.012
70	4.5E-07	10.8	24.2	0.376	5.6	0.209	0.011
80	4.5E-07	10.8	24.5	0.372	5.7	0.209	0.012
90	4.5E-07	10.8	24.8	0.37	5.7	0.208	0.012

C.4.3. *T* = 150 °C

Time (min)	K	Rc (nm)	Rhs (nm)	Φ	A (a.u.)	b (nm^{-1})	c
0	4.2E-07	9.6	20.8	0.406	0		
1	4.15E-07	9.6	21	0.407	0		
2	3.95E-07	9.6	21.1	0.408	0		
3	3.9E-07	9.6	21.2	0.408	0		
4	3.9E-07	9.6	21.3	0.408	0		
5	3.88E-07	9.6	21.4	0.408	0		
10	3.88E-07	9.7	21.7	0.407	0		
15	3.8E-07	9.8	22	0.406	0		
20	3.2E-07	9.8	22.2	0.407	1.3	0.187	0.015
25	3.1E-07	9.8	22.6	0.405	1.6	0.195	0.03
30	2.81E-07	9.9	23	0.403	2.4	0.2	0.025
35	2.9E-07	9.9	23.3	0.401	2.6	0.195	0.025

40	2.86E-07	9.9	23.6	0.399	3	0.195	0.024
45	2.78E-07	9.9	23.7	0.397	3.4	0.191	0.024
50	2.78E-07	9.9	24	0.393	3.8	0.191	0.024
55	2.8E-07	9.9	24.1	0.391	4	0.189	0.024
60	2.78E-07	9.9	24.3	0.388	4.2	0.189	0.024
70	2.76E-07	10	24.4	0.382	4.4	0.186	0.024
80	2.7E-07	10.1	24.7	0.376	4.5	0.186	0.024
90	2.67E-07	10.2	24.9	0.37	4.5	0.185	0.024
100	2.7E-07	10.2	25.1	0.363	4.6	0.184	0.024
110	2.65E-07	10.2	25.5	0.362	4.6	0.184	0.024
120	2.58E-07	10.3	25.9	0.356	4.7	0.184	0.024
130	2.55E-07	10.3	26.1	0.352	4.7	0.184	0.024
140	2.5E-07	10.3	26.8	0.351	4.8	0.184	0.024
150	2.3E-07	10.4	27.3	0.349	5	0.184	0.024

C.5. Kraton® D1161 – Piccotac™ 1095 Blends Isothermal Microphase Separation Kinetics

C.5.1. Blend: 90/10, *T* = 160 °C

Time (min)	**K**	**Rc (nm)**	**Rhs (nm)**	**Φ**	**A (a.u.)**	**b (nm^{-1})**	**c**
0	3.3E-07	9.6	20.8	0.405	0	0.21	0.02
1	3.3E-07	9.6	21	0.406	0	0.21	0.02
2	3.1E-07	9.7	21.1	0.406	0	0.21	0.02
3							
4							
5	3.1E-07	9.7	21.3	0.407	0	0.21	0.02
10	2.8E-07	9.9	21.4	0.407	0	0.21	0.02
15	2.6E-07	9.9	21.5	0.407	0.4	0.21	0.02
20	2.5E-07	10	21.6	0.406	0.8	0.215	0.02
25							
30	2.4E-07	10	21.7	0.404	1.5	0.212	0.015
35							
40	2.4E-07	10	21.7	0.402	1.6	0.21	0.02
45							
50	2.4E-07	10	21.8	0.4	1.7	0.208	0.02
55							
60	2.3E-07	10.1	21.8	0.397	2	0.203	0.02
70	2.3E-07	10.1	21.8	0.395	2.1	0.198	0.02
80	2.3E-07	10.1	21.9	0.391	2.3	0.195	0.02
90	2.3E-07	10.1	21.9	0.386	2.5	0.189	0.022
100	2.3E-07	10.2	21.9	0.383	2.5	0.182	0.022

110	2.2E-07	10.2	22	0.383	2.6	0.177	0.022
120	2.2E-07	10.2	22.1	0.382	2.8	0.173	0.021
130	2.2E-07	10.2	22.1	0.381	3	0.17	0.02
140	2.2E-07	10.2	22.1	0.38	3.1	0.169	0.02
150	2.2E-07	10.2	22.1	0.379	3.1	0.168	0.02
160	2.2E-07	10.2	22.2	0.378	3.1	0.166	0.021

C.5.2. Blend: 90/10, *T* = 150 °C

Time (min)	**K**	**Rc (nm)**	**Rhs (nm)**	**Φ**	**A (a.u.)**	**b (nm^{-1})**	**c**
0	3.7E-07	9.3	20.8	0.408	0	0	
1	3.65E-07	9.4	21	0.408	0	0	
2	3.5E-07	9.5	21	0.408	0	0	
3							
4							
5	3.3E-07	9.7	21.2	0.408	0	0	
10	3.1E-07	9.8	21.5	0.408	0	0	
15	2.8E-07	9.8	21.7	0.407	1.1	0.205	0.02
20	2.8E-07	9.9	21.8	0.406	1.3	0.202	0.018
25							
30	2.75E-07	9.9	21.9	0.406	1.5	0.202	0.018
35							
40	2.7E-07	10	21.9	0.404	2	0.202	0.015
45							
50	2.7E-07	10	21.9	0.403	2.2	0.202	0.015
55							
60	2.8E-07	10.1	21.9	0.402	2.5	0.204	0.015
70	2.8E-07	10.1	22	0.4	2.9	0.206	0.012
80	2.8E-07	10.1	22	0.399	3.2	0.206	0.012
90	2.8E-07	10.1	22	0.398	3.5	0.207	0.011
100	2.8E-07	10.2	22	0.397	3.7	0.208	0.01
110	2.8E-07	10.2	22	0.395	3.9	0.208	0.01
120	2.8E-07	10.3	22	0.394	4.1	0.209	0.01
130	2.7E-07	10.3	22	0.393	4.3	0.209	0.01
140	2.7E-07	10.3	22	0.392	4.5	0.209	0.009
150	2.7E-07	10.3	22	0.391	4.7	0.209	0.009
160	2.7E-07	10.3	22	0.39	4.8	0.209	0.009
170	2.7E-07	10.3	22	0.389	4.9	0.209	0.009
180	2.7E-07	10.3	22	0.388	5	0.209	0.009

C.5.3. Blend: 90/10, *T* = 140 °C

Time (min)	K	Rc (nm)	Rhs (nm)	Φ	A (a.u.)	b (nm^{-1})	c
0	3E-07	9.4	20.9	0.407	0		
1	2.85E-07	9.5	21	0.408	0		
2	2.8E-07	9.5	21	0.408	0		
3							
4							
5	2.6E-07	9.6	21.2	0.409	0		
10	2.6E-07	9.6	21.6	0.4085	0		
15							
20	2.7E-07	9.7	22.1	0.407	0		
25							
30	2.5E-07	9.7	22.4	0.404	1.2	0.189	0.02
35							
40	2.5E-07	9.8	22.7	0.402	1.7	0.181	0.015
45							
50	2.5E-07	9.8	22.8	0.399	2.2	0.178	0.015
55							
60	2.45E-07	9.8	22.9	0.397	2.7	0.176	0.015
70	2.45E-07	9.8	23	0.395	3	0.173	0.015
80	2.45E-07	9.9	23	0.393	3.2	0.171	0.015
90	2.4E-07	9.9	23	0.392	3.4	0.17	0.015
100	2.4E-07	9.9	23	0.391	3.6	0.168	0.015
110	2.4E-07	9.9	23	0.389	3.7	0.167	0.015
120	2.4E-07	9.9	23.1	0.388	3.8	0.166	0.015
130	2.4E-07	9.9	23.1	0.388	3.9	0.164	0.015
140	2.4E-07	9.9	23.1	0.385	4	0.163	0.017
150	2.4E-07	9.9	23.1	0.384	4	0.162	0.017
160	2.3E-07	10	23.1	0.383	4.1	0.161	0.017
170	2.3E-07	10	23.1	0.382	4.1	0.159	0.018
180	2.3E-07	10	23.1	0.382	4.2	0.158	0.018

C.5.4. Blend: 70/30, *T* = 150 °C

Time (min)	K	Rc (nm)	Rhs (nm)	Φ
0	3E-07	8.5	21.1	0.403
1	3E-07	8.5	21.2	0.404
2	3E-07	8.5	21.2	0.404
3	2.9E-07	8.5	21.3	0.405

4	2.9E-07	8.5	21.4	0.405
5	2.8E-07	8.6	21.4	0.405
10	2.8E-07	8.6	21.6	0.405
15	2.7E-07	8.6	21.7	0.406
20	2.3E-07	9	21.7	0.405
25	2.3E-07	9	21.8	0.405
30	2.3E-07	9	21.8	0.405
35	2.3E-07	9	21.8	0.405
40	2.3E-07	9	21.8	0.405
45	2.3E-07	9	21.8	0.405
50	2.3E-07	9	21.8	0.405
55				
60	2.3E-07	9	21.8	0.405
70	2.3E-07	9	21.8	0.405
80	2.3E-07	9	21.8	0.405
90	2.3E-07	9	21.9	0.405
100	2.3E-07	9	21.9	0.404
110	2.3E-07	9	21.9	0.404
120	2.3E-07	9	21.9	0.404
130	2.3E-07	9	21.9	0.404
140	2.3E-07	9	21.9	0.404
150	2.3E-07	9	22	0.404
160	2.3E-07	9	22	0.403
170	2.35E-07	9	22	0.403
180	2.32E-07	9	22	0.403

C.5.5. Blend: 70/30, *T* = 140 °C

Time (min)	**K**	**Rc (nm)**	**Rhs (nm)**	**Φ**	**A (a.u.)**	**b (nm^{-1})**	**c**
0	2.75E-07	9.3	20.8	0.408	0		
1	2.7E-07	9.2	21	0.409	0		
2	2.8E-07	9.2	21.1	0.409	0		
3	2.7E-07	9.3	21.1	0.409	0		
4	2.65E-07	9.3	21.2	0.409	0		
5	2.6E-07	9.3	21.3	0.409	0		
10	2.4E-07	9.3	21.5	0.409	1	0.2	0.015
15	2.4E-07	9.3	21.6	0.408	1.5	0.198	0.015
20	2.4E-07	9.3	21.8	0.406	2.2	0.197	0.015
25	2.4E-07	9.3	22	0.404	2.4	0.195	0.015

30	2.4E-07	9.3	22.1	0.403	2.6	0.192	0.015
35	2.4E-07	9.3	22.3	0.401	2.7	0.19	0.017
40	2.4E-07	9.3	22.4	0.4	2.8	0.186	0.017
45	2.4E-07	9.3	22.4	0.4	3	0.184	0.015
50	2.4E-07	9.3	22.5	0.398	3.1	0.182	0.016
55	2.4E-07	9.3	22.5	0.397	3.4	0.18	0.016
60	2.4E-07	9.3	22.6	0.397	3.4	0.178	0.016
70	2.5E-07	9.3	22.6	0.394	3.7	0.176	0.015
80	2.5E-07	9.3	22.6	0.394	3.8	0.174	0.015
90	2.5E-07	9.3	22.6	0.393	3.8	0.172	0.015
100	2.5E-07	9.4	22.7	0.392	3.8	0.17	0.015
110	2.5E-07	9.4	22.8	0.392	3.7	0.169	0.015
120	2.5E-07	9.4	22.9	0.392	3.8	0.167	0.015
130	2.5E-07	9.4	23	0.391	3.8	0.166	0.015
140	2.5E-07	9.4	23	0.391	4	0.163	0.017
150	2.5E-07	9.4	23.2	0.389	4	0.162	0.017
160	2.5E-07	9.4	23.2	0.389	4	0.161	0.017
170	2.5E-07	9.4	23.3	0.387	4	0.157	0.02
180	2.5E-07	9.4	23.3	0.387	4.1	0.156	0.02

C.5.6. Blend: 70/30, *T* = 130 °C

Time (min)	**K**	**Rc (nm)**	**Rhs (nm)**	**Φ**	**A (a.u.)**	**b (nm^{-1})**	**c**
0	2.1E-07	8.9	21.1	0.4	0		
1	2.1E-07	8.9	21.1	0.4	0		
2							
3	2.1E-07	8.9	21.2	0.4	0		
4							
5	2.1E-07	8.9	21.4	0.399	0		
10	2E-07	9	21.6	0.398	0		
15	2E-07	9	21.8	0.397	0		
20	1.75E-07	9	21.8	0.397	0.5	0.181	0.024
25	1.65E-07	9.1	21.9	0.395	0.6	0.181	0.024
30	1.5E-07	9.2	22	0.395	0.7	0.181	0.024
35	1.5E-07	9.2	22.1	0.394	0.8	0.178	0.024
40	1.48E-07	9.2	22.3	0.392	0.9	0.177	0.024
45	1.4E-07	9.3	22.6	0.391	0.9	0.176	0.024
50	1.4E-07	9.3	22.7	0.387	1	0.175	0.024
55							
60	1.38E-07	9.3	22.8	0.379	1.2	0.174	0.024

70	1.35E-07	9.3	22.9	0.378	1.3	0.168	0.024
80	1.35E-07	9.3	23	0.373	1.4	0.164	0.024
90	1.35E-07	9.3	23	0.371	1.4	0.16	0.024
100	1.35E-07	9.3	23.2	0.37	1.5	0.155	0.024
110	1.35E-07	9.3	23.4	0.369	1.5	0.152	0.024
120	1.35E-07	9.3	23.7	0.368	1.55	0.146	0.026
130	1.35E-07	9.3	23.7	0.367	1.6	0.145	0.024
140	1.32E-07	9.3	23.8	0.366	1.6	0.143	0.024
150	1.32E-07	9.3	23.9	0.366	1.7	0.137	0.028
160	1.32E-07	9.3	24	0.366	1.8	0.132	0.028
170	1.3E-07	9.3	24.1	0.365	1.8	0.128	0.029
180	1.3E-07	9.3	24.1	0.365	1.9	0.123	0.03

C.5.7. Blend: 50/50, *T* = 120 °C

Time (min)	**K**	**Rc (nm)**	**Rhs (nm)**	**Φ**
0	1E-07	8.6	21.8	0.408
1	1E-07	8.6	21.8	0.408
2				
3				
4				
5	1E-07	8.9	22	0.407
10	9E-08	9	22.2	0.406
15	9E-08	9.1	22.4	0.406
20	8.5E-08	9.2	22.6	0.406
25	8.5E-08	9.3	22.8	0.405
30	8.5E-08	9.3	22.9	0.404
35	8.5E-08	9.3	23	0.404
40	8.5E-08	9.4	23.3	0.402
45				
50	9E-08	9.4	23.7	0.401
55				
60	9E-08	9.4	24	0.398
70	9.1E-08	9.4	24.4	0.396
80	9E-08	9.5	24.4	0.394
90	9E-08	9.5	24.5	0.393
100	9E-08	9.5	24.5	0.39
110	9E-08	9.5	24.6	0.389

C.5.8. Blend: 50/50, *T* = 110 °C

Time (min)	K	Rc (nm)	Rhs (nm)	Φ
0	5.5E-08	9.1	21.7	0.386
1	5.5E-08	9.1	21.8	0.388
5	5E-08	9.1	21.8	0.391
10	4.8E-08	9.2	21.9	0.39
15	4.6E-08	9.3	22	0.39
20				
25	4.5E-08	9.5	22.3	0.385
30	4.5E-08	9.5	22.4	0.384
35				
40	4.5E-08	9.5	22.5	0.382
45				
50	4.4E-08	9.5	22.8	0.381
55				
60	4.2E-08	9.5	23	0.381
70	4.1E-08	9.6	23.2	0.378
80	4.1E-08	9.6	23.4	0.378
90	4E-08	9.6	23.6	0.374
100	4E-08	9.6	23.8	0.372
110	4E-08	9.6	24	0.371
120	4E-08	9.6	24.3	0.368

C.6. Kraton® D1171 – Temperature Ramp Experiment.

Ramp Rate: 2 °C/min.

	I (q) (a.u.)								
q (nm^{-1})	**30 °C**	**60 °C**	**90 °C**	**120 °C**	**150 °C**	**180 °C**	**210 °C**	**240 °C**	**250 °C**
0.07	161.4956	158.3017	159.1011	159.53	167.0855	196.7519	279.5255	179.6706	200.6982
0.08	192.1588	189.9692	187.9609	181.6843	191.0965	199.2943	157.3681	197.6601	186.7927
0.09	149.4353	147.9324	145.4681	139.9905	148.2109	149.8236	114.99	153.3295	145.0208
0.1	99.18862	98.25204	96.82406	93.79234	99.54563	101.8035	82.62483	101.8337	96.27291
0.11	71.70072	70.8669	69.55933	67.22372	71.21089	73.76751	59.19709	74.11173	70.02064
0.12	49.8374	49.4204	48.49924	47.20971	50.15611	53.08275	42.71602	51.72208	49.36641

0.13	37.74766	37.49583	36.62763	35.7138	38.1114	41.44792	32.13222	39.07513	36.93823
0.14	30.24425	30.1349	29.48469	28.73241	30.77541	35.5122	25.99809	31.79019	29.97869
0.15	20.87202	20.81324	20.46942	20.14692	21.83311	28.71254	19.38618	22.25745	21.10261
0.16	15.13624	15.16189	15.07409	14.98848	16.36795	26.26526	15.08014	16.49177	15.78341
0.17	13.28936	13.52697	13.34042	13.26191	14.94161	27.84083	13.69719	14.25283	13.84745
0.18	13.99441	15.12146	15.75664	13.68732	14.98485	29.8196	13.25918	12.57136	12.34179
0.19	27.56858	31.8605	35.40248	27.05235	24.56607	34.76247	14.77632	12.45267	12.44048
0.2	42.84407	48.00325	58.89269	74.65812	62.04023	45.55862	18.60222	14.38314	13.99277
0.21	50.93123	57.3191	80.90479	116.9465	115.0253	59.46745	24.26972	17.41295	16.21558
0.22	53.54312	62.75369	78.45733	70.96239	70.21712	37.77864	29.96261	21.61872	18.73454
0.23	57.81886	62.69933	45.26081	19.26878	17.87679	15.33976	29.40533	23.49182	19.36961
0.24	43.18277	37.72191	17.68683	7.784472	8.53218	10.83892	22.95722	20.98285	17.25076
0.25	18.09997	13.56953	6.891161	5.113586	5.94069	8.392545	15.69499	16.19871	13.84237
0.26	6.956293	5.748891	4.243549	4.019185	4.707362	6.786474	10.94909	11.90539	10.68642
0.27	4.256581	4.01225	3.483424	3.44331	4.007906	5.802223	8.159524	9.068572	8.433459
0.28	3.229476	3.18914	2.909899	3.009288	3.462119	4.922171	6.277922	7.040303	6.707818
0.29	2.712441	2.723382	2.589518	2.648157	3.070966	4.288406	5.049323	5.653647	5.430223
0.3	2.379331	2.413643	2.341217	2.398277	2.777933	3.819093	4.311972	4.658969	4.546918
0.31	2.207078	2.241452	2.221938	2.200015	2.569453	3.389427	3.637519	3.930425	3.874715
0.32	2.113359	2.216293	2.263164	2.131396	2.405821	3.076626	3.151687	3.420777	3.328202
0.33	2.259816	2.466099	2.60713	2.259794	2.398629	2.845403	2.800678	3.008069	2.965959
0.34	2.46196	2.748265	3.13421	2.7751	2.59587	2.757392	2.502218	2.648582	2.616748
0.35	2.632918	2.992951	3.636648	3.894044	3.138765	2.742767	2.251955	2.361628	2.329379

0.36	2.61149	2.95524	3.773246	4.95239	4.408344	2.845769	2.035842	2.159359	2.110644
0.37	2.47091	2.836203	3.693053	4.474412	4.579137	2.822899	1.859901	1.929986	1.915668
0.38	2.322362	2.720045	3.352781	2.840159	2.685363	2.108038	1.685253	1.756775	1.707221
0.39	2.237779	2.675771	2.855111	1.846588	1.819972	1.671017	1.535533	1.602562	1.589282
0.4	2.107373	2.39365	2.155376	1.613257	1.542058	1.471868	1.372144	1.438545	1.429441
0.41	1.813156	1.902973	1.737894	1.679517	1.505132	1.3258	1.233779	1.289894	1.282088
0.42	1.423726	1.444278	1.425407	1.604388	1.601036	1.266972	1.11442	1.205764	1.199506
0.43	1.045109	1.102119	1.164544	1.217149	1.326777	1.121389	0.987051	1.080761	1.068737
0.44	0.860293	0.916176	0.962977	0.906619	0.941222	0.936253	0.907722	0.974982	0.984609
0.45	0.755473	0.797687	0.774431	0.707501	0.755547	0.833728	0.824123	0.901277	0.90148
0.46	0.63504	0.680102	0.639735	0.61179	0.663348	0.742026	0.751178	0.825616	0.814305
0.47	0.561798	0.583783	0.551289	0.544547	0.615943	0.689797	0.686382	0.750891	0.752941
0.48	0.505282	0.514153	0.497383	0.512305	0.564262	0.634281	0.632098	0.704304	0.710227
0.49	0.463406	0.465419	0.44525	0.468892	0.519721	0.582532	0.590399	0.637981	0.651565
0.5	0.422643	0.439033	0.414019	0.440614	0.484681	0.553516	0.551837	0.599658	0.605224

C.7. Kraton® D1171 – Determination of Morphological Transitions

1/T vs $1/I_{max}$ plot

T (°C)	1/T (K^{-1})	I_{max}	$1/I_{max}$
99	0.002687	94.85	0.010543
102	0.002666	99.89	0.010011
105	0.002644	104.15	0.009602
108	0.002624	107.34	0.009316
111	0.002603	110.71	0.009033
114	0.002583	113.09	0.008843
117	0.002563	115.43	0.008663
120	0.002544	116.95	0.008551
123	0.002524	118.22	0.008459

126	0.002505	118.97	0.008405
129	0.002487	119.81	0.008347
132	0.002468	119.54	0.008365
135	0.00245	119.53	0.008366
139	0.002426	119.33	0.00838
142	0.002409	118.76	0.00842
145	0.002391	117.32	0.008524
148	0.002374	115.94	0.008625
151	0.002358	115.02	0.008694
154	0.002341	112.91	0.008857
157	0.002325	110.61	0.009041
160	0.002309	106.88	0.009356
163	0.002293	101.45	0.009857
166	0.002277	94.73	0.010556
169	0.002262	86.37	0.011578
172	0.002246	78.67	0.012711
175	0.002231	71.98	0.013893
178	0.002217	66.2	0.015106
181	0.002202	59.46	0.016818
184	0.002187	53.12	0.018825
187	0.002173	49.05	0.020387
190	0.002159	43.43	0.023026
193	0.002145	36.02	0.027762
196	0.002132	35.04	0.028539
199	0.002118	33.97	0.029438
202	0.002105	33.04	0.030266
205	0.002091	32	0.03125
208	0.002078	30.93	0.032331
211	0.002065	29.96	0.033378
214	0.002053	28.91	0.03459
217	0.00204	28.18	0.035486
220	0.002028	27.48	0.03639
223	0.002016	26.54	0.037679
226	0.002003	26.08	0.038344
229	0.001991	25.54	0.039154
232	0.00198	25.08	0.039872
236	0.001964	24.64	0.040584
239	0.001953	23.49	0.042571
242	0.001941	22.34	0.044763
245	0.00193	21.24	0.047081
248	0.001919	19.76	0.050607

250	0.001911	19.37	0.051626

C.8. Kraton® D1171 – Sylvalite® RE 100L Blends - Determination of Morphological Transitions

C.8.1. Blend: 90/10, 1/T vs $1/I_{max}$ plot

T (°C)	1/T (K^{-1})	I_{max}	$1/I_{max}$
100	0.00268	8.874	0.112689
103	0.002659	9.372	0.106701
106	0.002637	9.852	0.101502
109	0.002617	10.42	0.095969
112	0.002596	11.244	0.088936
115	0.002576	11.868	0.08426
118	0.002557	12.511	0.07993
121	0.002537	12.69	0.078802
124	0.002518	13.17	0.07593
127	0.002499	13.7	0.072993
130	0.00248	14.192	0.070462
133	0.002462	14.522	0.068861
136	0.002444	14.979	0.06676
139	0.002426	15.653	0.063886
143	0.002403	16.41	0.060938
146	0.002386	17.095	0.058497
149	0.002369	17.515	0.057094
152	0.002352	17.03	0.05872
155	0.002336	17.929	0.055776
158	0.002319	17.378	0.057544
161	0.002303	15.402	0.064927
164	0.002288	12.108	0.08259
167	0.002272	18.626	0.053688
170	0.002257	34.466	0.029014
173	0.002241	38.698	0.025841
176	0.002226	37.433	0.026714
179	0.002212	37.576	0.026613
182	0.002197	36.583	0.027335
185	0.002183	35.055	0.028527
188	0.002168	33.238	0.030086
191	0.002154	31.308	0.031941
194	0.002141	29.333	0.034091
197	0.002127	27.077	0.036932
200	0.002113	24.795	0.040331

203	0.0021	18.16	0.055066
206	0.002087	13.101	0.07633
209	0.002074	9.851	0.101513
212	0.002061	7.648	0.130753
215	0.002049	6.059	0.165044
218	0.002036	4.814	0.207727
221	0.002024	3.822	0.261643
224	0.002011	3.181	0.314367
227	0.001999	2.627	0.380662
231	0.001984	2.262	0.442087
234	0.001972	2.16	0.462963
237	0.00196	1.779	0.562114
240	0.001949	1.604	0.623441
243	0.001937	1.449	0.690131
246	0.001926	1.407	0.710732
250	0.001911	1.322	0.75643

C.8.2. Blend: 70/30, 1/T vs $1/I_{max}$ plot

T (°C)	**1/T (K^{-1})**	**I_{max}**	**$1/I_{max}$**
100	0.00268	25.05	0.03992
103	0.002659	24.761	0.040386
106	0.002637	23.999	0.041668
109	0.002617	23.129	0.043236
112	0.002596	22.316	0.044811
115	0.002576	21.373	0.046788
118	0.002557	20.54	0.048685
121	0.002537	19.74	0.050659
124	0.002518	19.211	0.052054
127	0.002499	18.616	0.053717
130	0.00248	17.879	0.055932
133	0.002462	16.97	0.058928
136	0.002444	16.011	0.062457
140	0.00242	15.168	0.065928
143	0.002403	14.265	0.070102
146	0.002386	13.388	0.074694
149	0.002369	12.631	0.07917
152	0.002352	11.699	0.085477
155	0.002336	11.001	0.090901
158	0.002319	10.143	0.09859
161	0.002303	9.443	0.105899

164	0.002288	8.737	0.114456
167	0.002272	6.864	0.145688
170	0.002257	4.924	0.203087
173	0.002241	3.57	0.280112
176	0.002226	2.713	0.368596
179	0.002212	2.149	0.465333
182	0.002197	1.784	0.560538
185	0.002183	1.533	0.652316
188	0.002168	1.383	0.723066
191	0.002154	1.224	0.816993
194	0.002141	1.15	0.869565
197	0.002127	1.08	0.925926
200	0.002113	1.0365	0.964785

C.9. Kraton® D1171 – Piccotac 1095™ Blends - Determination of Morphological Transitions

C.9.1. Blend: 90/10, 1/T vs $1/I_{max}$ plot

T (°C)	1/T (K^{-1})	I_{max}	$1/I_{max}$
99	0.002687	45.17	0.022139
103	0.002659	47.4	0.021097
107	0.002631	49.09	0.020371
111	0.002603	50.2	0.01992
115	0.002576	50.03	0.019988
119	0.00255	49.07	0.020379
123	0.002524	46.82	0.021358
127	0.002499	43.66	0.022904
131	0.002474	39.07	0.025595
135	0.00245	37.05	0.026991
139	0.002426	35.12	0.028474
143	0.002403	33.29	0.030039
147	0.00238	31.57	0.031676
151	0.002358	29.64	0.033738
155	0.002336	28.26	0.035386
159	0.002314	26.66	0.037509
164	0.002288	24.24	0.041254
168	0.002267	21.36	0.046816
172	0.002246	18.72	0.053419
176	0.002226	17.98	0.055617
180	0.002207	18.44	0.05423
184	0.002187	18.94	0.052798
188	0.002168	18.67	0.053562

192	0.00215	18.35	0.054496
196	0.002132	17.65	0.056657
200	0.002113	16.89	0.059207
204	0.002096	16.26	0.061501
208	0.002078	15.35	0.065147
212	0.002061	14.45	0.069204
216	0.002044	13.4	0.074627
220	0.002028	10.53	0.094967
224	0.002011	5.26	0.190114
228	0.001995	2.76	0.362319
232	0.00198	2	0.5

C.9.2. Blend: 70/30, 1/T vs $1/I_{max}$ plot

T (°C)	**1/T (K^{-1})**	**I_{max}**	**$1/I_{max}$**
99	0.002687	36.25	0.027586
103	0.002659	35.7	0.028011
107	0.002631	35.25	0.028369
112	0.002596	34.86	0.028686
116	0.00257	34.35	0.029112
120	0.002544	34.16	0.029274
124	0.002518	33.68	0.029691
128	0.002493	32.73	0.030553
132	0.002468	31.58	0.031666
136	0.002444	30.29	0.033014
140	0.00242	30.8	0.032468
144	0.002397	31.26	0.03199
148	0.002374	31.36	0.031888
152	0.002352	30.99	0.032268
156	0.00233	29.61	0.033772
160	0.002309	27.09	0.036914
164	0.002288	24.12	0.041459
168	0.002267	19.82	0.050454
173	0.002241	16.95	0.058997
177	0.002221	14.47	0.069109
181	0.002202	13.36	0.07485
185	0.002183	12.91	0.077459
189	0.002164	12.2	0.081967
193	0.002145	11.16	0.089606
197	0.002127	7.56	0.132275
201	0.002109	2.62	0.381679

205	0.002091	1.66	0.60241